USDA

EPA

United States
Department of
Agriculture

Northeast Watershed
Center
University Park PA 16802

United States
Environmental Protection
Agency

Office of Environmental
Processes and Effects Research
Washington DC 20460

EPA-600/7-84-032
March 1984

Research and Development

Do not remove. This document
should be retained in the EPA
Region 5 Library Collection.

Atmosphere and Temperature Within a Reclaimed Coal-Stripmine and a Numerical Simulation of Acid Mine Drainage from Stripmined Lands

Interagency
Energy/Environment
R&D Program
Report

ATMOSPHERE AND TEMPERATURE WITHIN A RECLAIMED COAL-STRIPMINE AND A NUMERICAL SIMULATION OF ACID MINE DRAINAGE FROM STRIPMINED LANDS

by

D. B. Jaynes, A. S. Rogowski, and H. B. Pionke
U.S. Department of Agriculture, ARS
Northeast Watershed Research Center
University Park, Pennsylvania 16802

EPA-IAG-D5-763

Project Officer

Clinton W. Hall
Office of Energy, Minerals and Industry
Washington, D. C. 20250

Office of Research and Development
U.S. Environmental Protection Agency
Washington, D. C. 20250

U.S. Environmental Protection Agency
Region 5, Library (PL-12J)
77 West Jackson Boulevard, 12th Floor
Chicago, IL 60604-3590

DISCLAIMER

This report has been reviewed by the Office of Energy, Minesoils and Industry, U.S. Environmental Protection Agency, and approved for publication. Approval does not signify that the contents necessarily reflect the views and policies of the U.S. Environmental Protection Agency, nor does mention of trade names or commercial products constitute endorsement or recommendation for use.

FOREWORD

The Federal Water Pollution Control Act Amendments of 1972, in part, stress the control of nonpoint source pollution. Sections 102 (C-1), 208 (b-2,F) and 304(e) authorize basin scale development of water quality control plans and provide for area-wide waste treatment management. The act and the amendments include, when warranted, waters from agriculturally and silviculturally related nonpoint sources, and requires the issuance of guidelines for both identifying and evaluating the nature and extent of nonpoint source pollutants and the methods to control these sources. Research program at the Northeast Watershed Research Center contributes to the aforementioned goals. The major objectives of the Center are to:

- Study the major hydrologic and water-quality associated problems of the Northeastern U.S. and
- Initial emphasis is on land uses in the Northeast which most severely impact surface and subsurface hydrology and water quality.

Within the context of the Center's objectives, stripmining for coal ranks as a major and hydrologically severe land use. In addition, often the site is reclaimed and the conditions of the mining permit are met, stripmined areas revert legally from point to nonpoint sources. As a result, the hydrologic, physical, and chemical behavior of the reclaimed

land needs to be understood directly and in terms of control practices before the goals of Sections 102, 208 and 304 can be fully met.

Signed:

Harry B. Pionke
Director
Northeast Watershed
Research Center

ABSTRACT

Oxygen, O_2, carbon dioxide, CO_2 and temperature were measured with depth along a transect of an acid, reclaimed, coal stripmine over a two year period. Spoil-atmosphere O_2 concentrations decrease with depth but approach zero only in a small portion of the transect. Most of the mine remains well oxygenated (O_2 > 10% by volume) down to 12-meters depth. CO_2 concentrations ranged from near atmospheric levels to greater than 15%. At some locations, especially within 2 meters of the surface, variations in O_2 and CO_2 are correlated with changes in the spoil temperature. Spoil temperatures in layers below 3 meters remain in a range conducive to iron-oxidizing bacterial activity year around. Flux ratios of CO_2 and O_2 and the source/sink rates of the two gases indicate that carbonate neutralization of the acid produced by pyrite oxidation is the dominant source of CO_2.

In a second phase of the study, a numerical model describing the production and removal of acid and acid by-products from reclaimed coal-stripmines is presented. Both direct oxygen and bacterially catalyzed pyrite oxidation is considered. The pyrite oxidation rate is assumed to be controlled by first-order, solid-liquid kinetics and simple diffusion of oxidant into reactive, coarse, stone fragments. Oxygen supply into the reclaimed profile is considered to be governed by one-dimensional, gas diffusion.

Activity of the iron-oxidizing bacteria is controlled by the ferrous-ferric ratio, from which they obtain their energy, and from a combination of potentially inhibiting factors--the oxygen and hydrogen concentrations and the spoil temperature. Under all conditions modeled, excess acid, in the form of free hydrogen, must be removed if bacteria are to play an important role in accelerating pyrite oxidation. Leaching of the spoil by normal precipitation is insufficient in removing the excess hydrogen. Neutralization and buffering by the host rock is required for prolonged bacterial activity--the degree of hydrogen removal determining the maximum sustainable activity. At optimum conditions, bacteria can greatly increase pyrite oxidation.

As an offshoot of the diffusion portion of the study a comparison of Fick's Law for the diffusion of gas, i, in a vapor to the equations based on the kinetic theory of gases was made. The comparison shows that only for certain special conditions is the Fickian diffusion coefficient, D_{F_i}, independent of the mole fraction of i and the diffusional fluxes of the other gases. These conditions include the diffusion of a trace concentration of a gas through a gas mixture of any composition and equi-molar counter-current diffusion in a binary gas mixture, or in a ternary mixture where the third gas is stagnant. In an O_2, CO_2, N_2 atmosphere, variations in the diffusion coefficient of at least 10% from the tracer values are possible with variations in the mole fraction or flux ratio. The temperature and pressure dependence of the diffusion coefficient must also be recognized.

CONCLUSIONS

Oxygen, carbon dioxide and temperature measurements within a reclaimed coal-stripmine indicate that at this site, the spoil atmosphere is seldom depleted of oxygen despite the continuing oxidation of pyrite within the spoil. Increases in carbon dioxide concentrations were correlated with decreases in oxygen concentrations at most depths of each site. Oxygen and carbon dioxide concentrations were significantly correlated with spoil temperature at several locations but in general the correlation was weak. Average spoil temperatures to at least 60 cm deep are, in general, higher than temperatures found in a natural soil. Temperatures in the spoil below 300 cm remain within the tolerance range of iron-oxidizing bacteria year round.

We have presented a comprehensive model describing the *in situ* oxidation of pyrite and the removal of the oxidation products from reclaimed coal-stripmines. The rate of pyrite oxidation is assumed to be controlled by both the reaction kinetics and the diffusion rate of the products and reactants to the reaction site, where both oxygen and ferric iron may serve as the oxidant. Ferric iron concentrations are controlled by iron complexation and precipitation reactions which are assumed to be rapid. The only important source of ferric iron is oxidation of ferrous iron by iron-oxidating

bacteria. This model is unique in that the "activity" of the bacteria, which determines the rate of ferric iron production, is calculated from the energy available from the energy substrate and the deviation of the bacterial environment from ideal growing conditions. Pyrite oxidation and bacterial "activity" are linked through their modification of a shared environment.

Simulations, using the model, indicate that the lack of oxygen is the primary rate controlling factor in both pyrite oxidation and atuotrophic bacterial "activity." In zones where oxygen is not limiting, autotrophic activity can greatly increase the rate of pyrite oxidation. Whether or not bacteria are important in these zones, depends on the solution pH. The oxidation rate of pyrite will be affected by bacterially produced ferric iron only if the solution pH can be maintained in the range between reduced bacterial efficiency (pH > 2.0) and reduced ferric iron solubility (pH < 3.0). The interaction between hydrogen, produced by pyrite oxidation, and the rock matrix appears to be crucial in establishing the pH of the spoil solution.

Extensive testing of the model was not possible at this time, although its behavior seemed consistent with our current knowledge of acid formation in spoils. Further refinement of the model is necessary. The model is very sensitive to changes in the gas diffusion properties of the spoil. Although this property has been measured for spoils in the laboratory (Colvin, 1977)[2], field-based measurements, capable of incorporating the great heterogeneity of reclaimed spoil, would be desirable. The values of E'_{min}, x_T, x_{pH} and x_{O_2}, although based on experimental data, represent only best estimates. Laboratory experiments designed specifically to

determine these values and the form of their mathematical relationship would help establish the validity of the autotrophic "activity" model and the magnitude of the model parameters.

In view of the extreme sensitivity of the autotrophic "activity" to solution pH, the interaction of rock matrices with acid needs further study. These interactions are complex and varied mainly due to the wide range of minerals and reactions possible and the slow reaction kinetics associated with most interactions. It may be possible to develop a simple analytical technique, similar to that used to measure the acid potential of spoil (Caruccio, 1968), that combines all of the neutralization reactions into a simple empirical representation. Carbonate neutralization was considered separately in this model because of the great potential these materials represent for acid consumption. Further research on the reaction kinetics of carbonates, incorporating the effects and the development of iron coatings and diffusion control of reactants needs to be pursued.

CONTENTS

	Page
Foreword	iii
Abstract	v
Conclusions	vii
Figures	xii
Tables	xvi
Notation for Section 2	xviii
Notation for Section 3	xix
Notation for Section 4	xx
Notation for Appendix A	xxv
Notation for Appendix B	xxvii
1. Introduction	1
References	4
2. Spoil Atmosphere and Temperature in a Reclaimed Coal Stripmine	6
Introduction	6
Materials and Methods	8
Results	16
Discussion	31
References	36
3. Flux and Production Rates of Oxygen and Carbon Dioxide in a Reclaimed Coal-Stripmine	39
Introduction	39
Theory	42
Materials and Methods	44
Results and Discussion	48
Conclusions	55
References	58
4. A Numerical Model of Acid Drainage from Reclaimed Coal-Stripmines	60
Introduction	60
Description of Model	62
Basic Reactions	62
Basic Equations	63
Oxygen Diffusion	69
Q_{PY}	70
Q_{HB}	71
Q_{CHOX}	72
Q_{AB}	72
K_B	73
Chemical Species	83
Ferric Precipitation	84
Ferric Complexes	85

Page

Removal of Reaction Products. 86
Acid Neutralization. 86
Leaching 90
Solution Method 93
Results and Discussion 97
Role of Iron Oxidizing Bacteria 97
Model Sensitivity and Versatility 112
Effective Diffusion Coefficient. 112
Pyrite Distribution. 119
Inhibition of Bacteria. 123
Carbon Dioxide Generation 125
References 129

Appendices

A. Applicability of Fick's Law to Gas Diffusion. 135
B. Parameter Values Used in the Pyrite Oxidation Model 160
C. Computer Listing and Example Output of Acid Mine Drainage Model. 173

LIST OF FIGURES

Figure		Page
1	Location of monitoring sites 1-6 and the depth of the gas sample-chambers (crossbars) at each site in relation to the strip-mine stratigraphy.	11
2	Schematic of gas sample-chambers design	12
3	Schematic of O_2 measuring-chamber used in the field	14
4	Variation of temperature (^oC) over time for six depths at site 2. Depths shown are (▲) 30cm, (□) 60 cm, (■) 170 cm, (○) 320 cm, (△) 625 cm and (●) 945 cm	20
5	Variation of temperature (^oC) and the mole fractions of O_2 and CO_2 over time for the composite record at site 1. The temperature plot is shown as a line connecting the individual data points for clarity .	22
6	Variation of temperature (^oC) and the mole fractions of O_2 and CO_2 over time for the composite records at site 2. The temperature plot is shown as a line connecting the individual data points for clarity .	23
7	Variation of temperature (^oC) and the mole fractions of O_2 and CO_2 over time for the composite record at site 3. The temperature plot is shown as a line connecting the individual data points for clarity .	24
8	Variation of temperature (^oC) and the mole fractions of O_2 and CO_2 over time for the composite record at site 4. The temperature plot is shown as a line connecting the individual data points for clarity .	25
9	Variation of temperature (^oC) and the mole fractions of O_2 and CO_2 over time for the composite record at site 5. The temperature plot is shown as a line connecting the individual data points for clarity .	26
10	Variation of temperature (^oC) and the mole fractions of O_2 and CO_2 over time for the composite record at site 6. The temperature plot is shown as a line connecting the individual data points for clarity .	27

List of Figures (Continued)

Figure		Page
11	Schematic of spoil profile showing the division of the profile into layers as determined by the depths of the gas concentration measurements, Y_{O_2} and Y_{CO_2}. Fluxes, N_{O_2} and N_{CO_2}, are calculated for the top of each layer and assumed to be 0.0 at the profile bottom. Source terms, Q_{O_2} and Q_{CO_2}, are calculated for each layer.	47
12	Cross section of a coarse fragment containing pyrite.	64
13	Plots of the inhibition factors (solid lines). a) X_T versus termperature (^oC); dashed line is normalized data from Malouf and Prater, 1961; (●) normalized data from Silverman and Lundgren, 1959; (▲)normalized data from Belly and Brock, 1974. b) x_{pH} versus p_H; (●) normalized data from Silverman and Lundgre, 1959; (▲) normalized data from Schnaitman, et al., 1969. c) X_{O_2} versus oxygen mole fraction..	78
14	Neutralization curves as calculated from equation in text. G_B equals 1.0 in both plots. G_A equals 2.5 in plot 1 (■) and 2.8 in plot 2 (●).	91
15	Example leaching curve shows the normalized concentration versus water-filled pore volumes. Profile was 10 meters deep, divided into 20 layers with a water-filled pore volume of 0.13 and an infiltration rate of 50 cm/year.	94
16	Fraction of pyrite oxidized within entire profile versus time for Run 1 and Run 2.	98
17	The rate of leaching out of the profile of all iron species versus time for Run 1 and Run 2.	100

List of Figures (Continued)

Figure		Page
18	Oxidation rate of pyrite for each layer after 5 years of oxidation. Fine cross-hatching is total oxidation rate for Run 1. Open cross-hatching is rate of oxidation by direct osygen reaction with pyrite in Run 2. While cross-hatching on black is oxidation rate due to ferric iron reaction with pyrite in Run 2. Below 1 meter, ferric oxidation is negligible. Below 4 meters, oxidation rate of Run 1 and Run 2 are identical.	102
19	The ratio of ferric iron to ferrous iron in the water leaving the profile for Run 1 and Run 2.. . .	103
20	Fraction of pyrite oxidized within entire profile versus time for Runs 2, 3 and 4	105
21	The rate of leaching out of the profile of all iron species versus time for Runs 2, 3 and 4	107
22	The rate of leaching out of the profile of the potential and active acid for Runs 3 and 4.	110
23	Fraction of pyrite oxidized within entire profile versus time for Run 3 and Run 5	111
24	Fraction of pyrite oxidized within entire profile versus time for Runs 3, 6 and 7	114
25	The rate of leaching out of the profile of all iron species for Runs 3, 6 and 7.	116
26	The mole fraction of oxygen within the profile versus depth (m) after 5 years for Runs 1 and 6 . .	117
27	The mole fraction of oxygen within the profile versus depth (m) after 5 years for Runs 3 and 7 . .	118
28	The distribution of pyrite (wt./wt.) with depth (m) for a) Run 3; b) Run 8; c) Run 9.	120

List of Figures (Continued)

Figure		Page
29	Fraction of pyrite oxidized within entire profile versus time for Runs 3, 8 and 9	121
30	The mole fraction of oxygen within the profile versus depth (m) after 10 years for Runs 8 and 9.	122
31	The rate of leaching out of the profile of all iron species for Run 7 (no inhibition) and Run 10 (complete inhibition after 2 years).	124
A1	Values of the reduced Fickian diffusion coefficient, $D_{F_i}^*$, in a binary gas mixture plotted against the gas mole fraction of component i. Curve labels are the values of the flux ratio, r_{ij}, for which the curve was calculated.	143
A2	Values of the Fickian diffusion coefficient, D_F, for O_2 in an O_2-CO_2-N_2 atmosphere (in m^2/sec). The N_2 mole fraction is held constant at 0.790, while the O_2 mole fraction, plotted on the abscissa, is varied between 0.0 to 0.21. CO_2 comprises the balance of atmosphere. Values are for 20°C and 101 KPa with the N_2 flux being set to 0.0. Curve labels are the values of the flux ratio r_{CO_2,O_2}. Point represents value calculated in text	149
A3	Values for the Fickian diffusion coefficient, D_F, for CO_2 in an O_2-CO_2-N_2 atmosphere (in m^2/sec). The N_2 mole fraction is held constant at 0.790, while the O_2 mole fraction, plotted on the abscissa, is varied between 0.0 and 0.21. CO_2 comprises the remainder of the atmosphere. Values are for 20°C and 101 KPa with the N_2 flux being set for 0.0. Curve labels are the values of the flux ratio r_{CO_2,O_2}. Point represents value calculated in text.	150

LIST OF TABLES

Table		Page
1	Mean and range of selected properties of the spoil and drainage waters from the reclaimed stripmine used in this study.	9
2	Average, maximum and minimum values for O_2 and CO_2 concentrations and temperature for each depth of sites 1-6	17
3	Correlation, r, and regression coefficients, a and b, between the mole fractions of CO_2 and decreased O_2 $(0.210-Y_{O_2})$ for each depth at sites 1-6.	29
4	Correlation coefficients, r, between the mole fraction of CO_2 and temperature between the mole fraction of CO_2 and temperature for each depth at sites 1-6.	30
5	Pyrite and sulfate concentrations expressed as percent by weight sulfur for ten representative spoil layers from research site (Rogowski, 1977). Also, the CO_2 equivalent of the carbonate content required to neutralize the acid produced from columns 2 and 3 and the measured carbonate content expressed as CO_2 (columns 4 and 5). The last column gives the ratio CO_2 measured/CO_2 required in percent.	41
6	Means and coefficients of variation, C.V., for O_2 and CO_2 fluxes at the surface of the six sites and for all sites combined. The ratio of the fluxes, $r_n = N_{CO_2}/N_{O_2}$, was calculated from the mean values. .	49
7	Mean values and coefficients of variation, C.V., of the source terms for O_2 and CO_2 and for the ratio $r_Q = Q_{CO_2}$ at the individual depths at each site. The correlation between Q_{CO_2} and Q_{O_2}, r, is also listed.	52
8	Mean values and coefficients of variation, C.V., for the production rate of O_2 and CO_2 and for their ratio, $r_Q = Q_{CO_2}/Q_{O_2}$. Rates are for the entire spoil profile at each site averaged over time	56

List of Tables (Continued)

Table		Page
9	Coefficients used to calculate typical values of t_c and t_d	68
10	Measured E_M values and calculated X_T, X_{O_2}, X_{pH} and E_{min} values from phase II of experiment run by Bailey (1968)[4].	81
11	Measured and calculated coefficients for the bacterial "activity" model from phase I of experiment run by Bailey (1968)[4].	82
12	Iron complexes and log of the equilibrium constants for their formation and for sulfuric acid dissociation and amorphous ferric hydroxide precipitation.	87
13	Ratio of the flux of CO_2 to O_2 for Run 12 (heterotrophs active in layer I only), Run 13 (heterotrophs active in layer 20 only) and Run 14 (acid neutralization by carbonates in layer 20)	128
A1	Coefficients for calculating D^*_{ij} for gas pairs of interest in research (after Marrero and Mason, 1972). Coefficients were fit to data over the temperature range shown. The uncertainty in the calculated values is for the lower end of the temperature range listed.	154
B1	K_s values for Fe^{3+} and O_2 systems	164

NOTATION FOR PART II

a,b	empirical constants,
$a_{H_2CO_3}$	activity of H_2CO_3 moles
pCO_2	partial pressure at CO_2, atmosphere (101 kPa)
r	correlation coefficient, -
T	temperature, K
T_{30}	temperature at 30 cm depth, K
$\overline{X}$	mean value, (variable)
Y_{O2}	mole fraction of oxygen, -
Y_{CO_2}	mole fraction of carbon dioxide, -

NOTATION FOR PART III

C.V.	coefficient of variation, -
D_{F_i}	Fickian diffusion coefficients for component, cm^2/sec
DZ	weighing factor, cm^{-1}
N_i	flux rate of component i, $moles\text{-}cm^{-2}\text{-}sec^{-1}$
P	total pressure, kPa
Q_i	source term for component i, $moles\text{-}cm^{-3}\text{-}sec^{-1}$
r_n	flux ratio, $r_n = N_{CO_2}/N_{O_2}$, -
r_q	source ratio, $r_q = Q_{CO_2}/Q_{O_2}$, -
R	gas constant, $kPa\text{-}cm^{-3}\text{-}mole^{-1}\text{-}k^{-1}$
t	time
T	temperature, K
$\overline{X}$	mean
Y_i	mole fraction of component i
Z	depth, cm
τ	tortuosity, -
ϕ	air-filled porosity of spoil, cm^3/cm^3

NOTATION FOR PART IV

A_F	fragment surface area per volume spoil water, cm^{-1}
b	stoichiometric ratio between pyrite and oxidant consumption, -
C_{eff}	normalized concentration of solute in effluent, -
C_i	normalized concentration of solute in layer i, -
C_{in}	normalized concentration of solute in influent, -
C_{ox}	oxident concentration at the fragment surface, $moles/cm^3$
d_i	distance between layers, cm
D_c	effective diffusion coefficient for coupled oxidant-product counter diffusion, cm^2/sec
D_{O_2}	effective diffusion coefficient for O_2 in an O_2, N_2 and CO_2 atmosphere, cm^2/sec
D_W	diffusion coefficient at O_2 water, $moles\text{-}cm^{-1}\text{-}sec^{-1}$
D_{O_2,CO_2}, D_{O_2,N_2}, D_{CO_2,N_2}	binary diffusion coefficients for the gas pairs O_2 and CO_2, O_2 and N_2 and CO_2 and N_2, respectively cm^2/sec
E	electromotive force, volt
E_A	energy per unit time available to bacterial population, W
E_G	energy per unit time available to bacterial population for growth, W
E_M	energy per unit time available to bacterial population for maintenance, W
E_M'	energy per mole of electrons oxidized available to bacterial population, measured as a driving force, volts

Notation for Part Iv (Continued)

E'_{min}	minimum energy per mole of electrons oxidized required to sustain bacterial population, measured as a driving force, volts
F	the Faraday, C
Fe^{3+}	total iron concentration (all species), moles/L
FFR	fraction of coarse fragments in spoil, g/g
FPY	fraction of pyrite in coarse fragments, g/g
G_A, G_B	empirical constants, -
I	ionic strength, moles/kg
K_s	first-order surface reaction rate constant for pyrite oxidation per unit surface area of pyrite, cm/sec
K	equilibrium constant for chemical reactions, -
K_B	first-order reaction rate coefficient for bacterial oxidation of ferrous iron, sec^{-1}
K_C	first-order surface reaction rate constant for carbonate dissolution, $L\text{-}cm^{-2}\text{-}sec^{-1}$
K_{sp}	solubility constant for amorphous iron hydroxide, -
K_1, K_2	reaction coefficients for chemical oxidation of ferrous iron, $mole^2\text{-}L^{-2}\text{-}sec^{-1}$ and sec^{-1}, respectively
ℓ	one-half thickness of fragment, cm
MW_{py}	molecular weight of pyrite, g/mole
$N_{O_2}, N_{CO_2}, N_{O_2}$	gas flux of oxygen, carbon dioxide and nitrogen, respectively, $moles\text{-}cm^{-2}\text{-}sec^{-1}$
P	total pressure, kPa
Q_{AB}	oxygen source term, due to iron-oxidizing bacteria, $moles\text{-}cm^{-3}\text{-}sec^{-1}$

Notation for Part IV (Continued)

Q_C	rate of carbonate consumption per surface area of carbonate, moles-cm^{-2}-sec^{-1}
Q_{CHOX}	oxygen source term due to chemical oxidation of ferrous iron, moles-cm^{-3}-sec^{-1}
Q_{HB}	oxygen source term due to heterotrophic respiration, moles-cm^{-3}-sec^{-1}
Q_{HBB}	base rate of oxygen consumption from heterotrophic respiration, moles-cm^{-3}-sec^{-1}
Q_{O_2}	total oxygen source term, moles-cm^{-3}-sec^{-1}
Q_{py}	oxygen source term due to direct pyrite oxidation by oxygen, moles-cm^{-3}-sec^{-1}
r_1, r_2	ratios of the fluxes of CO_2, O_2 and N_2 to O_2, respectively, -
R	gas constant, cm^{-3}-KPa-mole^{-1}-K^{-1}
R_C	rate at which bacterial population oxidizes iron, moles of electrons/sec
R_S	radius of carbonate particles, cm
t	time, sec
t_C	time required for complete pyrite oxidation if chemical reactions are the rate controlling process, sec
t_D	total time required for complete pyrite oxidation if diffusion processes are the rate limiting steps, sec
T	temperature, K
x_i	general inhibition factor, -
x_T, x_{pH}, x_{O_2}	inhibition factors dependent on temperature, pH, and oxygen concentration, respectively, -
x	fraction of pyrite remaining in a fragment, -

Notation for Part IV (Continued)

x_C	fraction of carbonate particle remaining, -
Y_{O_2}	mole fraction of oxygen in spoil atmosphere, -
z	depth, cm
z_i	charge of the 9th chemical species, -
α	surface area of pyrite per unit volume fragment, cm^{-1}
$\gamma_1, \gamma_2, \gamma_3$	activity coefficients for H^+, Fe^{2+} and Fe^{3+}, respectively
∂	effective thickness of pyrite within which pyrite is oxidized
$\Delta\ell'$	thickness of water film covering fragments, cm
ΔG	energy released in iron oxidation, J
ΔG_R	change in standard free energy, J
ΔH_A	actual increase of H^+ in solution, moles
ΔH_R	H^+ produced through chemical reactions, moles
Π	product operator
ρ_B	bulk density of spoil, g/cm^3
ρ_C	molar density of carbonate in carbonate spheres, $moles/cm^3$
ρ_{O_2}	molar density of oxygen in the vapour phase, $moles/cm^3$
ρ_{py}	molar density of pyrite in fragments, $moles/cm^3$
Σ	summation operator
τ	tortuosity of gas diffusion path, -

Notation for Part IV (Continued)

ϕ_A	air-filled porosity, cm^3/cm^3
ϕ_W	water-filled porosity cm^3/cm^3
[]	concentration operator, moles/L

NOTATION FOR APPENDIX A

a,b,c	semi-empirical constants
C_i	concentration of gas component k, kg m^{-3}
$\bar{v}_i, \bar{v}_j$	average velocity of gas i and j, respectively, m sec^{-1}
D_{F_i}	Fickian diffusion coefficient for component i, m^2 sec^{-1}
D_{ij}	binary diffusion coefficient, m^2 sec^{-1}
D^*_{ij}	temperature dependent, pressure independent binary diffusion coefficient, kPa m^2 sec^{-1}
D_T	coefficient of thermal diffusion, m^2 sec^{-1}
F_i, F_j	external force field acting on gas i and j, N/Kg
m_i, m_j	mass of molecules of gas i and j, respectively, Kg
M_o	Avagadrops number, mole -1
n_i, n_j	number density of gas i and j, respectively, m^{-3}
n_T	$= n_i + n_j$
N_i	molar flux of gas i, moles m^{-2} sec^{-1}
P	total pressure, KPa
q_i	mass flux of gas i, kg m^{-2} sec^{-1}
r	direction vector, m
R	universal gas constant, m^3 KPa $mole^{-1}$ K^{-1}
r_{ji}	flux ratio, $- N_j N_i$
t	time, sec
T	absolute temperature, K
Y_i	mole fraction of component i

z	distance or depth, m
α	combined air-filled porosity, tortuosity term
Π	product operator
ρ_i, ρ_j, ρ_T	density of gas i, j and the combined gas density, respectively, Kg m^{-3}
Σ	summation operator

NOTATION FOR APPENDIX B

b	shorthand notation, see text
C	concentration, moles/cm^3
C_1, C_2	integration constants, moles/cm^3
$C_{R\ell}$	concentration at the leached rim - oxidation zone interface, moles/cm^3
C, C_1, C_2	shorthand notation, see text
C_ℓ	same as C_R , moles/cm^3
D_c	diffusion coefficient in the spoil fragment, cm^2/sec
FFR	fraction of spoil mass composed of coarse fragments, -
FPY	fraction of fragment mass that is pyrite, -
K_s	first order reaction coefficient for pyrite oxidation per unit area, cm/sec
ℓ	one-half fragment thickness, cm
ℓ'	thickness at leached rim, cm
R_{dx}	reaction rate per fragment volume, dx, moles-cm^{-3}-sec^{-1}
R_t	total reaction rate per unit surface area of fragment, moles-cm^{-2}-sec^{-1}
X	thickness, cm
α	surface area of pyrite per unit volumn of fragment, cm^{-1}
ρ_B	bulk density of spoil, g/cm^3
ρ_{py}	molar density of pyrite in fragment, moles/cm^3
ϕA	air-filled porosity in spoil, cm^3/cm^3
ϕ_w	water-filled porosity in spoil, cm^3/cm^3
τ	tortuosity of diffusion path is spoil, -

SECTION 1

INTRODUCTION

The United States has the most extensive deposits of coal in the world. The rate at which we mine this coal must accelerate in the next century if we are to satisfy our increasing energy appetite and decrease our reliance on foreign sources of energy. Much of this coal will be mined by surface operations, such as stripmining. Stripmining will disturb millions of acres of land; land that must be restored if it is to become productive again. Unfortunately, reclaimed stripmines in the humid eastern United States have a tremendous potential for both acute short-term and significant long-term pollution of surface streams and lakes and subsurface aquifers (Collier et al., 1970). Water leaving many reclaimed stripmines contains acid, iron, sulfates and other constituents at levels far exceeding their concentration in natural waters. Agnew and Corbett (1973) found a large increase in the acidity of water draining from stripmined lands, especially during "flush outs" (large stream flows) caused by periods of heavy rain. Striffler (1973) found similar results for eastern Kentucky stripmine waters and concluded that primary watersheds, those directly draining stripmined areas, have a serious problem. Caruccio (1973), among others, has measured acid water draining from stripmine sites to have pH's as low as 2.8. At such low pH's, Warner (1973) found a severe decrease in stream invertebrates and algae populations and Kinney (1964) documented the adverse effects on fish and other vertebrates. Even though acid

pollution of streams caused a decrease in the stream biota, it does not directly cause any visual degradation. Iron pollution, on the other hand, can be readily observed when it precipitates in surface waters to color them from red to yellow-orange. These stainings, commonly referred to as "yellow-boy," can greatly impact the scenic value of streams in the Appalachian coal region.

Fortunately, the amounts of pollutants leaving a mined area can be considerably reduced if proper reclamation techniques are used (Grimm and Hill, 1974). However, we can intelligently develop these proper reclamation techniques or best management practices only if we understand the basic physical and chemical processes that lead to acid drainage. Researchers have been intensively investigating acid drainage problems for more than 50 years. A synopsis of their finding can be found in many articles including review papers by The Ohio State University Research Foundation (1971) and Rogowski et al. (1977). A crucial area of the acid drainage problem in reclaimed stripmines that has not received sufficient attention is the oxygen status of the mine environment (Ohio State University Research Foundation, 1971). The first portion of this research was to investigate the oxygen status of a reclaimed stripmine. The results from this part of the study are presented in Part II. Part II expands upon the oxygen concentration findings and presents calculations of the oxygen and carbon dioxide gas fluxes and the related rates of consumption and production of these gases within the reclaimed mine spoil.

Another productive avenue for developing best reclamation techniques is to develop and use mathematical models that describe the acid drainage process. A model, based on basic chemical and physical processes, can serve as a useful tool for identifying and gaining insight into the important, rate controlling processes of acid drainage. A model that accurately predicts the behavior of actual stripmines can be used to develop alternative reclamation techniques where the consequences of each modification can be tested rapidly and inexpensively. Part IV presents the development of a general model for acid formation and leaching from reclaimed coal stripmines.

Included in the appendices is a review of the process of gas diffusion in the vapor phase and a listing of the magnitude and derivation of some of the parameters used in the model for acid drainage. Also listed in the appendices is a listing of the FORTRAN program of the model and example output for the program.

REFERENCES

1. Agnew, A. F. and D. M. Corbett. Hydrology of a Watershed Containing Flood-Control Reservoirs and Coal Surface-Mining Activity, Southwestern Indiana. In: Ecology and Reclamation of Devastated Land, R. J. Hutnik and G. Davis, eds. Gordon and Breach, New York, 1973. pp. 159-174.
2. Caruccio, F. T. Characterization of Strip-Mine Drainage by Pyrite Grain Size and Chemical Quality of Existing Groundwater. In: Ecology and Reclamation of Devastated Land, R. J. Hutnik and G. Davis, eds. Gordon and Breach, New York, 1973. pp. 193-226.
3. Collier, W. R., R. J. Pickering, and J. J. Musser. Influences of Strip Mining on the Hydrologic Environment of Parts of Beaver Creek Basin, Kentucky, 1955-56. U.S. Geological Survey Professional Paper 427-C, 1970.
4. Grimm, E. C. and R. D. Hill. Environmental Protection in Surface Mining of Coal. EPA-670/2-74/093, Environmental Protection Technology Series, U.S. Environmental Protection Agency, Cincinnati, Ohio, 1974. pp. 1-277.
5. Kinney, E. C. Extent of Acid Mine Pollution in the United States Affecting Fish and Wildlife. U.S. Department of the Interior, Bureau of Sport Fisheries and Wildlife Circular 191, 1964.
6. Ohio State University Research Foundation. Acid Mine Drainage Formation and Abatement. Water Pollution Control Research Series Program 14010 FPR, U.S. Environmental Protection Agency, Washington, D.C.

7. Rogowski, A. S., H. B. Pionke, and J. G. Broyan. Modeling the Impact of Strip Mining and Reclamation Processes on Quality and Quantity of Water in Mined Areas: A Review. J. Environ. Qual., 6:237-244, 1977.

8. Striffler, W. D. Surface Mining Disturbance and Water Quality in Eastern Kentucky. In: Ecology and Reclamation of Devastated Land, R. J. Hutnik and G. Davis, eds. Gordon and Breach, New York, 1973. pp. 175-192.

9. Warner, R. W. Acid Coal Mine Drainage Effects on Aquatic Life. In: Ecology and Reclamation of Devastated Land, R. J. Hutnik and G. Davis, eds. Gordon and Breach, New York, 1973. pp. 227-238.

SECTION 2

SPOIL ATMOSPHERE AND TEMPERATURE IN A RECLAIMED COAL STRIPMINE

Introduction

Within the past two decades, the problems caused by acid-drainage from reclaimed coal stripmines in the eastern United States have been the focus of numerous studies. These studies have shown the primary source of acid to be the oxidation of the iron sulfide mineral, pyrite. Two mechanisms for pyrite oxidation have been demonstrated (Ohio State University Research Foundation, 1971). The first involves oxygen reacting directly with pyrite and water and is summarized in Eq. [1].

$$FeS_2 + 3.5\ O_2 + H_2O \rightarrow Fe^{2+} + 2SO_4^{2-} + 2H^+ \qquad [1]$$

The second mechanism, shown in Eq. [2], uses ferric iron as the electron acceptor.

$$14Fe^{3+} + FeS_2 + 8H_2O \rightarrow 15Fe_4^{2-} + 2SO_4^{2-} + 16H^+ \qquad [2]$$

For this reaction to contribute significant levels of acid, ferric iron must be present. At the low pH's of acid-stripmine waters (pH < 4), resupply of the ferric iron in Eq. [2] is inhibited by the extremely slow, ferrous to ferric iron, oxidation kinetics (Singer and Stumm, 1970). However, certain aerobic, chemoautotrophic bacteria (*Thiobacillus ferrooxidans*) are known to use the ferrous-ferric oxidation reaction as an energy source (Dugan and Randles,

1968). Thus Eq. [2] is considered to be bacterially catalyzed within acid stripmine spoils because the ferric iron is produced by Eq. [3]:

$$14Fe^{2+} + 14H^{+} + 3.5\ O_2 \xrightarrow{\text{bacteria}} 14Fe^{3+} + 7H_2O \qquad [3]$$

Summing Eqs. [2] and [3] gives Eq. [1], thus regardless of mechanism, the result of pyrite oxidation is the same; two moles of H^+ are produced for every three and one-half moles of oxygen consumed. Moreover, significant oxidation of pyrite cannot take place far from the presence of gaseous O_2 because of the slow diffusion rates of O_2 in water (Ohio State University Research Foundation, 1971). Thus, the presence of oxygen in the spoil atmosphere is critical for <u>in situ</u> oxidation of pyrite.

The temperature of the spoil environment is also critical in determining the oxidation rate of pyrite. The rate of direct pyrite oxidation by O_2 and thus O_2 consumption increases with temperature (Clark, 1965). Autotrophic bacteria are also sensitive to temperature showing maximum activity at temperatures near 30°C and almost no activity for temperatures below 4°C and above 55°C (Malouf and Prater, 1961; Ehlrich and Fox, 1967; Cathles and Apps, 1975).

Although the mechanics of pyrite oxidation and leaching have been studied for years, almost no information is available on the environmental status of reclaimed stripmines (Ohio State University Research Foundation, 1971). As part of a comprehensive investigation of the chemical and physical processes of a reclaimed stripmine, we measured temperatures and spoil atmosphere compositions over an extended period of time and for the entire depth of the mine site.

Materials and Methods

Oxygen, carbon dioxide and temperature profiles were measured within a reclaimed bituminous coal stripmine. The sparsely grassed mine-site, located in Clearfield County, west-central Pennsylvania, has been described in detail elsewhere (Pedersen et al., 1978; Pedersen et al., 1980; Pionke and Rogowski, 1980). The mine was developed in Pennsylvanian-age deposits. Two coal seams were mined at the site, the middle Kittanning (C) coal seam and the lower Kittanning (B) seam that underlies the C. Noncalcareous, thin bedded sandstones and shales overlay the middle Kittanning seam while predominantly silt stones and shales overlay the lower seam. High pyrite contents are usually associated with the shale layers (Rogowski, 1977; Lovell et al., 1978). Typical values of some of the important properties of the mine spoil and drainage waters are shown in Table 1. All the parameters vary greatly, but the water draining the site has been consistently low in pH and high in acidity indicating that pyrite oxidation and leaching are taking place.

In the first 10 months of the study, the spoil atmosphere composition was monitored at four locations along a transect of the mine (sites 1-4, Fig. 1). Site 1 was located in an area between two stripmines composed of 440 cm of spoil overlying unmined, coal-bearing strata. Site 2 was placed in 1250 cm of spoil from Kittanning B-seam and sites 3 and 4 were placed in 700 and 1060 cm of spoil from the Kittanning C-seam. In general, the shale and pyrite content of the spoil decrease from sites 1-4, while the vegetation cover increases from virtually 0.0 to 3.2 metric tons/ha (Pionke and Rogowski, 1980).

Table 1. Mean and range for selected properties of the spoil and drainage waters from the reclaimed stripmine used in this study[†].

Spoil property	$\bar{x}$	range
% pyritic S (st/wt)	0.18	0.02
bulk density (kg/m^3)	1,560	640-1,790
% coarse fragments (wt/wt)	78	54-93
% carbon (wt/wt)	4.4	0.4-22.8
pH (1:1 spoil-water extract)	4.9	3.7-6.0
acidity (meq/100 g)	16.4	4.0-24.0
Drain-water property	**$\bar{x}$**	**range**
pH	2.8	2.3-3.7
acidity (meq/L)	15.0	9.0-19.0

[†]Data from Pedersen, et al., 1978; Pedersen, et al., 1980; Rogowski, 1977; Rogowski, et al., 1982; and Rogowski, A. S., personal communication.

At each site, a 15 cm (6 in) diameter bore-hole was drilled with a standard well-drilling rig down to or slightly deeper than the deepest extent of the stripmining process; a depth of between 870 and 1250 cm. Five or six gas-sampling chambers were placed at selected depths between 150 cm of the surface and the bottom of each bore-hole (Fig. 1). After location of the chambers, the bore-holes were backfilled a few centimeters at a time; each layer being packed with a metal rod. Clean, coarse, silica sand was placed around each chamber with a 10-cm thick bentonite berm placed above the sand. The remaining space between samplers was filled with spoil material that had been screened to remove stone fragments. Two additional holes were drilled at sites 1-4 with a Giddings soil auger[1]. The holes were 5 cm in diameter, 30 and 50 cm deep. Each hole was fitted with a gas sampler and backfilled as described above.

After the first 10 months of monitoring, two additional sites were added. Site 5 was located close to the buried highwall of the Kittanning B-seam. Site 6 was placed in an adjacent area overlying the unmined Kittanning B seam where the top 30 cm were composed of disturbed spoil material.

Design of the gas samplers is shown in Figure 2. The samplers consisted of an 8.25-cm chamber of either 2.5- or 5-cm (1- or 2-in) diameter pvc pipe. A series of 0.48-cm (3/15-in) holes were drilled

---

[1]The mention of trade names does not constitute an endoresement of the product by the U.S. Department of Agriculture over other products not mentioned.

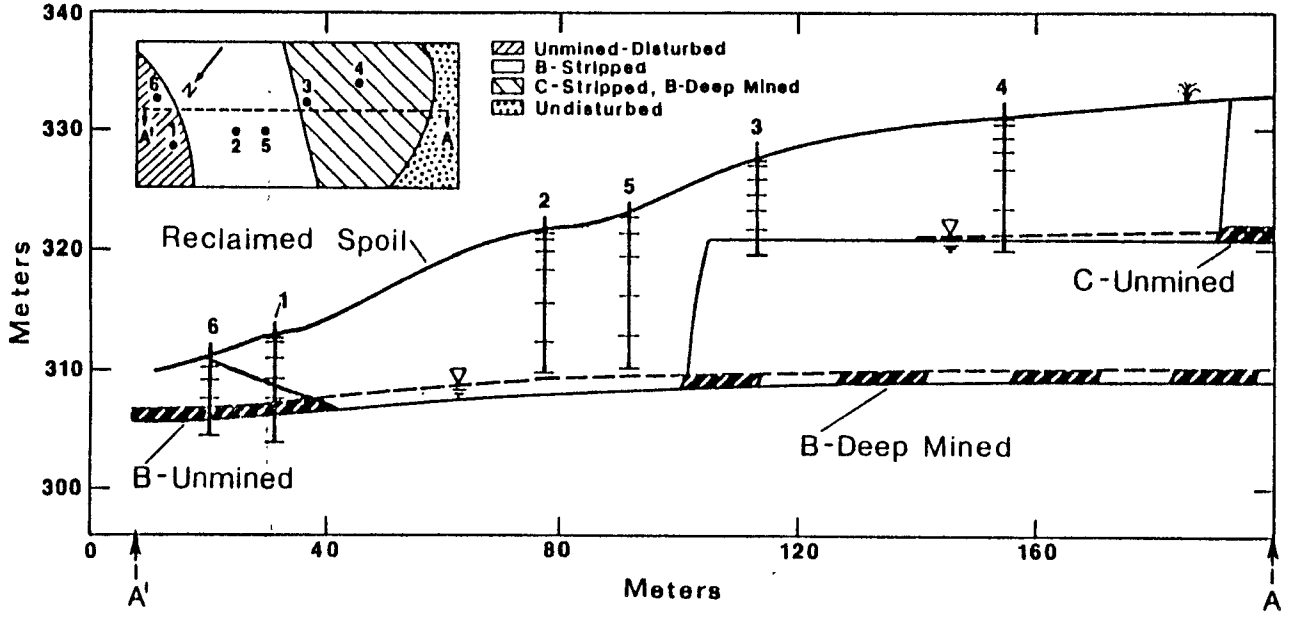

Figure 1. Location of monitoring sites 1-6 and the depth of the gas sample-chambers (crossbars) at each site in relation to the stripmine stratigraphy.

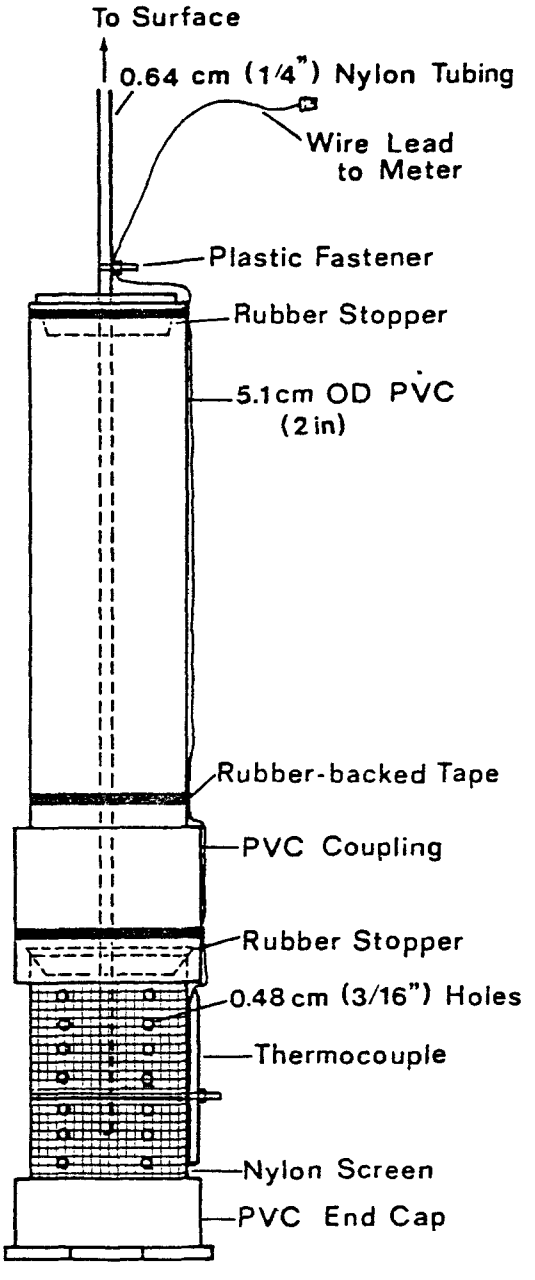

Figure 2. Schematic of gas sample-chambers design.

in each sample-chamber and were screened with a medium-mesh, nylon screen. The chambers were coupled to lengths of pvc pipe so that they could be placed at the desired depth. The sample-chambers were connected to the surface by a 0.64-cm (0.25-in) diameter nylon tube. At the surface, this tube was capped with a rubber septum except when gas samples were withdrawn. Each sample-chamber was also equipped with a thermocouple so spoil temperatures at each site could be measured. The thermocouple consisted of a 0.082-cm (0.032-in) diameter, copper/constantin, low-temperature element (Omega Engineering, Type T) silver soldered to 24-gauge, copper/constantin, unshielded wire (Omega Engineering, Type T Poly Rip Control). Soldered connections were protected by ceramic insulators. Each thermocouple was calibrated before installation. Temperature was measured directly using a Leeds and Northrop detector (Model 934 Numatron Digital Thermocouple Recorder, Type T, battery operated). An ice-water bath was used as a reference temperature when measurements were made.

Oxygen, carbon dioxide and temperature were measured at each sampler periodically (approximately every month). Initially, oxygen and carbon dioxide concentrations were measured in the field independently of each other. A gas sample was obtained by connecting the gas chamber access tube to a rubber bulb equipped with one-way valves. The bulb was used to pump air out of the gas samplers. For oxygen measurements, gas was pumped into a measuring chamber (Fig. 3) equipped with a dissolved oxygen probe (Lazar Research Labs,

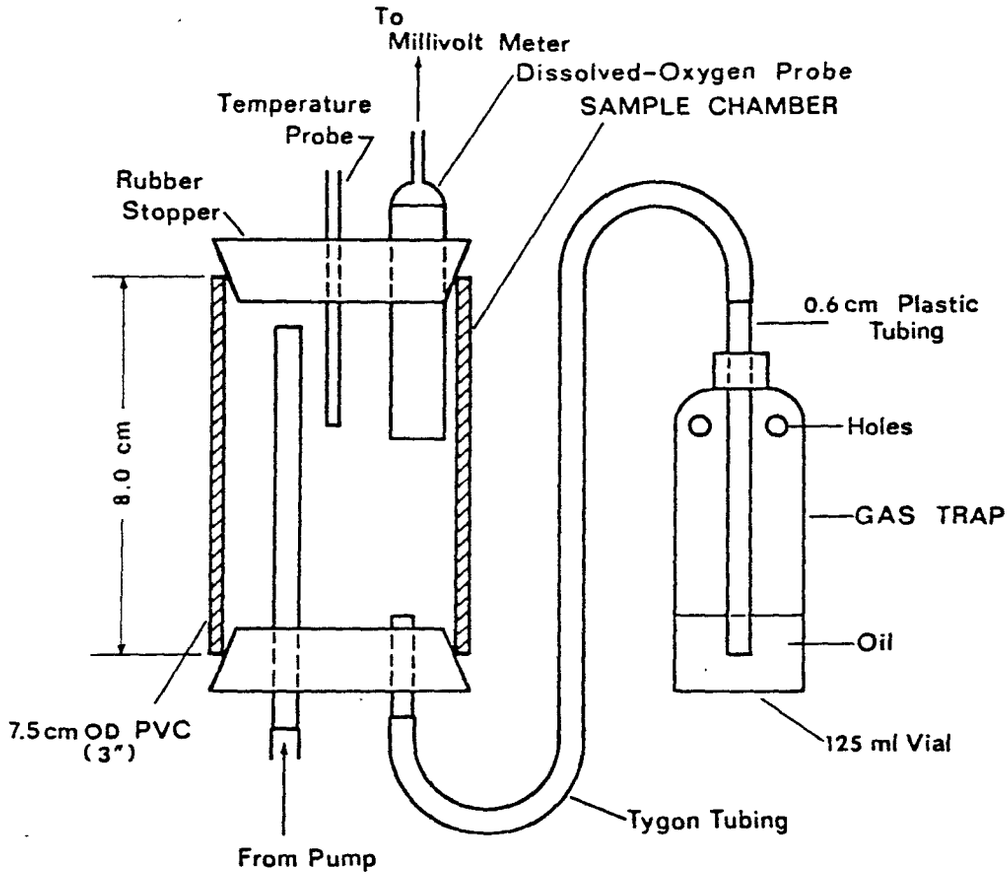

Figure 3. Schematic of O_2 measuring-chamber used in the field.

Inc., Model 00-166 Dissolved Oxygen Probe). Sufficient gas was pumped from the gas sampler to ensure a representative sample in the measuring chamber as indicated by steady O_2 readings. The required gas volume was approximately 1.6 liters, which corresponded to removing gas from a 9.4-liter spoil volume (1.5 g/cm^3 bulk density, 70% saturation) or a 26-cm diameter sphere centered at each probe. Oxygen levels were read directly from a millivoltmeter (Orion Research, Model 407A), which had been calibrated for O_2 concentrations in air (21% O_2) and bottled N_2 gas (0% O_2). CO_2 concentrations were measured by pumping a gas sample directly into a Lab-Line CO_2 Analyzer (Lab-Line, Inc.) which gave the CO_2 levels directly in percent.

For the past twelve months of the study, CO_2 and O_2 concentrations were measured in the laboratory. Field measurements were discontinued because the technique did not allow for measurements in the winter. For laboratory measurements, gas samples were collected in air tight bottles (150 ml volume), returned to the lab and measured with a gas chromatograph (Varian Aerograph, Model 1820) as described by Bollag and Barabasz (1979). The laboratory and field techniques were correlated with each other and found to be in good agreement for both O_2 and CO_2 measurements.

Statistical analysis was performed using standard procedures. Duncan's new multiple-range test, adjusted for unequal sample size, was used to compare the means of O_2 and CO_2 for each layer at each site (Steel and Torrie, 1960, p. 114). Homogeneity of regression equations was tested as described by Steel and Torrie (1960, p. 319).

Results

Average, maximum and minimum values for O_2, CO_2 and temperature for each depth at the six sites are shown in Table 2. The average mole fraction of O_2 ranged from 0.010 to 0.207, while the range in individual values was between atmospheric levels (0.210) to below the detection limit (< 0.001). Considerable variation in measured values was found for most layers. Several layers near the surface had variations in O_2 levels of less than 0.02 but most layers showed variations of greater than 0.05 mole fraction. In general, the average values decreased with depth at any one site, as did the values measured at any one time. At sites 1, 2 and 3, the O_2 concentrations showed a tendency to decrease with depth until a minimum was reached and then start to increase again. This pattern was consistent over time. Site 1 showed the extreme decrease of O_2 with depth, where average O_2 values dropped to 0.01 within 410 cm of the surface. The low O_2 levels in the deeper layers of sites 1 and 6 were distinctly different from the other values as indicated by Duncan's new multiple-range test. Other than at sites 1 and 6, however, the oxygen levels were consistently high indicating that most of the reclaimed mine site was well oxygenated.

Oxygen and carbon dioxide concentrations in the surface layers were in general not very different from atmospheric levels. One reason for this may have been the contamination of gas samples by air from the soil surface. The gas samplers used in this study were primarily designed for obtaining samples at deeper depths. The large

Table 2. Average, maximum and minimum values for O_2 and CO_2 concentrations and temperature for each depth at sites 1-6.

	Depth	O_2			CO_2			Temperature		
		$\bar{x}$	max	min	$\bar{x}$	max	min	$\bar{x}$	max	min
	cm	mole fraction						°C		
Site 1	30	.205 a†	.210	.170	.0045 a	.025	n.d.‡	14.2	25.2	-2.6§
	60	.206 a	.210	.190	.0046 a	.020	n.d.	16.0	24.0	1.2
	105	.147 g	.210	.090	.040 ef	.104	.002	13.9	24.5	-2.5
	260	.022 j	.082	n.d.	.132 i	.168	.062	12.3	17.5	3.0
	410	.010 j	.066	n.d.	.144 ij	.187	.104	12.2	14.8	5.3
	565	.016 j	.115	n.d.	.147 j	.187	.088	10.8	13.4	7.6
Site 2	30	.190 abcd	.210	.143	.011 ab	.034	n.d.	14.5	23.7	-2.3
	60	.194 abc	.207	.154	.010 ab	.033	.001	16.6	24.5	-1.8
	170	.178 cd	.210	.129	.017 bc	.045	.001	12.6	20.4	1.5
	320	.171 de	.209	.126	.023 cd	.052	.002	11.6	16.1	6.6
	625	.143 g	.187	.103	.048 fg	.082	.027	11.8	13.6	10.4
	945	.152 fg	.199	.090	.040 ef	.082	.013	12.2	12.9	11.2
	1250	.156 efg	.204	.121	.039 ef	.060	.006	12.3	13.3	11.2
Site 3	30	.207 a	.210	.185	.0022 a	.009	n.d.	13.9	25.2	-1.4
	60	.203 a	.210	.195	.046 a	.014	n.d.	13.8	23.5	-1.0
	150	.191 abc	.207	.169	.013 abc	.024	.004	12.6	21.2	0.8
	305	.194 abc	.209	.149	.012 ab	.027	.002	12.2	18.7	4.4
	455	.183 bcd	.205	.140	.013 abc	.033	.002	11.4	15.3	7.0
	610	.155 efg	.194	.116	.030 de	.055	.011	11.3	13.2	9.5
	810	.188 abcd	.208	.153	.012 ab	.033	.004	11.5	12.4	9.9

Site 4	30	.201	a	.210	.160	.0032	a	.018	n.d.	14.0	23.4	-0.9
	60	.179	cd	.207	.097	.012	ab	.024	.002	14.2	23.4	-0.1
	185	.194	abc	.204	.177	.010	ab	.022	.002	11.9	20.6	3.1
	335	.199	ab	.209	.181	.008	ab	.019	n.d.	12.6	18.6	6.1
	490	.192	abc	.206	.175	.015	abc	.028	.002	12.5	16.4	8.3
	790	.189	abcd	.208	.141	.018	bc	.050	.001	12.2	13.7	10.4
Site 5	30	.197	abc	.210	.169	.005	ab	.019	n.d.	10.0	25.0	-3.0
	145	.193	abc	.210	.152	.011	ab	.033	.001	10.2	19.7	1.2
	325	.186	abcd	.204	.131	.014	abc	.036	.004	10.8	15.4	6.2
	630	.186	abcd	.208	.155	.015	abc	.034	.002	11.5	13.0	10.1
	935	.179	cd	.207	.134	.022	bcd	.044	.004	11.6	12.6	10.5
	1240	.170	df	.190	.139	.032	de	.048	.020	11.8	12.4	10.6
Site 6	150	.114	h	.156	.040	.056	g	.103	.015	9.9	19.7	0.0
	305	.046	i	.141	n.d.	.098	h	.136	.059	11.1	14.7	6.1

†Numbers followed by the same letter in a column are not significantly different at p = 0.05.

‡Below detected limits (< .001).

§Data during the winter is missing.

volumes of air required to obtain a sample may have permitted short-circuiting of surface air through large pores to the sample chambers located near the surface.

Table 2 also shows the mean and extreme values of CO_2 for each site and layer. Average CO_2 mole fractions ranged from 0.009 to 0.147. Individual measurements ranged from less than 0.001 to 0.187. High CO_2 concentrations (< 0.10) were observed only at sites 1 and 6. The high average values of CO_2 at those two sites and for the 625 cm layer of site 2 were tested to be distinctly different than the other values. Site 4 consistently had the lowest CO_2 concentrations with no average value over 0.02 mole fraction for any layer. The surface layers at every site normally showed the lowest CO_2 concentrations with the concentrations increasing with depth. As in the case of O_2, sites 2 and 3 showed a tendency to reach maximum CO_2 concentrations at an intermediate depth and then start to decrease with depth.

Mean and extreme values for temperature are also shown in Table 2. Mean values for sites 5 and 6 are considerably lower than sites 1-4 because temperatures were measured over a period including two winters and only one summer, while the data for sites 1-4 span a period including two summers and winters. As expected, spoil temperatures showed an annual cyclic fluctuation, with the amplitude of the fluctuation decreasing and the phase lagging as depth increased. This behavior is shown in Figure 4, where the temperature is plotted for five depths at site 2 for a portion of the data record. Temperature showed little variation at depths below 500 cm.

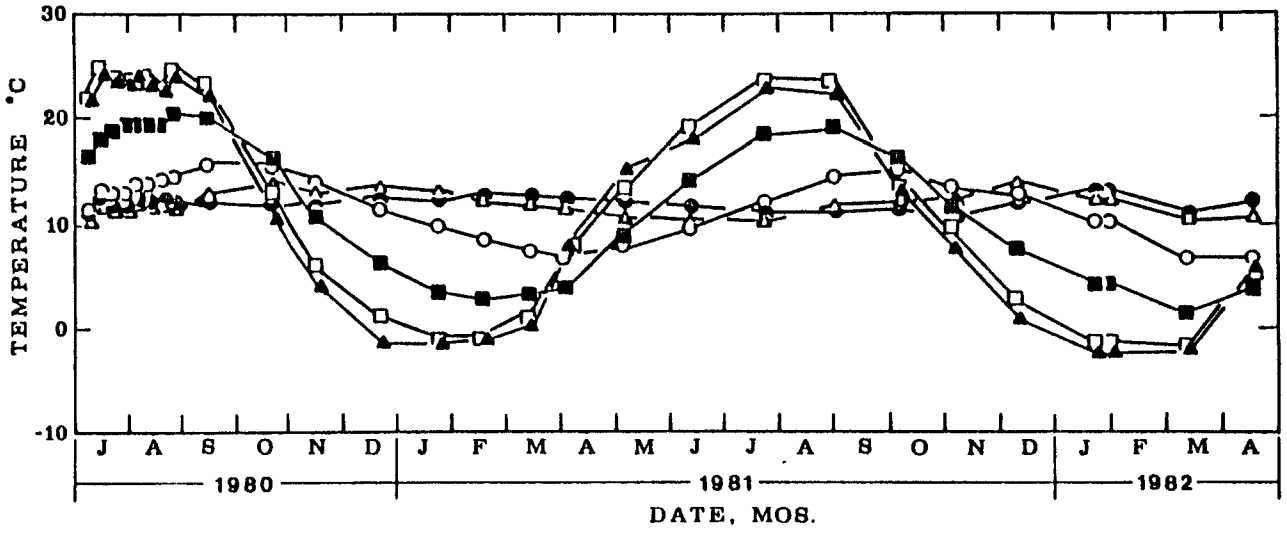

Figure 4. Variation of temperature (^{o}C) over time for six depths at site 2. Depths shown are (▲) 30 cm, (□) 60 cm, (■) 170 cm, (○) 320 cm, (△) 625 cm, and (●) 945 cm.

Although the mean values shown in Table 2 give a good indication of the spoil atmosphere characteristics, the oxygen and carbon dioxide levels also showed distinct seasonal tendencies. These tendencies are best shown in Figures 5-10 where O_2 and CO_2 mole fractions and temperature are plotted against time for each layer at the six sites. Data spanning three years are superimposed on a single Julian year. In Figures 5-10 temperature is shown as a continuous line connecting the individual data points for clarity. Much of the discontinuity in the temperature plot is due to the superimposition of the three years of data. Figures 5-10 illustrates that, at least for some depths at each site, there is a strong tendency for the CO_2 levels to increase during the summer months (150-273 days), while remaining low during the remainder of the year. The increase in CO_2 is accompanied by a decrease in O_2 concentrations. This behavior is especially well illustrated at the 105 cm depth of site 1 (Fig. 5) and all layers of site 2 (Fig. 6). Near the surface, the increase in CO_2 and decreases in O_2 coincide with the maximum in the spoil temperatures. However, at the lower depths these extremes in CO_2 and O_2 still occur during the summer while the temperature either experiences a maximum later in the year (320 cm, site 2, Fig. 5) or exhibits almost no variation over time (625 cm and deeper, site 2, Fig. 5).

A relationship between O_2 and CO_2 concentrations and between O_2 and temperature and CO_2 and temperature is suggested by Figures

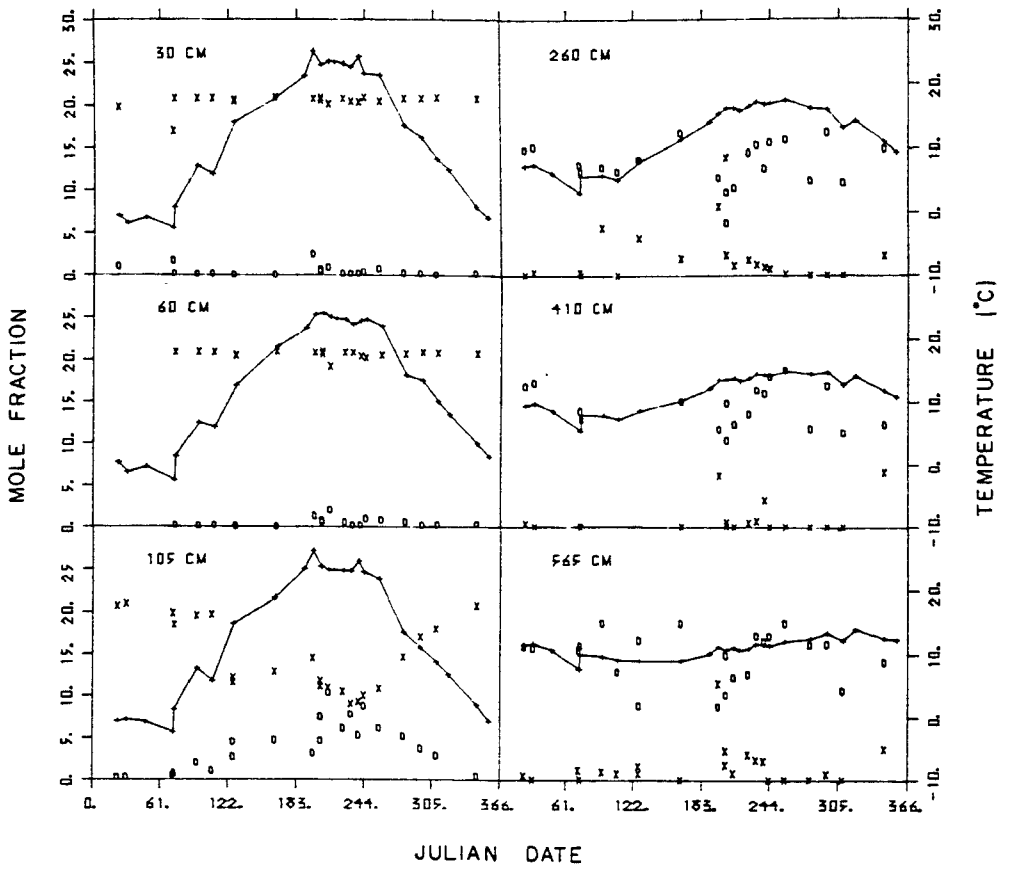

Figure 5. Variation of temperature and the mole fractions of O_2 (X) and CO_2 (O) over time for the composite record at site 1. The temperature plot is shown as a solid line connecting the individual points for clarity.

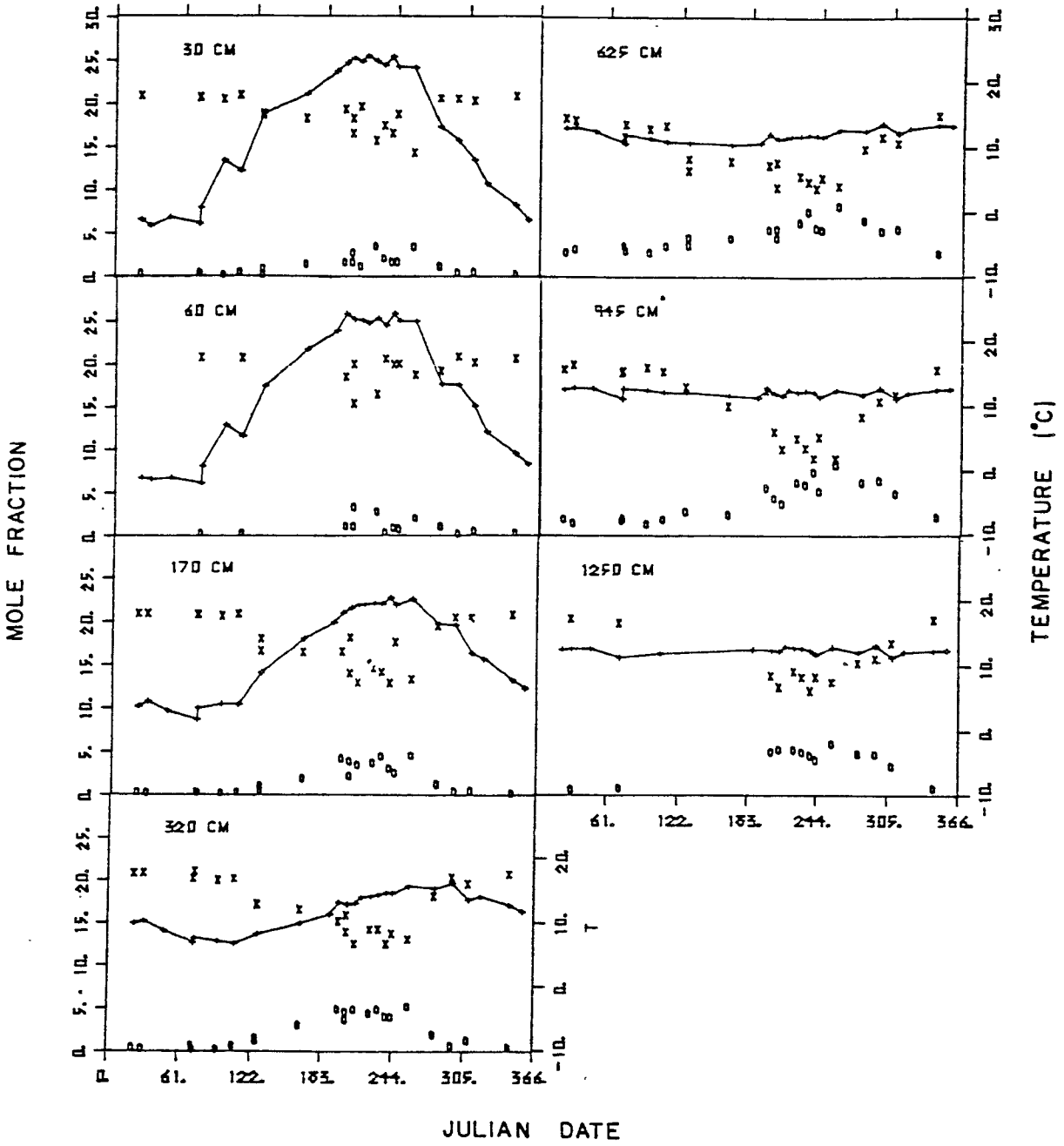

Figure 6. Variation of temperature and the mole fractions of O_2 (X) and CO_2 (O) over time for the composite record at site 2. The temperature plot is shown as a solid line connecting the individual points for clarity.

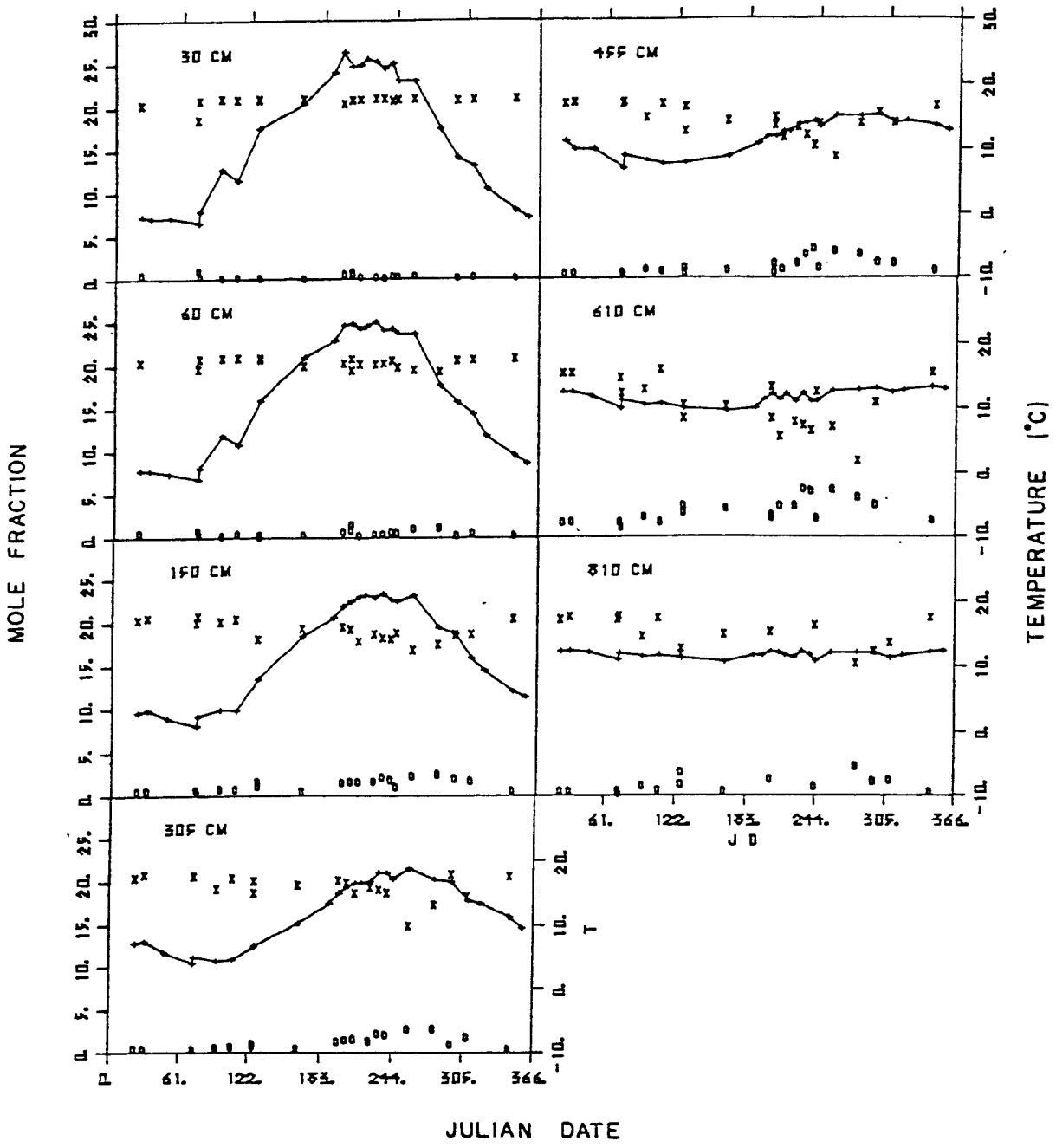

Figure 7. Variation of temperature and the mole fractions of O_2 (X) and CO_2 (O) over time for the composite record at site 3. The temperature plot is shown as a solid line connecting the individual points for clarity.

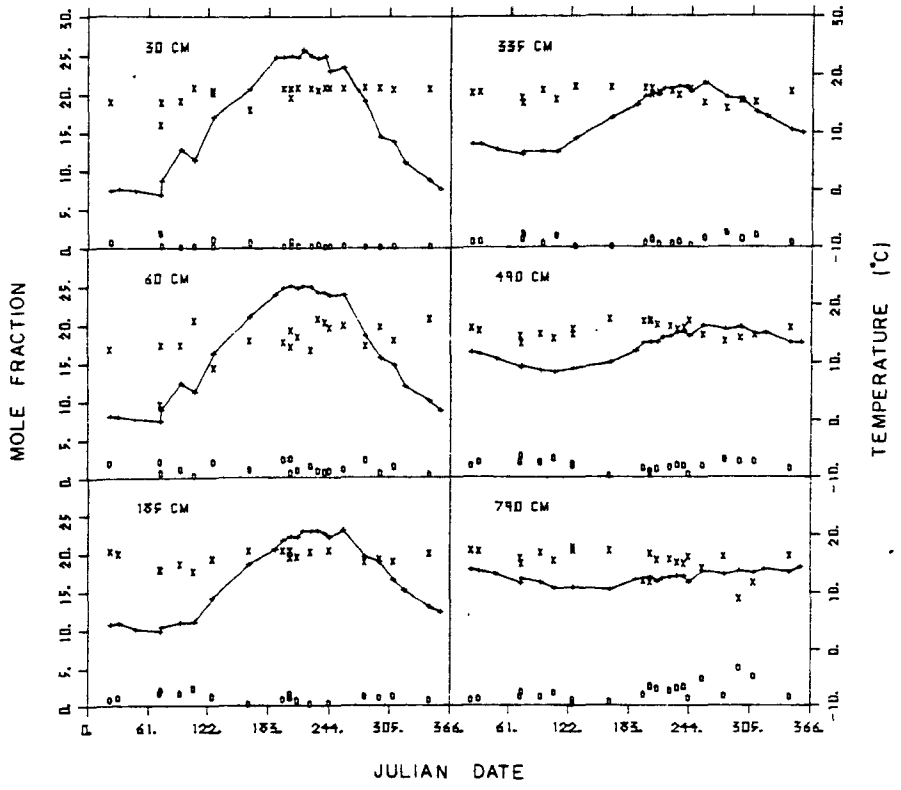

Figure 8. Variation of temperature and the mole fractions of O_2 (X) and CO_2 (O) over time for the composite record at site 4. The temperature plot is shown as a solid line connecting the individual points for clarity.

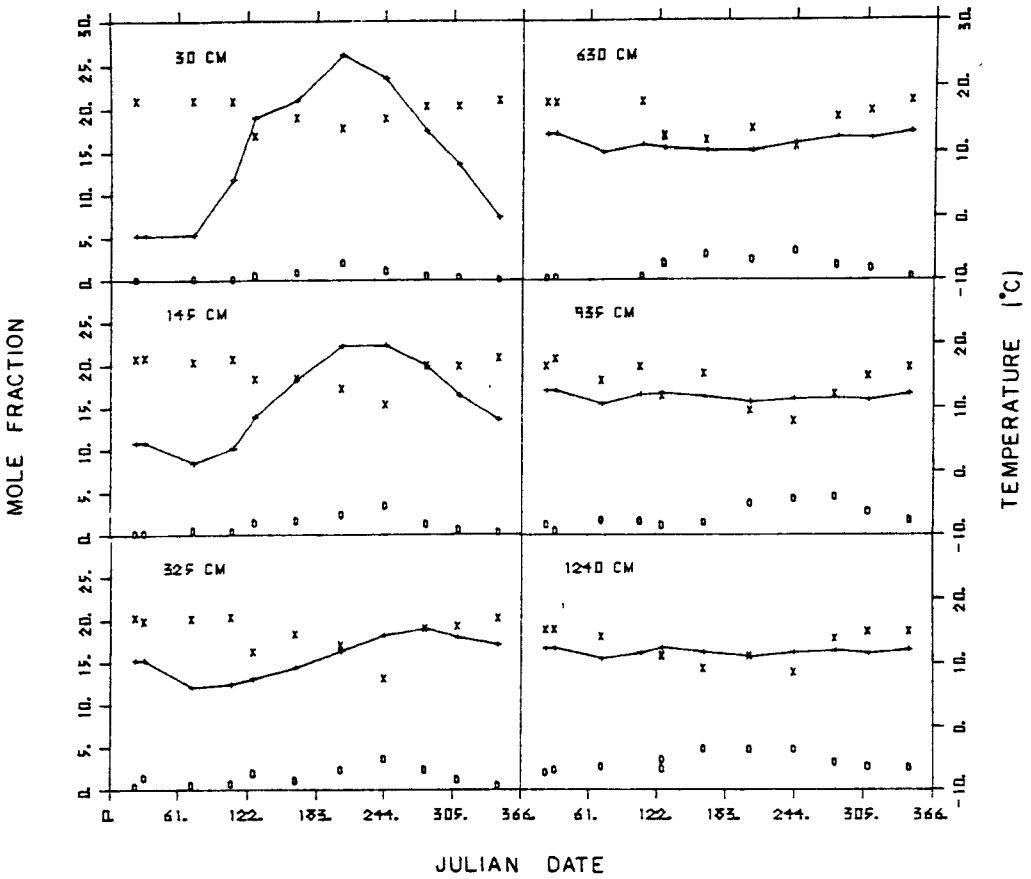

Figure 9. Variation of temperature and the mole fractions of O_2 (X) and CO_2 (O) over time for the composite record at site 5. The temperature plot is shown as a solid line connecting the individual points for clarity.

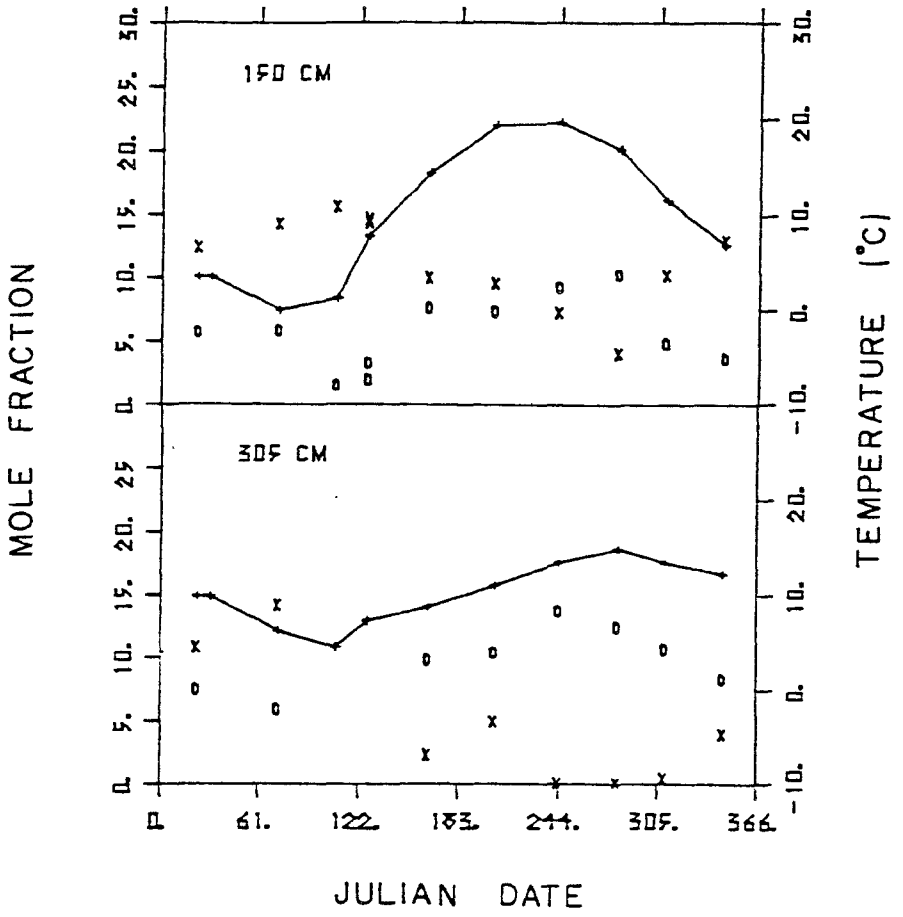

Figure 10. Variation of temperature and the mole fractions of O_2 (X) and CO_2 (O) over time for the composite record at site 6. The temperature plot is shown as a solid line connecting the individual points for clarity.

5-10. To test the relationship between O_2 and CO_2, regression and correlation coefficients were calculated for the relation:

$$Y_{CO_2} = a + b\ (0.210 - Y_{O_2}) \qquad [4]$$

where Y_{CO_2} and Y_{O_2} are the mole fraction of CO_2 and O_2, respectively and a and b are regression coefficients. Table 3 shows the values for a, b and r, the correlation coefficient, for O_2 and CO_2 at the different layers of each site. Correlations between Y_{CO_2} and the term $0.210 - Y_{O_2}$ range between -0.29 and 0.97, although the smallest absolute value for r, significant at the 5% level, is -0.51. Values for b range from 0.19 to 0.88 and for a from -0.014 to 0.074. Although the degree of correlation is high in most cases, the fraction of the variation in Y_{CO_2} that can be attributed to variation in Y_{O_2} (represented by r^2, Steele and Torrie, 1960, p. 187) ranges from 0.26 to 0.94 when the r value is significant at the 5% level.

To test the relationship between temperature and Y_{O_2} and Y_{CO_2}, correlation coefficients were calculated for temperature, T, and Y_{O_2}, T and Y_{CO_2}, and also between temperature at the 30 cm depth for sites 1-5 and Y_{O_2} and Y_{CO_2}. These r values are listed in Table 4. Correlations between Y_{O_2} and T are in general rather poor with only 5 values having an absolute value greater than 0.75 (excluding site 6). Correlations between Y_{CO_2} and T are even poorer with only 6 layers having an absolute correlation greater than 0.75 (excluding site 6). Correlations between T and Y_{CO_2} and Y_{O_2} are much stronger for most depths when the temperature at the 30 cm depth of each site, T_{30}, is used. Thirteen layers have an absolute correlation greater

Table 3. Correlation, r, and regression coefficients, a and b, between the mole fractions of CO_2 and decreased O_2 ($.210-Y_{O_2}$) for each depth at sites 1-6†.

	Depth (cm)	a	b	r		Depth (cm)	a	b	r
Site 1	30	.0029	.38	.51*	Site 4	30	.0009	.27	.76**
	60	.0016	.88	.68**		60	.0061	.19	.69**
	105	.0030	.59	.87**		185	.0021	.55	.87**
	260	.050	.43	.57**		335	.0016	.61	.91**
	410	.074	.35	.29		490	.0026	.70	.93**
	565	.028	.62	.59**		790	.0057	.58	.82**
Site 2	30	.0018	.48	.10**	Site 5	30	.0014	.31	.72**
	60	.0016	.58	.97**		145	.0013	.56	.98**
	170	.0015	.50	.91**		325	.0052	.39	.89**
	320	.0004	.60	.96**		630	.0029	.52	.95**
	625	.0192	.43	.77**		935	.0081	.47	.78**
	945	.0141	.46	.81**		1240	.014	.46	.83**
	1250	.0075	.59	.93**					
Site 3	30	.0013	.34	.74**	Site 6	150	-.0145	.74	.90**
	60	.0016	.51	.72**		305	.028	.43	.89**
	150	.0033	.51	.85**					
	305	.0050	.44	.81**					
	455	.0025	.39	.77**					
	610	.0098	.32	.80**					
	810	.0026	.42	.84**					

*Significant at the 5% level.

**Significant at the 1% level.

†$Y_{CO_2} = a + b\ (.210-Y_{O_2})$.

Table 4. Correlation coefficients, r, between the mole fraction of O_2 and temperature and between the mole fraction of CO_2 and temperature for each depth at sites 1-6.

	Depth (cm)	O_2-T	CO_2-T	O_2-T_{30}	CO_2-T_{30} †
Site 1	30	.40	.05	--	--
	60	-.27	.56**	-.28	.53*
	105	-.92**	.84**	-.91**	.84**
	260	.11	-.06	.34	-.16
	410	.13	.08	.02	.10
	565	.08	.03	.34	-.13
Site 2	30	-.72**	.74**	--	--
	60	-.53*	.57*	-.53*	.55*
	170	-.79**	.85**	-.84**	.87**
	320	-.54**	.60**	-.91**	.92**
	625	.34	.12	-.90**	.70**
	995	.28	-.06	-.80**	.68**
	1250	-.30	.39	-.93**	.88**
Site 3	30	.40	.01	--	--
	60	-.31	.38	-.32	.40
	150	-.70**	.74**	-.66**	.68**
	305	-.49*	.80**	-.42	.70**
	455	-.56**	.74**	-.77**	.56**
	610	-.13	.19	-.78**	.65**
	810	.16	-.19	-.51	.56*
Site 4	30	.50*	-.30	--	--
	60	.36	.03	.34	.06
	185	.56**	-.58**	.58**	-.50*
	335	-.09	-.02	.25	-.29
	490	.11	-.21	.58**	-.58**
	790	-.26	.44*	-.13	.20
Site 5	30	-.80**	.88**	--	--
	145	-.80**	.84**	-.86**	.88**
	325	-.30	.53	-.78**	.82**
	630	.77**	-.73**	-.87**	.91**
	935	.55	-.62*	-.78**	.57
	1240	.13	-.41	-.82**	.92**
Site 6	150	-.83**	.72**		
	305	-.82**	.80**		

*Significant at the 5% level **Significant at the 1% level

†Correlation coefficients between oxygen and temperature; carbon dioxide and temperature; oxygen and the temperature at the 30 cm depth, T_{30}; and carbon dioxide and T_{30}, respectively.

than 0.75 between Y_{O_2} and T_{30}, while eight layers have absolute values greater than 0.75 for Y_{CO_2} and T_{30}. The number of significant correlations at the 5% level increases from 12 to 17 for T_{30} and Y_{O_2} and from 15 to 19 for T_{30} and Y_{CO_2}. For layers where the correlation is significant at the 5% level, the correlations are positive between Y_{CO_2} and temperature and negative between Y_{O_2} and temperature. Two layers at site 4 exhibit the reverse behavior but the correlations for these two layers are fairly weak ($|r| < 0.6$).

Discussion

Oxygen concentrations remained fairly high for sites 2-5 during the entire period of this study. This is a fairly surprising result considering the abundance of pyrite within the spoil at this site and is contrary to earlier calculations and observations of *in situ* pyrite oxidation in reclaimed mines and refuse dumps where only limited penetration of O_2 was calculated or measured (Colvin, 1977[2]; Good, 1970[3]). The increase in O_2 concentrations with depth after reaching a minimum value at several sites indicates that gaseous exchange between the spoil and atmosphere may also be accompanied by exchange between the spoil and a deeper layer, perhaps the water table or more likely the zone of deep-mined, B coal (Fig. 1). Carbon dioxide showed the same behavior with depth.

[2]Colvin, S. L. 1977. Oxygen diffusion in strip-mine soils. Unpublished M.S. Thesis, Iowa State Univ., Ames, Iowa.

[3]Good, D. M. 1970. The relation of refuse pile hydrology to acid production. Unpublished M.S. Thesis, The Ohio State Univ., The Ohio State Univ., Columbus, Ohio.

Only at sites 1 and 6 did Y_{O_2} approach 0.0. At both of these sites, trace levels of methane were detected during spring measurements when Y_{O_2} was below detection levels indicating that anaerobic conditions existed at least during part of the year. Low O_2 levels at site 6 can be attributed in part to slower diffusion rates than at the other sites since this site was located in undisturbed shale-overburden. Low O_2 concentrations at site 1 must be due to higher consumption rates than at sites 2-5 with perhaps impeded diffusion at the lowest depth where again undisturbed material was encountered. The low O_2 concentrations at sites 1 and 6 were accompanied by very large increases in CO_2. We have not found any other reports of such high CO_2 values in soil or spoil materials. At all sites, the decrease in O_2 is strongly correlated to the increase in CO_2. This behavior suggests that respiration of plant roots or soil organisms is responsible for the changes in O_2 and CO_2. The high carbon content of these spoils (Table 1) may support considerable activity by heterotrophic bacteria.

Another possible source of CO_2 is neutralization of acid by carbonate minerals. The acid produced by pyrite oxidation will react with the gangue material (Rogowski et al., 1971). If the gangue contains carbonates or other salts of weak acids, they will react to neutralize the acid. For carbonate reactions in acid stripmines (pH < 4), carbonic acid will be the dominant species present since the first pK_a for H_2CO_3 is 6.4 (Garrels and Christ, 1965, p. 76). The reaction for any carbonate species is:

$$M - CO_{3_s} + 2H^+ \rightarrow M^{2+} + H_2CO_{3_{aq}} . \qquad [5]$$

Carbonic acid will in turn be in equilibrium with gaseous CO_2, the relation being governed by Henry's Law (Garrels and Christ, 1965, p, 76).

$$a_{H_2CO_3} = 10^{-1.47} \cdot pCO_2 \qquad [6]$$

where:

pCO_2 is the partial pressure of CO_2 (atmospheres)

$a_{H_2CO_3}$ is the activity of carbonic acid in solution, where by convention, all $CO_{2_{aq}}$ is treated as $H_2CO_{3_{aq}}$ (see Kern, 1960 for further discussion on this relationship).

Lovell, et al. (1978) have observed almost complete carbonate neutralization of acid in stripmine spoils and data presented by Rogowski, et al. (1982) indicate that some carbonate neutralization is taking place at this site. Where carbonates are present in stripmine spoils, appreciable CO_2 can be generated over much of the active lifetime of a reclaimed stripmine.

The correlation between O_2 and T and CO_2 and T is fairly weak. This is similar to the result found by DeJong (1981) between CO_2 and T in native and cultivated soils. The stronger correlation between the temperature at 30 cm and the gas concentrations in some of the deeper layers, particularly for sites 2, 3 and 5, indicates that processes taking place near the surface are the dominant processes

controlling the O_2 and CO_2 concentrations in these deeper layers. We should expect this to be true only if gas diffusion through the spoil was the dominant process of gas movement and if consumption and production processes for O_2 and CO_2 in the deeper layers were considerably less than in the surface layers.

The mean values for temperature at the 30 and 60 cm depth for sites 1-4 were 14.2 and 15.2°C, respectively. These values are about five degrees higher than those measured by Carter and Ciolkosz (1980) for a natural soil at approximately the same elevation and location as the research site. They found average temperatures of about 9.2°C at 25 cm and 9.3°C at 50 cm. Part of this difference is due to a bias in the data used to calculate the means, since more measurements were taken during the summer months. However, even the time-weighted average for mean temperature, 10.4°C at 30 cm and 11.0°C at 60 cm, is 1.2 to 1.7°C higher than the natural soil. These higher temperatures are probably due to the differences in vegetative cover, allowing greater solar heating of the surface spoil materials (Deely and Borden, 1978). The natural soil was located under a closed forest canopy while the mine spoil had no tree cover and only a sparse covering of grasses and herbaceous plants (Table 1). The spoil showed a greater temperature variation in the top 30 cm layer than the natural soil studies by Carter and Ciolkosz (1980), with the temperature dropping below 4°C in the top 300 cm for a portion of the year. Temperatures below 4°C should inhibit autotrophic bacteria activity if the autotrophs are present in these layers (Ehlrich and

Fox, 1967). The deeper soil stayed within the temperature tolerance range of iron-oxidizing bacteria, though apparently 10-20°C below the temperature of maximum activity (Table 2, Silverman and Lundegren, 1959).

REFERENCES

1. Bollag, J. M. and W. Barabasz. Effects of Heavy Metals on the Denitrification Process in Soil. J. Environ. Qual., 8:196-201, 1979.
2. Carter, B. J. and E. J. Ciolkosz. Soil Temperature Regimes of the Central Appalachians. Soil Sci. Soc. Am. J., 44:1052-1058, 1980.
3. Cathles, L. M. and J. A. Apps. A Model of the Dump Leaching Process that Incorporates Oxygen Balance, Heat Balance and Air Convection. Metall. Trans., 63:617-624, 1975.
4. Clark, C. S. The Oxidation of Coal Mine Pyrite. Ph.D. Thesis, John Hopkins University, University Microfilms International, Ann Arbor, Michigan, 1965.
5. Deeley, D. J. and F. Y. Borden. High Surface Temperatures on Strip-Mine Spoils. In: Ecology and Reclamation of Devastated Land, R. J. Hutnik and G. Davis, eds. Gordon and Breach, New York, 1973. pp. 69-79.
6. DeJong, E. Soil Aeration as Affected by Slope Position and Vegetation Cover. Soil Sci., 131:34-43, 1981.
7. Dugan, P. R. and C. I. Randles. The Microbial Flora of Acid Mine Water and its Relationship to Formation and Removal of Acid. Project Completion Report A-002-2410, to Office of Water Resour. Rec., U.S. Department of the Interior, 1968.
8. Ehlrich, H. L. and S. I. Fox. Environmental Effects on Bacterial Copper Extraction from Lower Grade Copper Sulfide Ores. Biotech. Bioeng., 9:471-485, 1967.

9. Garrells, R. M. and C. L. Christ. Solutions, Minerals and Equilibria. Freeman, Cooper and Company, San Francisco, California, 1965.

10. Kern, D. B. The Hydration of Carbon Dioxide. J. Chem. Ed., 37: 14-23, 1960.

11. Lovell, H. L., R. R. Parizek, D. Forsberg, M. Martin, D. Richardson, and J. Thompson. Environmental Control Survey of Selected Pennsylvania Strip Mining Sites. Final Report to Agronne National Laboratory, Contract No. 31-109-38-3497, 1978.

12. Malouf, E. E. and J. D. Prater. Role of Bacteria in the Alteration of Sulfide Minerals. J. Metals., 1961:353-356, 1961.

13. Ohio State University Research Foundation. Acid Mine Drainage Formation and Abatement. Water Pollution Control Research Series Program 14010 FPR, U.S. Environmental Protection Agency, Washington, D.C., 1971.

15. Pedersen, T. A., A. S. Rogowski, and R. Pennock, Jr. Comparison of Morphological and Chemical Characteristics of Some Soils and Minesoils. Reclam. Rev., 1:143-156, 1978.

16. Pedersen, T. A., A. S. Rogowski, and R. Pennock, Jr. Physical Characteristics of Some Minesoils. Soil Sci. Soc. Am. J., 44:321-328, 1980.

17. Pionke, H. B. and A. S. Rogowski. Implications for Water Quality on Reclaimed Lands. In: Economics, Ethics and Ecology: Roots of Productive Conservation, W. E. Jeske, ed. Soil Conservation Society of America, Ankeny, Iowa, 1981. pp. 426-440.

18. Rogowski, A. S. Acid Generation within a Spoil Profile: Preliminary Experimental Results. In: Seventh Symposium on Coal Mine Drainage Research, NCA/BCR Coal Conference and Expo IV, Oct. 18-20, Louisville, Kentucky, 1977. pp. 25-40.

19. Rogowski, A. S., H. B. Pionke, and J. G. Broyan. Modeling the Impact of Strip Mining and Reclamation Processes on Quality and Quantity of Water in Mined Areas: A Review. J. Environ. Qual., 6:237-249, 1972.

20. Rogowski, A. S., H. B. Pionke, and B. E. Weinrich. Some Physical and Chemical Aspects of Reclamation. Preprint, paper presented at the North Atlantic Region ASAE 1982 Annual Meeting, 1982.

21. Singer, P. C. and W. Stumm. Acidic Mine Drainage: The Rate Determining Step. Science, 167:1121-1123.

22. Steele, R. G. D. and J. H. Torrie. Principles and Procedures of Statistics. McGraw-Hill Book Company, Inc., New York, 1960.

SECTION 3

FLUX AND PRODUCTION RATES OF OXYGEN AND CARBON DIOXIDE IN A RECLAIMED COAL-STRIPMINE

Introduction

In Part II we presented data on the oxygen and carbon dioxide status within a reclaimed coal-stripmine. An unexpected finding was the prevalance of CO_2 within the spoil profile. Carbon dioxide concentrations ranging from 0.02 to 0.16 mole fraction were found in the stripmine atmosphere. The higher values were restricted to only one portion of the study area, but greatly exceed the highest values reported for natural soils (DeJong, 1981; Russell and Appleyard, 1915). We proposed two possible sources for the observed CO_2: i) heterotrophic respiration by soil bacteria within the spoil bank and ii) carbonate neutralization within the mine of the acid produced by pyrite oxidation with subsequent release of CO_2 gas. If either of these mechanisms accounts for the observed CO_2, the implications for acid generation and leaching within reclaimed stripmine is significant. In the first case, uptake of O_2 by micro-organisms would help reduce pyrite oxidation by reducing the O_2 concentration in the spoil atmosphere since the oxidation rate of pyrite is directly proportional to the gaseous O_2 concentration (Clark, 1965; Ohio State University Research Foundation, 1971). On the other hand, if the CO_2 is from carbonate neutralization of acid, the effect would be to reduce the acidity leaving the stripmine, while the production

rate of pyrite oxidation products remains unchanged. Both mechanisms would serve to reduce the amount of acid leaving a stripmine. However, in the first case, the reduction is from a decrease in the production rate of acid, while in the second case, the reduction is from an in situ neutralization of the acid produced. The objective of this study was to see if either i or ii could be identified as the dominant process at this reclaimed mine.

Neither mechanisms can be ruled out at this site. Heterotrophic respiration in the surface layers must take place at this site since a plant cover is well established. Also, heterotrophic activity appears to be occurring in the deeper depths as indicated by the formation of methane during the wet, presumably most poorly aerated times of the year (Part II). Carbonate neutralization of acid is also a possibility at this site, despite being located in an area low in carbonate-containing overburden. Water quality data presented by Rogowski, et al. (1982) indicates that some carbonate neutralization is taking place at this site.

Table 5 shows the pyrite and sulfate content expressed as percent by weight sulfur for ten representative spoil layers from this reclaimed mine (Rogowski, 1977). The fourth column in Table 5 represents the amount of carbonate, expressed as percent by weight CO_2, required to neutralize all the acid produced if all the pyrite oxidizes as shown in Eq. [8] and one-half of the sulfate content is in the form of sulfuric acid. The fifth and sixth column show the

Table 5. Pyrite and sulfate concentrations expressed as percent by weight sulfur for ten representative spoil layers from research site (Rogowski, 1977). Also, the CO_2 equivalent of the carbonate content required to neutralize the acid produced from columns 2 and 3 and the measured carbonate content. The last column gives the ratio $CO_{2\ measured}/CO_{2\ required}$ in percent.

Layer	Pyritic S	Sulfate S	$CO_{2\ required}$	$CO_{2\ measured}$	Potential neutralization
	% by weight				%
1	.095	.085	.122	.03	25
2	.112	.079	.130	.01	8
3	.136	.089	.158	.01	7
4	.088	.070	.108	.02	19
5	.124	.049	.118	.03	25
6	.082	.059	.096	.03	31
7	.064	.056	.082	.03	37
8	.060	.077	.094	.30	319
9	.066	.055	.082	.01	12
10	1.967	.738	1.86	1.16	62

amount of CO_2 forming minerals present in these layers and the percentage of the CO_2 requirement these minerals represent. From these data it can be seen that appreciable CO_2 can be generated over much of the active lifetime of a reclaimed stripmine.

Theory

One possible means of identifying whether mechanism i or ii dominates the production of CO_2 is to compare the consumption and production rates of O_2 and CO_2. For aerobic hetertrophic respiration by plant roots or microorganisms we would expect the ratio of consumption of CO_2 to O_2, r_q to be near -1.0 although values between -0.6 and -4.0 have been reported (Bridge and Rixon, 1976; Rixon and Bridge, 1968; Bunt and Rovira, 1955). To estimate r_q for mechanism ii, the stoichiometry of carbonate neutralization of acid and pyrite oxidation must be considered. For pyrite oxidation we know that 3.5 moles of O_2 will oxidize 1.0 mole of pyrite to form 2.0 moles of H^+.

$$FeS_2 + 3.5\ O_2 + H_2O \rightarrow Fe^{2+} + 2SO_4^{2-} + 2H^+ \qquad [8]$$

This result is true regardless of whether O_2 reacts directly with pyrite or if an intermediary oxidant, such as ferric iron, is involved (Ohio State University Research Foundation, 1971). The ferrous iron produced in Eq. [8] may or may not oxidize and precipitate within the mine to form more acid:

$$Fe^{2+} + 1/4\ O_2 + 2.5\ H_2O \rightarrow Fe\ (OH)_3 + 2H^+ \qquad [9]$$

Thus, from 0.57 to 1.07 moles of H^+ can be produced for every mole of O_2 consumed during pyrite oxidation.

For carbonate neutralization in acid stripmines (pH < 4), carbonic acid will be the dominant species in solution since the first pKa for H_2CO_2 is 6.4 (Garrels and Christ, 1965, p. 76). The equation for any carbonate species is:

$$M\text{-}CO_3 + 2H^+ \rightarrow M^{2+} + H_2CO_{3_{aq}} \quad [10]$$

The carbonic acid formed in Eq. [10] will in turn be in equilibrium with gaseous CO_2, the relation being governed by Henry's Law (Garrels and Christ, 1965, p. 76).

$$a_{H_2CO_3} = 10^{-1.47} \cdot pCO_2 = 10^{-3.47} \cdot P \cdot Y_{CO_2} \quad [11]$$

where a is activity, pCO_2 is the partial pressure of CO_2 (atmospheres), P is total pressure (kPa), and Y_{CO_2} is the mole fraction of CO_2 (-). If we assume that the movement of water through the spoil is sufficiently slow so that the water is always in equilibrium with gaseous CO_2, we can rewrite Eq. [10].

$$M\text{-}CO_3 + 2H^+ \rightarrow M^{2+} + H_2O + CO_{2_g} \quad [12]$$

Thus, the neutralization of 2.0 moles of H^+ will produce 1.0 mole of CO_2.

The areas in the mine where O_2 is consumed would correspond to the areas containing pyrite, whereas CO_2 production would take place only in zones where acidic waters come in contact with carbonates. These areas may not be the same. Table 5 shows that the presence of

CO_2 producing materials does not correspond to pyrite abundance. If all the acid produced by Eq. [8] is neutralized by carbonates, before it moves far in the profile, r_q would equal -0.29. If no neutralization occurs, r_q could be 0.0 and could go as high as -0.54 or higher if iron precipitates within the mine as described by Eq. [11] or if acid formed in one area of the mine is concentrated by leaching to a high carbonate zone where it is neutralized. Even if this latter case is true, the r_q value for the reclaimed site on the whole will be between 0.0 and -0.54. This range is considerably different from the range expected for heterotrophic respiration (-.6 to -4.0). The difference in the two ranges for r_q may serve as a means of differentiating between mechanisms i or ii, making it possible to identify the dominant process of CO_2 production.

Materials and Methods

Oxygen and carbon dioxide concentrations for selected depths at 6 sites on a reclaimed coal-stripmine were presented in Part II. The consumption and production rates for O_2 and CO_2 at these sites can be calculated from the gas concentration profiles if we assume that the dominant means of gas movement through the spoil material is by diffusion in the vertical direction only (Evans, 1965). The diffusion of gas component i into the spoil can be described in one dimension by:

$$- d/dz\ (N_i) + Q_i = d/dt\ (\phi\ \rho_i y_i) \qquad [13]$$

where N_i is the flux of component i (moles-cm^{-2}-sec^{-1}, positive downwards), Q_i is the source/sink (+/-) term for component i (moles-cm^{-3}-sec^{-1}), ϕ is the air-filled fraction of the spoil (-), Y_i the mole fraction (-), z is depth (cm), and t is time (sec). At steady or quasi-steady state, the gas concentration per unit volume of soil is constant or changing slowly. The right side of Eq. [13] can then be set equal to zero since ϕ, ρ_i and Y_i are constant with time and Eq. [13] can be rearranged:

$$d/dz\ (N_i) = Q_i \qquad [14]$$

The molar flux, N_i, can be found from the mole fraction form of Fick's Law (see Appendix A).

$$N_i = -\ \phi/\tau\ D_{F_i}\ \frac{P}{RT}\ dY_i/dz \qquad [15]$$

where P is pressure (kPa), R the gas constant (kPa-cm^3-$mole^{-1}$-K^{-1}), T is temperature (K), τ is the tortuosity (-) and D_{F_i} the Fickian diffusion constant for component i (cm^2/sec, see Appendix A). The Fickian diffusion coefficient in an open system, D_{F_i}, is adjusted by ϕ/τ in Eq. [15] to account for the reduced air-filled cross section and tortuous path of gas diffusion in soils (Troeh, et al., 1982). A constant tortuosity term of 5 was used for the coarse spoil material at sites 1-5 (Cathles and Apps, 1975). ϕ was assumed to be 0.12 at these sites based on an average bulk density of 1.57 g/cm^3 and a water-saturation percentage of 0.7 for the stripmine land (Pedersen, et al., 1980). Since site 6 was located in an undisturbed area, values of 10 and 0.06 were used for τ and ϕ, respectively.

D_{F_i} was calculated by assuming that O_2 and CO_2 diffusion were taking place in a four-component atmosphere comprised of O_2, CO_2, Ar and N_2, where N_{N_2} and N_{Ar} were 0.0. Since $D_{F_{O_2}}$ and $D_{F_{CO_2}}$ are dependent on N_{O_2} and N_{CO_2} (Appendix A), an iterative scheme was used to solve for N_{O_2}, N_{CO_2}, $D_{F_{O_2}}$ and $D_{F_{CO_2}}$. Nitrogen and argon concentrations were not measured directly so their values were set by assuming $Y_{N_2} + Y_{Ar} = 1 - Y_{O_2} - Y_{CO_2}$ and that the nitrogen-argon ratio was constant and equal in the atmospheric ratio of 0.012. At each site, the mine profile was divided into a number of layers corresponding to the depths at which O_2 and CO_2 were measured (Fig. 11). Flux values for O_2 and CO_2 were calculated at each layer by using the unequal-spacing, central-difference form of the first-order space derivation in Eq. [15] (Peaceman, 1977, p. 38). In general:

$$N_{i,j} = -\phi_j/t_j \, D_{F_{i,j}} \frac{P}{R} \left[\left[\frac{Y_{i,j+1}}{T_{i,j+1}} - \frac{Y_{i,j}}{T_{i,j}} \right] DZ_{j+1/2} + \left[\frac{Y_{i,j}}{T_{i,j}} - \frac{Y_{i,j-1}}{T_{i,j-1}} \right] DZ_{j-1/2} \right] \qquad [16]$$

where the subscript j refers to the depth, increasing downwards, and DZ is the distance weighing factor;

$$DZ_{j+1/2} = \frac{z_{j+1} - z_j}{(z_{j+1} - z_j)\,(z_j - z_{j-1}) + (z_j - z_{j-1})^2} \qquad [17]$$

At each site the flux was assumed to be 0.0 at the spoil-bedrock or spoil-water table boundary. Oxygen and carbon dioxide concentrations at the spoil surface were assumed to be at atmospheric levels. After

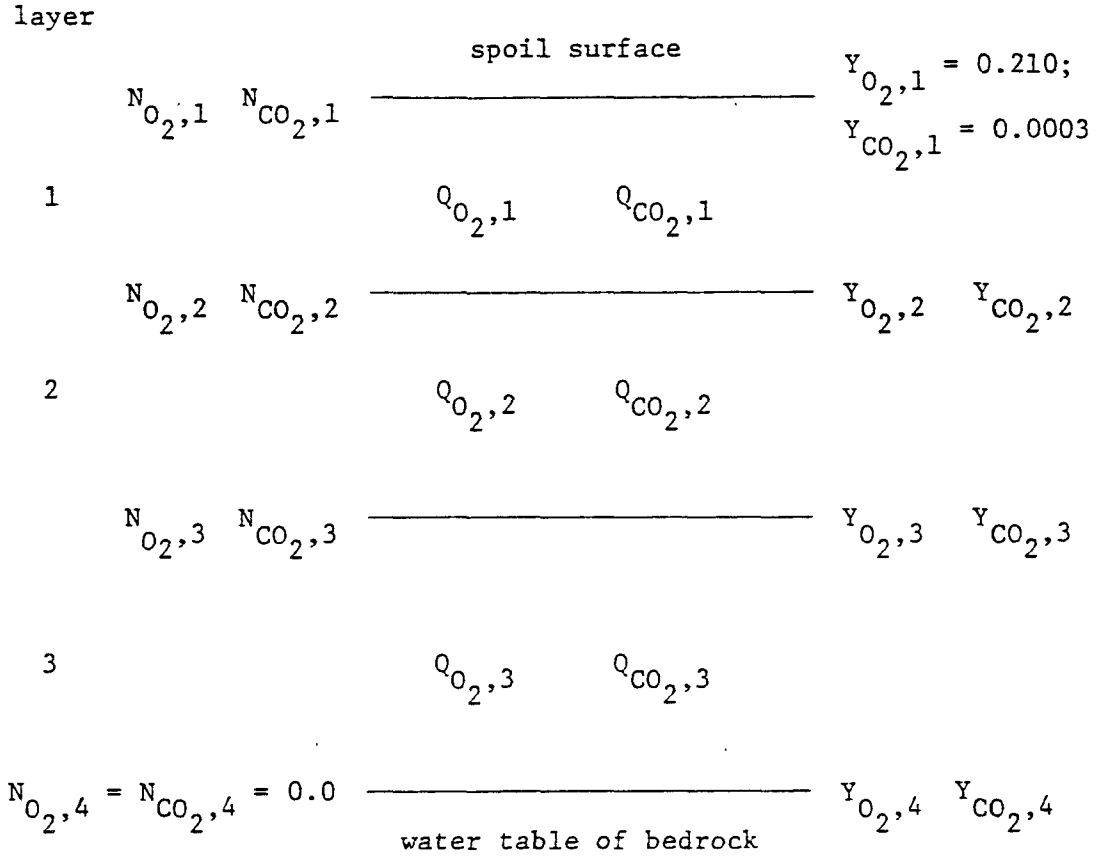

Figure 11. Schematic of spoil profile showing the division of the profile into layers as determined by the depths of the gas concentration measurements, Y_{O_2} and Y_{CO_2}. Fluxes N_{O_2} and N_{CO_2} are calculated for the top of each layer and are assumed to be 0.0 at the profile bottom. Source terms, Q_{O_2} and Q_{CO_2}, are calculated for each layer.

the fluxes were calculated, the average Q_{O_2} and Q_{CO_2} values were found for the layers between the probes (Fig. 11), by using the difference form of Eq. [14]:

$$Q_{i,j+1/2} = \frac{N_{i,j+1} - N_{i,j}}{z_{j+1} - z_j} \qquad [18]$$

Fluxes and source terms for O_2 and CO_2, and the rates, $r_Q = Q_{CO_2}/Q_{O_2}$ and $r_N = N_{CO_2}/N_{O_2}$ were calculated from the data presented earlier.

Results and Discussion

The calculated fluxes showed considerable variation over time at each site. Table 6 shows the flux values, averaged over time, for oxygen and carbon dioxide at the soil surface of the six sites and for all sites combined. Coefficients of variation, C.V., for both N_{O_2} and N_{CO_2} are also shown in Table 6. The C.V. values range from 37 to 390%. Site 6 consistently showed less variation than the other sites and was also the only site located in undisturbed bedrock. This was probably because the diffusional process was more consistent and uniform in the bedrock than in the spoil material. This isn't surprising since we would expect greater heterogeneity of both porosity and pyrite content in the spoil, which would lead to nonuniform patterns of diffusion. In the extreme, heterogeneity could negate our assumption of one-dimensional diffusion, although the generally uniform variation of O_2 and CO_2 concentrations with

Table 6. Means and coefficients of variation, C.V., for O_2 and CO_2 fluxes at the surface of the six sites and for all sites combined. The ratio of the fluxes, $r_N = N_{CO_2} / N_{O_2}$, was calculated from the mean values.

Site	$N_{O_2} \times 10^{10}$		$N_{CO_2} \times 10^{10}$		
	$\bar{x}$	C.V.	$\bar{x}$	C.V.	r_N
	$\frac{\text{moles}}{\text{cm}^2\text{-sec}}$	%	$\frac{\text{moles}}{\text{cm}^2\text{-sec}}$	%	--
1	0.78	160	-.27	210	-.35
2	2.2	110	-.82	110	-.37
3	0.49	140	-.07	270	-.14
4	0.96	110	-.10	390	-.10
5	1.41	130	-.23	200	-.16
6	.45	37	-.20	43	-.46
all	1.2	130	-.37	170	-.31

depth (Part II) indicates that vertical flow still dominates at this reclaimed mine.

No significant difference at the 10% significance level was measured between any site for the flux of O_2 and CO_2. For all the sites the average flux of O_2 at the surface was 1.2×10^{-10} moles-cm^{-2}-sec^{-1}, while for CO_2 the average flux was $-.37 \times 10^{-10}$ moles-cm^{-2}-sec^{-1}. The CO_2 fluxes measured for these minesoils are, in general, less than the fluxes of CO_2 measured by DeJong (1981) in grassland and cultivated soils. DeJong (1981) found CO_2 fluxes ranging from near 0.0 to -7×10^{-10} moles-cm^{-2}-sec^{-1} (-3×10^{-8} g-cm^{-2}-sec^{-1}), with fluxes normally near -2×10^{-10} moles-cm^{-2}-sec^{-1}. The lower CO_2 fluxes in the minesoils may be due to the lack of plant cover and freshly deposited organic matter at the sites measured, although no consistent pattern was obvious in the data.

Undoubtedly, much of the variation found in the flux values was due to the fact that we assumed a constant air-filled porosity - tortuosity term in the diffusion calculation when, in fact, this term would vary over time as the water content of the minesoils changed (Troeh, et al., 1982). The value we used was only approximate, thus, the magnitude of the flux terms shown in Table 6 are also approximate. However, the ratio of the CO_2 flow to O_2 flux is an absolute comparison since the effect of diffusion path in the spoil is identical for O_2 and CO_2 (Penman, 1940) and cancels out when we take the ratio, $r_N = N_{CO_2}/N_{O_2}$. Table 6 lists the r_N for the

average of the fluxes at the surface of each site. The r_N ranges from -.10 at site 4 to -.46 at site 6 and is equal to -.31 for all the sites combined. The lower values for r_N occur at sites 3, 4 and 5 which are located on the upper portion of the mine site in the predominantly sandstone overburden. The differences between r_N at sites 3, 4 and 5 and 1, 2 and 6 are not significant however, because of the great variability in the flux values. These r_N values indicate that, on the average, from 2 to 10 times as much O_2 is entering the spoil material as CO_2 is leaving.

The source term Q was calculated for O_2 and CO_2 for each layer at the six sites. Table 7 summarizes the results, showing the mean values of Q_{O_2} and Q_{CO_2} (moles-cm^{-3}-sec^{-1}) and the coefficients of variation for these values. The variation in the Q terms was large enough that no significant difference could be found between the different layers, but several trends are obvious from the data.

The layers of greatest consumption of O_2 are the surface layers at almost every site. The rate of O_2 uptake in these layers is consistently greater than for the deeper layers. This finding is consistent with the fact that plant roots and soil organisms are most active in the surface layers and would be removing oxygen during respiration. The rate of O_2 uptake in the surface layer at the six sites averaged -1.2×10^{-12} moles-cm^{-3}-sec^{-1} or 0.065 μliters-g^{-1}-hr^{-1} if a bulk density of 1.57 g/cm^3 is assumed. This value is much lower than the values found by Stroo and Jencks (1982) for O_2 uptake in minesoils. Even for barren minesoils they found the lowest O_2 uptake

Table 7. Mean values and coefficients of variation of the source terms for O_2 and CO_2 and for the ratio $r_Q = Q_{CO_2}/Q_{O_2}$ at the individual depths at each site. The correlation between Q_{CO_2} and Q_{O_2}, r, is also listed.

	Depth	$Q_{O_2} \times 10^{12}$		$Q_{CO_2} \times 10^{12}$		r_Q		
		$\bar{x}$	C.V.	$\bar{x}$	C.V.	$\bar{x}$	C.V.	r
	cm	$\frac{\text{moles}}{\text{cm}^3\text{-sec}}$	%	$\frac{\text{moles}}{\text{cm}^3\text{-sec}}$	%	--	%	--
Site 1	15	-3.6	123	1.5	150	-.38	87	-.85**
	45	3.6	64	-1.8	88	-.48	44	-.90**
	82	3.1	36	-1.4	33	-.49	32	-.63**
	182	- .92	110	.41	110	-.50	100	-.84**
	335	- .55	42	.23	64	-.47	57	-.47*
	488	- .073	260	.021	580	-.15	930	-.36
	602	.048	720	.13	220	-.29	470	-.42
Site 2	15	-5.5	150	2.5	98	-.51	180	-.86**
	45	-3.0	110	1.2	81	-.48	130	-.85**
	115	1.0	120	- .38	79	-.24	200	-.68**
	245	- .079	270	.020	410	-.45	130	-.77**
	472	- .013	280	.010	130	-.18	310	-.15
	785	- .045	62	.029	59	-.54	140	-.63**
	1098	.027	99	- .014	86	-.59	130	-.49*
Site 3	15	-2.1	150	.35	240	-.32	50	-.81**
	45	- .51	220	- .004	8000	-.78	290	-.88**
	105	.003	7900	.033	350	-.53	340	-.60**
	228	- .072	140	.059	71	-.79	160	-.71**
	380	.17	92	- .064	56	-.23	270	-.46*
	532	- .12	80	.039	92	-.45	110	-.58**

Site 4	15	.22	1400	.18	750	-.25	365	.22
	45	.082	180	-.27	180	-.56	390	-.77**
	122	-1.10	93	.28	96	-.24	200	-.53*
	260	.12	140	-.027	160	-.36	92	-.59**
	412	.029	140	-.017	100	-.42	120	-.79**
	640	.003	1500	.004	630	-.45	87	-.69**
	900	- .010	580	.006	560	-.39	53	-.66**
Site 5	15	-2.5	160	.055	1620	-.23	245	-.30
	88	- .58	130	.13	160	-.32	100	-.63*
	235	- .028	327	.017	170	-.29	120	-.50
	478	- .009	310	-.001	1500	-.16	310	-.91**
	782	.007	270	-.008	130	-.56	130	-.81**
	1088	- .014	120	.011	110	-.91	44	-.83**
Site 6	75	- .090	110	.038	110	-.53	110	-.86**
	228	- .052	90	.030	100	-.52	75	-.88**
	342	- .20	78	.075	80	-.46	51	-.88**

*Significant at the 5% protection level.

**Significant at the 1% protection level.

rates to be 0.58 μliters-g^{-1}-hr^{-1} or about ten times the values found in this study. This large difference may be due to differences in the studied site, but is more likely due to the different techniques used to measure Q; a laboratory respirometer by Stroo and Jencks (1982), and concentration gradients in this study. Also, since only estimated values for the porosity - tortuosity term were used here to calculate N_{O_2} and thus Q_{O_2}, the absolute magnitude of Q_{O_2} is unknown. Comparing the two data sets, the coefficient ϕ/τ would have to be increased by a factor of 10 for the uptake rates to agree. Such an increase is certainly feasible but would result in greater C_{O_2} flux rates for the minesoil than for the natural soils studied by DeJong (1981). Problems in measuring Y_{O_2} at shallow depths, discussed in Part II, may also contribute to the difference, as well as smearing of the O_2 gradient as a result of atmosphere-pressure fluctuations (Morth, et al., 1972). Smearing of the gradients because of pressure fluctuations and deviation from strictly vertical diffusion because of spatial variability in the porosity of the minesoil may also account for the seemingly contradictory result that the layers just below the surface act as O_2 sources and CO_2 sinks (Table 7).

Problems with using the data resulting from uncertainty in the absolute magnitude of Q_{O_2} and Q_{CO_2} is avoided by comparing the ratio of the fluxes $r_Q = Q_{CO_2}/Q_{O_2}$ and the correlation of the relative uptake terms. Table 7 shows the correlation coefficient between Q_{CO_2} and Q_{O_2} and the ratio, r_Q, for each layer. In general, the

correlation is strongest near the surface at each site indicating a greater dependency of the changes in CO_2 and O_2. The r_Q values are extremely variable and range from -.15 to -.91. Table 8 shows the average values for the source term of O_2 and CO_2 and the r_Q values for the entire depth at each site. Again the values are extremely variable which prevents any significant statistical comparison between the sites. However, there is a trend in the data for r_Q similar to that found for r_N where the r_Q values for sites 3, 4 and 5 are less than sites 1, 2 and 6. The average r_Q value for all the sites was -0.30 which indicates that more than 3 times as much O_2 is being consumed as CO_2.

Conclusions

Both the ratios of the diffusional flux of CO_2 to O_2 and the ratios of the source terms for CO_2 and O_2 showed considerable variability. Site 6 showed considerably less variation than the other sites possibly because it was the only site located in undistrubed bedrock where our assumption of strict vertical diffusion was more valid. The r_N ranged from -.10 to -.46 for the six sites and was equal to -.31 for all the sites combined. The r_Q for the entire profile at each site ranged from -.12 to -.46 and averaged -.30 for the combined site. Both r_Q and r_N indicate that from 2 to 10 times as much O_2 is being consumed as CO_2 with 3.3 times as much for all the sites combined. These values lie well within the range expected for carbonate neutralization of the acid formed from pyrite oxidation and indicate that this mechanism accounts for the bulk of the CO_2 measured at this site although heterotrophic

Table 8. Mean values and coefficients of variation, C.V., for the production rate of O_2 and CO_2 and for their ratio, $r_Q = Q_{CO_2}/Q_{O_2}$. Rates are for the entire spoil profile at each site averaged over time.

Site	$Q_{O_2} \times 10^{10}$		$Q_{CO_2} \times 10^{10}$			
	$\bar{x}$	C.V.	$\bar{x}$	C.V.	r_Q	C.V.
	$\frac{\text{moles}}{\text{cm}^2\text{-sec}}$	%	$\frac{\text{moles}}{\text{cm}^2\text{-sec}}$	%	--	%
1	-.66	210	0.22	280	-.44	350
2	-1.9	130	0.78	110	-.40	180
3	-.47	140	0.063	300	-.15	550
4	-.24	480	-.047	880	-.24	450
5	-1.0	170	0.16	250	-.12	230
6	-.45	37	0.20	42	-.46	33
all	-.91	180	0.29	220	-.30	330

respiration is undoubtedly still taking place. The more negative ratios at the sites located on the lower portions of the mine site may be as a result of greater concentrations of carbonate in this portion of the mine. The more negative ratios may also be due to waters containing acid formed in the upper reaches of the mine site flowing through the lower sites and producing increased amounts of CO_2 for neutralization reactions. This may also explain the poor correlation between Q_{O_2} and Q_{CO_2} at the 488 and 602 cm layers at site 1, where Y_{CO_2} was very high. The r_Q values indicate that a considerable amount of the acid produced within the mine is being neutralized before it leaves the site.

REFERENCES

1. Bridge, B. J. and A. J. Rixon. Oxygen Uptake and Respiration Quotient of Field Soil Cores in Relation to their Air-Filled Pore Space. J. Soil Sci., 27:279-286, 1976.
2. Bunt, J. S. and A. D. Rovira. Microbial Studies of Some Sub-antartic Soils. J. Soil Sci., 6:119-128, 1955.
3. Cathles, L. M. and J. A. Apps. A Model of the Dump Leaching Process that Incorporates Oxygen Balance, Heat Balance and Air Convection. Metall. Trans., 6B:617-624, 1975.
4. Clark, C. S. The Oxidation of Coal Mine Pyrite. Ph.D. Thesis, John Hopkins University, University Microfilms International, Ann Arbor, Michigan, 1965.
5. DeJong, E. Soil Aeration as Affected by Slope Position and Vegetation Cover. Soil Sci., 131:34-43, 1981.
6. Evans, D. D. Gas Movement. In: Methods of Soil Analysis, C. A. Black, ed. American Society of Agronomy, Madison, Wisconsin, 1965. Agronomy 9:319-330.
7. Garrels, R. M. and C. L. Christ. Solutions, Minerals and Equilibria. Freeman, Cooper and Company, San Francisco, California, 1965.
8. Morth, A. H., E. E. Smith, and K. S. Shumate. Pyritic Systems: A Mathematical Model. Environmental Protection Agency Technology Series 14010 EAH, Contract No. 14-12-589, Report No. 665771, U.S. Environmental Protection Agency, Washington, D.C., 1972.
9. Ohio State University Research Foundation. Acid Mine Drainage Formation and Abatement. Water Pollution Control Research Series Program 14010 FPR, U.S. Environmental Protection Agency, Washington, D.C., 1971.

10. Peaceman, D. W. Fundamentals of Numerical Reservoir Simulation. Elsevier Scientific Publishing Company, New York, 1977.

11. Pedersen, T. A., A. S. Rogowski, and R. Pennock, Jr. Physical Characteristics of Some Minesoils. Soil Sci. Soc. Am. J., 44:321-328, 1980.

12. Penman, H. L. Gas and Vapour Movements in the Soil. II. The Diffusion of Carbon Dioxide through Porous Solids. J. Agr. Res., 30:570-581, 1940.

13. Rixon, A. J. and B. J. Bridge. Respiratory Quotient Arising from Microbial Activity in Relation to Matric Suction and Air-Filled Pore-Space of Soil. Nature, 218:961-962, 1968.

14. Rogowski, A. S. Acid Generation within a Spoil Profile: Preliminary Experimental Results. In: Seventh Symposium on Coal Mine Drainage Research, NCA/BCR Coal Conference and Expo IV, Oct. 18-20, Louisville, Kentucky, 1977. pp. 25-40.

15. Rogowski, A. S., H. B. Pionke, and B. E. Weinrich. Some Physical and Chemical Aspects of Reclamation. Reprint, paper presented at the North Atlantic Region ASAE 1982 Annual Meeting, 1982.

16. Russell, E. J. and A. Appleyard. The Atmosphere of the Soil: Its Composition and the Causes of Variation. J. Agric. Sci., 7:1-48, 1915.

17. Stroo, H. F. and E. M. Jencks. Enzyme Activity and Respiration in Minesoils. Soil Sci. Soc. Am. J., 46:548-553, 1982.

18. Troeh, F. R., J. D. Jabro, and D. Kirkham. Gaseous Diffusion Equations for Porous Materials. Geoderma, 27:239-253, 1982.

SECTION 4

A NUMERICAL MODEL OF ACID DRAINAGE FROM RECLAIMED COAL-STRIPMINES

Introduction

Acid drainage from reclaimed coal stripmines can be a severe problem in the humid Eastern United States (Collier, et al., 1970). The amount of pollutants leaving the reclaimed site can be reduced by using proper-reclamation techniques when restoring the land (Grim and Hill, 1974). However, the development and evaluation of best reclamation and management techniques is difficult because of the great expense and time required to implement and assess the value of a specific practice and because of the great variability between even adjacent-stripmine sites. The development of a mathematical model that describes the acid production and leaching from stripmined lands would facilitate the development of sound-management practices by allowing assessment of each technique for any given condition to be made in minutes rather than years. Although several models for pyrite weathering have been presented (Morth, et al., 1972; Colvin, 1977; Cathles and Apps, 1977; Cathles, 1979) none is completely suitable for describing the process in reclaimed coal-stripmines. The model described by Morth, et al., (1972) is for pyrite oxidation in deep mines and assumes that pyrite oxidation takes place only on the surface of cracks and voids and not within the rock matrix. They assumed oxygen flux due to diffusion and

atmospheric-pressure fluctuations. Their model is reasonable for deep mines but does not seem representative of pyrite oxidation within mine spoil composed of coarse fragments. Colvin (1977) describes a model for pyrite oxidation of reclaimed stripmines where diffusion serves as the mechanism of replacing oxygen with the profile. However, the model uses representative values of pyrite oxidation rates and does not attempt to relate the oxygen consumption rate to pyrite content and distribution within the spoil fragments nor does it differentiate between pyrite oxidation mechanisms. Cathles and Apps (1977) present a model for oxidation and leaching of sulfide-bearing fragments where the pyrite distribution, degree of weathering, and oxidation kinetics are considered. However, they assumed air-convection to be the main mechanism of oxygen movement and that pyrite was oxidized by ferric iron, where the ferric iron was maintained at a constant concentration by bacterial activity. While these conditions represent reasonable assumptions for the very coarse, copper-waste dumps they modelled, they do not apply well to reclaimed coal-stripmines where diffusion processes probably dominate and the role of iron-oxidizing bacteria is unclear. This paper presents a parametric model of <u>in situ</u> oxidation of pyrite and subsequent leaching of the acid products from reclaimed coal-stripmines, based on oxygen diffusion, pyrite oxidation kinetics and combined oxygen and ferric iron oxidation of pyrite, where the activity of iron-oxidizing bacteria depends on the energy available

from their substrate and the suitability of their environment for cell viability and is calculated independently.

Description of Model

Basic Reactions.

The chemistry of pyrite oxidation is extremely complex and only partially understood. However, the overall stoichiometry of the reaction can be summarized by four equations (Singer and Stumm, 1968). Two mechanisms for pyrite oxidation are possible (Ohio State University Research Foundation, 1970). One possibility is that oxygen can react directly with pyrite to form sulfate and acid.

$$FeS_2 + 3.5\ O_2 + H_2O \rightarrow Fe^2 + 2SO_4^{2-} + 2H^+ \qquad [19]$$

Alternatively, ferric iron can replace oxygen as the direct oxidant.

$$FeS_2 + 14Fe^{3+} + 8H_2O \rightarrow 15Fe^{2+} + 2SO_4^{2-} + 16H^+ \qquad [20]$$

In stripmine spoil, the only important source of ferric iron in Eq. [20] is assumed to be the *in situ* oxidation of ferrous iron (Lau, et al., 1970; Singer and Stumm, 1968);

$$14Fe^{2+} + 3.5\ O_2 + 14H^+ \rightarrow 14Fe^{3+} + 7H_2O \qquad [21]$$

While the oxidation of ferrous iron is thermodynamically favorable, the kinetics are extremely slow at normal pH's of stripmine waters (pH < 4; Singer and Stumm, 1970). However, certain chemoautotrophic bacteria (*Thiobacillus ferrooxidans*) are known to use the energy released by Eq. [21] as their energy source and can significantly increase the oxidation rate (Lundgren, 1975; Beck, 1960). Thus, Eq.

[21] and consequently Eq. [20] are thought to be bacterially catalyzed since ferric oxidation of pyrite can be significant only when bacteria are active.

As a final step in the pyrite oxidation process, the ferric iron produced by Eqs. [19] and [20] may precipitate as a ferric hydroxide.

$$Fe^{3+} + 3H_2O \rightarrow Fe(OH)_3 + 3H^+ \qquad [22]$$

This reaction often takes place after the iron has been leached from the stripmine site, with the iron hydroxide precipitation in surface streams and ponds. Summing Eqs. [20] and [21] results in Eq. [19], thus regardless of mechanism the result is the same; two moles of acid are produced for every mole of pyrite and three and a half moles of oxygen consumed.

Basic Equations

The reclaimed-mine environment in which Eqs. [19]-[21] and possibly [22] take place can be described as consisting primarily of coarse (> 2mm) fragments. Pedersen, et al. (1980) and Ciolkosz, et al. (1977) found coarse fragments composing 50-90% of the spoil volume. In this model, we consider all the pyrite oxidation to take place within coarse fragments. Since pyrite oxidation is a surface reaction (Garrels and Thompson, 1960), the oxidant must diffuse from the fragment surface through the fine pores of the fragment, which we assume to be water saturated, to the pyrite mineral surface (Fig. 12). Evidence indicates that the fine-grained or framboidal form of pyrite is the most reactive (Clark, 1965 and Caruccio, 1973).

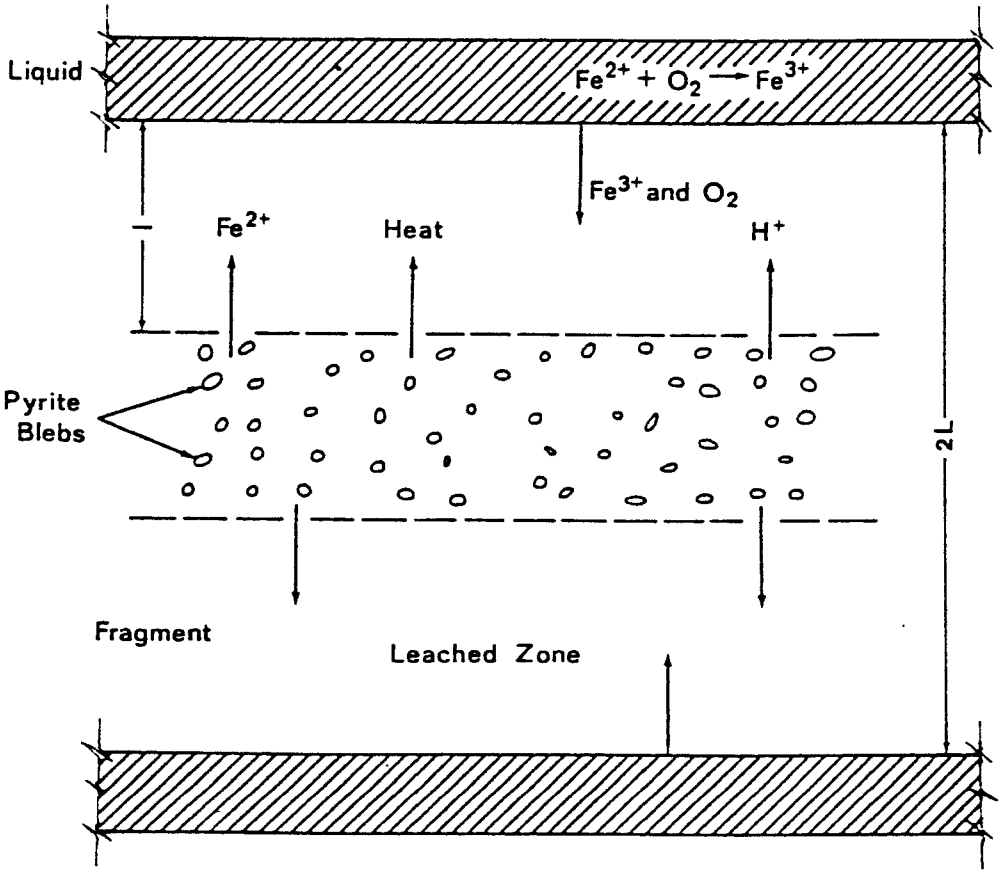

Figure 12. Cross section of a coarse fragment containing pyrite.

The framboidal form may be the result of the mineral being deposited by microorganisms that were active in the original sediments (Emrich and Thompson, 1968). Possibly for this reason, framboidal pyrite is evenly distributed within the rock formations in which it is found and the fragments derived from these strata during mining (Arora, et al., 1978). The rate at which pyrite and oxidant react may be controlled either by the chemical reaction rate or by the rate of diffusion of oxidant into the fragment, or by both. This process can be described by a standard shrinking-core model (Levenspiel, 1972). If we consider the fragments to be thin plates and the oxidation of pyrite to be first order with respect to oxidant concentration and pyrite surface area, we can express the oxidation rate of pyrite within a fragment by:

$$dX/dt = \frac{-1}{2t_D(1-X)+t_C} \qquad [23]$$

where:

X = fraction of pyrite remaining in fragment, (-)

t_D = time for complete oxidation of fragment if diffusion of oxidant is much slower than reaction rate, (sec)

t_C = time for complete oxidation of fragment if chemical oxidation is much slower than oxidant diffusion, (sec)

and

t = time (sec)

t_D represents the total time required to oxidize all the pyrite within a fragment when the diffusion of reactants and products between the fragment surface and the pyrite grain is the rate-controlling step. t_D can be calculated from (Levenspiel, 1972):

$$t_D = \frac{\rho_{py} \ell^2}{2bD_C C_{ox}} \qquad [24]$$

where:

ρ_{py} = molar density of pyrite within the fragment, (moles/cm^3)

ℓ = one half thickness of fragment, (cm)

b = stoichiometric ratio between pyrite and oxidant consumption, (-)

D_C = effective diffusion coefficient for coupled oxidant-product counter diffusion, (cm^2/sec)

C_{ox} = concentration of oxidant at fragment surface, (moles/cm^3).

t_C is the total time required for complete pyrite oxidation within a fragment if the resupply rate of oxidant to the pyrite surface is much faster than the chemical oxidation of pyrite. t_C can be calculated from (after Levenspiel, 1972; Cathles and Apps, 1975):

$$t_C = \frac{\rho_{py}}{bK_S C_{ox} \partial\alpha} \qquad [25]$$

where:

K_S = first-order surface reaction rate constant for pyrite oxidation per unit surface area of pyrite, (cm/sec); i.e.,

$\rho_{py} \ell \, dx/dt = -bK_S C_{ox}$

α = surface area of pyrite per unit volume of fragment, (cm^{-1})

and

∂ = effective thickness of fragment within which pyrite is oxidized (cm, see Appendix B).

From Eq. [23] it is obvious that the oxidation of pyrite will be independent of diffusion rates at initial times, ($X \approx 1$), but may or may not become important as the pyrite is leached, depending on the magnitudes of t_C and t_D. For $t_C >> t_D$, diffusion will never be an important rate-controlling step and the fragment will weather uniformly throughout its thickness. For $t_D >> t_C$, diffusion is the rate-controlling step and a rim depleted of pyrite will form and slowly grow at the fragment surface.

When both oxygen and ferric iron are present the rate of pyrite oxidation is the sum of the rates of each oxidant acting alone (Ohio State University Research Foundation, 1970) and their reaction rates can be summed.

$$dX/dt = \frac{-1}{t_D(O_2)(1-X)+t_C(O_2)} + \frac{-1}{t_D(Fe^{3+})(1-X)+t_C(Fe^{3+})} \qquad [26]$$

Values for t_C and t_D can be calculated from typical values for spoil and Eqs. [24] and [25]. For the values shown in Table 9, the calculated values are $t_D(O_2) = 27 \times 10^8$ sec, $t_D(Fe^{3+}) = 35 \times 10^8$ sec, $t_C(O_2) = 4 \times 10^8$ sec, and $t_C(Fe^{3+}) = .7 \times 10^8$ sec. These calculated values indicate that we would expect diffusion to be the rate-controlling step for both the oxygen and iron oxidants and would expect that a leached rim, surrounding a relatively unweathered core, would form in the fragment. This agrees with the weathering

Table 9. Coefficients used to calculatee typical values of t_c and t_0.

Parameter	Value
ρ_{py}	4.4×10^{-5} moles cm^{-3} (.13% pyrite S)
ℓ	1 cm
$b(O_2)$	1/3.5
$b(Fe^{3+})$	1/14.
D_c	10^{-7} cm^2-sec^{-1}
$C_{ox}(O_2)$	0.29×10^{-6} moles-cm^{-3} (.21 mole fraction)
$C_{ox}(Fe^{3+})$	0.89×10^{-6} moles-cm^{-3} (50 mg/ℓ)
$K_s(O_2)$	$83. \times 10^{-7}$ cm-sec^{-1}
$K_s(Fe^{3+})$	4.4×10^{-6} cm-sec^{-1}
α	217 cm^{-1}
∂ (O_2)	.0745 cm
∂ (Fe^{3+})	.0102 cm

pattern observed for sulfide-bearing fragments (Cathles, 1979; Braum, et al., 1974).

Oxygen Diffusion

We assume the main mechanism for resupply of O_2 to the fragment surface to be diffusion within the interfragment voids of the spoil profile. Atmospheric pressure fluctuations (Morth, et al., 1972), air pumping from rising and falling water-table levels, convection due to temperature and compositional differences (Cathles, 1979) and dissolved oxygen contained in percolating water may contribute to the O_2 flux within the spoil but diffusion should dominate, especially where a fine-textured, surface soil layer is present (Evans, 1965). For one-dimensional diffusion of O_2 into a rigid spoil-bank at constant total pressure in which uptake of O_2 is taking place and the water content remains constant over time, the process can be described by:

$$\phi_A \, d/dt \, (\rho_{O_2} Y_{O_2}) = \frac{P}{R} \, d/dz \left[\frac{D_{O_2}}{T\tau} \frac{\phi_A \, dY_{O_2}}{d_z} \right] + Q_{O_2} \qquad [27]$$

where:

ϕ_A = air filled porosity, (-)

ρ_{O_2} = molar density O_2, (moles/cm^3-air)

Y_{O_2} = mole fraction of O_2 in gas, (-)

P = total pressure, (kPa)

R = universal gas constant, (8.31 kPa-cm^3/mole-K)

T = temperature, (K)

τ = tortuosity of gas diffusion path, (-)

Q_{O_2} = O_2 uptake rate, (moles/cm^3)

Z = depth, cm

D_{O_2} is the effective diffusion coefficient of O_2 in an O_2, CO_2, N_2 atmosphere and is found from the binary diffusion coefficients and the flux ratios, $r_1 = N_{CO_2}/N_{O_2}$ and $r_2 = N_{N_2}/N_{O_2}$ (Appendix A).

$$D_{O_2} = \left[\frac{Y_{CO_2}}{D_{O_2,\,CO_2}} + \frac{Y_{N_2}}{D_{N_2,CO_2}} - Y_{O_2} \left[\frac{r_1}{D_{O_2,CO_2}} + \frac{r_2}{D_{O_2,N_2}} \right] \right]^{-1} \qquad [28]$$

For gaseous diffusion into spoil banks, the bottom of the spoil profile can be assumed to act as an effective diffusion barrier since below this boundary the air-filled porosity of the bedrock is significantly less than the spoil and commonly coincides with the water table.

Q_{O_2} in Eq. [27] may be partitioned into four separate processes of O_2 consumption:

$$Q_{O_2} = Q_{PY} + Q_{AB} + Q_{CHOX} + Q_{HB} \qquad [29]$$

Q_{PY} represents oxygen consumption by direct pyrite oxidation. Q_{AB} is the oxygen consumption rate of iron oxidation by autotrophic bacteria as shown in Eq. [21]. Q_{CHOX} is the rate of O_2 uptake by chemical oxidation of ferrous iron, and Q_{HB} represents the uptake of oxygen due to respiration by plant roots or other soil organisms. The magnitude of each factor in Eq. [29] can be calculated separately.

$\underline{Q_{PY}}$. Q_{PY} can be calculated from Eq. [23], modified to account for the number of fragments per cm^3 of spoil, $\left(\frac{FFR\ FPY\ \rho_B}{MW_{PY}}\right)$ and the stoichiometric ratio of pyrite consumption to O_2 consumption, $b(O_2)$.

$$Q_{PY} = \frac{-b(O_2)^{-1}}{2t_D(O_2)(1-X)+t_C(O_2)} \frac{FFR\ FPY\ \rho_B}{MW_{PY}} \qquad [30]$$

For a given fragment configuration and pyrite content, the magnitude of Q_{PY} depends on the O_2 concentration at the fragment surface and the degree to which the fragment has weathered.

$\underline{Q_{HB}}$. Q_{HB} represents the rate at which O_2 is consumed through respiration by plant roots and other soil organisms. The magnitude of Q_{HB} depends on type and extent of plant cover, time of the year and the presence of biodegradable organic matter in the reclaimed profile. Since Q_{HB} does not affect pyrite oxidation other than decreasing the available O_2 (Colvin, 1977), we have chosen a simple temperature and O_2 concentration dependent function to describe the process. O_2 uptake rates for bare (winter) and cropped (summer) surface soils have been measured to range between 1.5 and 16.0 x 10^{-12} moles O_2-sec^{-1}-cm^{-3} (soil) (Russell, 1973). If we let the rate equal zero at 0^oC and a maximum value of 16.0 x 10^{-12} moles O_2-sec^{-1}-cm^{-3} at 30^oC and assume that the observed values occurred at an O_2 mole fraction of 0.17, but would drop to zero linearly as the O_2 concentration goes to zero, we can represent Q_{HB} as:

$$Q_{HB} = 2Y_{O_2} T\ Q_{HBB} \qquad T > 0^oC$$
$$= 0.0 \qquad T < 0^oC \qquad [31]$$

Where Q_{HBB} is the base rate of O_2 production by respiration and would be equal to 0.0 when no plants or biodegradable organic matter are present in the soil and to -1.5 x 10^{-12} moles O_2-sec^{-1}-cm^{-3}-$^oC^{-1}$ for a well established agronomic soil.

Q_{CHOX}. The rate of chemical oxidation of ferrous iron is very slow at low pH's and pH dependent throughout the remaining pH range. Singer and Stumm (1970) found that for pH > 4.5 the rate of ferrous iron oxidation at normal atmospheric pressure can be expressed by:

$$d\,[Fe^{2+}]/dt = -\,K_1\,[Fe^{2+}]\,Y_{O_2}\,[H^+]^{-2} \qquad [32]$$

with $K_1 = 1.3 \times 10^{-16}\ mole^2\text{-}L^{-2}\text{-}sec^{-1}$

where the brackets indicate concentration. Below a pH of 3.0, the rate can be expressed as:

$$d[Fe^{2+}]/dt = -K_2\,[Fe^{2+}]\,Y_{O_2} \qquad [33]$$

$$K_2 = 1.7 \times 10^{-9}\ sec^{-1}$$

For the entire pH range, Eqs. [32] and [33] can be combined and since the oxygen uptake rate is equal to one fourth of the ferrous iron oxidation rate (Eq. [21]), we find the O_2 uptake rate per cubic centimeter to be:

$$Q_{CHOX} = \frac{\phi_w}{4000}\,d[Fe^{2+}]\,/dt_{chem} = -\,\frac{\phi_w}{4000}\,[Fe^{2+}]\,Y_{O_2}(\,K_1[H^+]^{-2} + K_2) \qquad [34]$$

where ϕ_w is the water-filled porosity.

Q_{AB}. The rate at which chemoautotrophic bacteria can oxidize ferrous iron, consuming O_2 in the process, is extremely variable and depends on the size of the bacterial population and the condition of the bacterial environment. Expressing Q_{AB} in a manner similar to chemical oxidation we have:

$$Q_{AB} = \frac{\phi_w}{4000}\,\frac{d\,[Fe^{2+}]}{dt} = -\,\frac{\phi_w}{4000}\,K_B\,[Fe^{2+}]\,Y_{O_2} \qquad [35]$$

Where K_B is the factor that accounts for the bacterial "activity the reclaimed spoil. The lower limit for K_B is 0.0 when the autotrophs are not active. An upper limit to K_B is set by assuming that

at maximum "activity," the bacteria are limited by the diffusion rate of O_2 to their surface. If we assume the bacteria are attached to the fragment surface within the water film surrounding the fragment (Malouf and Prater, 1961), the maximum oxidation rate must just equal the diffusion rate of O_2 through the film.

$$\frac{1}{4000} K_B \quad Fe^{2+} \quad Y_{O_2} = A_F D_W Y_{O_2} / \Delta\ell' \qquad [36]$$

where A_F is the fragment surface area per milliliter spoil water, D_W is the diffusion rate of O_2 in water, where O_2 concentration is expressed as mole fraction and 101 kPa (1 atmosphere) total pressure is assumed, Y_{O_2} is the mole fraction of O_2 at the film surface (the O_2 concentration at the fragment/bacterial surface is set equal to 0.0), and $\Delta\ell'$ is the film thickness. Rearranging Eq. [36]

$$K_B = \frac{4000 \; A_F D_W}{\Delta\ell' [Fe^{2+}]} \qquad [37]$$

For $\Delta\ell' = 0.01$ cm (ElBoushi, 1975) and $D_W = 2.75 \times 10^{-11}$ moles O_2-$cm^{-1}sec^{-1}$, the upper limit of K_B can be calculated for any pyrite and fragment content. Between the upper and lower limits, the magnitude of K_B is found from the bacterial "activity," which depends on the energy available to the bacteria.

$\underline{K_B}$. The primary concern of this model is the long term (e.g., months) leaching of stripmined lands. Since on this time scale bacterial population fluctuations are comparatively rapid, we can consider the bacterial "activity" to be in dynamic equilibrium with the environment at all but initial times. It is also desirable to include the effects of the bacterial "activity" directly without

having to be concerned with the exact population size and metabolic kinetics. Most bacterial models are thus of little use to us since they are concerned with population size or growth rate (Lacey and Lawson, 1970; Schaitman, et al., 1969; Landesman, et al., 1966; Lundgren, 1975). Instead, we must devise a scheme that accounts for the activity of chemoautotrophic bacteria directly.

Treating the bacteria population as a single, idealized organism, we can represent the energy available to the population per unit time, E_A, as being divided into two separate parts. First, the population must obtain sufficient energy in order to maintain its current activity. This maintenance energy, E_M, represents energy required to obtain nutrients from the environment, regenerate cell components, and sustain metabolic porcesses. E_M also includes the energy required to shield each cell in the population from hostile environmental conditions such as too low or too high of a pH or high-salt concentrations. If E_A exceeds E_M then the remainder of the energy available per unit time is put into population growth. The total energy available to the population is partitioned between maintenance needs and growth.

$$E_A = E_M + E_G \qquad [38]$$

An increase in cell numbers will only occur if $E_A > E_M$ and the cells will cease to function or "die" and the population collapse when $E_A > E_M$, where both E_M and E_G have incorporated into them the efficiency with which the specific organisms transfer energy from external sources to internal uses.

The energy requirement of an organism can be related to the rate at which it consumes its energy substrate. Arkesteyn (1980) found that Thiobacillus ferrooxidans serves as the primary autotroph in increasing the oxidation rate of pyrite. These organisms use the energy released from the ferrous-ferric oxidation reaction as their only energy source. He found that the sulfur-oxidizing bacteria were incapable of oxidizing pyrite directly but could use the sulfur released from chemical or T. ferrooxidans induced pyrite oxidation. Therefore, in this model we'll assume that the ferrous-ferric oxidation reaction is the sole energy source for the pyrite-oxidizing autotrophs. If we let R_C represent the rate at which the entire population oxidizes iron (moles of electrons/ unit time) and let ΔG represent the energy released in iron oxidation (energy/mole of electrons) then:

$$E_A = R_C \, \Delta G = E_M + E_G \qquad [39]$$

which, when the population is stable, ($E_G = 0$), reduces to:

$$R_C \, \Delta G = E_M \qquad [40]$$

Since we are assuming that the population can adjust itself rapidly enough to always be in equilibrium with its environment, Eq. [40] should always be true.

We can combine the bacterially dependent terms in Eq. [40] by solving for ΔG:

$$\Delta G = E_M/R_C = E_M' \qquad [41]$$

The magnitude of ΔG can be calculated if we know the iron ion concentrations in the spoil solution. ΔG can be found from:

$$\Delta G = - FE \qquad [42]$$

where F is the Farady and E (volts) is found from the combined Nernst equations for the exchange of one electron in the ferrous iron oxidation and oxygen reduction half-cell reactions at normal pressure.

$$E = 0.46 - 8.6 \times 10^{-5}\ T \ln \left[\frac{\gamma_3 [Fe^{3+}]}{\gamma_2 [Fe^{2+}]} \ \frac{1}{\gamma_1 [H^+] Y_{O_2}^{1/4}} \right] \qquad [43]$$

where γ_1, γ_2 and γ_3 are the activity coefficients for H^+ and Fe^{2+} and Fe^{3+}, respectively. Since ΔG is proportional to the driving force, E, we will consider the two interchangeable and talk of the energy as though it were measured by the driving force, E and thus let $E'_M = E$ at constant cell population size.

The value of E'_M will vary in relation to the environment of the organism, increasing when adverse conditions are encountered. This can be represented by:

$$E'_M = E'_{min} / \prod_{i=1}^{n} x_i \qquad [44]$$

where E'_{min} is the minimum value of E'_M for ideal conditions and x_i represents the inhibiting effect caused by the ith inhibition agent. x_i varies from 1.0 for no inhibition to 0.0 for total inhibition and subsequent cell "death" and population collapse. For <u>T. ferrooxidans</u>, we will consider only 3 inhibition agents. These are defined as:

$x_T \equiv$ Temperature dependence of cell viability. <u>T. ferrooxidans</u> are mesophiles and based on work by Silverman and Lundgren (1959), Landesmann, et al.

(1966), Belly and Brock (1974), Lundgren (1975) and Malouf and Prater (1961), we have assigned the peak cell activity (x_T = 1.0) to be at 28°C, falling to zero at 4°C (Ehrlich and Fox, 1967) and 55°C (Cathles and Apps, 1975). A cubic equation was fit through these points such that

$$x_T = -1.23 \times 10^{-5}\ T^3 - 4.33 \times 10^{-4}\ T^2 + .0657\ T - .255 \qquad 4^oC < T < 55^oC \qquad [45]$$

$$x_T = 0.0 \qquad \text{otherwise}$$

Figure 13a shows the calculated value of x_T versus the normalized cell "activity" data from Belly and Brock (1974), Silverman and Lundgren (1959) and Malouf and Prater (1961).

x_{pH} ≡ T. ferrooxidans are sensitive to pH. At low pH's, cell activity decreases probably due to acid attack of cell membranes. At high pH's, activity also decreases perhaps due to a decrease in efficiency of metabolic processes that are tuned to low pH's. From the work by Silverman and Lundgren (1959), Landesmann, et al. (1966), Schnaitman, et al. (1969), Ehrlich and Fox (1966) and Malouf and Prater (1961), the maximum activity is between pH 2.5 and 4.0. A quadratic expression was fit to the data given by Silverman and Lundgren (1959) and Schnaitman, et al. (1969) and is shown in Fig. 13b. From this data:

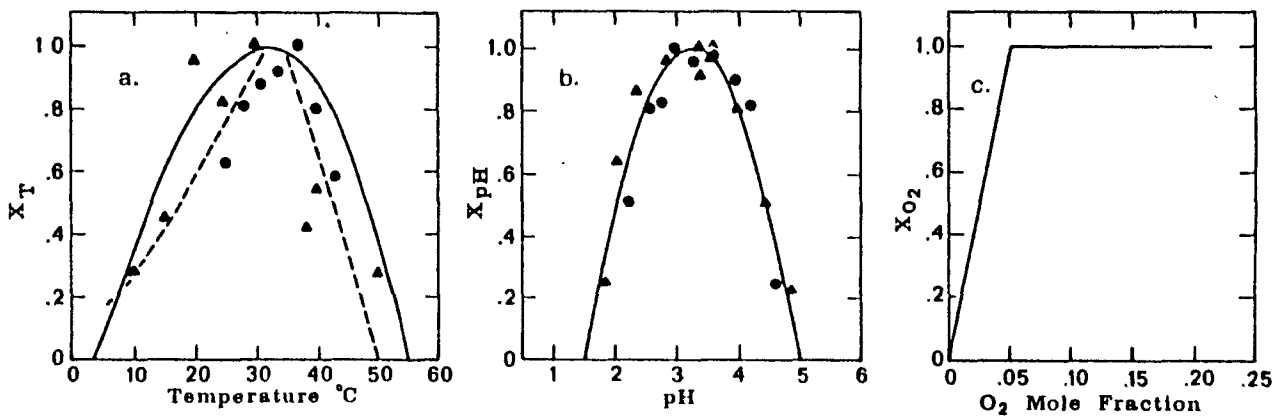

a. b. c.

Figure 13. Plots of the inhibition factors (solid lines). a) x_T versus temperature (^oC); dashed line is normalized data from Malouf and Prater, 1961; (●) normalized data from Silverman and Lundgren, 1959; (▲) normalized data from Belly and Brock, 1974. b) x_{pH} versus pH; (●) normalized data from Silverman and Lundgren, 1959; (▲) normalized data from Schnaitman et al., 1969. c) x_{O_2} versus oxygen mole fraction.

$$x_{pH} = -.348\ pH^2 + 2.26\ pH - 2.66 \qquad 1.54 < pH < 4.95 \qquad [46]$$
$$= 0.0 \qquad \text{otherwise}$$

the maximum ($x_{pH} = 1.0$) occurring at pH = 3.25.

x_{O_2} ≡ Oxygen dependence of chemoautotrophic bacteria. *T. ferrooxidans* are obligate aerobes whose activity ceases when O_2 is depleted. At 25°C, Myerson (1981) found their activity to decline when O_2 concentrations fell below 5% of saturated levels. Thus, at normal atmospheric pressure:

$$x_{O_2} = 1.0 \qquad Y_{O_2} > .01$$
$$[47]$$
$$x_{O_2} = Y_{O_2}/.01 \qquad Y_{O_2} < .01$$

The $x_{O_2} - O_2$ relation is shown in Fig. 13c.

Thus, E_M' can then be written as:

$$E_M' = E_{min}'/(x_T x_{O_2} x_{pH}) \qquad [48]$$

the magnitude of E_M' varying with environmental conditions. At this point, we need to evaluate E_{min}'. No *a priori* relationships seem obvious so instead we must turn to experimental data.

We have found only one report in the literature with sufficient detail to evaluate E_{min}'. Bailey (1968)[4] ran culture experiments with pyrite solutions innoculated with iron-oxidizing bacteria. From his observations of ferric, ferrous and bacterial concentrations as a function of time, we can evaluate E_M'. Initially, his solutions showed

[4]Bailey, J. R. 1968. Biological oxidation pyrite. Unpublished M.S. Thesis, The Ohio State University, Columbus, Ohio.

rapid bacterial growth (doubling time $\sim$ 10 hr), but as the system approached steady state conditions the population stabilized, in agreement with our model, and remained fairly constant thereafter ($\Delta G = E_M'$).

Analysis of the results of Bailey (1968)[4] are shown in Tables 10 and 11. The experimental results are divided into two phases. Phase 1 represents the growth phase of the bacterial population when $\Delta G > E_M'$, while phase 2 represents the steady state condition when $\Delta G = E_M'$. To evaluate for E_{min}', the data from the second phase of the experiment was used to calculate E and E_M' from Eq. [43] and to find x_T, x_{O_2} and x_{pH}. E_{min}' was then found by rearranging Eq. [48]. The average value for E_{min}' from eight measurements during phase 2 was 0.173 volts (Table 10). This value was then used with the data from phase 1. Table 11 shows the analysis of the results from five measurements during the intial growth phase. The values for E_M' were calculated by correcting the value for E_{min}' found in Table 10 for x_T, x_{O_2} and x_{pH}. Values for ΔG were found from Eq. [43]. E_G' is the difference between ΔG and E_M', in each case $E_G' >$ 0.0 indicating that a surplus of energy is available for population growth. The last column in Table 11 shows the normalized growth rates of the bacteria. Comparing the last two columns, we find that the growth rate is roughly proportional to the surplus energy, E_G (especially after 224 hours) which is consistent with our simple growth model.

Table 10. Measured E_M' values and calculated x_T, x_{O_2}, x_{pH} and E_{min}' values from Phase II of experiment by Bailey (1968).[4]

hr	pH	x_T	x_{O_2}	x_{pH}	E_M'	E_{min}'
593	3.10	.80	1.0	1.00	.224	.179
639	3.05	.80	1.0	.996	.231	.184
688	2.95	.80	1.0	.979	.202	.158
758	2.85	.80	1.0	.954	.230	.175
833	2.80	.80	1.0	.940	.223	.168
880	2.80	.80	1.0	.940	.209	.157
929	2.80	.80	1.0	.940	.249	.187
1002	2.70	.80	1.0	.905	.240	.173
					Ave. =	.173

Table 11. Measured and calculated coefficients for the bacterial "activity" model from Phase I of experiment run by Bailey (1968)[4].

hr	pH	x'_T	x_{O_2}	x_{pH}	ΔG	E'_M †	E'_G ‡	RR §
224	3.71	.800	1.00	.935	.312	.231	.081	0.42
362	3.90	.800	1.00	.861	.301	.251	.050	1.00
412	3.50	.800	1.00	.987	.258	.219	.039	0.55
439	3.40	.800	1.00	1.00	.233	.216	.017	0.39
459	3.35	.800	1.00	1.00	.226	.216	.009	0.26

† E'_M is calculated based on E'_{min} of 0.173.

‡ $E_G = E_A - E_M$.

§ RR is the measured normalized growth rate of the bacterial population.

On the basis of this model of bacterial growth, we can calculate the ferric/ferrous ratio at any time and for any conditions by rearranging Eq. [43] and by using Eq. [48] to calculate E_M'.

$$\frac{[Fe^{3+}]}{Fe^{2+}} = \frac{\gamma_2\gamma_1}{\gamma_3} [H^+] Y_{O_2}^{1/4} \exp[\frac{.46-E_M'}{T\ 8.8 \times 10^{-5}}] \qquad [49]$$

The actual oxidation rate of Fe^{2+} by bacteria must be such that Eq. [49] is satisfied. That is the valueof K_B in Eq. [35] is adjusted such that the ferric/ferrous ratio calculated in Eq. [49] is met.

To extend the model of pyrite oxidation beyond steady-state conditions of bacterial population "activity", allowances for population growth and decline must also be included. Population growth is modeled by allowing the "activity" (K_B) to double every 12 hours if conditions are favorable (e.g., $\Delta G > E_M'$). This compares to the doubling times for population size found by Bailey (1968)[4] of between 7.5 and 51 hours. When environmental conditions deteriorate in relation to sustaining population size, the population "activity" is assumed to respond instantly and K_B decreases.

Chemical Species

Chemical species that are followed in the model include H^+, Fe^{2+}, Fe^{3+}, SO_4^{2-}, HSO_4^- and the complexes of ferric iron. Concentrations for each are calculated using the activity coefficient for the ion as calculated by the Davies equation (Davies, 1967, p. 60).

$$\gamma_i = \exp\left[-0.5\ z_i^2 \left[\frac{I^{1/2}}{1+I^{1/2}} - 0.3I\right]\right] \qquad [50]$$

which is satisfactory for ionic strengths less than about 0.3 moles/kg.

Ferric Precipitation. The precipitation and complexation of ferric iron must be considered. One such step, is the precipitation of ferric hydroxide:

$$Fe^{3+} + 3H_2O \rightarrow Fe(OH)_{3_c} + 3H^+ \qquad [51]$$

The change in standard free energy per mole of electrons for this reaction is $\Delta G_R^o = -210.kJ$ and thus is spontaneous as written. The equilibrium concentrations of Fe^{3+} can be calculated from this reaction, but the very low values for ferric concentration don't agree well with measured values from acid-mine drain-waters (Nordstrom, et al., 1979), when crystaline forms of iron hydroxide are used. This is probably due to one of two factors, either the kinetics of the above reaction have not been considered and may be slow or the crystaline form of $Fe(OH)_3$ may not be the controlling species for Fe^{3+} solubility. Amorphous $Fe(OH)_3$ or some other species may instead be the control (Langmuir and Whittemore, 1971).

Fresh solutions can be significantly supersaturated with respect to ferric hydroxide precipitates (Langmuir, 1971), but this seems to be primarily a function of nucleation kinetics. In strip mines, where nucleation surfaces are abundant, precipitation of ferric hydroxide would not be a problem. Analysis of acid-mine drain-waters has, in fact, shown this to be true (Nordstrom, et al.,

(1979), the waters seldom being supersaturated with respect to $Fe(OH)_{3\ amor}$:

$$Fe(OH)_{3\ amor} + 3H^+ \rightarrow Fe^{3+} + 3H_2O \quad \log K_{sp} = 4.9 \qquad [52]$$

We can thus assume that $Fe(OH)_{3\ amor}$ controls the Fe^{3+} concentration and that the kinetics are sufficiently fast to assume constant equilibrium. However, we must also account for the strong complexing characteristics of ferric iron.

Ferric Complexes. As can be seen from Eq. [52], ferric iron concentration when in equilibrium with amorphous ferric hydroxide is extremely pH dependent and is practically insignificant at pH's > 4. Yet many measurements of total ferric iron concentrations exceed the calculated values (Bailey, 1968[4]; Pionke, et al., 1980). This is primarily due to ferric complexes. Ferric iron complexes strongly with hydroxides and sulfates, which can raise the aqueous concentration of Fe^{3+} a hundred to a thousand times at moderate pH's (pH $\sim$ 5). Thus, the complexed forms of ferric iron must be accounted for.

Another reason we must take account of iron complexes is that in most kinetic studies of pyrite oxidation or bacterial catalysis of ferrous iron, ferric complexes have been ignored and values reported as Fe^{3+} concentrations, are in reality, total aqueous Fe^{3+}, Fe_T^{3+}. Thus, the reaction kinetics are based on total dissolved ferrous iron not just the Fe^{3+} ion.

For calculating the pyrite oxidation rate in this model, the Fe_T^{3+} concentration in solution is used in the rate expressions.

Fe_T^{3+} is found in one of two ways. If the hydroxide solid is present Eq. [52] is used to calculate the ferric iron concentration from which the concentration of the complexes can be found. The solid iron hydroxide is then adjusted for changes in total dissolved iron minus pyrite dissolution. If no solid hydroxide is present, the dissolved iron species are adjusted so that the mass balance is preserved and the species are in equilibrium with each other. The complexes considered in this model and their equilibrium constants are shown in Table 12.

Removal of Reaction Products

The dissolved products of the pyrite and bacterial-oxidation reactions must be removed from the spoil profile. Two possible methods exist for H^+ removal; acid neutralization with a possible increase in reserve acidity and leaching by deep percolation. For sulfate and iron, only leaching is assumed to remove the ions from the profile.

Acid Neutralization. Acid produced by pyrite oxidation may be neutralized or modified by the surrounding rock matrix or gangue material (Rogowski, et al., 1977). These H^+ - gangue reactions appear to be quite significant. Lovell, et al., (1978) found that *in situ* neutralization reactions were significant in all three mine sites they studied, effectively removing all of the acidity in two of the sites. Although not of the same magnitude, considerable neutralization and transformation to reserve acidity was observed in a small column-leaching study (Pionke, et al., 1980).

Table 12. Iron complexes and log of the equilibrium constants for their formation and for sulfuric acid dissociation and amorphous ferric hydroxide precipitation.

Reaction	logK	Reference†
$H_2O+Fe^{3+} \leftrightarrow Fe(OH)^{2+}+H^+$	- 2.94	1
$2H_2O+Fe^{3+} \leftrightarrow Fe(OH)_2^+ + 2H^+$	- 5.70	1
$2H_2O+2Fe^{3+} \leftrightarrow Fe_2(OH)_2^{4+} + 2H^+$	- 5.22	1
$3H_2O+Fe^{3+} \leftrightarrow Fe(OH)_{3\,aq} + 3H^+$	-12.	2
$4H_2O+Fe^{3+} \leftrightarrow Fe(OH)_4^- + 4H^+$	-21.60	2
$Fe^{3+}+HSO_4^- \leftrightarrow FeHSO_4^{2+}$	0.60	1
$HSO_4^- \leftrightarrow H^+ + SO_4^{2-}$	- 1.14	1
$3H^+ + FeOOH + H_2O \leftrightarrow Fe^{3+} + 3H_2O$	4.9	3

†References refer to: 1) Sapieszko, et al., 1977; 2) Baes and Mesmer, 1976; and 3) Nordstrom, et al., 1979.

Although not reported in the study, approximately 10% and 20% of the H^+ formed from pyrite oxidation was consumed by neutralization and transformation to reserve forms of acidity (mostly aluminum), respectively (H. B. Pionke, personal communication). Column studies by Braun, et al., (1974) have shown similar results.

Carbonates may be very reactive with H^+ and are capable of maintaining the water percolating through them at pH's near neutrality (Freeze and Cherry, 1979). The carbonate-H^+ reaction is treated separately from other gangue-H^+ reactions because of this large neutralization capacity and because of their use as liming materials on reclaimed stripmines. The reaction of carbonates with H^+ is assumed to be controlled by the chemical kinetics. The rate of carbonate consumption per unit area of carbonate can be described by (Wentzler, 1977).[5]

$$Q_c = - K_c \; [H^+] \qquad [53]$$

where Q_c is the rate of carbonate consumption (moles-sec^{-1}-cm^{-2}) and K_c the first-order rate constant (2.9×10^{-6} L/cm^2-sec). Assuming the carbonate is in the form of distinct, pure fragments that dissolve completely with time, we can describe the consumption of carbonate mathematically in a manner similar to the consumption of pyrite [Eq. 23] but without the diffusional control term (t_D). For spherical particles, Levenspiel (1972) gives the rate of change of the fraction of carbonate sphere remaining, X_c, to be:

[5]Wentzler, T. H. 1977. A study of the interactions of limestone in acid solutions. Unpublished M.S. Thesis, The Pennsylvania State University, University Park, Pa.

$$dX_c/dt = \frac{3\ X_c^{2/3}\ K_c[H^+]}{\rho_c\ R_s} \qquad [54]$$

where ρ_c is the molar density of the sphere and R_s its original radius. The rate of carbonate consumption and thus H^+ consumption can then be calculated from Eq. [54] and the number of carbonate fragments per volume.

Reactions between H^+ and other gangue minerals that need to be considered include neutralization of H^+ to form weak acids, such as orthoclase reacting to form kaolinite (Birkeland, 1974, p. 61).

$$\underset{\text{(orthoclase)}}{2KAlSi_3O_8} + 2H^+ + 9H_2O \rightarrow \underset{\text{(kaolinite)}}{H_4Al_2Si_2O_9} + 4H_4SiO_4 + 2K^+ \qquad [55]$$

or the exchange of H^+ for other cations on clay colloids and oxides. Reserve acidity in the form of aluminum and aluminum hydroxides may also serve as a sink for hydrogen. In general, the amount of pH modification caused by the gangue would depend on the mineralogy and pH. For this model a simple empirical relation was used to partition the H^+ produced into active solution-H^+ and combined neutralized- or reserve--H^+. The relation has the form:

$$\Delta H^+ = \Delta H_R^+\ (1.0 - \exp\ (G_B(G_A - pH))\ ) \qquad [56]$$

where ΔH_A^+ and ΔH_R^+ are the actual increase in free H^+ and the amount of H^+ produced by all the remaining reactions respecively, and G_A and G_B are empirical constants. G_A has the physical significance that when the solution pH equals G_A all the H^+ produced is consumed by the gangue and the pH remains constant. G_B is a scaling factor which determines the rate at which the condition of constant pH is

approached. The shape of the neutralization curves used in this study are shown in Fig. 14.

Leaching. Water percolating through the reclaimed-spoil profile will flush the oxidation products out of the profile. Intuitively, it would seem unrealistic to assume that Darcy type flow governs the movement of water in coarse-spoil material. Indeed, ElBoushi (1975), measuring infiltration into coarse-stone rubble, and Rogowski and Weinrich (1981), modeling infiltration into reconstructed-spoil profiles, have demonstrated the shortcomings of Darcy's Law for describing water movement in coarse materials. In addition, since it is assumed in this model that the water content of the spoil remains constant over time, infiltration studies like those quoted above are of limited help here. Considerable progress has been made in understanding and modeling the leaching of coarse materials (Rao, et al., 1980 a and b), but such treatments are beyond the intent of this model where only a simple removal mechanism of solutes is desired.

Instead, we first recognize that the model will be solved by finite-difference techniques and therefore divide the spoil profile into a number of horizontal layers. Within each layer, the water is assumed to be completely mixed and homogeneous, which represents a major simplification of the leaching process. In strongly structured soils, it has been shown that infiltrating water can penetrate very deeply in a short time with very little or no interaction with the intervening soil layers (Quissenberry and

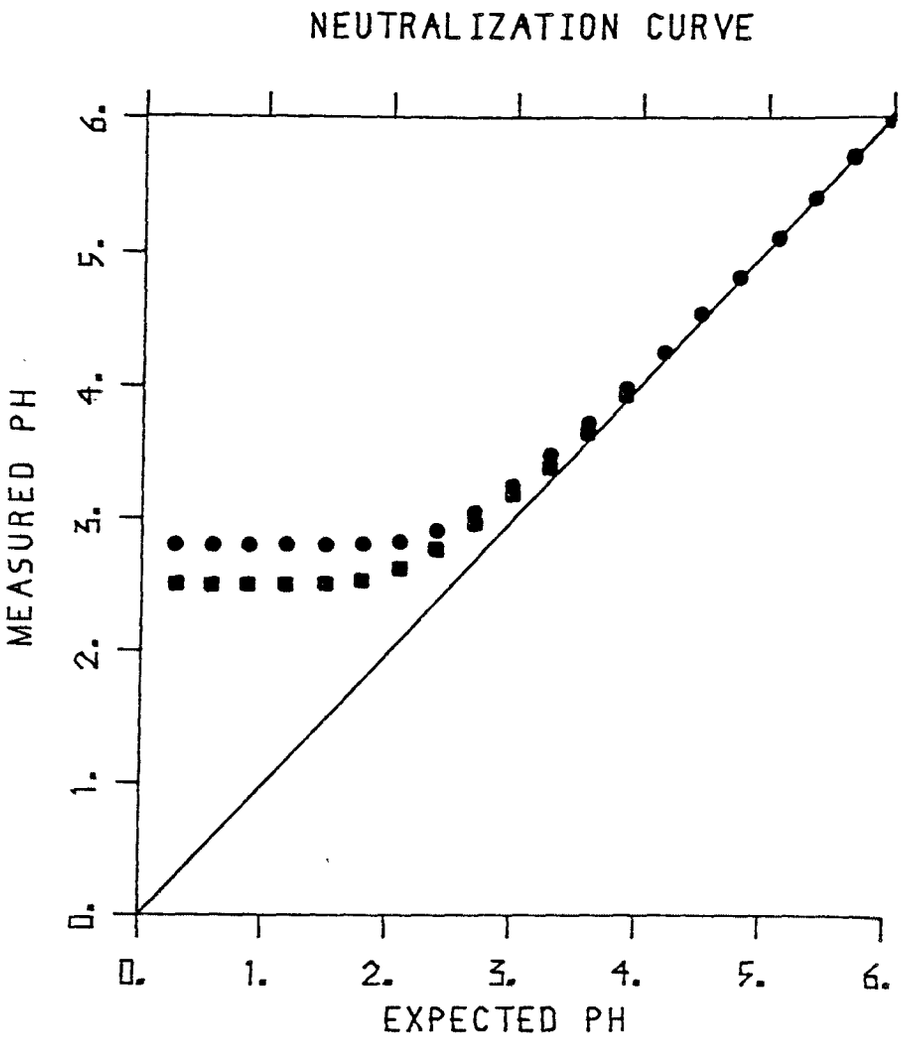

Figure 14. Neutralization curves as calculated from equation in text. G_B equals 1.0 in both plots. G_A equals 2.5 in plot 1 (■) and 2.8 in plot 2 (●).

Phillips, 1976; Bouma and Dekker, 1978). Incorporating this phenomena into the leaching process, we assume that water leaving any layer is partitioned to the underlying layers in proportion to the inverse of the distance separating them, 1/d. Water traveling between two layers does not interact with the intervening layers.

For an n layer system, water infiltrating the surface is partitioned among all layers proportional to the inverse of the depth to the layer (the distance is measured from the surface to the center of the layer). The fraction of infiltrating water entering any layer, i, is:

$$\text{fraction} = 1/d_i / \sum_{j=1}^{n} 1/d_j \qquad [57]$$

Water leaving any layer will also be partitioned proportional to 1/d to the underlying layers. The fraction entering any layer j from layer i where layer 1 is at the surface is:

$$\text{fraction}_{i \to j} = 1/(d_j - d_i) / \sum_{k=i+1}^{n} 1/(d_k - d_i) \qquad [58]$$

The amount of water leaving any layer is equal to the amount entering, which is just the sum of all the fractional contributions from overlying layers, the 0 layer indicating surface precipitation:

$$\text{outflow}_j = \sum_{i=0}^{j-1} [1/(d_j - d_i) / \sum_{k=i+1}^{n} 1/(d_k - d_i)] \text{ outflow}_i . \qquad [59]$$

H^+, Fe^{2+}, total sulfur, total dissolved ferric iron, and the acid-neutralization products are carried with the percolating water and leached from the mine profile. The chemical load entering any layer is equal to the sum of water coming from each overylying layer

multiplied by the species concentration in the layer. The amount of each constituent leaving a layer is just the concentration of the species in the layer multiplied by the outflow.

An example of leaching as described by Eq. [58] is shown in Fig. 15. The figure shows the normalized concentration of a non-interacting solute in the water leaving a 10-meter deep profile that is divided into 20 layers. The profile has a water-filled pore volume of 0.13 and the water is infiltrating at a constant rate of 50 cm/year. The initial and boundary conditions for the solute concentration are:

$$\begin{aligned} C_i &= 1.0 \qquad 1 < i < 20;\ t = 0.0 \\ C_{in} &= 0.0 \qquad t > 0.0 \end{aligned} \qquad [60]$$

Figure 15 shows a considerable smearing of the solute front, with the concentration slowly tailing off to zero after more than 3 pore-volumes have passed through the profile. The method of inverse weighting of water flow between layers mimics a system where diffusion - dispersion processes are of considerable magnitude (Rose, 1977).

Solution Method

Equations [27], [28], [30], [31], [34], [35] and [49] serve as the basis of a model for describing *in situ* pyrite-oxidation. Equations [53], [56], [59] and the expressions listed in Table 12 are used to adjust the concentrations of each species and calculate the leaching rate of the reaction products, where water is assumed to

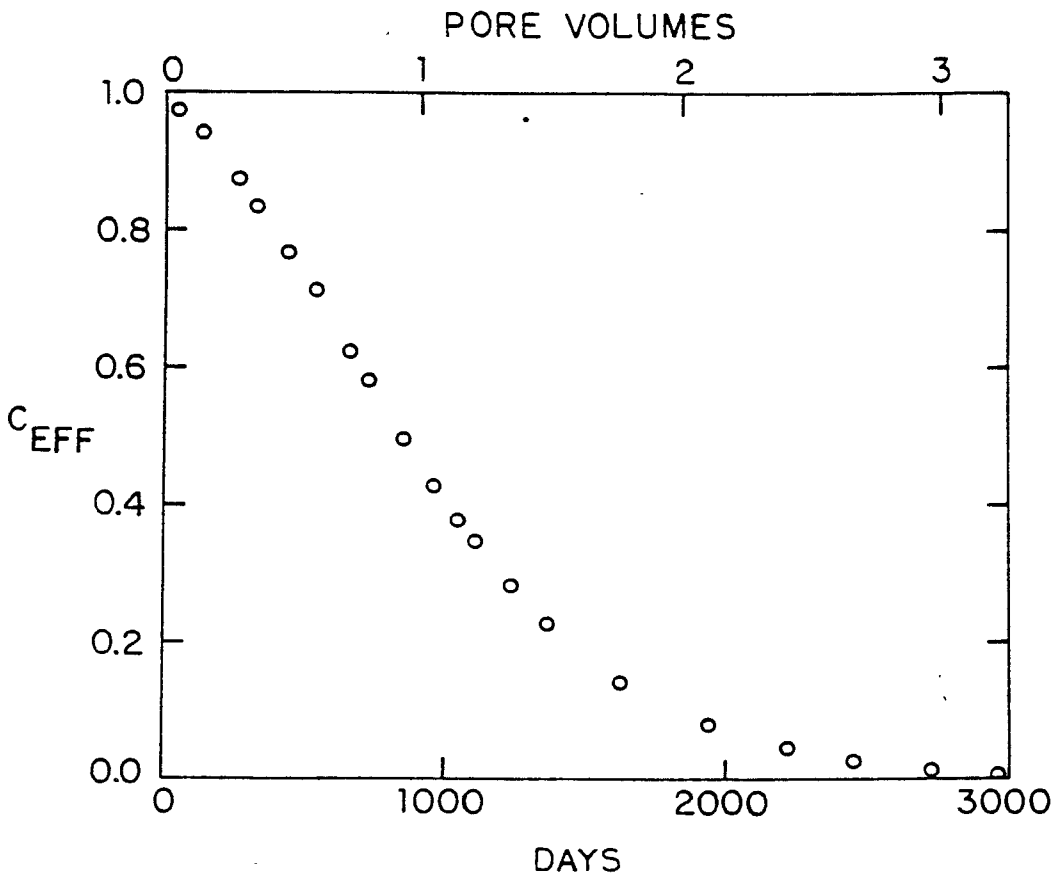

Figure 15. Example leaching curve showing the normalized concentration versus water-filled pore volumes. Profile was 10 meters deep, divided into 20 layers with a water-filled pore volume of 0.13 and an infiltration rate of 50 cm/year.

move downward only at a uniform annual rate. For air movement in the vertical direction only, Eq. [27] is a nonlinear, nonhomogeneous, parabolic equation. Equation [27] can be solved using an implicit, finite-difference technique in which the reclaimed-mine profile is divided into N horizontal layers.

The solution of these series of equations is very unstable due to the complicated interdependence of the variables and to the non-linear form of some of the equations (e.g., Eq. [49]. The solution procedure involved estimating values for all of the variables at time $t + \Delta t$, calculating the diffusion coefficients and source/sink terms from Eq. [28], [30], [31], [34] and [35] and then solving Eq. [27]. The calculated values for the O_2, CO_2, Fe^{3+}, Fe^{2+} and H^+ concentration were then used to recalculate the diffusion coefficients and source/sink terms and Eq. [27] was solved again. This procedure was repeated until the values for O_2, CO_2, Fe^{3+}, Fe^{2+} and H^+ concentrations had converged. Values for K_B and the leaching rates of each chemical species were then updated for $t + \Delta t$ and the entire process repeated a maximum of 25 times or until all values had converged. The iterative scheme has proven to be stable and capable of handling large ($\sim$ 6 months) time steps for all cases studied.

A comprehensive testing of the model, comparing the model results to measured values, was not possible due to the lack of a sufficiently complete data set for an active, oxidizing-leaching pyrate body. However, several simulations were run to determine the

interaction of several parameters in the model and to compare the simulator results to known stripmine behavior. For all simulations, a reclaimed profile, 10 meters deep and divided into 20 equal horizontal layers, was used. Unless otherwise noted, each layer contained 75% (wt/wt) coarse fragments (ℓ = 1 cm), containing a pyrite content of 0.25% (wt/wt) and a 20% water-filled porosity. The bulk density of each layer was 1800 kg/m^3 and a constant water saturation of 70% was used.

At the beginning of each simulation the profile air-space contained 0.21 mole fraction O_2 and 0.0003 CO_2. The spoil water contained 0.28 mg/L Fe^{2+}, 4.8 mg/L sulfate, less than 1 mg/L Fe^{3+} and was at a pH of 5.0. No soluble ferric hydroxide was assumed to be present. These values for dissolved species may be unrealistically low for spoil water in newly reclaimed mine-sites because of the large content of soluble salts in spoil material (Lovell, et al., 1978), but were used so that the formation of oxidation products could be observed more easily. After the pyrite started to oxidize, the water infiltrating the surface of the profile was assumed to be at a pH of 5.0 and contain no dissolved iron, with sulfate at a concentration of 4.8 mg/L. In the simulations where iron-oxidizing bacteria are active, a 32 day "innoculation" period was assumed. During these first 32 days, the bacteria were assumed not to be active. After this time a base "activity" for the bacteria, represented by $K_B = 10^{-15}$, was used. That is, the base rate of ferrous oxidation catalyzed by bacteria was set to less than 0.1% of the minimum chemical oxidation rate of ferrous iron.

Results and Discussion

Two major aspects of the model were investigated. The significance of iron-oxidizing bacteria was studied, since the way in which the model calculates their "activity" from the energy subtrate and environmental conditions is unique. Several other simulations were also performed to illustrate the flexibility of the model and compare the model output to expected behavior.

Role of Iron Oxidizing Bacteria

Since this model is unique in the way that the activity of iron-oxidizing bacteria is accounted for, the effect of bacteria on pyrite weathering as predicted by the model was examined. In the first simulation, Run 1, iron-oxidizing bacteria were assumed not to be active and thus the only source of ferric iron was chemically oxidized ferrous iron. Figure 16 shows the fractional amount of pyrite consumed within the entire profile from 0 days, when pyrite oxidation begins, to 10,000 days or approximately 27 years. The pyrite is consumed slowly, with just over 22% consumed after 10,000 days, the consumption is due almost exclusively to direct O_2 reaction. The ferric iron concentration never exceeds 0.5 μmoles/L at any time in any layer. The rate of pyrite oxidation due to ferric iron is never greater than 0.07% of the direct O_2 pyrite oxidation rate. The rate of pyrite oxidation is slightly faster at initial times, but is virtually constant (slope in Fig. 16 is constant) after 3000 days. A similar trend is observed in Fig. 17, where the rate of total iron

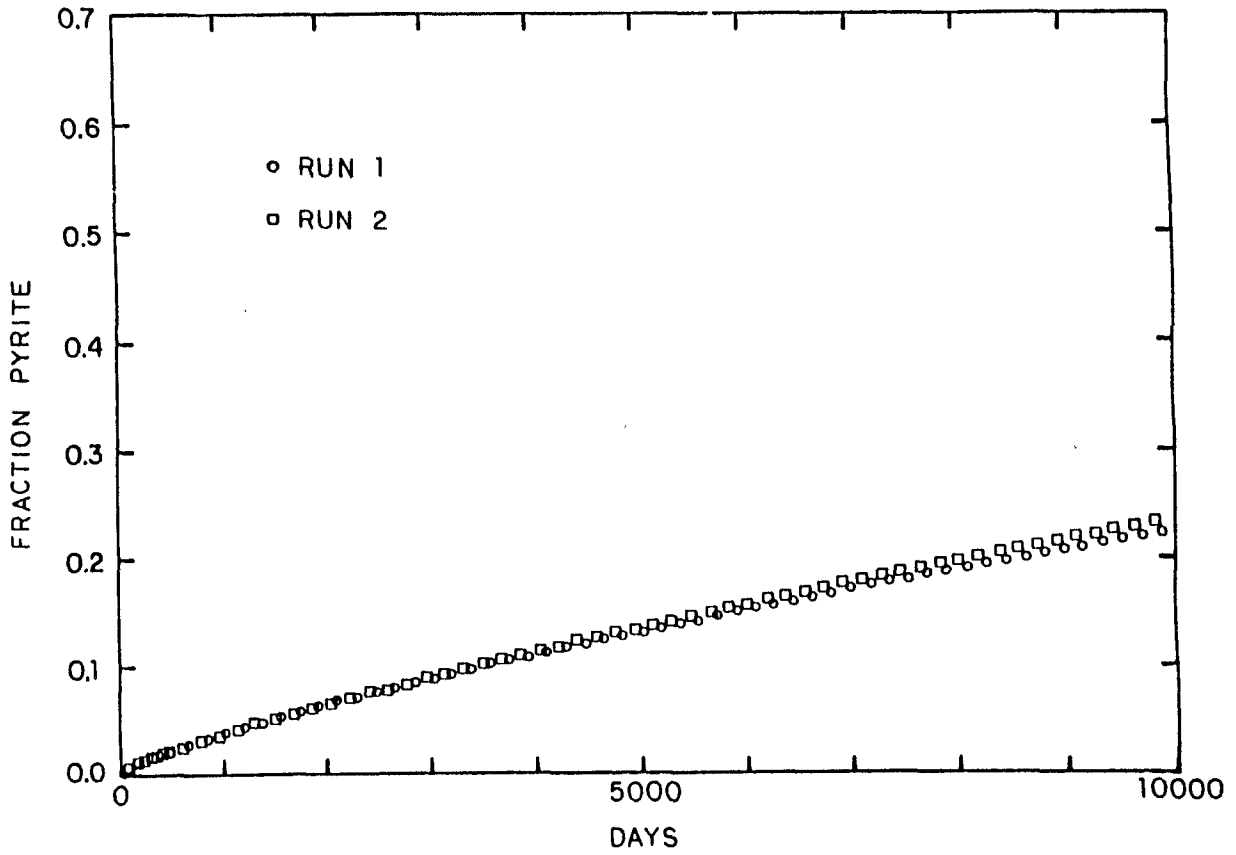

Figure 16. Fraction of pyrite oxidized within entire profile versus time for Run 1 and Run 2.

being leached from the profile (moles/m^2-day) is plotted against time for the 0 to 10,000 day period. A marked peak in the leach rate is observed at 2,100 days (5.75 years), which then levels off slowly to an almost constant value. The average concentration of Fe^{2+} within the profile after 2,100 days of pyrite oxidation is 0.0054 moles/L. The average pH of the spoil water is 1.99. After 10,000 days of weathering, the ferrous iron concentration and average pH of the spoil water are 0.0032 moles/L and 2.22, respectively. While the Fe^{2+} concentrations seem to be well within the range of values found for water samples removed from below a reclaimed stripmine, the pH values appear to be about 0.5 of a pH unit lower than measured values (Rogowski, et al., 1982).

In the second simulation, Run 2, iron-oxidizing bacteria were allowed to interact with the pyrite system as predicted by the model. Figure 16 also shows the amount of pyrite consumed over time for this simulation. The consumption of pyrite is almost identical to the results of Run 1, where no bacteria are active, the relative increase in oxidation being less than 3%, which represents an absolute increase in pyrite oxidation of 0.7% after 10,000 days. The plot for Run 2 in Fig. 17 shows the same behavior, almost no difference is observed in the rate of total-iron removal for Run 1 and Run 2.

The lack of impact by the bacteria in this case is explained by the fact that the pH of the spoil water drops rapidly below 2.6 for all layers after only 200 days and remains between 1.8 and

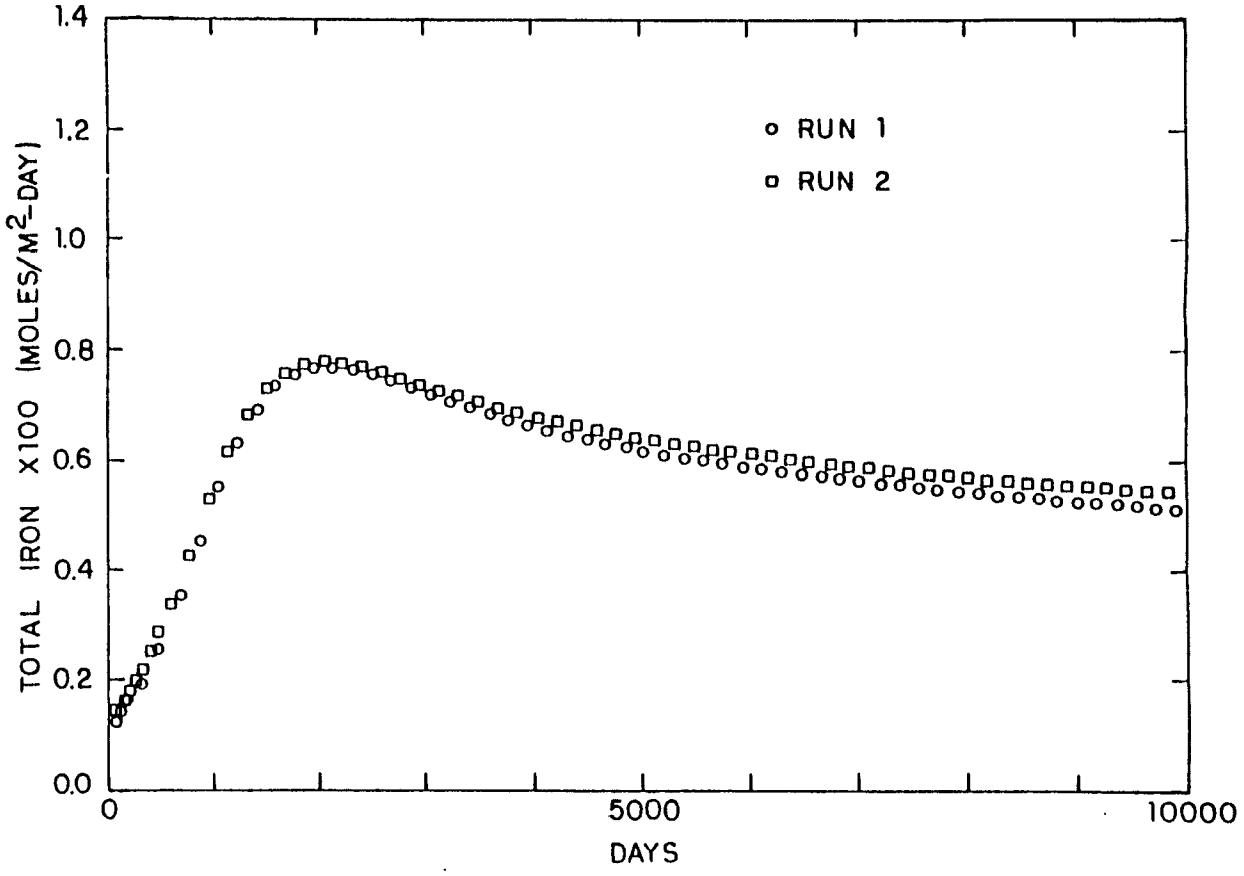

Figure 17. The rate of leaching out of the profile of all iron species versus time for Run 1 and Run 2.

2.3 for most layers for the remainder of the simulation. Examination of Fig. 13b shows that at these lower pH's, x_{pH} drops to between 0.2 and 0.7 indicating decreased "activity" of the bacteria because of adverse H^+ activity and a decreased role for ferric iron - pyrite oxidation. However, it is misleading to believe that the bacteria exert no influence under these conditions. Figure 18 shows the rate of pyrite oxidation (moles/cm^3-sec) as a result of direct O_2 and ferric oxidation for Runs 1 and 2 after 5 years of oxidation. Although the overall rate of pyrite oxidation is similar, in Run 1, O_2 is the only important oxidizer while in Run 2 bacterially produced ferric iron begins to become important in the surface layer, where the pH remains higher due to infiltration of water at pH 5. This increase in ferric iron concentration can also be seen in Fig. 19 where the ferric/ferrous concentration ratio in the water leaving the profile is plotted against time. The ratio is about 100 times greater during Run 2 than during Run 1.

Two additional simulations were run under the same conditions, but where interactions between the acid produced by pyrite weathering and the rock matrix were assumed to occur. Figure 20 shows the fraction of pyrite consumed versus time for these two runs compared to Run 2. In Run 3, the gangue material is assumed to react with H^+ so that the pH never falls below 2.5 (G_A = 2.5). In Run 4, the system is maintained at a pH of 2.8 or above (G_A = 2.8). The H^+ produced by pyrite oxidation, but not assumed to contribute to the

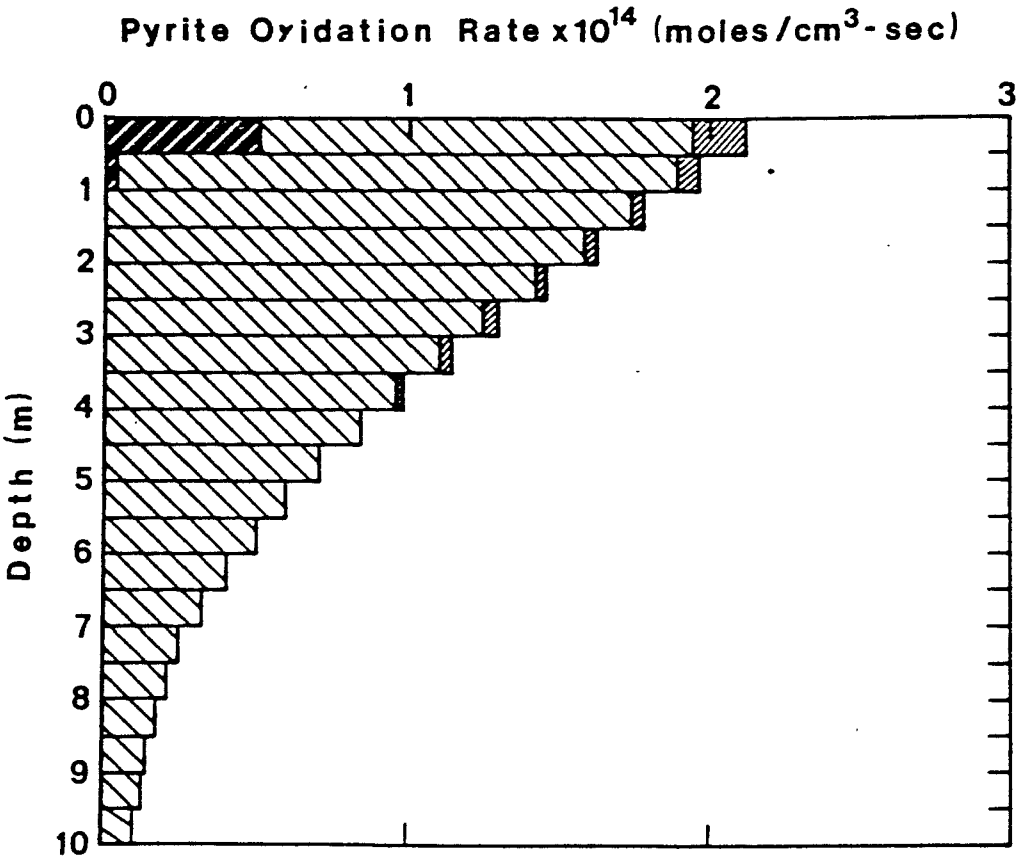

Figure 18. Oxidation rate of pyrite for each layer after 5 years of oxidation. Fine cross-hatching is total oxidation rate for Run 1. Open cross-hatching is rate of oxidation by direct oxygen reaction with pyrite in Run 2. White cross-hatching on black is oxidation rate due to ferric iron reaction with pyrite in Run 2. Below 1 meter, ferric oxidation is negligible. Below 4 meters, oxidation rates of Run 1 and Run 2 are identical

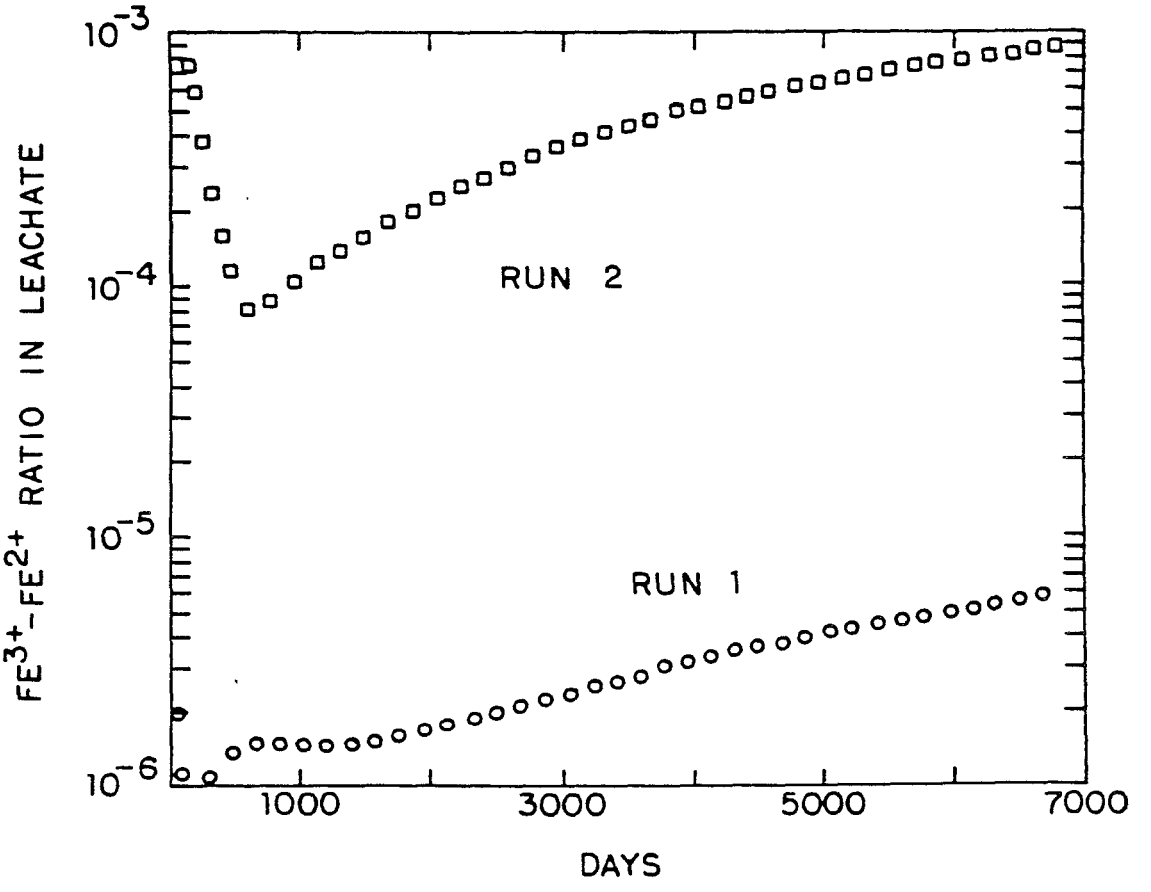

Figure 19. The ratio of ferric iron to ferrous iron in the water leaving the profile for Run 1 and Run 2.

H^+ activity, is represented by the reserve acidity in the spoil solution.

Raising the pH of the system has the effect of increasing the x_{pH} function value and thus increasing bacterial "activity." In Run 3, where the pH is maintained at 2.5 or higher, Fig. 20 shows a considerable increase in the amount of pyrite consumed over time. After 10,000 days, 30.5% of the pyrite is consumed for a relative increase of 36% over the unbuffered, bacterial Run 2. Most of this increase occurs before 2,000 days, after which the rate of pyrite consumption is very similar to Run 2 (plots are parallel). When the system pH is maintained at 2.8 and above, 36% of the pyrite is consumed after 10,000 days for a relative increase of 61% over the unbuffered run. Again, most of this increase over Run 2 occurs before 2,000 days, but the rate of pyrite oxidation continues to be greater than Run 2 or Run 3 as indicated by the continuously diverging plots.

To maintain the pH at 2.5 and 2.8, a considerable proportion of the H^+ formed by Eqs. [18], [19] and [21] must be converted to acidity by reactions with the gangue. In Run 3, 39% of the acid formed from pyrite oxidation is converted to acidity after 10,000 days of oxidation. Again, it should be remembered that in this model the acidity term represents both neutralization and conversion to reserve forms of acidity such as Al^{3+}. In Run 4, 56% of the acid

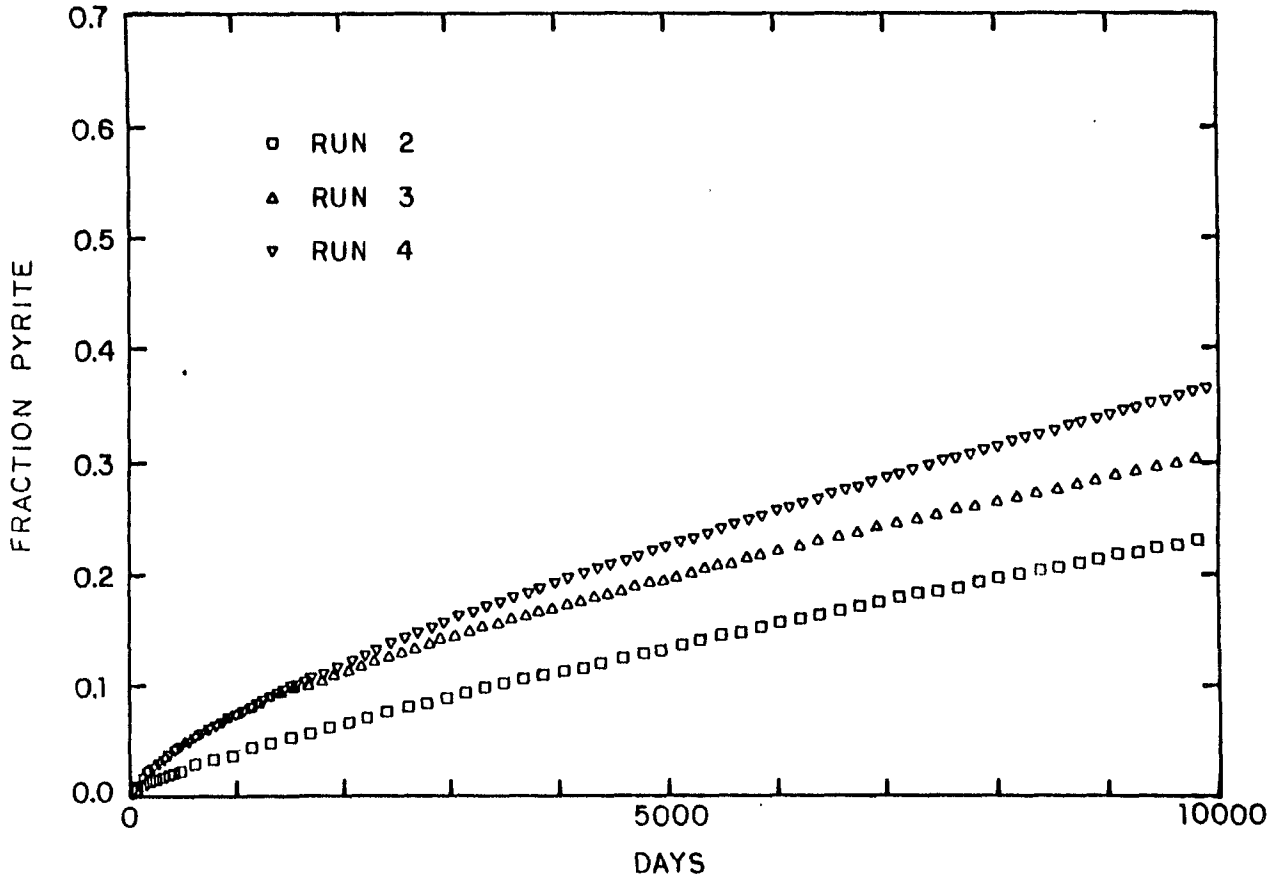

Figure 20. Fraction of pyrite oxidized within the entire profile versus time for Runs 2, 3, and 4.

from pyrite oxidation is converted to acidity in order to maintain the pH at 2.8 or higher. Although these percentages seem high, they certainly fall within the range of observed behavior for strip-mine lands (Lovell, et al., 1978).

Figure 21 shows the rate of removal of total iron over time for Run 3 and Run 4. Run 2 is replotted on this figure for ease of comparison. For Run 3, where the pH is maintained at 2.5 or higher, the peak in the total iron-leaching rate occurs at 1,750 days ($\sim$ 5 years). The rate of leaching is considerably greater than Run 2 throughout most of the simulation, being almost double when the maximum rate is observed. Although greater in magnitude, the shape of the rate vs. time plot for Run 3 is very similar to Run 1 and Run 2, Run 4, however, shows a considerably different behavior. The plot for Run 4, where the pH is maintained at 2.8 or higher, shows a tendency for the rate to reach a plateau value of about 0.0065 moles/m^2-sec and then slowly oscillate around this value while the plateau rate slowly decreases with time. This behavior is due to two factors. As O_2 penetrates a layer at a sufficient rate to permit bacterial activity, the ferric iron concentration increases, which increases the overall rate of pyrite oxidation, which in turn increases the total iron in solution and in the leachate. This process is what is occurring within the 250 to 300 cm layer between 3,300 and 4,000 days in Run 4. A point is reached, however, where the bacterially catalyzed-ferric iron concentration within the

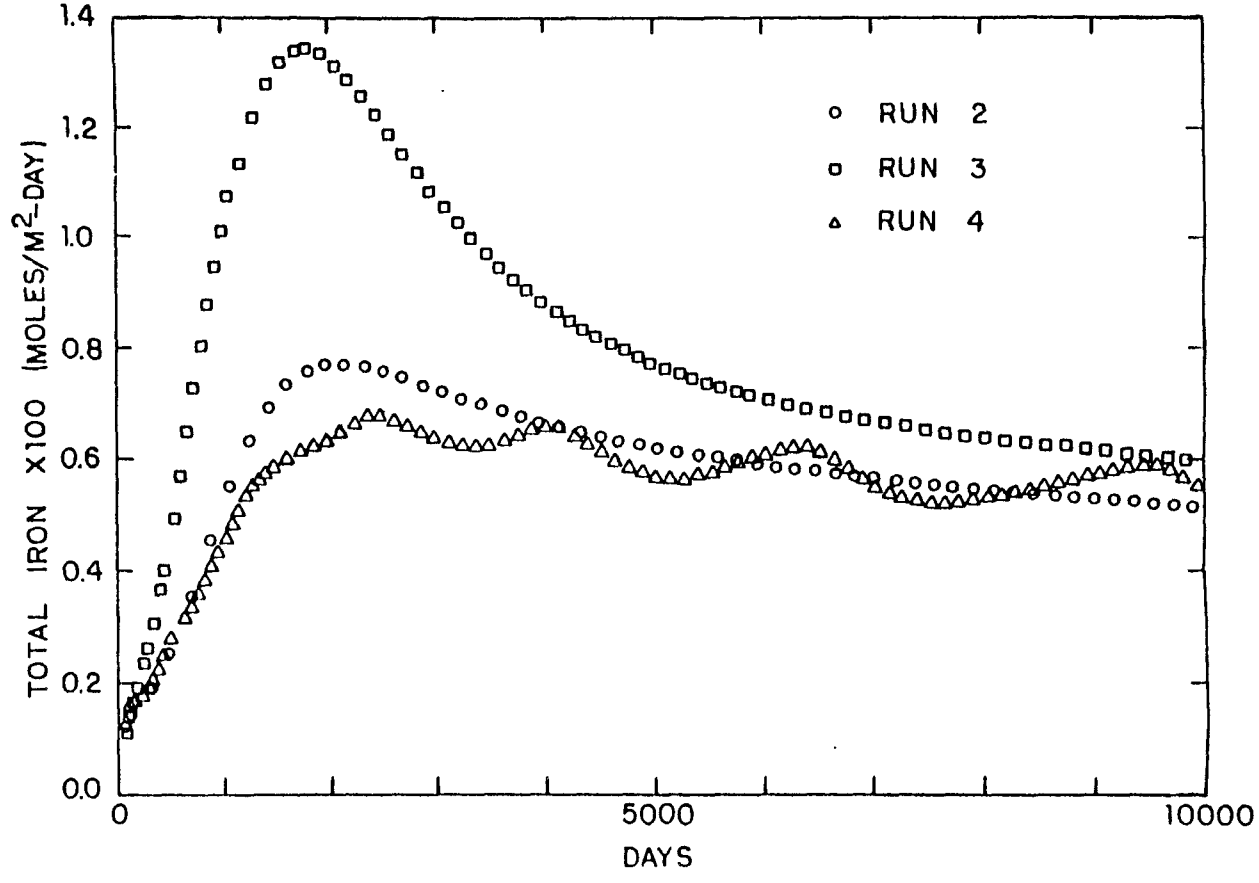

Figure 21. The rate of leaching out of the profile of all iron species versus time for Runs 2, 3, and 4.

layer exceeds the ferric iron solubility as controlled by amorphous ferric hydrooxide at pH 2.8. The ferric iron then starts to precipitate, removing iron from solution and from the leaching water. The rate of leaching then starts to decline because the Fe^{3+} oxidant is maintained at a stable concentration while the pyrite concentration decreases. From Eq. [26], where t_D is greater than t_C (pyrite oxidation rate is controlled by diffusion), it can be seen that as X decreases the rate of pyrite oxidation decreases. This is what is occurring between 4,000 and 5,100 days, where X, for the layer between 250 and 300 cm in which the maximum rate of pyrite oxidation is taking place, decreases from 0.646 to 0.449. After 5,100 days the pyrite concentration in the layer is sufficiently low that the oxidation rate and consumption of O_2 has decreased to a point that increased levels of O_2 are diffusing to the next deepest layer raising that layer's O_2 concentration. The process is then repeated in the deeper layer. The iron concentration in the deeper layer and the profile as a whole and in the leach water starts to increase again. Thus, the oscillating behavior of Run 4 in Fig. 21 is due to the division of the profile into distinct layers, while the constant value of the leaching rate is controlled by the precipitation of ferric iron within the profile when the pH is maintained at 2.8 or higher. This is the first simulation discussed where iron precipitation is observed.

A better indication of the rate of pyrite oxidation and acid leaching for Run 4 compared to Run 3 is shown in Figure 22, where

the total acidity being removed from the profile in the leach water versus time is plotted. The total acidity is the sum of the concentrations in the leachate of H^+, one-half the acidity value calculated from the gangue-H^+ interaction, and three times the ferric iron values. One-half of the acidity value is used in calculating the total acidity in an attempt to partition the gangue-H^+ interaction between neutralization processes and the formation of reserve acidity. As can be seen in Fig. 22, the two plots are of similar shape with the plot for Run 4 indicating an increase in the rate of acid leaching of about 30% over Run 3 after 1,950 days of pyrite oxidation.

One other simulation was run to investigate the response of the bacterial "activity" model. Run 5 was conducted assuming no gangue-H^+ interaction but where the x_{pH} function [47] was lowered one-half pH unit so that the maximum, $x_{pH} = 1.0$, occurred at pH 2.75. This simulation was run because the mathematical form and value of the coefficients in Eq. [48] represent only a first approximation and are not absolute. Differences in bacterial strains, substrate type, and means of measuring bacterial activity may cause discrepancies between the leaching studies cited in estimating the x_i values and bacterial activity within stripmine material. Figure 23 shows the plots of pyrite consumed versus time for Run 5 and Run 3. The plots are of similar magnitude, although buffering the pH at 2.5 or higher results in greater consumption of pyrite at

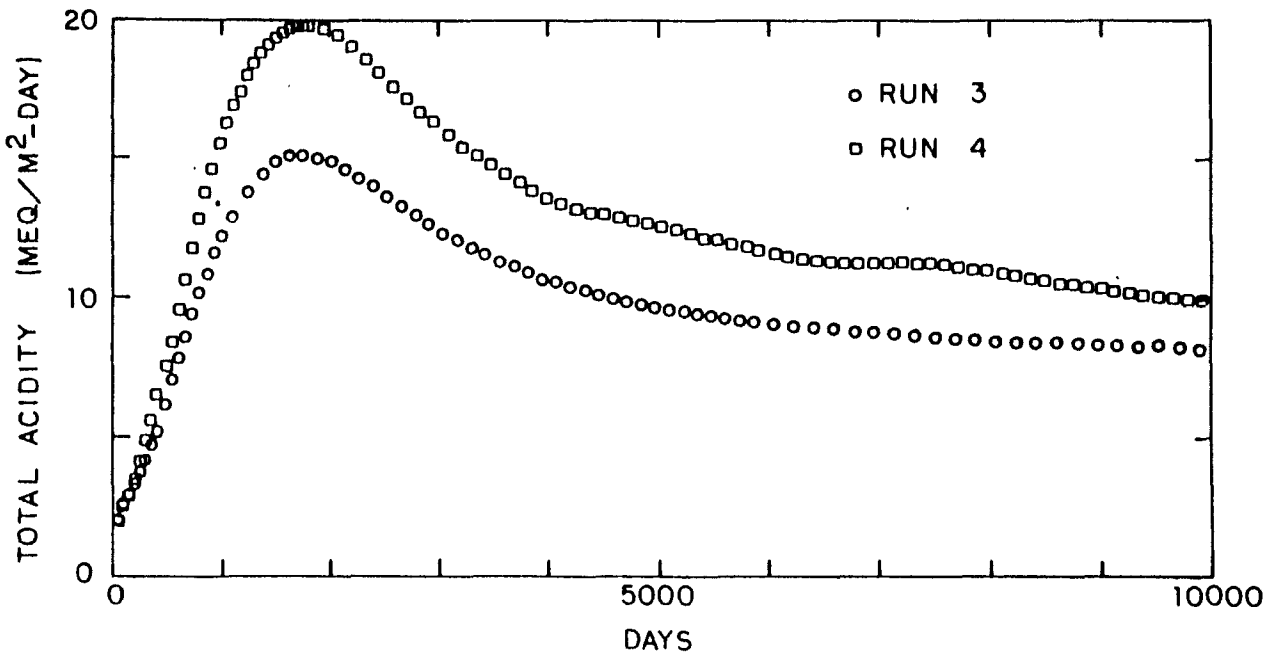

Figure 22. The rate of leaching out of the profile of the potential and active acid for Runs 3 and 4.

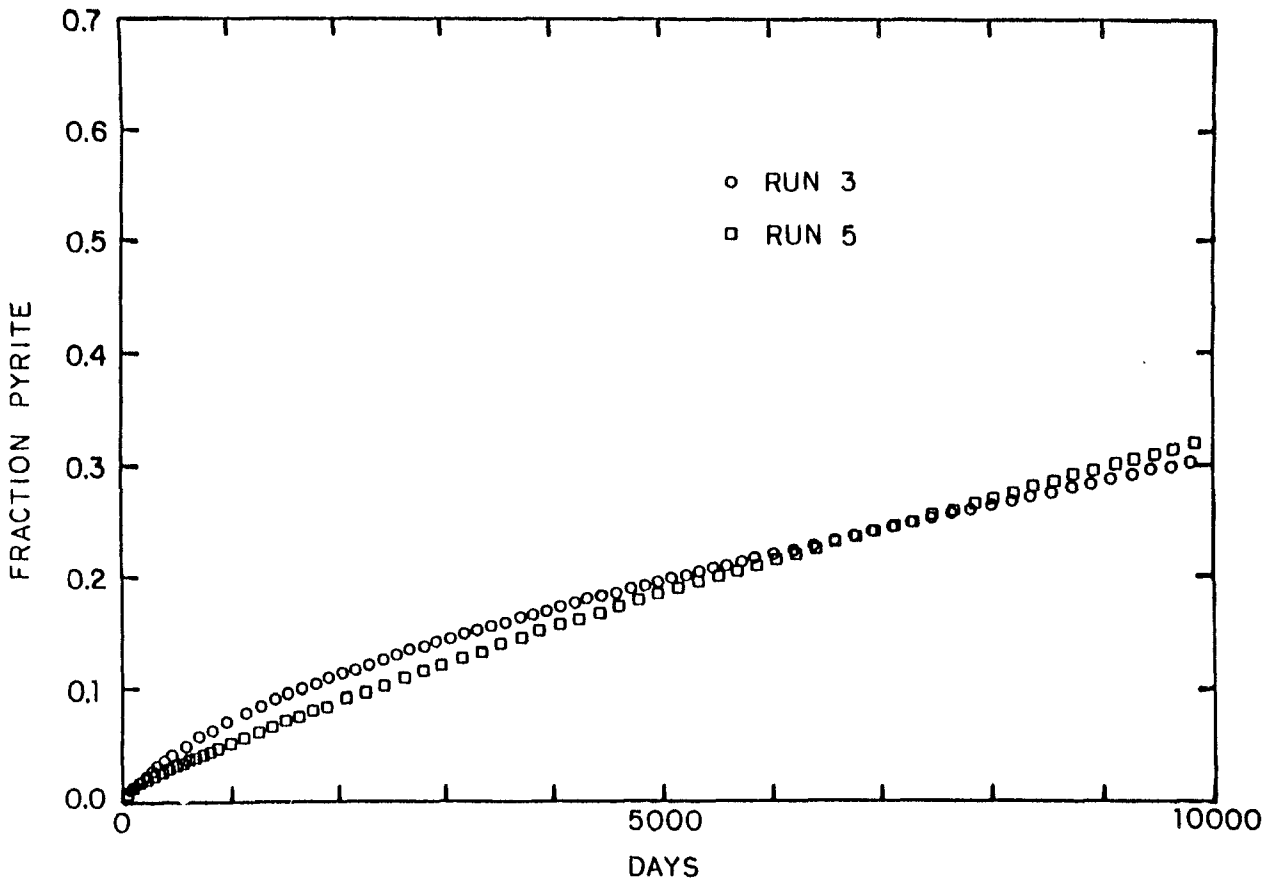

Figure 23. Fraction of pyrite oxidized within entire profile versus time for Run 3 and Run 5.

early times, but less consumption after 8,800 days or after about 28% of the pyrite is consumed.

Runs 1-4 indicate that, at least for the parameters used, the iron-oxidizing bacteria increase the pyrite oxidation rate only if the pH is maintained above ambient levels of interactions with the rock matrix. Removal of H^+ by leaching alone (Run 2), was insufficient in preventing the pH in dropping to levels where the bacterially produced ferric iron only compensates for the loss in direct O_2 pyrite oxidation caused by the drop in O_2 concentrations due to bacterial consumption of O_2. The oxidation rate in Run 4, where the pH is maintained at 2.8 or higher is controlled intermittently by ferric solubility and bacterial "activity," with bacterial "activity" controlling the oxidation rate until the solubility of ferric iron is exceeded. The solubility then controls the oxidation rate until bacteria start to increase in the next deepest layer because of increased O_2 levels.

Model Sensitivity and Versatility

Although it is beyond the scope of this paper to perform an extensive sensitivity analysis of all the parameters in the model or to model all possible management alternatives to reclaiming a given mine profile, several possible combinations of parameters were studied to demonstrate the versatility of the model.

Effective Diffusion Coefficient. Ultimately, the rate of pyrite oxidation can exceed the rate at which O_2 is supplied to the oxidation zone. In this model, O_2 is assumed to be transported through the mine profile by gas diffusion which is very sensitive to the

air-filled porosity and tortuosity of the flow path. To observe the effect of varying the porosity and tortuosity on the results, two simulations were run where the air-filled porosity from Runs 1-5 was doubled and the tortuosity was halved. Examining Eq. [27], it can be seen that this combination results in increasing the effective diffusion coefficient, D_{O_2}, by a factor of 4. In Run 6, iron-oxidizing bacteria are assumed not to be active within the profile, analogous to Run 1. For Run 7, bacteria are assumed to be active as calculated by the model, with the spoil solution pH maintained at a pH of 2.5 or higher (G_A = 2.5). This is comparable to Run 3.

Figure 24 shows the plots for Run 6 and 7 for the consumption of pyrite over time. Run 3 is included for reference. The oxidation of pyrite increases significantly with the increase in the effective diffusion coefficient. Run 6, without the bacteria, shows a significant increase over Run 3, with 40% of the pyrite consumed after 10,000 days. When the bacteria are allowed to be active, Run 7 shows that a very large increase in the amount of pyrite consumed is obtained, with 70% of the pyrite consumed after 10,000 days. This represents a 133% increase in pyrite oxidized over Run 3 and a 75% increase over Run 6. At the reduced air-filled porosity, when bacteria were included at a buffered pH of 2.5 the amount of pyrite oxidized increased by 24% over the case where no bacteria were present (Run 3 compared to Run 1, Figs. 16 and 20). Thus, at the greater air-filled porosity, the effect of bacteria is increased (75% increase in pyrite oxidation versus a 25% increase). The

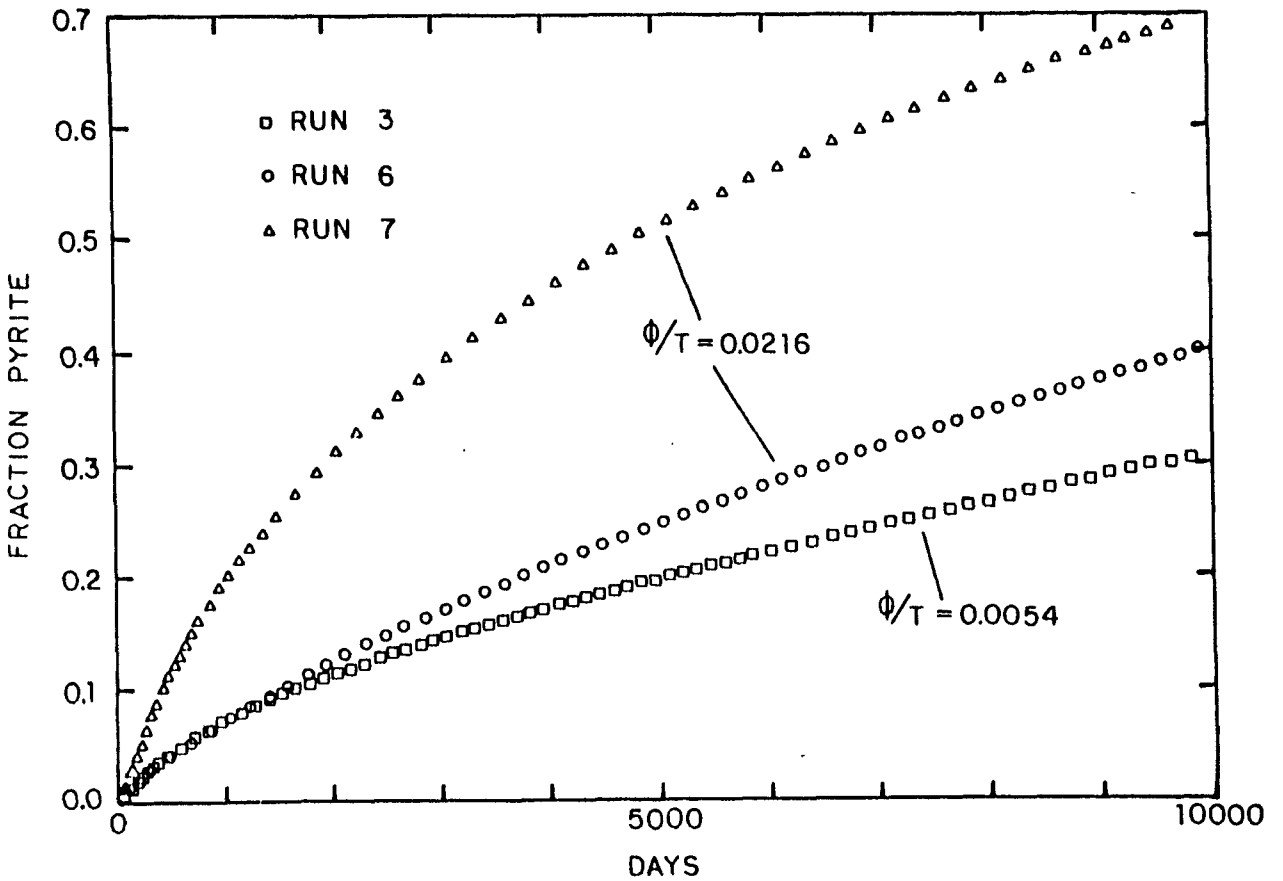

Figure 24. Fraction of pyrite oxidized within entire profile versus time for Runs 3, 6, and 7.

effect of increased pyrite consumption is even greater at early times. After 500 days, 3 times as much pyrite is consumed in Run 7 than Run 6.

The effect of increased diffusion can also be seen in Fig. 25 where the rate of total iron leaching from the profile is plotted against time. The plot for Run 3 is also shown for comparisons with Runs 6 and 7. The leach rate of iron shows a similar pattern over time for the three runs, however, the magnitude is greater at all times for Runs 6 and 7 compared to Run 3. The leaching rate is particularly greater in Run 7 where iron-oxidizing bacteria are present.

The effect of increasing the diffusion rate is perhaps better shown in Fig. 26 and 27 where the O_2 concentration with depth after 1,825 days ($\sim$ 5 years) of pyrite oxidation is plotted. Figure 26 shows Runs 1 and 6 where bacteria are not allowed to be active. O_2 concentrations at the deeper depths are much higher for Run 6. The shape of the curves reflect a process where the consumption term is proportional to the concentration (Kirkham and Powers, 1972). This is in contrast to Fig. 27 where Runs 3 and 7 are plotted. These O_2 profiles show a near linear decrease with depth similar to diffusion through a non-interacting zone to a layer of complete O_2 consumption. O_2 does not penetrate as deeply in the profiles where bacteria are active due to the concentration of pyrite oxidation in the first few layers of high pyrite concentration rather than slower oxidation rates distributed over several layers as is the case when bacteria are not active.

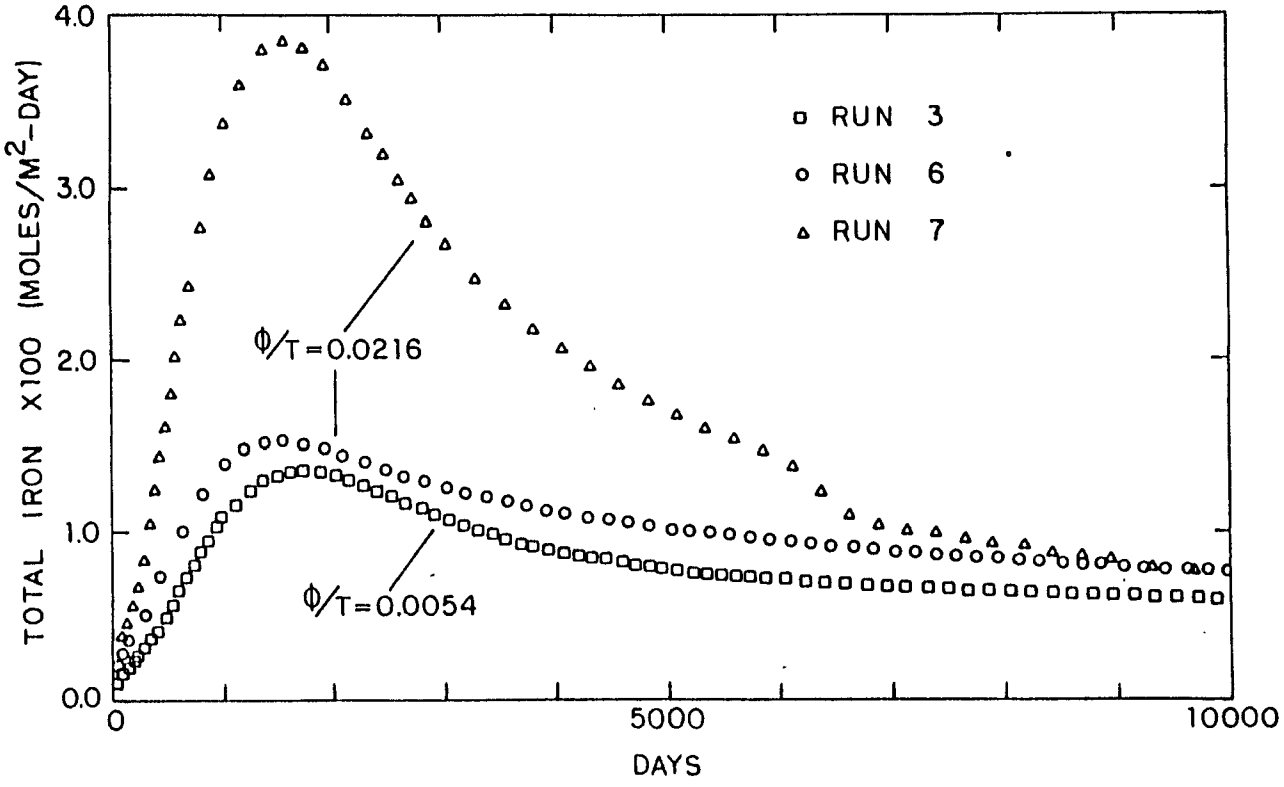

Figure 25. The rate of leaching out of the profile of all iron species versus time for Runs 3, 6, and 7.

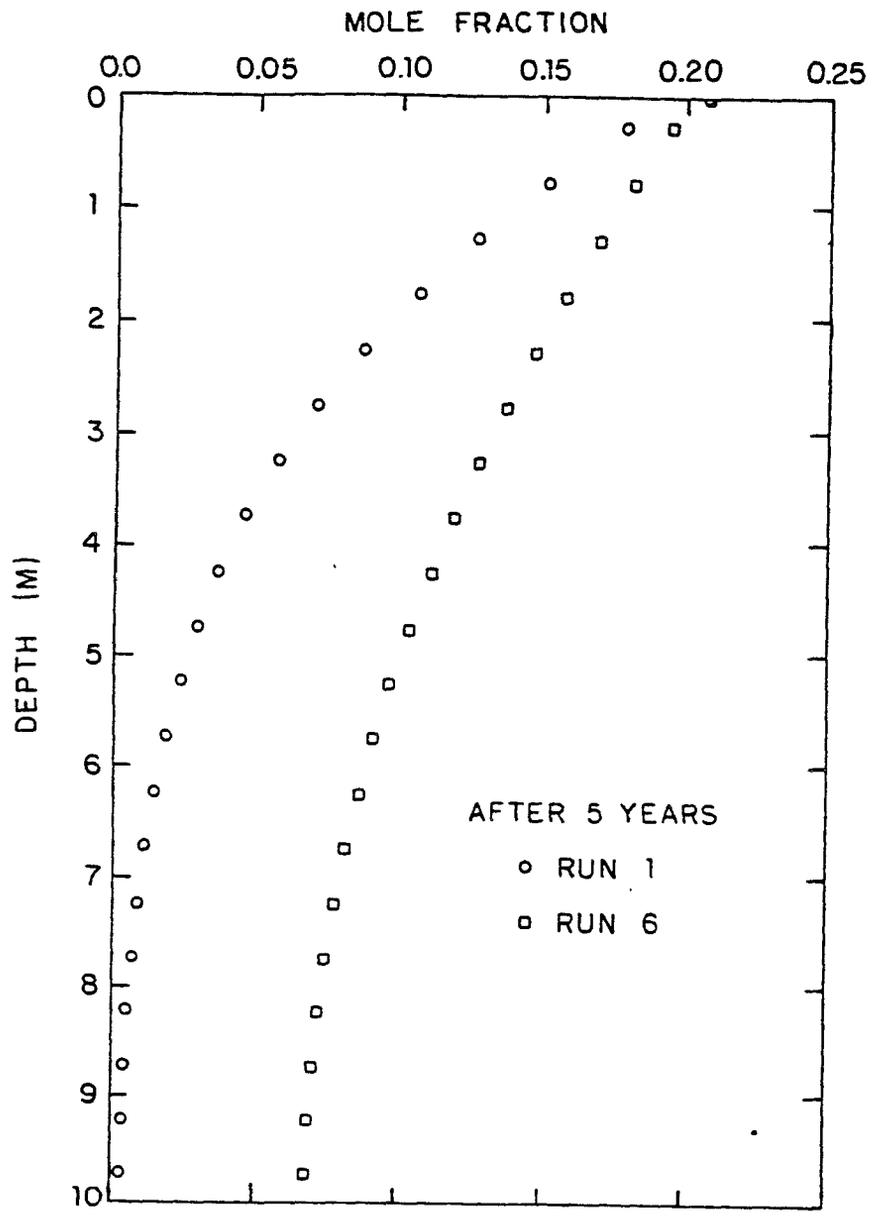

Figure 26. The mole fraction of oxygen within the profile versus depth (m) after 5 years for Runs 1 and 6.

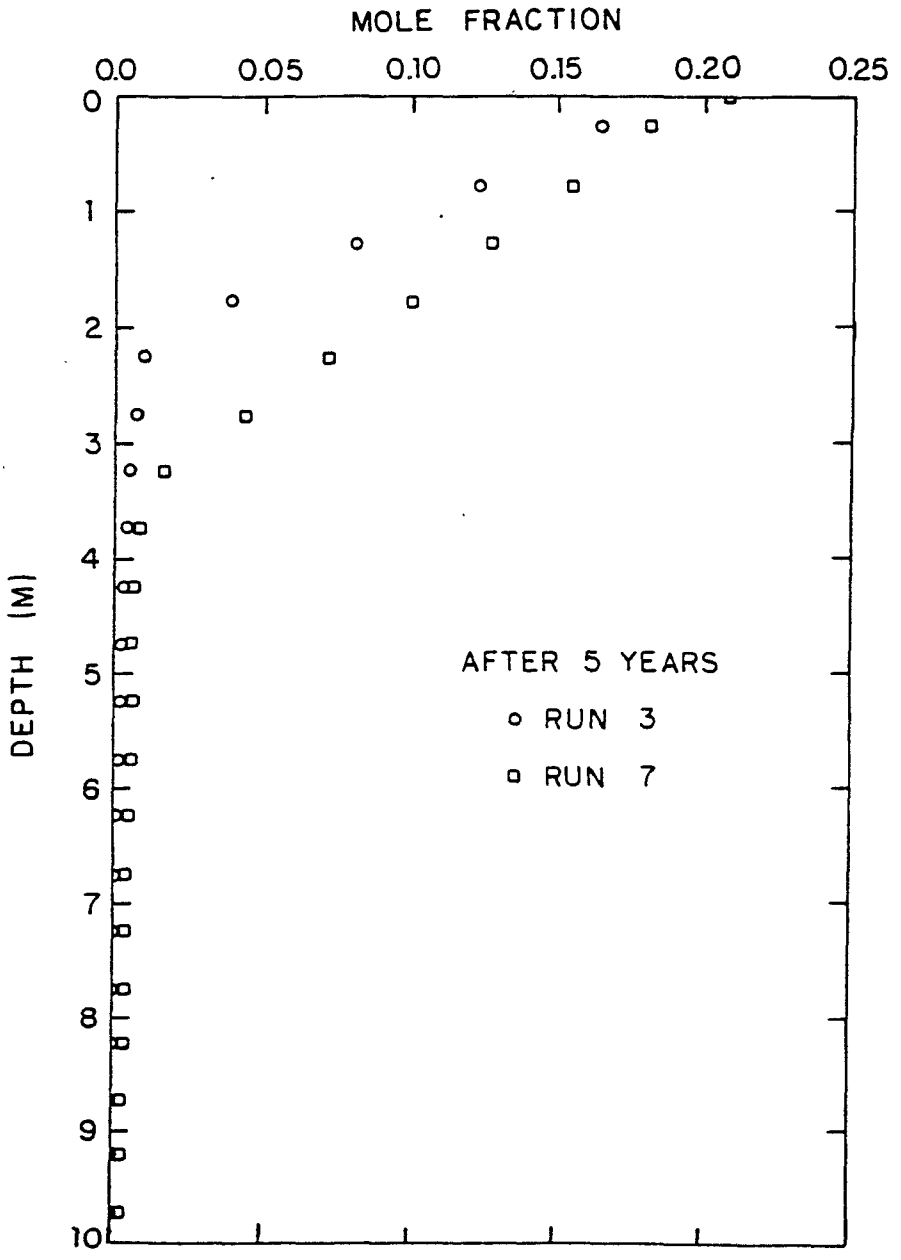

Figure 27. The mole fraction of oxygen within the profile versus depth (m) after 5 years for Runs 3 and 7.

Pyrite Distribution. Runs 1-7 were conducted with a uniform pyrite distribution with depth to simplify the comparisons between the runs. Two simulations were performed to illustrate the dependence of pyrite oxidation on pyrite distribution. The two simulations were run under conditions similar to Run 3 except that the initial pyrite distributions were as shown in Fig. 23. These distributions are analogous to burying a "worst" pyrite layer at either 4.75 meters or 9.75 meters and replacing the best material or material with the lowest pyrite content near the surface.

Figure 29 shows the amount of pyrite consumed from 0 to 4,000 days for these two runs and Run 3. Both Run 8, where the worst layer is half-buried and Run 9 where the layer is completely buried, show a marked reduction in pyrite oxidation. However, Runs 8 and 9 show very little differences in pyrite oxidation, indicating that for the combination of parameters used, the position of the worst layer is not as important as the position of the first layer having a sufficient pyrite content to support an oxidation rate that effectively consumes all of the oxygen. This is best illustrated in the O_2 versus depth plots for these two runs after 3,650 days (10 years). Figure 30 shows these O_2 profiles. In each case, O_2 does not penetrate significantly beyond the first layer having a pyrite content gerater than 0.25% (wt/wt), which is sufficient to consume most of the O_2.

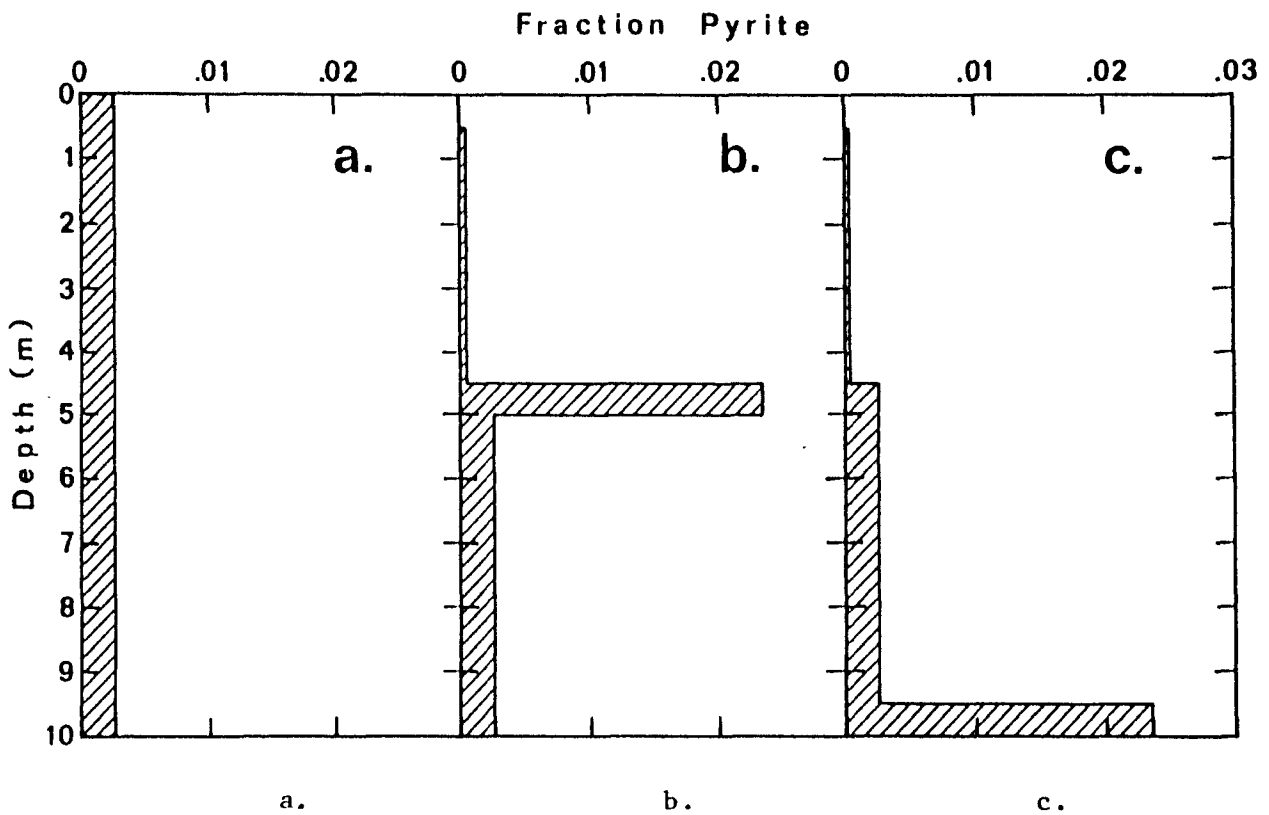

Figure 28. The distribution of pyrite (wt./wt.) with depth (m) for a) Run 3; b) Run 8; and c) Run 9.

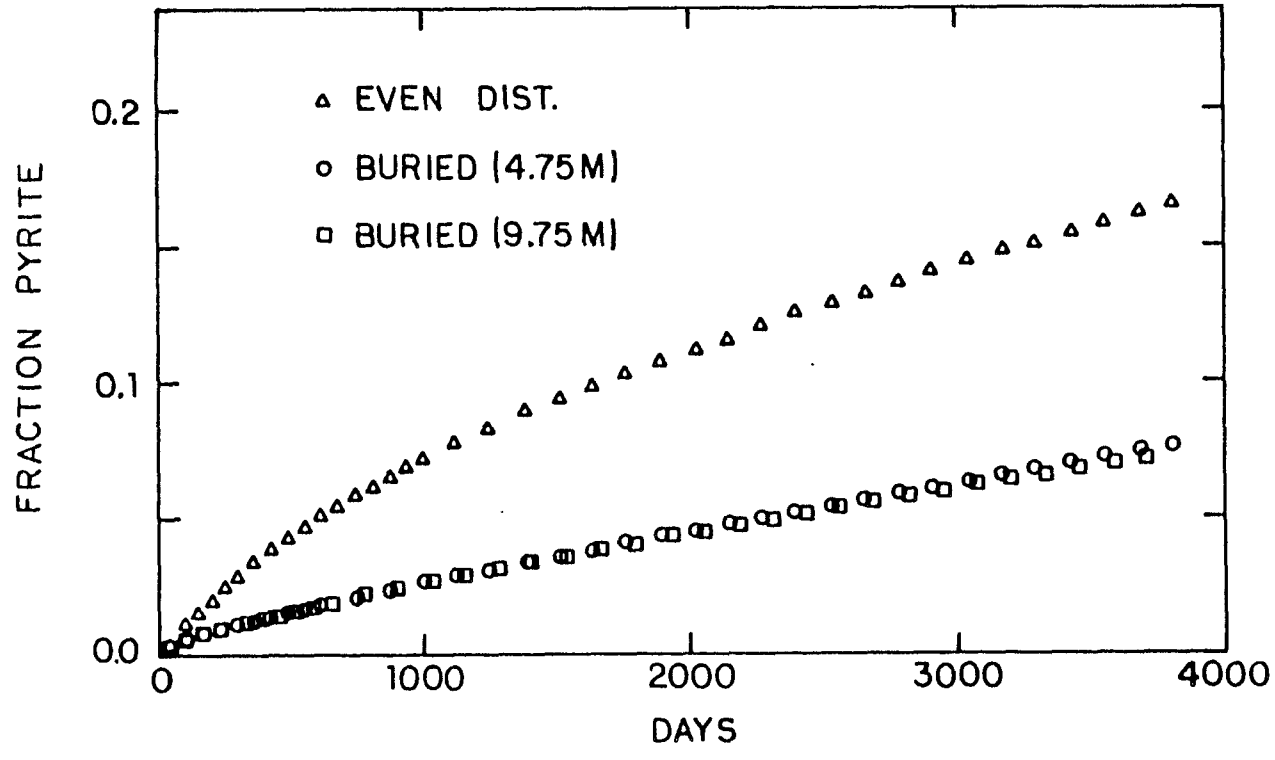

Figure 29. Fraction of pyrite oxidized within entire profile versus time for Run 3 (even distribution), Run 8 (buried at 4.75 m), and Run 9 (buried at 9.75 m).

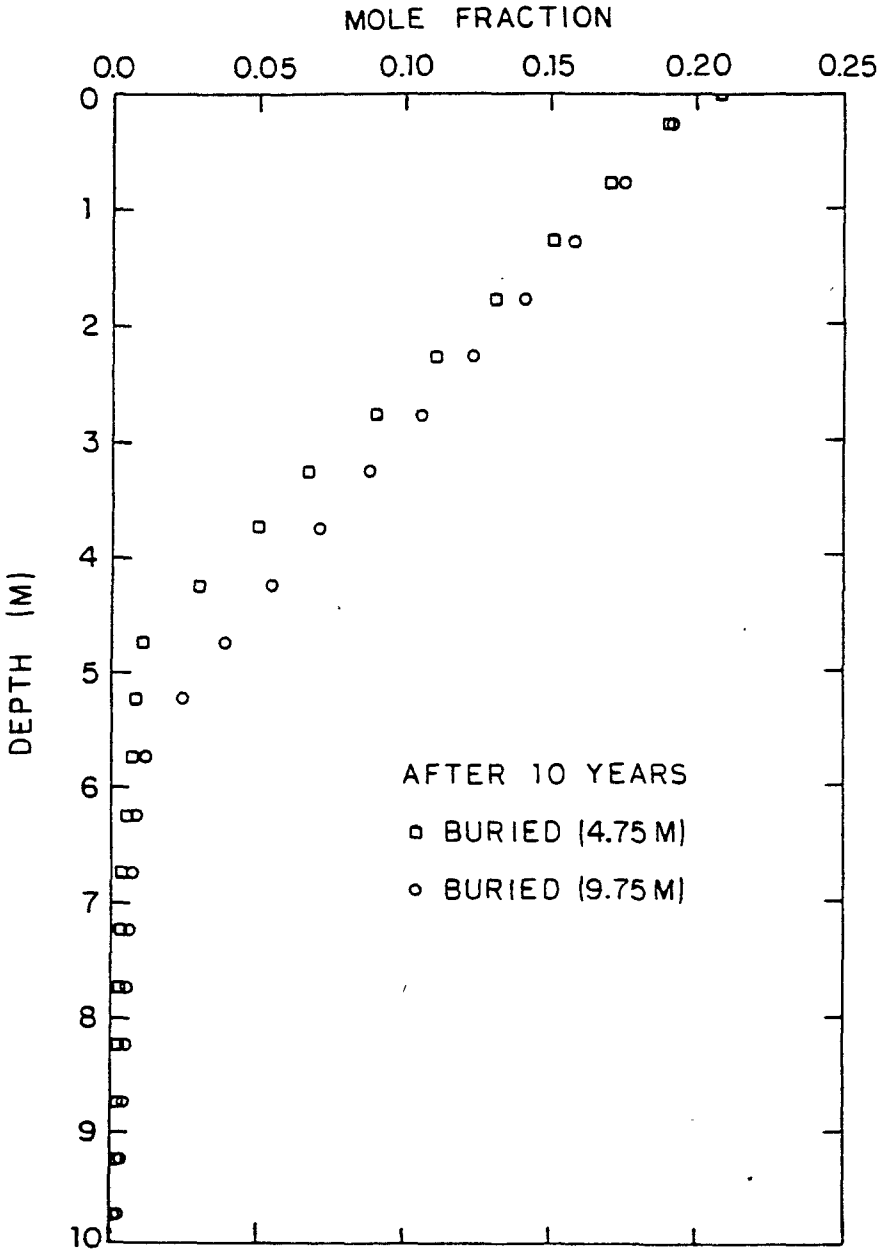

Figure 30. The mole fraction of oxygen within the profile versus depth (m) after 10 years for Run 8 (buried at 4.75 m) and Run 9 (buried at 9.75 m).

Inhibition of Bacteria

Comparing Run 1 to Run 3 or Run 4, it is apparent that, at least under some circumstances, a considerable reduction in the oxidation of pyrite over time can be achieved if a system can be shifted from bacterially catalyzed Fe^{3+} oxidation of pyrite to direct O_2 oxidation. Indeed, techniques for inhibiting bacterial activity have been proposed as a means of reducing acid drainage from reclaimed stripmines (Kleinmann and Erickson, 1981). If bacteria can be inhibited from the beginning of pyrite oxidation, a reduction of the magnitude represented by the difference between Run 3 or 4 and Run 7 and Run 6 may be possible. Amending the stripmine spoil after oxidation has started and bacteria have been established in order to inhibit bacterial activity and reduce acid drainage has also been suggested (Kleinman and Erickson, 1981). To simulate the situation in which iron-oxidizing bacteria are inhibited after they have become established, a run was made identical to Run 7 but where the bacterial activity was assumed to cease after approximately two years of oxidation. This represents the extreme case where the addition of a bacteriacide is 100% effective in destroying the bacteria throughout the profile. Figure 31 shows the rate of leaching of total iron over time for this simulation along with the results of Run 7 for comparison. Although the bacterial activity ceases after 700 days, allowing the oxidation system to shift from Fe^{3+}-dominant to O_2-dominant, no difference in the leaching rate of

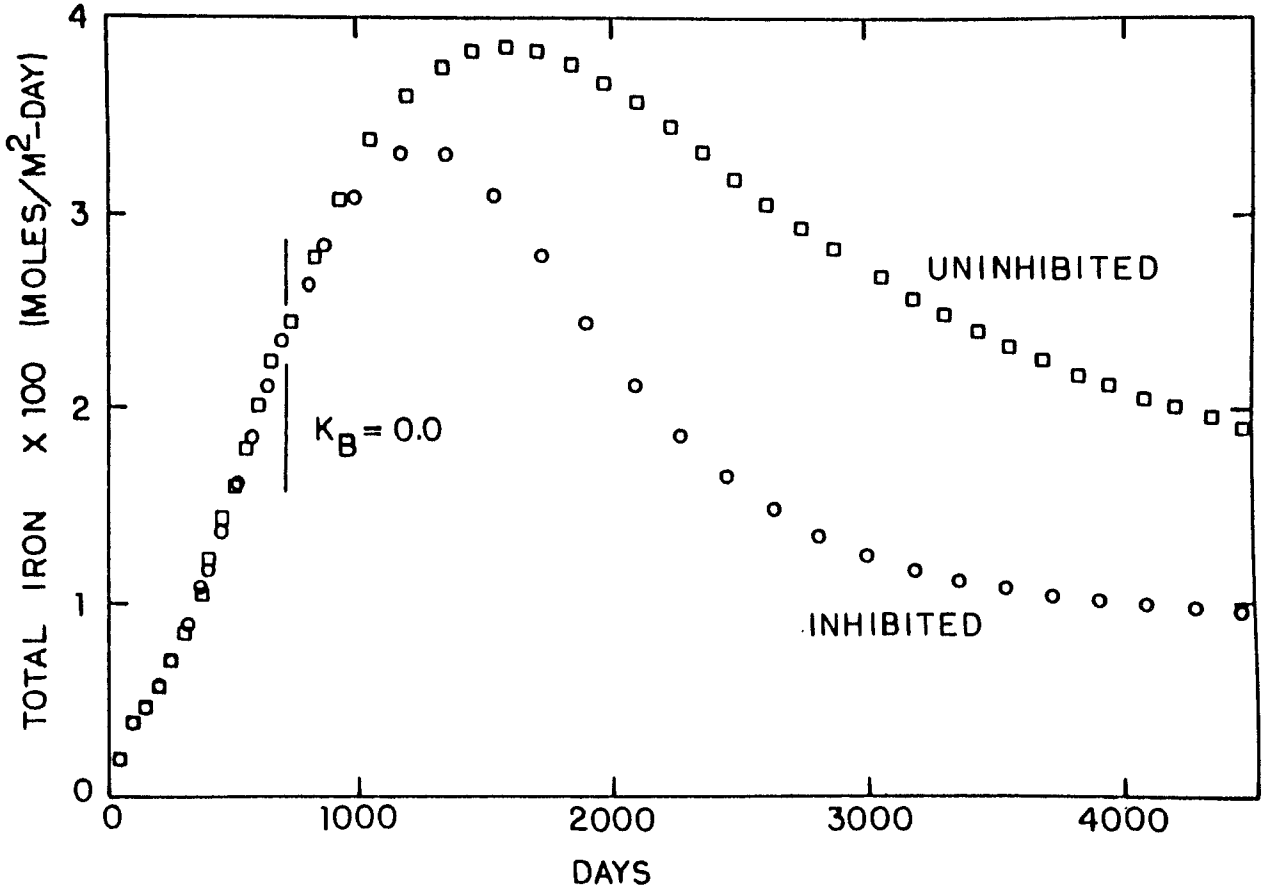

Figure 31. The rate of leaching out of the profile of all iron species versus time for Run 7 (no inhibition) and Run 10 (complete inhibition after 2 years).

iron is observed until 250 days later. From 950 days onward, the plots continue to diverge such that a large reduction is observed after 3,000 days, or 2,300 days (6.3) years after bacterial inhibition. The system demonstrates an apparent sluggishness in response to the decreased oxidation rate. One reason is that not until after day 800 does the ferric iron concentration fall below levels allowing the direct O_2 oxidation mechanism to become dominant. Another reason is that at the assumed leaching-rate of 50 cm/year, 2.16 years are required to remove one water-filled pore volume from the 10-meter deep profile. Thus, any change in oxidation rate will not be fully expressed in the leach water until months and perhaps years later.

Carbon Dioxide Generation

Several simulations were made to examine the way in which the model handled carbon dioxide production and flux within the mine profile. Four simulations were run for a period of five years; Run 11, a control where no source of carbon dioxide was assumed, Run 12, where heterotrophic respiration was assumed to be occurring in the top 50 cm of the profile, Run 13, where respiration was assumed to be occurring in the bottom layer of the profile only, and Run 14, where carbonates were assumed present in the bottom layer only. Run 12 is analogous to a mine profile with a well established vegetative cover, where $Q_{BB} = -0.3 \times 10^{-12}$ moles

O_2-cm^{-3}-sec^{-1}-$^oC^{-1}$ in Eq. [31]. Run 13 represents the case where heterotrophs are active deep within the mine profile, utilizing buried organic matter or digestible coal. Q_{HBB} for Run 13 was also set to -0.3×10^{-12} moles O_2-cm^{-3}-sec^{-1}-$^oC^{-1}$. Run 14 was run to simulate carbonate neutralization of acid. Only one layer was assumed to contain carbonate at a content of 0.083% (wt/wt). The low carbonate content in the profile was used because the H^+-carbonate reaction rate as predicted by the model was very rapid and dominated the pyrite oxidation reaction even at very low-carbonate contents. Although rapid reactivity of carbonates in acid spoil has been observed (Geidel and Caruccio, 1977), we believed the neutralization rate used in this model to be unrealistically fast mainly because it was based on work with freshly exposed limestone (Wentzler, 1977)[5] and ignored diffusion controlled kinetics and possible build-up of iron coatings on the carbonate surface (Geidel and Caruccio, 1977) both of which would reduce the neutralization rate. Even at the low-carbonate content used here, the pH of the bottom layer remained above 5.0 compared to approximately 2.5 for the other layers.

In every case the production of CO_2 reduced the oxidation of pyrite. After five years 73, 85 and 88% of the pyrite consumed in the control was consumed in Runs 12, 13 and 14, respectively. The reduction in pyrite oxidation is due primarily to the decreased oxygen concentration in the spoil profile. The reduction in O_2 concentrations in Run 12 was due mainly to O_2 consumption in the

surface layers. In contrast, reductions in O_2 concentrations in Runs 13 and 14 were primarily due to increased resistance to oxygen diffusion in the profile because of the counter-current CO_2 diffusion up through the profile (see Appendix A). In addition to reducing pyrite oxidation because of CO_2 production, Run 14 showed reduced levels of acid being flushed from the profile because of carbonate neutralization. Although Run 14 had a greater amount of pyrite oxided than Run 12, the acid removed from the profile after 5 years was the same; 73% of the control value for Runs 12 and 14 compared to 80% for Run 13.

Table 13 shows the flux ratio, $r_N = N_{CO_2}/N_{O_2}$, for each layer in Runs 12-14. Even for these simple examples it can be seen that the behavior of r_N with depth is fairly complicated. Values of r_N are both positive and negative in each run and may not show a uniform increasing or decreasing pattern with depth. For example, Run 12 shows a minimum r_N value below the surface layer at a depth of 275 cm. This may, in part, explain some of the difficulties encountered with the interpretation of measured fluxes in Part III.

Table 13. Ratio of the flux of CO_2 to O_2 for Run 12 (heterotrophs active in layer 1 only), Run 13 (heterotrophs active in layer 20 only), and Run 14 (acid neutralization by carbonates in layer 20).

Layer	Depth (cm)	N_{CO_2}/N_{O_2} Run 12	Run 13	Run 14
1	25†	-.47	.0003	.0003
2	75	.16	.0002	.0003
3	125	.12	-.0009	.0003
4	175	.10	-.0016	.0004
5	225	.093	-.0018	.0001
6	275	.089	-.0022	-.0013
7	325	.090	-.0028	-.0026
8	375	.096	-.0037	-.0033
9	425	.12	-.0053	-.0048
10	475	.21	-.010	-.0091
11	525	.57	-.028	-.027
12	575	.76	-.074	-.082
13	625	.83	-.10	-.13
14	675	.86	-.14	-.18
15	725	.90	-.18	-.26
16	775	.94	-.24	-.38
17	825	.99	-.33	-.57
18	875	1.0	-.45	-.88
19	925	1.1	-.61	-1.4
20	975	1.2	-.72	-1.8

†Depth to middle of layer.

REFERENCES

1. Arkesteyn, G. J. M. W. Pyrite Oxidation in Acid Sulfate Soils: The Role of Microorganisms. Plant and Soil, 54:119-134, 1980.
2. Arora, H. S., J. B. Dixon, and L. R. Hossner. Pyrite Morphology in Lignitic Coal and Associated Strata of East Texas. Soil Sci., 125:151-159, 1978.
3. Baes, C. F., Jr. and R. E. Mesmer. The Hydrolysis of Cations. John Wiley and Sons, New York, 1976.
4. Beck, J. V. A Ferrous-Ion-Oxidizing Bacteria. I. Isolation and Some General Physiological Characteristics. J. Bacteriol., 79:502-509, 1960.
5. Belly, R. T. and T. D. Brock. Ecology of Iron-Oxidizing Bacteria in Pyritic Materials Associated with Coal. J. Bacteriol., 117:726-732, 1974.
6. Birkeland, P. W. Pedology, Weathering and Gemorphological Research. Oxford University Press, New York, 1974.
7. Bouma, J. and L. W. Dekker. A Case Study on Infiltration Into Dry Clay Soil. I. Morphological Observations. Geoderma 20:27-40, 1978.
8. Braun, R. L., A. E. Lewis, and M. E. Wadsworth. In-Place Leaching of Primary Sulfide Ores: Laboratory Leaching Data and Kinetics Model. In: Solution Mining Symposium 1974, American Institute of Mining, Mettalurgical and Petroleum Engineers, Inc., New York, 1974. pp. 295-323.
9. Cathles, L. M. Predictive Capabilities of a Finite Difference Model of Copper Leaching in Low Grade Industrial Sulfide Waste Dumps. Mathematical Geol., 11:175-191, 1979.

10. Cathles, L. M. and J. A. Apps. A Model of the Dump Leaching Process that Incorporates Oxygen Balance, Heat Balance and Air Convection. Metal. Trans., 6B:617-624, 1975.

11. Ciolkosz, E. J., R. L. Cunningham, G. W. Peterson, and R. Pennock, Jr. Characteristic Interpretations and Uses of Pennsylvania Minesoils. Pa. Agric. Exp. Stn. Prog. Rep., 1977.

12. Clark, C. S. The Oxidation of Coal Mine Pyrite. Ph.D. Thesis, John Hopkins, University, University Microfilms, Inc., Ann Arbor, Michigan. No. 65-10-278, 1965.

13. Collier, W. R., R. J. Pickering, and J. J. Musser. Influences of Strip Mining on the Hydrologic Environment of Parts of Beaver Creek Basin, Kentucky, 1955-66. U.S. Geological Survey Professional Paper 427-C, 1970.

14. Davis, C. W. Electrochemistry. William Clowes and Sons., Limited, London, 1967.

15. Ehrlich, H. C. and S. J. Fox. Environmental Effects on Bacterial Copper Extraction from Lower Grade Copper Sulfide Ores. Biotech. and Bioeng., 9:471-485, 1967.

16. ElBoushi, I. M. Amount of Water Needed to Initiate Flow in Rubbly Rock Particles. J. Hydrol., 27:275-284, 1975.

17. Emrich, G. H. and E. G. Thompson. Some Characteristics of Drainage from Deep Bituminous Mines in Pennsylvania. In: Proceedings Second Symposium on Coal Mine Drainage Research, Mellon Institute, Pittsburgh, Pennsylvania, May 14, 1968.

18. Evans, D. D. Gas Movement. In: Methods of Soil Analysis, C. A. Black, ed. American Society of Agronomy, Madison, Wisconsin. Agronomy, 9:319-330, 1965.

19. Freeze, R. A. and J. A. Cherry. Groundwater. Prentice-Hall, Inc., Englewood Cliffs, New Jersey, 1979.

20. Garrels, R. M. and M. E. Thompson. Oxidation of Pyrite by Iron Sulfate Solutions. Am. J. Sci., Bradley Vol. 258-A:57-67, 1960.

21. Geidel, G. and F. T. Caruccio. Time as a Factor in Acid Mine Drainage Pollution. In: Proceedings Seventh Symposium on Coal Mine Drainage Research, Louisville, Kentucky, Oct. 18-20, National Coal Association, Washington, D.C., 1977.

22. Grim, E. C. and R. D. Hill, Environmental Protection in Surface Mining of Coal. EPA-670/2-74-093, U.S. Environmental Protection Technology Series, U.S. Environmental Protection Agency, Concinnati, Ohio, 1974. pp. 1-277.

23. Kleinmann, R. L. P. and P. M. Erickson. Field Evaluation of a Bactericidal Treatment to Control Acid Drainage. In: Symposium on Surface Mining, Hydrology, Sedimentation and Reclamation, Lexington, Kentucky, December 7-11, University of Kentucky, Lexington, Kentucky, 1981.

24. Lacey, D. T. and F. Lawson. Kinetics of the Liquid-Phase Oxidation of Acid Ferrous Sulfate by the Bacterium Thiobacillus ferrooxidans. Biotech. and Bioeng., 12:29-50, 1970.

25. Landesman, J., D. W. Duncan, and C. C. Walden. Iron Oxidation by Washed Cell Suspensions of the Chemoautotroph Thiobacillus ferrooxidans. Can. J. Microbial. 12:25-33, 1966.

26. Langmuir, D. Particle Size Effect on the Reaction Geothite = Hematite + Water. Am. J. Sci., 271:147-156, 1971.

27. Langmuir, D. and D. O. Whittemore. Variations in the Stability of Precipitated Ferric Oxyhydroxides. In: Nonequilibrium Systems in Natural Water Chemistry, R. F. Gould, ed. Advan. in Chem., Series 106, Amer. Chem. Soc., 1971. pp. 209-234.

28. Lau, C. M., K. S. Shumate, and E. E. Smith. The Role of Bacteria in Pyrite Oxidation Kinetics. In: Third Symposium on Coal Mine Drainage Research, May 19-20, Mellon Institute, Pittsburgh, Pennsylvania, 1970.

29. Levenspiel, O. Chemical Reaction Engineering. John Wiley and Sons, Inc., New York, 1972.

30. Lovell, H. L., R. R. Parizek, D. Forsberg, M. Martin, D. Richardson, and J. Thompson. Environmental Control Survey of Selected Pennsylvania Strip Mining Sites. Final Report to Agronne National Laboratories, #31-109-38-3497, 1978.

31. Lundgren, D. G. Microbiological Problems in Strip Mine Areas: Relationship to the Metabolism of Thiobacillus ferrooxidans. Ohio J. Sci., 75:280-287, 1975.

32. Malouf, E. E. and J. D. Prater. Role of Bacteria in the Alteration of Sulfide Minerals. J. Metals 1961:353-356, 1961.

33. Morth, A. H., E. E. Smith, and K. S. Shumate. Pyritic Systems: A Mathematical Model. Environmental Protection Agency Technology Series 14010 EAH, Contract No. 14-12-589, Report No. 665771, U.S. Environmental Protection Agency, Washington, D.C., 1972.

34. Myerson, A. S. Oxygen Mass Transfer Requirements During the Growth of Thiobacillus ferrooxidans on Iron Pyrite. Biotech. and Bioeng., 23:1413-1416, 1981.

35. Nordstrom, D. K., E. A. Jenne, and J. W. Ball. Redox Equilibria of Iron in Acid Mine Waters. In: Chemical Modeling in Aqueous Systems, E. A. Jenne, ed. American Chemical Society, Washington, D.C., 1979.

36. Ohio State University Research Foundation. Sulfide to Sulfate Reaction Mechanism. Water Pollution Control Research Series 14010, FPS 02/70, Federal Water Pollution Control Administration, Washington, D.C., 1970.

37. Pedersen, T. A., A. S. Rogowski, and R. Pennock, Jr. Physical Characteristics of Some Minesoils. Soil Sci. Soc. Am. J., 44:321-328, 1980.

38. Pionke, H. B., A. S. Rogowski, and R. J. DeAngelis. Controlling the Rate of Acid Loss from Strip Mine Spoil. J. Environ. Qual., 9:694-699, 1980.

39. Pionke, H. B., A. S. Rogowski, and C. A. Montgomery. Percolate Quality of Strip Mine Spoil. Trans. ASAE, 23:621-628, 1980.

40. Quisenberry, V. L. and R. E. Phillips. Percolation of Surface-Applied Water in the Field. Soil Sci. Soc. Am. J., 40:484-489, 1976.

41. Raats, P. A. C. Unstable Wetting Fronts in Uniform and Non-uniform Soils. Soil Sci. Soc. Am. Proc., 37:681-685, 1973.

42. Rao, P. S. C., R. E. Jessup, D. E. Rolston, J. M. Davidson, and D. P. Kilcrease. Experimental and Mathematical Description of Non-absorbed Solute Transfer by Diffusion in Spherical Aggregates. Soil Sci. Soc. Am. J., 44:684-688, 1980a.

43. Rao, P. S. C., D. E. Rolston, R. E. Jessup, and J. M. Davidson. Solute Transport in Aggregated Porous Media: Theoretical and Experimental Evaluation. Soil Sci. Soc. Am. J., 44:1139-1146, 1980b.

44. Rogowski, A. S., H. B. Pionke, and J. G. Broyan. Modeling the Impact of Strip Mining and Reclamation Processes on Quality and Quantity of Water in Mined Areas: A Review. J. Environ. Qual., 6:237-244, 1977.

45. Rogowski, A. S., H. B. Pionke, and B. E. Weinrich. Some Physical and Chemical Aspects of Reclamation. Preprint, paper presented at the North Atlantic Region ASAE 1982 Annual Meeting, 1982.

46. Rogowski, A. S. and B. E. Weinrich. Modeling Water Flux on Strip-Mined Land. Trans. ASAE, 24:935-940, 1981.

47. Rose, D. A. Hydrodynamic Dispersion in Porous Materials. Soil Sci., 123:277-283, 1977.

48. Russell, E. W. Soil Conditions and Plant Growth. Longmans, London, 1973.

49. Sapieszko, R. S., R. C. Patel, and E. Matijevic. Ferric Hydrous Oxide Soils. 2. Thermodynamics of Aqueous Hydroxo and Sulfate Ferric Complexes. J. Phys. Chem., 81:1061-1068, 1977.

50. Silverman, M. P. and D. G. Lundgren. Studies of Chemoautotrophic Iron Bacterium, Ferrobacillus ferrooxidans. II. Manometric Studies. J. Bacteriol., 78:326-331, 1959.

51. Singer, P. C. and W. Stumm. Acidic Mine Drainage: The Rate Determining Step. Science, 167:1121-1123, 1970.

APPENDIX A

APPLICABILITY OF FICK'S LAW TO GAS DIFFUSION

Introduction

The exchange of gases between the soil and the atmosphere is of primary concern to soil scientists. Gas movement in the soil can be caused by both convection and diffusion. Convection results when a difference in total gas pressure exists between two locations. Diffusion will occur even if the total pressure is uniform as long as there is a spatial difference in the chemical potential, normally represented by differences in concentration or partial pressure, of the components of a gas mixture (Kittel, 1969). While both processes are important in soils, diffusion is considered to dominate during normal gaseous exchange (Evans, 1965).

The fundamental equation used to describe one dimensional diffusion in soil is Fick's First Law.

$$q_i = - \alpha D_{F_i} dC_i/dz \qquad [A1]$$

where q_i is the mass transfer rate of component i per unit area ($ML^{-2}T^{-1}$), D_{F_i} is the Fickian diffusion coefficient for component i (L^2T^{-1}), C_i is the concentration of i (ML^{-3}), z is distance and α is the correction term that accounts for the air-filled porosity and tortuosity of the diffusion path in soils (Troeh, et al., 1982). Since in the remainder of this paper the magnitude of α is inconsequential as long as its magnitude is independent of gas type (Penman, 1940b), we will let it equal 1.0 and drop it from the remaining equations.

Alternatively, Eq. [A1] can be written in terms of mole fractions by invoking the equation of state for ideal gases and Dalton's Law to give:

$$N_i = - D_{F_i} \frac{P}{RT} dY_i/dz \qquad [A2]$$

where now N_i is the molar flux, P is the total gas pressure, R the universal gas constant, T absolute temperature, Y_i the mole fraction of component i and t is time. While useful in soil science, it must be remembered that Fick's Law when applied to gases is strictly an empirical relation, borrowed from studies with solutes and shown to agree well with observed diffusional processes in air (Kirkham and Powers, 1972, p. 429; Penman, 1940a and 1940b). The form of Eq. [A2], the flux of a gas being equal to its gradient multiplied by a single coefficient, is very misleading and requires closer examination.

The equations for gaseous diffusion were developed by Stefan (in Wilke, 1950) and Maxwell (1952) among others. The equations are based on the statistical mechanics description of ideal gases developed by Gibbs and Boltzman (Kittel, 1969). These equations have been extensively developed in the literature and found to agree very closely with experiments on gas-diffusion (Hirschfelder, et al., 1964; Fairbanks and Wilke, 1950). Since the interest in gas-diffusion in soils has increased in recent years (Smith, 1977; Bakker and Hidding, 1970; DeJong, et al., 1979;and others) and Fick's Law is used to describe the process in most soils literature (see

Wood and Greenwood, 1971 for an exception) it would seem advisable to compare Fick's Law (Eq. [A2]) to the Stefan-Maxwell diffusion equations in order to gauge its validity. This paper will examine several simple cases of diffusion of interest in soil science. It is not our intention to develop the Stefan-Maxwell equations in depth, nor to fully present the theory underlying them. For this, the reader is directed to the comprehensive works by Chapman and Cowling (1939) or Hirschfelder, et al. (1964), or to the excellent review by Marrero and Mason (1972). We shall, for the remainder of the paper, consider only diffusion in the gas phase, ignoring gas-liquid interactions, convection, turbulence or other mass flow phenomena, and for simplicity will consider only steady-state diffusion.

Stefan-Maxwell Equations for Gas Diffusion

Chapman and Cowling (1939, p. 244) have shown that for diffusion, the average velocity of one gas in relation to a second gas is represented by:

$$\bar{v}_i - \bar{v}_j = -\frac{n_T^2}{n_i n_j} D_{ij} \left[\frac{\partial (n_i/n_T)}{\partial r} + \frac{n_i n_j (m_j - m_i)}{\rho_T n_T} \frac{\partial \ln P}{\partial r} - \frac{\rho_i \rho_j}{P(\rho_i + \rho_j)} (F_i - F_j) + \frac{D_T}{D_{ij} T} \partial T/\partial r \right] \qquad [A3]$$

where the terms are defined at the end of this paper. For our purposes, it is only important to note that the difference in average velocities of two gases $(\bar{v}_i - \bar{v}_j)$ depends on four separate terms on the right side of Eq. [A3], which may be thought of as the chemical

potential for the gas pair (Kittel, 1969, p. 215). The first term represents ordinary or concentration diffusion, which we are concerned with in this paper. The second term represents diffusion caused by differences in total pressure but should not be confused with mass flow. As an example of pressure diffusion, lighter elements such as helium will concentrate in the upper portions of the atmosphere due to diffusion driven by pressure differences in the atmosphere. The gases respond to the pressure gradient created by gravity and not to gravity directly. The third term represents a diffusional flux created by an external force, such as a flow of charged particles in an electric field giving rise to an electric current. The final term represents thermal diffusion. In thermal diffusion, a temperature difference will cause diffusion within a gas mixture, with the lighter components concentrating near the warmer zone. If the temperature gradient is maintained, the gas components will continue to separate until ordinary diffusion exactly balances thermal diffusion. Of the four terms, only concentration or ordinary diffusion is important under normal circumstances in soil and plant processes, although thermal diffusion is used in commercial refining techniques for separating isotopes of some gases (Jones and Furry, 1946; Vasaru, et al., 1969).

For ordinary diffusion in one dimension of one gas, i, through another gas, j, where total pressure and temperature are constant, Eq. [A3] reduces to:

$$\bar{v}_i - \bar{v}_j = - \frac{n_T^2}{n_i n_j} D_{ij} \frac{d(n_i/n_T)}{dz} \qquad [A4]$$

Dividing by $\frac{n_T}{n_i n_j} D_{ij}$, Eq. [A4] can be rearranged such that:

$$\frac{\bar{v}_i \; n_i n_j - \bar{v}_j \; n_j n_i}{n_T D_{ij}} = - n_T \frac{d(n_i n_T)}{dz} \qquad [A5]$$

Dividing both sides of Eq. [A5] by Avagadro's number, M_o, convert the number densities to molar densities. Remembering that $N_i = v_i \; n_i/M_o$, Eq. [A5] becomes:

$$\frac{N_i n_j - N_j n_i}{n_T D_{ij}} = - \frac{n_T}{M_o} \frac{d(n_i/n_T)}{dz} \qquad [A6]$$

But since $Y_i = n_i/n_T$ and for unit volume $\frac{n_T}{M_o} = \frac{P}{RT}$ Eq. [A6] reduced to:

$$\frac{N_i Y_j - N_j Y_i}{D_{ij}} = - \frac{P}{RT} \frac{dY_i}{dz} \qquad [A7]$$

and D_{ij} is the mutual diffusion coefficient for gases i and j.

In a multicomponent gas mixture, the diffusion of component i can be represented by a linear summation of Eq. [A7] for each gas pair (Hirschfelder, et al., 1964). The equations for diffusion of each component in an n-component mixture commonly referred to as the Stefan-Maxwell equations are:

$$- \frac{P}{RT} dY_i/dz = \sum_{\substack{j=1 \\ j \neq i}}^{n} \frac{N_i Y_j - N_j Y_i}{D_{ij}} \qquad [A8]$$

We should note that D_{ij} in Eq. [A8] is not identical to the binary D_{ij} in Eq. [A7], since its magnitude is affected by the entire gas

mixture and not just i and j. However, this difference is slight (within the experimental error of measurement) and can be ignored (Marrero and Mason, 1972).

In general, Eq. [A8] represents n-1 independent equations for n unknowns (since $\sum_{i=1}^{n} Y_i = 1.0$) and as such the solution is indeterminate. However, under certain simplifying assumptions, solutions can be found for the series of equations. We will examine several of these situations applicable to soil and plant science.

Binary Gas System

For the simplest case of diffusion in a two-component system (i and j), Eq. [A8] yields only one unique equation, identical to Eq. [A7], since $Y_i + Y_j = 1.0$. Eq. [A7] can be rearranged into a form similar to Fick's Law (Eq. [A2]). By letting r_{ji} equal the negative value of the ratio of the fluxes, $r_{ji} = - N_j/N_i$, and substituting $1-Y_i$ for Y_j, we can rearrange Eq. [A7] to obtain:

$$N_i = \frac{-D_{ij}}{1-(1-r_{ji})Y_i} \frac{P}{RT} dY_i/dz \qquad [A9]$$

Comparing Eqs. [A9] and [A2] we find that:

$$D_{F_i} = \frac{D_{ij}}{1-(1-r_{ji})Y_i} \qquad [A10]$$

The Fickian diffusion coefficient depends not only on D_{ij}, but also on the flux ratio and mole ratio of component i. Two special circumstances immediately follow from Eq. [A10].

Tracer Diffusion

In cases where Y_i is present only in trace amounts (i.e., $Y_i \simeq 0.0$), Eq. [A10] for the Fickian diffusion coefficient reduces to:

$$D_{F_i} = D_{ij} \qquad [A11]$$

independent of flux ratios and concentration.

Closed System

A second possibility for binary gas diffusion is diffusion in a closed system where, since the total pressure remains constant, $N_i = - N_j$, $r_{ji} = 1.0$ and, from Eq. [A10], D_{F_i} again just equals D_{ij}.

Open System

A more general situation is the steady state diffusion of gases through an inert layer where the concentrations of the gases are held constant at one end because of an infinite source/sink for the gases (the atmosphere) and the concentrations are fixed at the other end by consumption or production processes. An example would be oxygen diffusing into a soil ped and oxidizing ferrous to ferric iron where oxygen and nitrogen comprise the ped atmosphere. For an open system Eqs. [A9] and [A10] cannot be solved without a priori knowledge of r_{ji}. Figure A1 illustrates the variation of D_{F_i} with changes in r_{ji} and Y_i as calculated by Eq. [A10]. The reduced Fickian diffusion coefficient, $D^*_{F_i} = D_{F_i}/D_{ij}$ is plotted for several values of r_{ji} and for $0.0 < Y_i < 1.0$. As discussed for equi-molar, counter-current diffusion in a closed system and for tracer diffusion, $D^*_{F_i}$ is constant for all values of Y_i when $r_{ji} = 1.0$ and for all

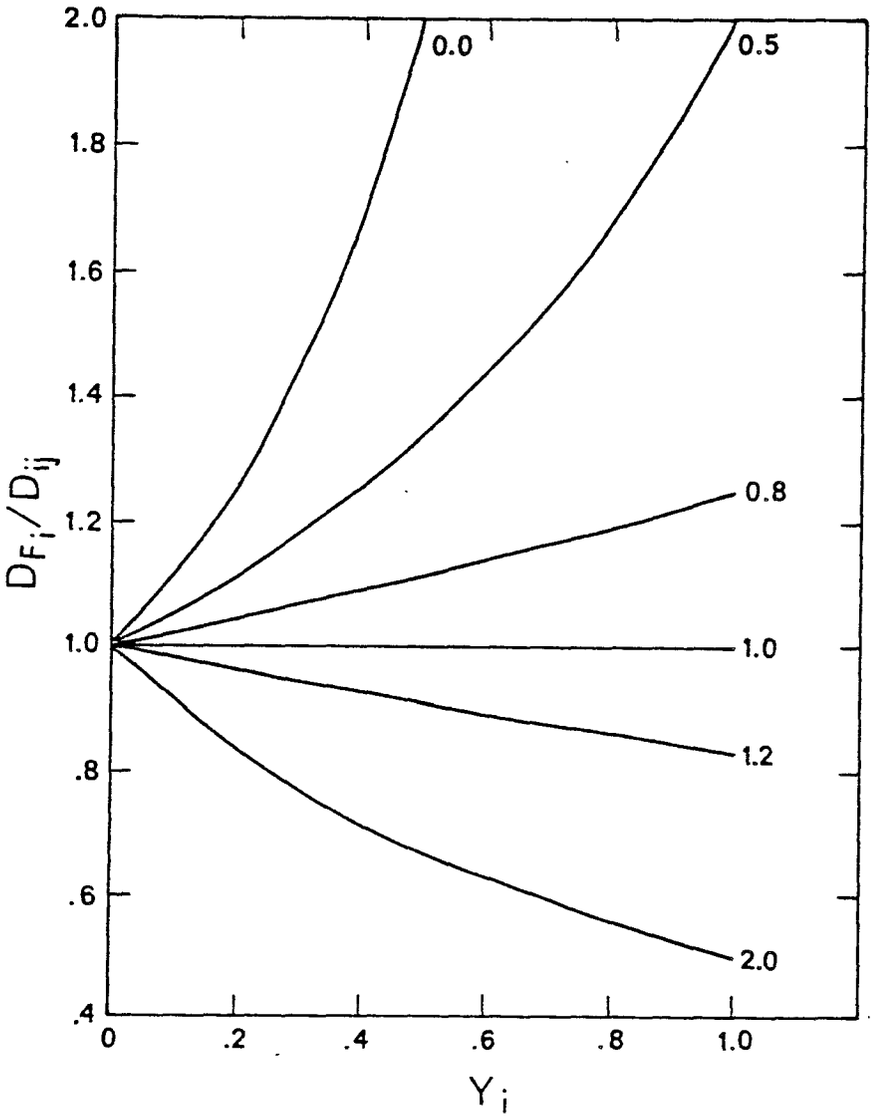

Figure A1. Values of the reduced Fickian diffusion coefficient, $D^*_{F_i}$, in a binary gas mixture plotted against the gas mole fraction of component i. Curve labels are the values of the flux ratio, r_{ji}, for which the curve was calculated.

values of r_{ji} when $Y_i \approx 0.0$. $D^*_{F_i}$ diverged rapidly however as Y_i increases, decreasing as r_{ji} becomes less (reduced resistance to diffusion) and increasing as r_{ji} increases. In the extreme it can be seen from Eq. [A10] that $D^*_{F_i}$ can become negative when the two gases are diffusing in the same direction ($r_{ji} < 0.0$), that is, gas i would diffuse against its gradient. This behavior has been measured by Duncan and Toor (1962).

Three Component Gas Systems

The soil atmosphere can normally be characterized as a three-component (ternary) system. In a ternary system composed of gases i, j and k, where $Y_i + Y_j + Y_k = 1$, Eq. [A8] yields two unique equations:

$$-\frac{P}{RT}\, dY_i/dz = \frac{N_i Y_j - N_j Y_i}{D_{ij}} + \frac{N_i Y_k - N_k Y_i}{D_{ik}} \qquad [A12]$$

$$-\frac{P}{RT}\, dY_j/dz = \frac{N_j Y_i - N_i Y_j}{D_{ij}} + \frac{N_j Y_k - N_k Y_j}{D_{jk}} \qquad [A13]$$

Again, the general solution of these equations is impossible without further simplifying assumptions.

Tracer Diffusion

If we let component i represent a gas at trace concentration, so that $Y_j + Y_k \approx 1$, then Eq. [A12] which describes the diffusion of i, becomes:

$$- \frac{P}{RT} dY_i/dz = N_i \left(\frac{Y_j}{D_{ij}} + \frac{Y_k}{D_{ik}} \right) \qquad [A14]$$

or upon solving for N_i:

$$N_i = \frac{- D_{ij} D_{ik}}{Y_j D_{ik} + Y_k D_{ij}} \frac{P}{RT} dY_i/dz \qquad [A15]$$

which is identical in form to Fick's Law with the Fickian diffusion coefficient dependent only on D_{ij}, D_{ik} and the mole fractions Y_j and Y_k.

$$D_{F_i} = \frac{D_{ij} D_{ik}}{Y_j D_{ik} + Y_k D_{ij}} \qquad [A16]$$

In general, for tracer diffusion in a n-component gas mixture, the tracer will diffuse according to Fick's Law where the diffusion coefficient is equal to:

$$D_{F_i} = \prod_{\substack{j=1 \\ j \neq 1}}^{n} D_{ij} / \sum_{\substack{j=1 \\ j \neq 1}}^{n} \left(Y_j \left(\prod_{\substack{k=1 \\ k \neq i \text{ or } j}}^{n} D_{ik} \right) \right) \qquad [A17]$$

and is independent of the diffusional fluxes of the other components.

<u>One Gas Stagnant</u>

Eqs. [A12] and [A13] can also be simplified if we assume one of the gases is stagnant. This is analogous to quasi-steady state respiration in a soil where oxygen and carbon dioxide are being exchanged with the atmosphere and nitrogen, the third gas component, (k), is stagnant. In this case with $N_k = 0.0$, Eqs. [A12] and [A13] become:

$$- P/RT \; dY_i/dz = N_i \left[\frac{Y_j}{D_{ij}} + \frac{Y_k}{D_{ik}} \right] - N_j \frac{Y_i}{D_{ij}} \qquad [A18]$$

$$- P/RT \; dY_j/dz = N_j \left[\frac{Y_i}{D_{ij}} + \frac{Y_k}{D_{jk}} \right] - N_i \frac{Y_j}{D_{ij}} \qquad [A19]$$

These equations can be solved for the molar fluxes N_i and if Y_i, Y_j and Y_k are known. In the case of counter-current, equi-molar diffusion, where $N_i = - N_j$ ($r_{ji} = 1.0$), Toor (1957) has solved these equations exactly and found that the solution must simultaneously satisfy Eqs. [A20] and [A21].

$$N_i = - N_j = \frac{D_{ik} \, D_{jk}}{D_{jk} - D_{ik}} \; \frac{P}{RTz} \ln \frac{Y_{k_2}}{Y_{k_1}} \qquad [A20]$$

$$\left(1 - \frac{D_{ij}}{D_{jk}}\right) (Y_{i_1} - Y_{i_2}) + \left(1 - \frac{D_{ij}}{D_{ik}}\right) (Y_{j_1} - Y_{j_2}) = \ln(Y_{k_2}/Y_{k_1}) \qquad [A21]$$

The second subscript on Y refers to the points 1 and 2 separated by the distance z. These equations can be used to describe diffusion in soils where the source and sink terms for O_2 (i) and CO_2 (j) are determined by plant root or soil organism respiration and the respiration quotient, CO_2 produced/O_2 consumed, is near 1.0 (e.g., r_{ji} = 1.0). However, it must be remembered that this is only a good approximation for respiration in soils during quasi-steady state conditions because if Y_i or Y_j is changing rapidly, $N_k \neq 0.0$ and the simplification is not justified.

In general, we can solve Eqs. [A18] and [A19] only if the ratio r_{ji} is known. Substituting $r_{ji}N_i$ for N_j in Eq. [A18] and solving

for N_i and substituting N_j/r_{ji} for N_i and solving for N_j in Eq. [A19] yields

$$N_i = \frac{-D_{ij}D_{ik}}{D_{ik}Y_j+D_{ij}Y_k+r_{ji}D_{ik}Y_i}\frac{P}{RT}\,dY_i/dz \qquad [A22]$$

$$N_j = \frac{-D_{ij}D_{jk}}{D_{jk}Y_i+D_{ij}Y_k+D_{jk}Y_j/r_{ji}}\frac{P}{RT}\,dY_j/dz \qquad [A23]$$

which are in the form of Fick's Law with diffusion coefficients:

$$D_{F_i} = \frac{D_{ij}D_{ik}}{D_{ik}Y_j+D_{ij}Y_k+r_{ji}D_{ik}Y_i} \qquad [A24]$$

$$D_{F_i} = \frac{D_{ij}D_{jk}}{D_{jk}Y_i+D_{ij}Y_k+D_{jk}Y_j/r_{ji}} \qquad [A25]$$

These equations demonstrate that the apparent diffusion coefficient in Fick's Law depends not only on the binary diffusion coefficients but also on the gas composition and the flux ratio, r_{ji}. As an example, D_F can be calculated for O_2 from Eq. [A24] and for CO_2 from Eq. [A25] in a ternary atmosphere where $i = O_2$, $j = CO_2$, $k = N_2$ and $N_{N_2} = 0.0$. For this case Eqs. [A24] and [A25] become:

$$D_{F_{O_2}} = \frac{D_{O_2,CO_2}D_{O_2,N_2}}{D_{O_2,N_2}Y_{CO_2}+D_{O_2,CO_2}Y_{N_2}+r_{CO_2,O_2}D_{O_2,N_2}Y_{O_2}} \qquad [A26]$$

$$D_{F_{CO_2}} = \frac{D_{O_2,CO_2}D_{CO_2,N_2}}{D_{CO_2,N_2}Y_{O_2}+D_{O_2,CO_2}Y_{N_2}+D_{CO_2,N_2}Y_{CO_2}/r_{CO_2,O_2}} \qquad [A27]$$

Values for the binary diffusion coefficients can be calculated from Table A1 (next section). For a temperature of 20°C and a pressure of 101 kPa these values are 0.159×10^{-4}, 0.202×10^{-4} and 0.159×10^{-4} (m^2/sec) for D_{O_2,CO_2}, D_{O_2,N_2} and D_{CO_2,N_2}, respectively. The Fickian

diffusion coefficients can then be calculated if values for Y_{O_2}, Y_{CO_2}, Y_{N_2} and r_{CO_2} are known. For example, with $Y_{O_2} = 0.15$, $Y_{CO_2} = 0.06$, $Y_{N_2} = 0.79$ and $r_{CO_2,O_2} = 0.5$, $D_{F_{O_2}}$ and $D_{F_{CO_2}}$ are calculated to be 0.210×10^{-4} and 0.150×10^{-4} m^2/sec, respectively. These two points are indicated on Fig. A2 and A3 where the values of $D_{F_{O_2}}$ and $D_{F_{CO_2}}$ are plotted for various flux ratios. In both figures Y_{N_2} is held constant at 0.790 while Y_{O_2} varies from 0.0 to 0.21. Carbon dioxide comprises the remainer of the atmosphere ($0.21 < Y_{CO_2} < 0.0$).

The apparent diffusion coefficients for both O_2 and CO_2 vary little for r_{CO_2,O_2} near 1.0. As the flux ratio deviates further from 1.0, the O_2 diffusion coefficient diverges rapidly as Y_{O_2} increases (Fig. A2). D_F for CO_2 is less variable but can deviate markedly from its value at $r_{CO_2,O_2} = 1.0$ at low values of the flux ratio and high CO_2 (low O_2) concentrations (Fig. A3). Values for the flux ratio in soils have been reported ranging between 0.6 and 4.0 (Bunt and Rovira, 1955; Rixon and Bridge, 1968; Bridge and Rixon, 1976). Although none of these authors reported the O_2 and CO_2 mole fractions at which these ratios were found, extreme values of 0.0 to 0.21 for O_2 and 0.0 to 0.09 for CO_2 have been measured (Russell and Appleyard, 1915). Using the values of 0.05 for Y_{CO_2} and 0.15 for Y_{O_2} and a flux ratio of 2.0, we can see from Figs. A2 and A3 that deviations in the fickian diffusion coefficients of 15% for O_2 and 9% for CO_2 from the values at $r_{CO_2,O_2} = 1.0$ are possible. Figures A2 and A3 illustrate the potential hazard of applying values of the Fickian diffusion coefficient from one situation to another

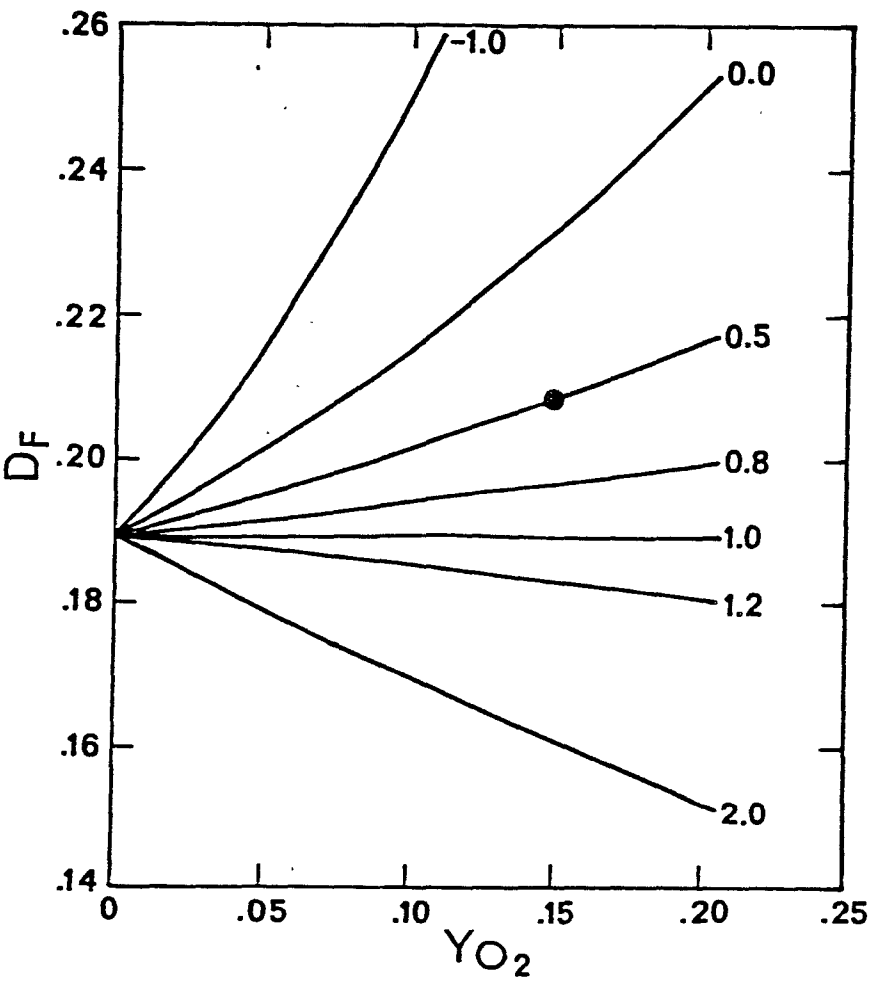

Figure A2. Values of the Fickian diffusion coefficient, D_F, for O_2 in an O_2-CO_2-N_2 atmosphere (in m^2/sec). The N_2 mole fraction is held constant at 0.790, while the O_2 mole fraction, plotted on the abscissa, is varied between 0.0 and 0.21. CO_2 comprises the balance of the atmosphere. Values are for 20°C and 101 kPa with the N_2 flux being set to 0.0. Curve labels are the values of the flux ratio r_{CO_2,O_2}. Point represents value calculated in text.

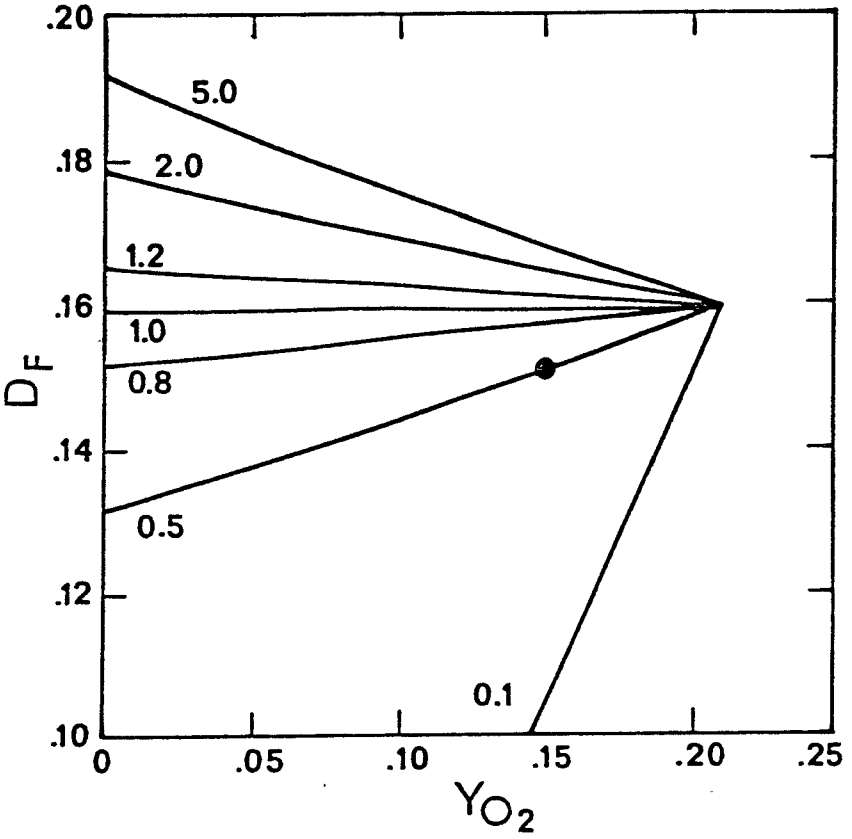

Figure A3. Values for the Fickian diffusion coefficient, D_F, for CO_2 in an O_2-CO_2-N_2 atmosphere (in m^2/sec). The N_2 mole fraction is held constant at 0.790, while the O_2 mole fraction, plotted on the abscissa, is varied between 0.0 and 0.21. CO_2 comprises the remainder of the atmosphere. Values are for 20°C and 101 kPa with the N_2 flux being set to 0.0. Curve labels are the values of the flux ratio r_{CO_2,O_2}. Point represents value calculated in text.

where the flux ratio and gas composition may not be the same. This may be, at least in part, the reason why flux calculations based concentration gradients do not compare well to other techniques for measuring flux (DeJong, et al., 1979).

Equation [A8] also applies to diffusion in four-component or greater gas mixtures. O_2, CO_2, N_2 and Ar or O_2, CO_2, N_2, Ar and H_2O vapor atmospheres would be mixtures of interest in soils. However, as in the ternary case, unless some simplifying assumptions can be made, the exact solution for diffusion in these mixtures is not possible.

Binary Diffusion Coefficient

D_{ij} is the proportionality coefficient relating the flux of i and j to their gradient in a binary gas system. Conceptually D_{ij} can be thought of as a macroscopic averaging of the interactions or collisions between components i and j. The greater the number of collisions, the more diffusion is impeded and the smaller D_{ij} must be. For this reason, D_{ij} must be inversely proportional to density, and thus pressure since the number of collisions will increase linearly with pressure at constant temperature. Thus:

$$D_{ij} = D^*_{ij}/P \qquad [A28]$$

where D^*_{ij} is the temperature dependent, pressure independent binary diffusion coefficient. However, any decrease in D_{ij} due to a pressure increase will be exactly balanced by an increase in the

number of molecules or flux carriers per volume of gas (increased concentration, C). This can be seen by substituting Eq. [A28] into Eq. [A29] for the flux in a binary system:

$$N_i = - \frac{D^*_{ij}/P}{1-(1-r_{ji})Y_i} \frac{P}{RT} dY_i/dz \qquad [A29]$$

the pressure terms drop out and the diffusion equation is pressure independent when expressed in mole fractions:

$$N_i = - \frac{D^*_{ij}}{1-(1-r_{ji})Y_i} \frac{1}{RT} \frac{dY_i}{dz} \qquad [A30]$$

When working with the concentration form of the diffusion equation (Eq. [A1]), the pressure dependence of the diffusion coefficient must be retained:

$$q_i = - \frac{D_{ij}}{1-(1-r_{ij})Y_i} \frac{P_1}{P_2} dC_i/dz \qquad [A31]$$

where P_1 is the total pressure at which D_{ij} is known and P_2 is the pressure at which diffusion is taking place.

Relations for calculating D^*_{ij} for any gas pair, based on classical statistical mechanics were independently developed by Chapman and by Enskog (Chapman and Cowling, 1939). The solution involves successive approximations to D^*_{ij}. The approximations converge rapidly, so that the first approximation, which is temperature dependent but independent of gas composition and at most the second approximation, which introduces slight compositional variation, is

sufficient for calculating D^*_{ij} to within at most several percent error (Marrero and Mason, 1972).

Values for D^*_{ij} (more commonly D_{ij}), can be found in numerous papers in the literature (see Marrero and Mason, 1972), with some recent values for carbon dioxide, nitrous oxide, ethylene and ethane presented by Pritchard and Currie (1982). Marrero and Mason (1972) have compiled an extensive tabulation of binary diffusion coefficients taken from the literature. Based on the Chapman-Enskog equations and extensive experimental results, they have compiled semi-empirical relations for the first approximation of over 70 gas pairs. Diffusion coefficients for gas pairs of interest in soil research are tabulated in Table A1. In all cases shown, the second approximation to D^*_{ij}, which is based on the compositional ratio of component i to component j, represents a correction to the first approximation of less than 1.0% at normal temperatures for the entire compositional range. This correction is within the experimental error of the measured values and can be neglected for all the gas pairs listed. The equation used by Marrero and Mason (1972) to calculate D^*_{ij} is:

$$\ln(D^*_{ij}) = \ln(a) + b \ln(T) - c/T. \qquad [A32]$$

They computed the constants a, b and c by matching Eq. [A32], whose form is suggested by the theoretical work of Chapman-Enskog, to a compilation of experimental data for each gas pair. The temperature

Table A1. Coefficients for calculating D^*_{ij} † for gas pairs of interest in soil research (after Marrero and Mason, 1972).

Gas Couple	a x 10^7	b	c	T range	Uncertainty† limits
	KPa-m^2/sec-K^b	--	K		%
Ar-CH_4	0.792	1.785	0.0	307-10^{-4}	3
Ar-N_2	0.913	1.752	0.0	244-10^4	2
Ar-O_2	0.987	1.736	0.0	243-10^4	3
Ar-air	0.926	1.749	0.0	244-10^4	3
Ar-CO_2	1.76	1.646	89.1	276-1800	3
CH_4-N_2	1.01	1.750	0.0	298-10^4	3
CH_4-O_2	1.68	1.695	44.2	294-10^4	3
CH_4-air	1.04	1.747	0.0	298-10^4	3
N_2-O_2	1.14	1.724	0.0	285-10^4	3
N_2-H_2O	0.188	2.072	0.0	282-373	4
N_2-CO_2	3.18	1.570	113.6	288-1800	2
O_2-H_2O	0.191	2.072	0.0	282-450	7
O_2-CO_2	1.58	1.661	61.3	287-1083	3
Air-H_2O	0.189	2.072	0.0	282-450	5
Air-CO_2	2.73	1.590	102.1	280-1800	3
H_2O-CO_2	9.33	1.500	307.9	296-1640	10
CO_2-N_2O	0.284	1.866	0.0	195-550	3

†$\ln(D^*_{ij}) = \ln(a) + b \ln(T) - c/T$, where T is temperature, (K).

‡Uncertainty in D^*_{ij} term at lower end of listed temperature range.

range over which these coefficients were fit and the uncertainty limits in D^*_{ij} at the lower end of the temperature range are also given in Table A1.

An example calculation of D^*_{ij} using values in Table A1 is as follows. The pressure-independent, diffusion coefficient for the gas pair O_2-CO_2 is calculated from Eq. [A32] with the coefficients from Table A1 of a = 1.58 x 10^{-7}, b = 1.661 and c = 61.3 At a temperature of 293 K:

$$\ln(D^*_{O_2,CO_2}) = \ln(1.58 \times 10^{-7}) + 1.661 \ln(293) - 61.3/293. \quad [A33]$$

$$D^*_{O_2,CO_2} = 0.00160 \ m^2\text{-KPa-sec}^{-1}$$

or at atmospheric pressure, from Eq. [A28]

$$D_{O_2,CO_2} = 0.00160/101.$$
$$= 0.159 \times 10^{-4} \ m^2/sec \quad [A34]$$

The diffusion coefficients are highly sensitive to temperature with a 30% variation possible under normal, seasonal soil temperature fluctuations. For example, the binary diffusion coefficient for the O_2-CO_2 gas pair is equal to 0.136 x 10^{-4} at 0^oC (273 K) and 0.165 x 10^{-4} at 30^oC (303 K) or D_{O_2,CO_2} is 22% greater at 30^oC than 0^oC.

SUMMARY

The comparison of the Stefan-Maxwell equations and Fick's Law for diffusion of gas through vapor shows that only under certain, special circumstances is the diffusion coefficient for Fick's Law, D_{F_i}, a constant independent of the mole fraction of i and the diffusion flux of other gases. These special cases are the diffusion of a trace amount of component i and equi-molar, counter-current diffusion in a binary gas mixture, or equi-molar, counter-current diffusion of two gases in a ternary system with the third gas stagnant. In general, D_{F_i} is dependent on the binary diffusion coefficients, the composition of the gas mixture, and the diffusional flux ratios of the gas components. Measured values of D_{F_i} can only be accurately extrapolated to other circumstances when all the above conditions are similar. In an O_2, CO_2 and N_2 atmosphere where N_2 is stagnant, variations on the order of 10% from the tracer value of D_F for O_2 and CO_2 are possible with variations in the mole fraction, or flux ratio. The diffusion coefficients are most sensitive to changes in the flux ratio for ratios less than 0.8 or greater than 1.2. The temperature and pressure dependent nature of the diffusion coefficient must also be considered.

REFERENCES

1. Bakker, J. W. and A. P. Hidding. The Influence of Soil Structure and Air Content on Gas Diffusion in Soils. Neth. J. Agric. Sci., 18:37-48, 1970.
2. Bridge, B. J. and A. J. Rixon. Oxygen Uptake and Respiratory Quotient of Field Soil Cores in Relation to their Air-Filled Pore Space. J. Soil Sci., 27:279-286, 1976.
3. Bunt, J. S. and A. D. Rovira. Microbial Studies of Some Sub-anarctic Soils. J. Soil Sci., 6:119-128, 1955.
4. Chapman, S. and T. G. Cowling. The Mathematical Theory of Nonuniform Gases. Cambridge University Press, London, 1939.
5. Curtiss, C. F. and J. O. Hirschfelder. Transport Properties of Multicomponent Gas Mixtures. J. Chem. Physics, 17:550-555, 1949.
6. DeJong, E., R. E. Redmann, and E. A. Ripley. A Comparison of Methods to Measure Soil Respiration. Soil Sci., 127:299-306, 1979.
7. Duncan, J. B. and H. C. Toor. An Experimental Study of Three Component Gas Diffusion. Am. Inst. Chem. Eng., 8:38-41, 1962.
8. Evans, D. D. Gas Movement. In: Methods of Soil Analysis, C. A. Black, ed. American Society of Agronomy, Madison, Wisconsin, 1965. Agronomy 9:319-330.
9. Fairbanks, D. F. and C. R. Wilke. Diffusion Coefficients in Multicomponent Gas Mixtures. Indust. Eng. Chem., 42:471-475, 1950.
10. Hirschfelder, J. O., C. F. Curtiss, and R. B. Bird. Molecular Theory of Gases and Liquids. John Wiley and Sons, Inc., New York, 1964.

11. Jones, R. C. and W. H. Furry. The Separation of Isotopes by Thermal Diffusion. Rev. Modern Phys., 18:151-224, 1946.

12. Kirkham, D. and W. L. Powers. Advanced Soil Physics. Wiley-Interscience, New York, 1972.

13. Kittel, C. Thermal Physics. John Wiley and Sons, Inc., New York, 1969.

14. Marrero, T. R. and E. A. Mason. Gaseous Diffusion Coefficients. J. Phys. Chem. Ref. Data, 1:3-118, 1972.

15. Maxwell, J. C. Scientific Papers, II. Dover Publications, Inc., New York, 1952.

16. Penman, H. L. Gas and Vapour Movements in the Soil. I. The Diffusion of Vapours through Porous Solids. J. Agr. Res., 30:437-462, 1940a.

17. Penman, H. L. Gas and Vapour Movements in the Soil. II. The Diffusion of Carbon Dioxide through Porous Solids. J. Agr. Res., 30:570-581, 1940b.

18. Pritchard, D. T. and J. A. Currie. Diffusion Coefficients of Carbon Dioxide, Nitrous Oxide, Ethylene and Ethane in Air and their Measurement. J. Soil Sci., 33:175-184, 1982.

19. Rixon, A. J. and B. J. Bridge. Respiratory Quotient Arising from Microbial Activity in Relation to Matric Suction and Air-Filled Pore-Space of Soil. Nature, 218:961-962, 1968.

20. Russell, E. J. and A. Appleyard. The Atmosphere of the Soil. Its Composition and the Causes of Variation. J. Agric. Sci., 7:1-48, 1915.

21. Troeh, F. R., J. D. Jabro, and D. Kirkham. Gaseous Diffusion Equations for Porous Materials. Geoderma, 27:239-253, 1982.

22. Smith, K. A. Soil Aeration. Soil Sci., 123:284-291, 1977.

23. Toor, H. L. Diffusion in Three-Component Gas Mixtures. Appl. Ind. Chem. Eng. J., 3:198-207, 1957.

24. Vasaru, G., G. Miller, G. Reinhold, and T. Fodor. The Thermal Diffusion Column. Veb Deutscher Verlag der Wissenschaften, Berlin, 1969.

25. Wilke, C. R. Diffusional Properties of Multicomponent Gases. Chem. Eng. Prog., 46:95-104, 1950.

26. Wood, J. T. and D. J. Greenwood. Distribution of Carbon Dioxide and Oxygen in the Gas Phase of Aerobic Soils. J. Soil Sci., 22:281-288, 1971.

APPENDIX B

PARAMETER VALUES USED IN THE PYRITE OXIDATION MODEL

D_c

The coupled counter-current diffusion coefficient for the diffusion of reactants and products within the coarse fragments was assigned a value comparable to measure diffusion coefficients in soil. Cathles (1979) used a value of 1.6×10^{-7} cm^2/sec for D_c in stone fragments. Elgawhary et al. (1970) and Palmer and Blanchar (1980) measured values of about 1.8×10^{-7} and from $0.3 - 1.0 \times 10^{-6}$ cm^2/sec for zinc diffusion and for potassium diffusion in soils, respectively. A value from the lower range was used for this model and was equal to 1.0×10^{-7} cm^2/sec.

K_s

Numerous workers have investigated pyrite oxidation rates, unfortunately most have ignored the fact that pyrite oxidation is a surface reaction, which makes estimation of K_s difficult. McKay and Halpern (1958) and Braley (1954) showed pyrite oxidation rate is proportional to pyrite surface area. Lorenz and Tarpley (1964) studied the reaction rate for three different pyrite sizes under a variety of oxidizing conditions. Clark (1965) combined their results with those of Braley (1954), (which gave surface area of pyrite fragments versus particle size as measured by screen sieving), to show the relationship between reaction rate, oxidant concentration and pyrite surface area. Making surface area determinations for irregularly shaped, framboidal pyrite grains is extremely difficult.

Extrapolating these results from one set of samples to another must be done with extreme caution due to the great variety of pyrite grain shapes and sizes. However, we can assume that the most finely ground pyrite will tend to have the most uniform fragment shape and use these values to calculate K_s from the data presented by Clark (1965). This gives a value of 1.8×10^{-9} cm/sec for K_s when oxygen is the oxidizer (curve 1, Clark, 1965, Figure 12, p. 113), and 8.6×10^{-4} cm/sec (curve 3) and 8.1×10^{-8} cm/sec (curve 4) when Fe^{3+} is the oxidizer.

Singer and Stumm (1968) in studying the reduction rate of Fe^{3+} by pyrite found that the reaction is first-order with respect to Fe^{3+} concentration, but conversely, they found the reaction rate constant was inversely dependent on the Fe^{3+} concentration. They had no explanation for this apparent contradiction, but from the data it appears that their assumption of non-limiting pyrite surface area was in error. This can be seen in their Figures 5-18 where doubling the surface area at fixed Fe^{3+} concentrations caused a doubling of the reaction rate. If available surface area was not limiting an increase would not be expected. Extension of the experiments to greater pyrite surface area-Fe^{3+} concentration ratios should verify this relationship. Using the Singer and Stumm (1968) values for the reaction rate constant and the surface area information presented by Clark (1965), we calculate K_s values for Fe^{3+} oxidation to be 4.4×10^{-6} cm/sec when available pyrite surface area is least

limiting and 10.0×10^{-6} cm/sec when most limiting. The former value is preferred in view of the argument above.

In a study by the Ohio State University Research Foundation (1970) reaction rate and surface area determinations were made for both Fe^{3+} and O_2 oxidants of primary sulphur ball pyrite. They found the maximum value of K_s for O_2 reduction, to be 12.0×10^{-8} cm/sec when dissolved O_2 concentrations were the least and a minimum K_s value of 4.4×10^{-8} cm/sec when dissolved O_2 concentrations were the greatest. These values indicate a slight coupling effect of available surface area with O_2 concentrations. They also found K_s for the Fe^{3+} system to equal a maximum of 4.4×10^{-6} cm/sec for the minimum Fe^{3+} concentration studied and 7.5×10^{-8} cm/sec for the highest Fe^{3+} concentration.

Pionke, et al. (1980) measured pyrite oxidation rates for fresh shale fragments, exposed to 20% O_2, to be 0.45 mg SO_4^{2-} per hour. They did not specify pyrite grain size or surface area, but measured the pyrite concentration in the shale to be 3.8% by weight. From the work of Caruccio (1973), we can assume that the active-pyrite grains in their samples were on the order of 0.2 microns in size. Using this approximation and assuming the grains to be spherical, we can calculate the K_s value for their material to be 8.3×10^{-8} cm/sec, in excellent agreement with the other values. K_s values for the O_2 system, $K_s(O_2)$, and for the Fe^{3+} system, $K_s(Fe^{3+})$, are summarized in Table B1. In this model a value of 8.3×10^{-8}

Table B1. K_s values for Fe^{3+} and O_2 system.

Source	K_s (cm/hr)	
	Fe^{3+}	O_2
	---------- oxidant ----------	
Clark (1965)	8.6×10^{-8}	$18. \times 10^{-8}$
	8.1×10^{-8}	----
Singer and Stumm (1968)	4.4×10^{-6}	----
	$10. \times 10^{-8}$	----
OSURF (1970)	4.4×10^{-6}	$12. \times 10^{-8}$
	7.5×10^{-8}	4.4×10^{-8}
Pionke, et al. (1980)	----	8.3×10^{-8}

cm/sec was used for $K_s(O_2)$ and a value of 4.4×10^{-6} cm/sec for $K_s(Fe^{3+})$ was used.

$\underline{\alpha}$

The surface area of pyrite per unit volume of fragment was calculated from the pyrite content of a fragment. Donaldson, et al. (1977) measured the surface area for sandstone to be approximately 10^4 cm^2/g. This surface area was then modified by the pyrite content and the pyrite and fragment densities. In particular:

$$\alpha = 10^4 \cdot \rho_{FR} \cdot (FPY\ \rho_{Fr}/\rho_{py})^{2/3} \qquad [B1]$$

where ρ_{FR} is the fragment density (g/cm^3), ρ_{py} is the pyrite density (5.0 g/cm^3), and FPY is the fraction of pyrite in a fragment (g/g). For a fragment having a 0.002 pyrite fraction and a bulk density of 2.1 g/cm^3, α equals 187 cm^2/cm^3.

$\underline{\partial}$

The thickness of the fragment in which pyrite is being oxidized can be calculated in a manner similar to that used by Cathles (1979). First, we assume that the oxidant is diffusing through a leached rim of the fragment, where no uptake is occurring, to a zone where pyrite is oxidizing at a rate proportional to the oxidant concentration.

$$D_c\ d^2C(x)/dx^2 - \alpha\ K_s C(x) = 0 \qquad [B2]$$

or:

$$d^2C(x)/dx^2 - \frac{\alpha\ K_s}{D_c} D(x) = 0 \qquad [B3]$$

where C is concentration of the oxidant, α the surface area of pyrite per unit volume, D_c the diffusion coefficient of the oxidant in the fragments, K_s the first-order reaction rate constant and x is depth into the fragment. The solution to Eq. [B3] is of the form

$$C(x) = C_1 \exp(\alpha K_a/D_c)^{1/2} + C_2 \exp[-(\alpha K_s/D_c)^{1/2}] \quad [B4]$$

Eq. [B4] can be solved subject to the boundary conditions:

$$dC(x)/dx = 0.0 \qquad x = \ell, \text{ one-half thickness of fragment} \quad [B5]$$

$$C(x) = C_{R\ell} = C_{\ell'} \qquad x = \ell' = R\ell \quad [B6]$$

where ℓ' is the depth of the leached rim and R = 1.0 - fraction pyrite remaining/initial pyrite fraction. Taking the derivative of Eq. [B4] with respect to x and using Eq. [B5] gives:

$$0.0 = b\, C_1 \exp(b\ell) - b\, C_2 \exp(-b\ell) \quad [B7]$$

where $b = (\alpha K_s/D_c)^{1/2}$

Rearranging Eq. [B7]:

$$C_1 = C_2 \exp(-b\ell)/\exp(b\ell) = C_2 \exp(-2b\ell) \quad [B8]$$

From Eqs. [B4] and [B6] we find:

$$C_{R\ell} = C_1 \exp(bR\ell) + C_2 \exp(-bR\ell) \quad [B9]$$

or rearranging:

$$C_1 = \{C_{R\ell} - C_2 \exp(bR\ell) / \exp(bR\ell)\} \quad [B10]$$

Eqs. [B8] and [B10] can be used to find the values of C_1 and C_2, giving:

$$C_1 = \frac{C_{R\ell}\exp(-2b\ell)}{\exp(bR\ell-2b\ell)+\exp(-bR\ell)} = C_{R\ell}\ C_1' \qquad [B11]$$

$$C_2 = \frac{C_{R\ell}}{\exp(bR\ell-2b\ell)+\exp(-bR\ell)} = C_{R\ell}\ C_2' \qquad [B12]$$

The reaction rate, R_{dx}, for the fragment can be expressed for a unit area and depth, dx, as:

$$R_{dx} = \alpha\ K_s\ C(x)\ dx \qquad [B13]$$

The rate per unit surface area for the entire fragment is:

$$R_T = \int_0^{\ell} \alpha\ K_s C(x)\ dx = \int_{R\ell}^{\ell} \alpha\ K_s C(x)\ dx \qquad [B14]$$

Since no reaction is taking place in the leached rim, $0 < x < R\ell$. Substituting Eq. [B4] for C(x) and Eqs. [B11] and [B12] for C_1 and C_2, Eq. [B14] becomes

$$R_T = \alpha\ K_s \int_{R\ell}^{\ell} [C_{R\ell}\ C_1'\ \exp(bx) + C_{R\ell}\ C_2'\ \exp(-bx)]\ dx \qquad [B15]$$

which upon integration becomes:

$$R_T = \alpha\ K_s C_{R\ell}/b \left[C_1'\ [\exp(b\ell) - \exp(bR\ell)] - C_2'\ [\exp(-b\ell) - \exp(-bR\ell)]\right] \qquad [B16]$$

For the pyrite oxidation model, we want to replace the expression for R_T with one of the form

$$R_T = \alpha\ K_s\ C_{x=o}\ \partial \qquad [B17]$$

Combining Eqs. [B16] and [B17] and solving for ∂ gives:

$$\partial = \frac{C_R}{C_{x=\theta}} \left[C_1' \left[\exp(b\ell) - \exp(bR\ell)\right] - C_2' \left[\exp(-b\ell) - \exp(-bR\ell)\right]\right] = \frac{C_{R\ell}}{C_{x=o}\ b} \cdot C' \qquad [B18]$$

Within the depleted rim there is no uptake of oxidant and the C(x) vs x curve will be linear. The flux of oxidant, Q_o, can be expressed as:

$$R_T = Q_o = -D_c\ dC(x) = -D_c\ \frac{C_{x=o} - C_{R\ell}}{0.0 - R\ell} \qquad [B19]$$

and

$$\frac{C_{R\ell}}{C_{x=o}} = 1.0 - R\ell/D_c\ Q_o/C_{x=o}$$

$$= 1.0 - R\ell/D_c\ R_T/C_{x=o} \qquad [B20]$$

Substituting Eq. [B17] into Eq. [B20] gives

$$C_{R\ell}/C_{x=o} = 1.0 - R\ell/D_c \alpha\ K_s\ \partial \qquad [B21]$$

which when substituted into Eq. [B18] gives:

$$\partial = C'\ (1.0 - R\ell/D_c\ \alpha\ K_s\ \partial)/b \qquad [B22]$$

which can be rearranged

$$\partial = C'/(b + R\ell/D_c\ \alpha\ K_s\ C') \qquad [B23]$$

Eq. [B23] was then used to calculate ∂ as a function of oxidant concentration, reaction rate, diffusion rate and degree of pyrite weathering.

FFR

The fraction of fragments composing the spoil, FFR, was assumed to 0.75 (wt./wt.) This compares with values measured by Pedersen, et al. (1980) of from 0.5 to 0.9.

FPY and ρ_{py}

The average pyrite content of the spoil composing a reclaimed stripmine was measured by Rogowski (1977) to be approximately 0.001 pyritic S by weight or 0.002 pyrite by weight. In this model we assume all the pyrite to be contained within the coarse fragments which comprise 75% of the total spoil weight. Thus, we set FPY equal to .002/.75 or 0.0025. For a bulk density of 1.5 and a fragment fraction of 0.75, this value of FPY corresponds to a molar density of pyrite of $\rho_{py} = 0.0025 \cdot 0.75 \cdot 1.5/120. = 23 \times 10^{-6}$ moles pyrite/cm^3.

ρ_B, ϕ_A and ϕ_w

The bulk density for minesoils was measured by Pedersen, et al. (1980) to average about 1.57 g/cm^3, which corresponds to a total porosity of 0.4 (particle density = 2.62 g/cm^3). We have assumed a percent water saturation of 75% in this model based on measured values (Rogowski, et al., 1982). With these values for total porosity and water content, a good estimate for the air-filled porosity, ϕ_A, is 0.12 cm^3/cm^3 and 0.28 cm^3/cm^3 for ϕ_w.

Unfortunately, a mistake was made in running the simulations where ϕ_A was set to 0.06 cm^3/cm^3 instead. This corresponds to a bulk density of 1.7 g/cm^3, which is still within the range measured by Pedersen, et al. (1980).

$\underline{\tau}$

Colvin (1977)[2] measured the diffusion coefficient for O_2 in shale spoil. He found the ratio of the diffusion coefficient in spoil to the coefficient in air to be 0.013 at an air-filled porosity of 0.13. For these conditions τ can be calculated to be $\tau = 0.13/.013 = 10$, which was the base value in the model.

REFERENCES

1. Braley, S. A. Summary Report on Commonwealth of Pennsylvania, Department of Health Industrial Fellowship, Nos. 1, 2, 3, 4, 5, 6 and 7. Mellon Institute, Fellowship No. 326B, 1954.
2. Caruccio, F. T. Characterization of Strip-Mine Drainage by Pyrite Grain Size and Chemical Quality of Existing Groundwater. In: Ecology and Reclamation of Devastated Land, R. J. Hutnik and G. Davis, eds. Gordon and Breach, New York, 1973. pp. 193-226.
3. Cathles, L. M. Predictive Capabilities of a Finite Difference Model of Copper Leaching in Low Grade Industrial Sulfide Waste Dumps. Mathematical Geol., 11:175-191, 1979.
4. Clark, C. S. The Oxidation of Coal Mine Pyrite. Ph.D. Thesis, John Hopkins University, University Microfilms, Inc., Ann Arbor, Michigan. No. 65-10-278, 1965.
5. Donaldson, E. C., R. F. Kendall, and B. A. Baker. Surface-Area Measurement of Geologic Materials. Soc. Petrol. Eng. J., 15:111-116, 1975.
6. Elgawhary, S. M., W. L. Lindsay, and W. D. Kemper. Effect of EDTA on the Self-Diffusion of Zinc in Aqueous Solution and in Soil. Soil Sci. Soc. Am. J., 44:925-929, 1970.
7. Lorentz, W. L. and E. L. Tarpley. Oxidation of Coal Mine Pyrites. Report of Invest. No. 6247, U.S. Bureau of Mines, 1963.
8. Mckay, O. R. and J. Halpern. A Kinetic Study of the Oxidation of Pyrite in Aqueous Suspension. Trans. Met. Soc., AIME 212:301-309, 1958.

9. Ohio State University Research Foundation. Sulfide to Sulfate Reaction Mechanism. Water Pollution Control Research Series 14010 FPS 02/70, Federal Water Pollution Control Administration, Washington, D.C., 1970.

10. Palmer, C. J. and R. W. Blanchar. Prediction of Diffusion Coefficients from the Electrical Conductance of Soil. Soil Sci. Soc. Am. J., 44:925-929, 1980.

11. Pedersen, T. A., A. S. Rogowski, and R. Pennock, Jr. Physical Characteristics of Some Minesoils. Soil Sci. Soc. Am. J., 44:321-328, 1980.

12. Pionke, H. B., A. S. Rogowski, and C. A. Montgomery. Percolate Quality of Strip Mine Spoil. Trans. ASAE, 23:621-628, 1980.

13. Rogowski, A. S. Acid Generation within a Spoil Profile: Preliminary Experimental Results. In: Seventh Symposium on Coal Mine Drainage Research, NCA/BCR Coal Conference and Expo IV, Oct. 18-20, Louisville, Kentucky, 1977. pp. 25-40.

14. Rogowski, A. S., H. B. Pionke, and B. E. Weinrich. Some Physical and Chemical Aspects of Reclamation. Preprint, paper presented at the North Atlantic Region ASAE 1982 Annual Meeting, 1982.

15. Singer, P. C. and W. Stumm. Acidic Mine Drainage: The Rate Determining Step. Science, 167:1121-1123, 1970.

APPENDIX C

COMPUTER LISTING AND EXAMPLE OUTPUT OF ACID MINE DRAINAGE MODEL

Computer Listing of Acid Mine Drainage Model

```
//MNWXXXXX      JOB      (DXJ79)
// EXEC PGM=UMSG,PARM=(INTERACT,'TO D1J JOB RUNNING')
//DELETE DD VOL=REF=MEN.P65440.D1J.LIB,
//  DSN=MEN.P65440.D1J.DMNLS8,
//  DISP=(OLD,DELETE)
/*
// EXEC FWCG,PARM=NOSOURCE
/*JOBPARM FULLSKIPS,UCS=TN,FORMS=16,V=NORMAL
//SYSIN DD *
      IMPLICIT REAL*8 (A-H,O-Z)
      INTEGER O,OPRINT
      REAL*8 NA,NB,NAI,NBI,KB(50),KBMAX,NC2,NC(50),NCI,NCIO,LSMAX,
     1KBO,KB1,KB2,KBO(50),KBA(50),KBH(50),KBL(50),LS(50),LSO(50)
      REAL*4 KSP,K11,K12,K13,K14,K22,KML,KMHL,KA2,KOX1,KOX2,INFILR,
     1L,KSO,KSF,DCO,DCF,KLS,MWLS,DCO2
      DIMENSION X(50),YA(50),YB(50),NA(50),H2CO3(50),OH2CO3(50),
     1NB(50),R(50),T(50),PHI(50),FFR(50),RHOB(50),TE(50),TO(50),
     2FPY(50),RHOFR(50),UA(50),UB(50),UAN(50),EA(50),EB(50),
     3DX(50),DA(50),DB(50),FA(50),FB(50),TA(50),YAO(50),YBO(50),
     4PYO(50),QA(50),QB(50),PY(50),YAX(50),YBX(50),YAH(50),YAL(50),
     5PYX(50),NAI(50),NBI(50),UAO(50),UBO(50),U(50),RR(50),
     6ALPHA(50),DELTAO(50),DXFO(50),DXF(50),TB(50),CO3FL(50),TFE3C(50),
     7AFE3T(50),FE2(50),FE3(50),PYF(50),PYO2(50),TFE3CX(50),
     8ST(50),FE2X(50),YAXO(50),YBXO(50),GA(50),GB(50),
     9FFEO(50),WC(50),OIO(50),OH(50),OE3(50),OEOH(50),OEOH2(50),
     1OEOH4(50),OE2OH2(50),OESO4(50),OEHSO4(50),OEOOH(50),OSO4(50)
     2,H(50),FEOOH(50),OEOH3(50),OST(50),OE2(50),OHBOX(50),HBACT(50),
     3OE2OX(50),OHSO4(50),G1(50),DELTAF(50),HC(50),AHLS(50),AHLSX(50),
     4OE2B(50),OHC(50),FE3FL(50),FE2FL(50),HFL(50),DX2(50),
     5STFL(50),HCFL(50),CAFL(50),CA(50),OCA(50),RLS(50),FLS(50)
      EXTERNAL DO,DCO2,DAB,DBC,DAC,FLUX
      COMMON/ADEL/KSO,DCO,KSF,DCF,L
     1/ACHEMI/FE31,H1,TFE3C,KSP,KA2,K11,K12,K13,K14,K22,KML,KMHL,MCHEMI
     1/ACHCAL/OIO,OEOH,OEOH2,OEOH3,OEOH4,OE2OH2,OESO4,
     2OEHSO4,OEOOH,OSO4,OHSO4,ST,FE2,OH,OE3,OE2,
     3OST,CA,OCA,H2CO3,OH2CO3,I/AHADJ/HC,OHC,HCFL,GA,GB/AFLUX1/H,FE3,X,
     4DX,DT,INFILR,N
      EQUIVALENCE (FFEO,OE2B)
      CALL ERRSET(208,256,-1,1)
      CALL TIMREM(IREMO)
      READ, IDUMP
C*****************************************************************C
C                                                                 C
C                        SET IN CONSTANTS                         C
C                                                                 C
C*****************************************************************C
      MCHEMI=-10
      MM=MSWEEP=M=0
      RHOPY=5.0
      PI=3.14159265
      KSP=79433.0
      KA2=.073
      K11=.00116
      K12=2.0E-06
      K13=1.0E-12
      K14=2.5E-22
      K22=6.0E-06
      KML=84.0
      KMHL=4.0
      KOX1=1.3E-19
      KOX2=1.7E-12
      BO=1./3.5
      BF=1./14.
      EMIN=.173
      IF(IDUMP.EQ.1) THEN
C*****************************************************************C
C                                                                 C
C                        INITIALIZE VALUES IF T=0.                C
C                              (IDUMP=1)                          C
C                                                                 C
C*****************************************************************C
```

```
      READ31,OPRINT,MBAT,L,RADIUS,Y,Z,
     1DCO,KSO,DCF,KSF,KLS,P,RG,E1,ET,MT,INFILR,MWLS,RHOLFR
      INFILR=INFILR/(365.*86400.)
      PR=P/RG
      DX(1)=1.
      X(1)=-.5
      IF(MT.EQ.1) THEN
      DDT=DT=86400.*2.
      ELSE
      DDT=DT=MT
      END IF
      READ35,DEPTH,NL,VINC,NPL
      N=NL*NPL+1
      IF(N.EQ.1) READ31,N
      READ36,X(2),YA(1),YB(1),T(1),PHI(1),WC(1),FFR(1),
     1RHOB(1),FPY(1),FFEO(1),RHOFR(1),TE(1),GA(1),GB(1),HBACT(1),
     2RLS(1),FLS(1)
      DO 30 I=2,N
      IF(X(2).GT.0.0) X(I)=X(I-1)+X(2)
      IF(YA(1).NE.-1.) YA(I)=YA(I-1)
      IF(YB(1).NE.-1.) YB(I)=YB(I-1)
      IF(FFR(1).NE.-1.) FFR(I)=FFR(1)
      IF(RHOB(1).NE.-1.) RHOB(I)=RHOB(1)
      IF(FPY(1).NE.-1.) FPY(I)=FPY(1)
      IF(FFEO(1).NE.-1.) FFEO(I)=FFEO(1)
      IF(RHOFR(1).NE.-1.) RHOFR(I)=RHOFR(1)
      IF(T(1).NE.-1.) T(I)=T(1)
      IF(PHI(1).NE.-1.) PHI(I)=PHI(1)
      IF(WC(1).NE.-1.) WC(I)=WC(1)
      IF(TE(1).NE.-25.) TE(I)=TE(1)
      IF(GA(1).NE.-1.) GA(I)=GA(1)
      IF(GB(1).NE.-1.) GB(I)=GB(1)
      IF(RLS(1).NE.-1.) RLS(I)=RLS(1)
      IF(FLS(1).NE.-1.) FLS(I)=FLS(1)
      IF(HBACT(1).NE.1.) HBACT(I)=HBACT(1)
      IF(I.NE.21) FLS(I)=0.
30    CONTINUE
31    FORMAT(I2,/,I2,/,13(G10.0,/),I10,3(/,G10.0))
35    FORMAT(G10.0,/,I2,/,G10.0,/,I2)
36    FORMAT(G10.0)
      IF(X(2).EQ.-1.) READ,(X(I),I=1,N)
      IF(X(2).EQ.0.) THEN
      NI=NPL
      DO 32 I=2,NL
      NI=NI+NPL*VINC**(I-1)
32    CONTINUE
      DI=DEPTH/NI
      II=2
      DO 34 J=1,NL
      DO 33 I=1,NPL
      DX(II)=DI
      X(II)=X(II-1)+DX(II)/2.+DX(II-1)/2.
      II=II+1
33    CONTINUE
      DI=DI*VINC
34    CONTINUE
      END IF
      IF(YA(1).EQ.-1.) READ,(YA(I),I=1,N)
      IF(YB(1).EQ.-1.) READ,(YB(I),I=1,N)
      IF(T(1).EQ.-1.) READ,(T(I),I=1,N)
      IF(PHI(1).EQ.-1.) READ,(PHI(I),I=1,N)
      IF(WC(1).EQ.-1.) READ,(WC(I),I=1,N)
      IF(FFR(1).EQ.-1.) READ,(FFR(I),I=1,N)
      IF(RHOB(1).EQ.-1.) READ,(RHOB(I),I=1,N)
      IF(FPY(1).EQ.-1.) READ,(FPY(I),I=1,N)
      IF(FFEO(1).EQ.-1.) READ,(FFEO(I),I=1,N)
      IF(RHOFR(1).EQ.-1.) READ,(RHOFR(I),I=1,N)
      IF(TE(1).EQ.-25.) READ,(TE(I),I=1,N)
      IF(GA(1).EQ.-1.) READ,(GA(I),I=1,N)
      IF(GB(1).EQ.-1.) READ,(GB(I),I=1,N)
      IF(HBACT(1).EQ.1) READ,(HBACT(I),I=1,N)
      IF(RLS(1).EQ.-1) READ,(RLS(I),I=1,N)
      IF(FLS(1).EQ.-1) READ,(FLS(I),I=1,N)
      NBAT=51
      O=0
      TZ1=TZ2=TZ3=TZ4=TZ5=TZ6=TZ7=TZ8=TFEO=TT=TUT=0.
      PRINT756,T(2),PHI(2),WC(2),FFR(2),RHOB(2),FPY(2),FFEO(2),
     1RHOFR(2),TE(2),GA(2),GB(2),HBACT(2),RLS(2),FLS(2),RHOLFR,L
756   FORMAT(10X,'T= ',F6.3,10X,'PHI= ',F6.3,10X,'WC= ',F6.3,
```

```
151.          1/,10X,'FFR= ',F6.3,8X,'RHOB= ',F6.3,9X,'FPY= ',F7.4,/,10X,
152.          2'FFEO= ',F6.3,7X,'RHOFR= ',F6.3,8X,'TE= ',F6.3,/,10X,
153.          3'GA= ',F8.4,7X,'GB= ',F6.3,11X,'HBACT= ',F6.3/,10X,'RLS= ',
154.          4F8.4,6X,'FLS= ',F8.4,8X,'RHOLFR= ',F8.4,/,10X,'L= ',F6.3)
155.           DO 40    J=1,N
156.           I=N-J+1
157.           RLS(I)=2.*MWLS*KLS/(RLS(I)*RHOLFR)
158.           FLS(I)=FLS(I)*RHOB(I)/(2.*MWLS)
159.           H2CO3(I)=DCO2(TE(I))*YB(I)
160.           TO(I)=TE(I)=TE(I)+273.
161.           ALPHA(I)=(FPY(I)*RHOFR(I)/RHOPY)**(2./3.)*RHOFR(I)*10000.
162.           Z1=WC(I); Z2=PHI(I)
163.           WC(I)=Z2*Z1
164.           PHI(I)=Z2*(1.-Z1)
165.           T(I)=PHI(I)/T(I)
166.           OHBOX(I)=OE2B(I)=OE2OX(I)=UB(I)=0.
167.           HC(I)=1.D-20
168.           KBA(I)=KBO(I)=KB(I)=0.D-15
169.           LSO(I)=LS(I)=PYO(I)=UAO(I)=DXFO(I)=PY(I)=1.0;PYF(I)=PYO2(I)=1.D-25
170.           IF(FPY(I).EQ.0.0) PY(I)=0.0
171.           IF(RLS(I)*FLS(I).EQ.0.0) LSO(I)=LS(I)=0.0
172.           YAXO(I)=YAX(I)=YAO(I)=YA(I)
173.           YBXO(I)=YBX(I)=YBO(I)=YB(I)
174.           CALL DELCAL(ALPHA(I),PY(I),DELTAO(I),DELTAF(I))
175.           NAI(I)=NA(I)=1.0; NBI(I)=NB(I)=-1.
176.           CA(I)=OE2(I)=FE2(I)=5.0D-07
177.           ST(I)=5.0D-05
178.           FEOOH(I)=1000.*FFEO(I)*RHOB(I)/(89.*WC(I))
179.           H(I)=1.0D-05
180.           CALL CHEMI(-1,H(I),FE3(I),FEOOH(I),AFE3T(I),G1(I))
181.           H(I)=OH(I); FE3(I)=OE3(I)
182.           UAN(I)=-DCO*RHOB(I)*FFR(I)*DO(TE(I))*ALPHA(I)*KSO/(32.*RHOFR(I)*L)
183.           UA(I)=YA(I)*UAN(I)*DELTAO(I)/(ALPHA(I)*DELTAO(I)*KSO*
184.          1L*(1.-PY(I))+DCO)
185.           U(I)=UA(I)/YA(I)
186.           DXF(I)=-120.*BF*DCF*ALPHA(I)*KSF/(RHOFR(I)*FPY(I)*L)
187.           R(I)=-0.05
188.     40    CONTINUE
189.           T(1)=T(2)
190.           LSO(1)=LS(1)=PY(1)=UA(1)=DXF(1)=UAO(1)=UAN(1)=FEOOH(1)=0.0
191.           OCA(1)=CA(1)=ST(1)=FE2(1)=HC(1)=FE3(1)=1.0D-15
192.     C*****************************************************************C
193.     C                                                                 C
194.     C                        RETRIEVE DUMPED VALUES                   C
195.     C                              (IDUMP=0)                          C
196.     C                                                                 C
197.     C*****************************************************************C
198.           ELSE
199.           READ(43,202) OPRINT,O,N,NBAT,MBAT,MT,E1,PR,DT,DDT,TT,ET,TUT,
200.          1TZ1,TZ2,TZ3,TZ4,TZ5,TZ6,TZ7,TZ8,KSO,DCO,KSF,DCF,L,INFILR,TFEO
201.           READ(43,201) (YA(I),I=1,N)
202.           READ(43,201) (YB(I),I=1,N)
203.           READ(43,201) (PY(I),I=1,N)
204.           READ(43,201) (PYO(I),I=1,N)
205.           READ(43,201) (TE(I),I=1,N)
206.           READ(43,201) (TO(I),I=1,N)
207.           READ(43,201) (X(I),I=1,N)
208.           READ(43,201) (DX(I),I=1,N)
209.           READ(43,201) (T(I),I=1,N)
210.           READ(43,201) (UAN(I),I=1,N)
211.           READ(43,201) (UA(I),I=1,N)
212.           READ(43,201) (UAO(I),I=1,N)
213.           READ(43,201) (ALPHA(I),I=1,N)
214.           READ(43,201) (PHI(I),I=1,N)
215.           READ(43,201) (WC(I),I=1,N)
216.           READ(43,201) (RHOB(I),I=1,N)
217.           READ(43,201) (RHOFR(I),I=1,N)
218.           READ(43,201) (FFR(I),I=1,N)
219.           READ(43,201) (FPY(I),I=1,N)
220.           READ(43,201) (FEOOH(I),I=1,N)
221.           READ(43,201) (ST(I),I=1,N)
222.           READ(43,201) (FE3(I),I=1,N)
223.           READ(43,201) (FE2(I),I=1,N)
224.           READ(43,201) (H(I),I=1,N)
225.           READ(43,201) (DXF(I),I=1,N)
```

```
226.          READ(43,201) (DXFO(I),I=1,N)
227.          READ(43,201) (OE2B(I),I=1,N)
228.          READ(43,201) (OE2OX(I),I=1,N)
229.          READ(43,201) (KB(I),I=1,N)
230.          READ(43,201) (KBO(I),I=1,N)
231.          READ(43,201) (OIO(I),I=1,N)
232.          READ(43,201) (HC(I),I=1,N)
233.          READ(43,201) (HBACT(I),I=1,N)
234.          READ(43,201) (OHBOX(I),I=1,N)
235.          READ(43,201) (R(I),I=1,N)
236.          READ(43,201) (OE3(I),I=1,N)
237.          READ(43,201) (OE2(I),I=1,N)
238.          READ(43,201) (OH(I),I=1,N)
239.          READ(43,201) (YAO(I),I=1,N)
240.          READ(43,201) (YBO(I),I=1,N)
241.          READ(43,201) (GA(I),I=1,N)
242.          READ(43,201) (GB(I),I=1,N)
243.          READ(43,201) (CA(I),I=1,N)
244.          READ(43,201) (LS(I),I=1,N)
245.          READ(43,201) (LSO(I),I=1,N)
246.          READ(43,201) (RLS(I),I=1,N)
247.          READ(43,201) (FLS(I),I=1,N)
248.          READ(43,201) (H2CO3(I),I=1,N)
249.          READ(43,201) (OH2CO3(I),I=1,N)
250.          FPY(1)=0.0; PYF(1)=PYO2(1)=1.0D-25; E1=.00001
251.          DO 38 I=1,N
252.          CALL DELCAL(ALPHA(I),PY(I),DELTAO(I),DELTAF(I))
253.          CALL CHEMI(1,H(I),FE3(I),FEOOH(I),AFE3T(I),Z)
254.          KBA(I)=KB(I)
255.          NAI(I)=NA(I)=1.0; NBI(I)=NB(I)=-1.
256.          G1(I)=1.0
257.     38   CONTINUE
258.          IF(1.EQ.2) THEN; TT=TT-DT/86400.
259.          DT=DDT=DT*2.
260.          TT=TT+DT/86400. ; END IF
261.          END IF
262.          HCFL(1)=0.
263.          EB(1)=EA(1)=1.0
264.          DA(1)=DB(1)=0.
265.          PYX(1)=PYO(1)=PY(1)
266.          U(1)=NA(1)=NB(1)=0.0
267.          OHC(1)=HC(1)
268.          KBA(1)=KB(1)
269.          QA(1)=YAX(1)=YA(1)
270.          QB(1)=YBX(1)=YB(1)
271.          NAI(N)=NBI(N)=TB(N)=TA(N)=0.
272.           Z=FLUX(0)
273.     C*****************************************************************C
274.     C                                                                 C
275.     C    CONSTANT PART OF TRANSMISSIBILITIES ARE CALCULATED           C
276.     C                                                                 C
277.     C*****************************************************************C
278.     400  CALL TIMREM(IREM)
279.          IF(2.*IREM-IREMO.LT.50) GO TO 200
280.          IF(TT.GT.1850.) GO TO 200
281.          IREMO=IREM
282.          PRINT789
283.     789  FORMAT('1')
284.          DO 70 I=1,N
285.          TEMP=TE(I)
286.          TA(I)=T(I)*DAB(TEMP)*DAC(TEMP)/TEMP
287.          TB(I)=T(I)*DAB(TEMP)*DBC(TEMP)/TEMP
288.     70   CONTINUE
289.     C*****************************************************************C
290.     C                                                                 C
291.     C    CALCULATE EXTRAPOLATED VALUES AND LEACH RATES                C
292.     C                                                                 C
293.     C*****************************************************************C
294.          YAXO(1)=YAX(1)=YA(1); YBXO(1)=YBX(1)=YB(1)
295.          DO 50 I=2,N
296.          ASX=LS(I)+(LS(I)-LSO(I))
297.          LSO(I)=LS(I)
298.          LS(I)=DMAX1(ASX,0.0D+00)
299.          YAX(I)=YA(I)+(YA(I)-YAO(I))
300.          YBX(I)=YB(I)+(YB(I)-YBO(I))
301.          IF(YAX(I).LT.0.) YAX(I)=YA(I)/2.; IF(YBX(I).LT.0.) YBX(I)=YB(I)/2.
302.          IF(O.GE.1) THEN
303.          Z3=H(I)+(H(I)-OH(I))
304.          Z1=FE3(I)+(FE3(I)-OE3(I))
305.          Z2=FE2(I)+(FE2(I)-OE2(I))
306.          OE3(I)=FE3(I)
```

```
307.          OE2(I)=FE2(I)
308.          IF(Z1.GT.0.) THEN; FE3(I)=Z1; ELSE; FE3(I)=FE3(I)/2.; END IF
309.          IF(Z2.GT.0.)THEN;FE2X(I)=FE2(I)=Z2;ELSE;FE2X(I)=FE2(I)=FE2(I)/2.
310.          END IF
311.          OH(I)=H(I)
312.          IF(Z3.GT.0.0) THEN; H(I)=Z3; ELSE; H(I)=H(I)/2.; END IF
313.          YBO(I)=YB(I)
314.          YAO(I)=YA(I)
315.          YA(I)=YAXO(I)=YAX(I)
316.          YB(I)=YBXO(I)=YBX(I)
317.          PYX(I)=PY(I)+(PY(I)-PYO(I))
318.          IF(PYX(I).LT.0.0) PYX(I)=PY(I)
319.          PYO(I)=PY(I)
320.          PY(I)=PYX(I)
321.          ELSE
322.          PYX(I)=PYO(I)=PY(I)
323.          END IF
324.    50    CONTINUE
325.    C*************************************************************C
326.    C                                                             C
327.    C     SIP COEFFICIENTS ARE CALCULATED FOR A AND B             C
328.    C                                                             C
329.    C*************************************************************C
330.    450   LSMAX=FLMAX=0.
331.          DO 55 I=2,N
332.          TFE3CX(I)=TFE3C(I)
333.          IF(MSWEEP.EQ.0)THEN; Z1=Z2=Z3=Z5=0.; ELSE
334.          Z1=HFL(I)
335.          Z2=FE3FL(I)
336.          Z3=FE2FL(I)
337.          Z5=HCFL(I)
338.          END IF
339.          H2CO3(I)=DCO2(TE(I))*YB(I)
340.          HFL(I)=FLUX(1)/WC(I)
341.          FE3FL(I)=FLUX(2)/WC(I)
342.          FE2FL(I)=FLUX(3)/WC(I)
343.          STFL(I)=FLUX(4)/WC(I)
344.          HCFL(I)=FLUX(5)/WC(I)
345.          CAFL(I)=FLUX(6)/WC(I)
346.          CO3FL(I)=FLUX(7)/WC(I)
347.          IF(MSWEEP.GT.0) THEN; HFL(I)=(HFL(I)+Z1)/2.
348.          FE2FL(I)=(FE2FL(I)+Z3)/2.
349.          HCFL(I)=(HCFL(I)+Z5)/2.
350.          END IF
351.          IF(HFL(I).NE.0.) FLMAX=DMAX1(FLMAX,DABS(1.-Z1/HFL(I)))
352.          IF(FE3FL(I).NE.0.) FLMAX=DMAX1(FLMAX,DABS(1.-Z2/FE3FL(I)))
353.          IF(FE2FL(I).NE.0.) FLMAX=DMAX1(FLMAX,DABS(1.-Z3/FE2FL(I)))
354.          IF(HCFL(I).NE.0.) FLMAX=DMAX1(FLMAX,DABS(1.-Z5/HCFL(I)))
355.    55    CONTINUE
356.          IF(0.EQ.0) GO TO 110
357.    500   NCI0=0.0
358.          RMAX=0.0
359.          DO 80 J=1,N
360.          I=N+1-J
361.          IF(M+MSWEEP.EQ.0) THEN
362.          KB(I)=(KB(I)+KBA(I))/2.; END IF
363.          IF(J.EQ.1) THEN
364.          YA2=YA3=YA(I)
365.          YB2=YB3=YB(I)
366.          X2=X(I)
367.          DA3=DB3=TA3=TB3=0.0
368.          X3=X2+(X2-X(I-1))
369.          ELSE
370.          DA3=DA2; DB3=DB2
371.          YA3=YA2; YB3=YB2
372.          YA2=YA1; YB2=YB1
373.          X3=X2; X2=X1
374.          TA3=TA2; TB3=TB2
375.          DAC3=DAC2; DAB3=DAB2; DBC3=DBC2
376.          TE3=TE2
377.          END IF
378.          IF(I.NE.1) THEN
379.          YA1=YA(I-1)
380.          YB1=YB(I-1)
381.          X1=X(I-1)
382.          XX1=(X2-X1)/((X3-X2)*(X2-X1)+(X3-X2)**2)
383.          XX2=(X3-X2)/((X3-X2)*(X2-X1)+(X2-X1)**2)
384.          ELSE; XX2=0.; XX1=1./(X3-X2)
385.          END IF
386.          T2=T(I); TA2=TA(I); TB2=TB(I)
387.          TE2=TE(I)
388.          DAC2=DAC(TE2); DAB2=DAB(TE2); DBC2=DBC(TE2)
389.          NCI=PHI(I)*PP/TE(I)*DX(I)/T**(NAO(I)-YBO(I)-YA2-YB2 +NCI0
```

```
      NC2=(NC1-NC10)/2.+NC10
      NC10=NC1
      IF(M.GT.0) NC2=(NC2+NC(I))/2.
      NC(I)=NC2
      Z=1.; MMM=0
      WHILE(Z.GT.1.0D-14.AND.MMM.LT.22)
      Z1=NA(I); Z2=NB(I)
      NA(I)=T2*DAB2*DAC2/(YB2*(DAC2-DAB2)-YA2*DAB2+DAB2)*(Z2*YA2/
     1(T2*DAB2)+NC2*YA2/(T2*DAC2)-PR/TE2*((YA3-YA2)*XX1+(YA2-YA1)*XX2))
      NB(I)=T2*DAB2*DBC2/(YA2*(DBC2-DAB2)-YB2*DAB2+DAB2)*(NA(I)*YB2/
     1(T2*DAB2)+NC2*YB2/(T2*DBC2)-PR/TE2*((YB3-YB2)*XX1+(YB2-YB1)*XX2))
      Z=DABS(NA(I)-Z1)+DABS(NB(I)-Z2)
      MMM=MMM+1
      END WHILE
74    IF(NA(I).EQ.0.0) THEN
      RR(I)=R2=-1.0D+16
      IF(NB(I).EQ.0.0) RR(I)=R(I)=R2=PI
      DA2=1.
      ELSE
      R2=RR(I)=NB(I)/NA(I)
      RMAX=DMAX1(RMAX,1.-DABS(R(I)/R2))
      R(I)=R2=(RR(I)+R(I))/2.
      DA2=YB2*(DAC2-DAB2)-YA2*(R2*DAC2+DAB2)+DAB2
      END IF
      IF(R2.EQ.0.0) THEN
      DB2=1.
      ELSEIF(R2.EQ.PI) THEN
      DB2=1.
      ELSE
      IF(R2.EQ.-1.0D+16) THEN
      Z=0.0
      ELSE
      Z=DBC2/R2
      END IF
      DB2=YA2*(DBC2-DAB2)-YB2*(Z+DAB2)+DAB2
      END IF
      FA(I)=4.*PR*TA3*TA2/(TA3*DA2+TA2*DA3)
      FB(I)=4.*PR*TB3*TB2/(TB3*DB2+TB2*DB3)
      DX2(I)=(X2-X1)*(X3-X2)+(X3-X2)**2
80    CONTINUE
      Z=0.0
      DO 85 J=2,N
      I=N+2-J
      DA(I)=FA(I-1)/DX2(I)
      DB(I)=FB(I-1)/DX2(I)
      FA(I)=FA(I)/DX2(I)
      FB(I)=FB(I)/DX2(I)
      FE21=FE2(I)
      H1=H(I)
      IF(NB(I).EQ.0.0) FB(I)=DB(I)
      U(I)=UAN(I)*DELTAO(I)/(ALPHA(I)*DELTAO(I)*KSO*
     1L*(1.-PY(I))+DCO)
      IF(O.EQ.0) UAO(I)=U(I)*YA(I)
      X1=DMIN1(0.0D+00,2.*HBACT(I)*(TE(I)-273.))
      EA(I)=-(DA(I)+FA(I)-(U(I)-WC(I)/4.*FE21*(KB(I)+KOX1
     1*H1**(-2)+KOX2)+X1))-PHI(I)*PR/(TE(I)*DT)
      EB(I)=-(DB(I)+FB(I)+DCO2(TE(I))/(DT*1000.))
      QA(I)=-PHI(I)*PR*YAO(I)/(TO(I)*DT)
      QB(I)=X1*YA(I)-((OH2CO3(I)+CO3FL(I))/1000.+(LSO(I)-LS(I))*FLS(I))
     1/DT
      Z=1.+Z+DABS(QB(I))+YB(I)/TE(I)-YBO(I)/TO(I)
      IF(Z.EQ.0.0) THEN
      QB(I)=YB(I)
      EB(I)=1.0
      DB(I)=FB(I)=FB(I-1)=0.
      ELSE
      EB(I)=EB(I)-PHI(I)*PR/(TE(I)*DT)
      QB(I)=QB(I)-PHI(I)*PR*YBO(I)/(TO(I)*DT)
      END IF
85    CONTINUE
      FA(1)=FB(1)=0.
C*****************************************************************C
C                                                                 C
C     SOLVE  FOR A AND B                                          C
C                                                                 C
C*****************************************************************C
      NTO=N
      NTTO=N
      CALL THOMAS(DA,EA,FA,QA,NTO,YAX)
      CALL THOMAS(DB,EB,FB,QB,NTTO,YBX)
C
C
      FCMAX=BMAX=FEPMAX=KBMAX=AMAX=PYMAX=PMAX=FEMAX=0.0
```

```
      DO 87 J=2,N
      IF(YAX(J).LT.0.) THEN; YAX(J)=YA(J); YA(J)=YA(J)/2.
      PRINT,J,YAX(J),'=YAX',YA(J),'=YA'; END IF
      IF(DB(J).EQ.0.) THEN
      YBX(J)=YBX(J-1)*DEXP((NA(J)/T(J)+NA(J-1)/T(J-1))*(X(J)-X(J-1))/
     1(2.*DAB(TE(J))*PR/TE(J)))
      END IF
      YAX(J)=YA(J)=(YA(J)+YAX(J))/2.; YBX(J)=YB(J)=(YB(J)+YBX(J))/2.
87    CONTINUE
      UT=0.
120   DO 115 J=1,N
      I=N+1-J
C*************************************************************C
C                                                             C
C      PYRITE CONSUMPTION IS CALCULATED                       C
C                                                             C
C*************************************************************C
      IF(I.EQ.1) GO TO 115
      TOE3C=OEOH(I)+OEOH2(I)+OEOH3(I)+OEOH4(I)+2.*OE2OH2(I)+OEHSO4(I)
     1+OESO4(I)+OEOOH(I)
      AMAX=DMAX1(AMAX,DABS(YAX(I)-YAXO(I)))
      BMAX=DMAX1(BMAX,DABS(YBX(I)-YBXO(I)))
      YA2=YA1=YA(I)
      YB1=YB(I)
      YAXO(I)=YAX(I); YBXO(I)=YBX(I)
      IF(FPY(I).EQ.0.) THEN; Z3=Z4=0.0; GO TO 111; END IF
      Z3=DT*U(I)*YA1*BO*120./(RHOB(I)*FFR(I)
     1*FPY(I))
      Z4=DT*DXF(I)*AFE3T(I)*FE3(I)*DELTAF(I)/(L*DELTAF(I)*ALPHA(I)
     1*KSF*(1.-PY(I))+DCF)
      PY(I)=PYO(I)+Z3+Z4
      IF(PY(I).LT.0.0) THEN
      PY(I)=PYO(I)/2.
      Z3=-Z3*PY(I)/(2.*(Z3+Z4))
      Z4=-(PY(I)+Z3)/2.
      END IF
      IF(O.NE.0)CALL DELCAL(ALPHA(I),PYO(I),DELTAO(I),DELTAF(I))
111   IF(O.EQ.0) THEN
      PY(I)=PYO(I)
      UAO(I)=U(I)*YA1
      END IF
C*************************************************************C
C                                                             C
C              KB IS CALCULATED                               C
C                                                             C
C*************************************************************C
      IF(O.EQ.0) THEN
      AFE21=AFE22=DFE2OX=ASO4=0.
      ELSE
      FE32=FE31=FE3(I)
      FE32=FE31
      H2=H1=H(I)
      KB2=-1.
      KB1=KB(I)
      AFE21=-Z3*1000.*RHOB(I)*FFR(I)*FPY(I)/(120.*WC(I))
      AFE22=-15.*Z4*1000.*RHOB(I)*FFR(I)*FPY(I)/(120.*WC(I))
      FE21=FE2(I)
      FE22=FE2X(I)
      TC=(TO(I)+TE(I))/2.-Z73.
      XTE=-1.23D-05*TC**3-4.33D-04*TC**2+0.0657*TC-0.255
      IF(H2.LE.0.) PRINT,I,H2,'=H2',M
      PH=-DLOG10(H2)
      XPH=-.348*PH**2+2.26*PH-2.66
      IF(XPH.LE.0.0) THEN; Z25=KB2=Z5=KB(I)=0.0; GO TO 803; END IF
      XO2=YA2/.01
      IF(XO2.GT.1.) XO2=1.0
      EM=EMIN/(XTE*XO2*XPH)
      IF(XTE.LE.0..OR.XPH.LE.0.0.OR.XO2.LE.0.) THEN
      PRINT,I,XTE,'=XT',XO2,'=XO2',XPH,'=XPH',YA2,'=YA'
      KB(I)=KB1/100.
      GO TO 803
      END IF
      IF(EM.GT.1.18) THEN; KB(I)=0.0; GO TO 803; END IF
      Z25=Z5=G1(I)**(-4)*H2*YA2**.25*DEXP((.46-EM)/(8.6D-05*TE(I)))
      Z18=Z5=(FE31-Z5*FE22)/(1.+Z5)
      Z5=FE22+Z5
      KB2=KB(I)=(OE2(I)+AFE21*YA2/YA1+AFE22*(1.-Z18/FE31)+FE2FL(I)
     1-Z5)/(Z5*DT*YA2*1000.)
      IF(KB(I).LT.0.0) KB(I)=.01*DSQRT(KB1)*3.3D-08
803   Z11=2.*DT/86400.
      Z11=DMIN1(2.0D+01,Z11)
      KB(I)=DMIN1(KB(I),KBO(I)*2.**Z11)
      Z16=4.*WC(I)*2.75D-11/(.01**2*FE22)
```

```
476.          PRINT,J,YAX(J),'=YAX',YA(J),'=YA'; END IF
477.          IF(DB(J).EQ.0.) THEN
478.          YBX(J)=YBX(J-1)*DEXP((NA(J)/T(J)+NA(J-1)/T(J-1))*(X(J)-X(J-1))/
479.         1(2.*DAB(TE(J))*PR/TE(J)))
480.          END IF
481.          YAX(J)=YA(J)=(YA(J)+YAX(J))/2.; YBX(J)=YB(J)=(YB(J)+YBX(J))/2.
482.    87    CONTINUE
483.          UT=0.
484.    120   DO 115 J=1,N
485.          I=N+1-J
486.    C*************************************************************C
487.    C                                                             C
488.    C      PYRITE CONSUMPTION IS CALCULATED                       C
489.    C                                                             C
490.    C*************************************************************C
491.          IF(I.EQ.1) GO TO 115
492.          TOE3C=OEOH(I)+OEOH2(I)+OEOH3(I)+OEOH4(I)+2.*OE2OH2(I)+OEHSO4(I)
493.         1+OESO4(I)+OEOOH(I)
494.          AMAX=DMAX1(AMAX,DABS(YAX(I)-YAXO(I)))
495.          BMAX=DMAX1(BMAX,DABS(YBX(I)-YBXO(I)))
496.          YA2=YA1=YA(I)
497.          YB1=YB(I)
498.          YAXO(I)=YAX(I); YBXO(I)=YBX(I)
499.          IF(FPY(I).EQ.0.) THEN; Z3=Z4=0.0; GO TO 111; END IF
500.          Z3=DT*U(I)*YA1*BO*120./(RHOB(I)*FFR(I)
501.         1*FPY(I))
502.          Z4=DT*DXF(I)*AFE3T(I)*FE3(I)*DELTAF(I)/(L*DELTAF(I)*ALPHA(I)
503.         1*KSF*(1.-PY(I))+DCF)
504.          PY(I)=PYO(I)+Z3+Z4
505.          IF(PY(I).LT.0.0) THEN
506.          PY(I)=PYO(I)/2.
507.          Z3=-Z3*PY(I)/(2.*(Z3+Z4))
508.          Z4=-(PY(I)+Z3)/2.
509.          END IF
510.          IF(O.NE.0)CALL DELCAL(ALPHA(I),PYO(I),DELTAO(I),DELTAF(I))
511.    111   IF(O.EQ.0) THEN
512.          PY(I)=PYO(I)
513.          UAO(I)=U(I)*YA1
514.          END IF
515.    C*************************************************************C
516.    C                                                             C
517.    C              KB IS CALCULATED                               C
518.    C                                                             C
519.    C*************************************************************C
520.          IF(O.EQ.0) THEN
521.          AFE21=AFE22=DFE2OX=ASO4=0.
522.          ELSE
523.          FE32=FE31=FE3(I)
524.          FE32=FE31
525.          H2=H1=H(I)
526.          KB2=-1.
527.          KB1=KB(I)
528.          AFE21=-Z3*1000.*RHOB(I)*FFR(I)*FPY(I)/(120.*WC(I))
529.          AFE22=-15.*Z4*1000.*RHOB(I)*FFR(I)*FPY(I)/(120.*WC(I))
530.          FE21=FE2(I)
531.          FE22=FE2X(I)
532.          TC=(TO(I)+TE(I))/2.-273.
533.          XTE=-1.23D-05*TC**3-4.33D-04*TC**2+0.0657*TC-0.255
534.          IF(H2.LE.0.) PRINT,I,H2,'=H2',M
535.          PH=-DLOG10(H2)
536.          XPH=-.348*PH**2+2.26*PH-2.66
537.          IF(XPH.LE.0.0) THEN; Z25=KB2=Z5=KB(I)=0.0; GO TO 803; END IF
538.          XO2=YA2/.01
539.          IF(XO2.GT.1.) XO2=1.0
540.          EM=EMIN/(XTE*XO2*XPH)
541.          IF(XTE.LE.0..OR.XPH.LE.0.0.OR.XO2.LE.0.) THEN
542.          PRINT,I,XTE,'=XT',XO2,'=XO2',XPH,'=XPH',YA2,'=YA'
543.          KB(I)=KB1/100.
544.          GO TO 803
545.          END IF
546.          IF(EM.GT.1.18) THEN; KB(I)=0.0; GO TO 803; END IF
547.          Z25=Z5=G1(I)**(-4)*H2*YA2**.25*DEXP((.46-EM)/(8.6D-05*TE(I)))
548.          Z18=Z5=(FE31-Z5*FE22)/(1.+Z5)
549.          Z5=FE22+Z5
550.          KB2=KB(I)=(OE2(I)+AFE21*YA2/YA1+AFE22*(1.-Z18/FE31)+FE2FL(I)
551.         1-Z5)/(Z5*DT*YA2*1000.)
552.          IF(KB(I).LT.0.0) KB(I)=.01*DSQRT(KB1)*3.3D-08
553.    803   Z11=2.*DT/86400.
554.          Z11=DMIN1(2.0D+01,Z11)
555.          KB(I)=DMIN1(KB(I),KBO(I)*2.**Z11)
556.          Z16=4.*WC(I)*2.75D-11/(.01**2*FE22)
```

```
557.          KB(I)=DMIN1(KB(I),Z16)
558.          KBA(I)=KB(I)
559.          KB(I)=KB1
560.          IF(KBA(I)*YA1*FE21.LT.1.0D-22) KBA(I)=0.0
561.          IF(KBA(I)*KB(I).NE.0.) THEN; KBMAX=DMAX1(KBMAX,DABS(KB(I)-KBA(I))
562.         1/KB(I))
563.          ELSE; KBMAX=DMAX1(KBMAX,DABS(KBA(I))); END IF
564.          IF(KBA(I).EQ.KB2) FERMAX=DMAX1(FERMAX,DABS(Z25-FE31/FE22)/Z25)
565.    C*************************************************************C
566.    C                                                             C
567.    C              FE3,FE2 AND H ARE CALCULATED                   C
568.    C                                                             C
569.    C*************************************************************C
570.          FE2X(I)=(OE2(I)+AFE21+AFE22+FE2FL(I)
571.         1)/(1.+DT*1000.*YA1*(KOX1*H1**(-2)
572.         2+KOX2+KB(I)))
573.          WHILE(FE2X(I).LT.0.)
574.          FE2FL(I)=FE2FL(I)/2.
575.          FE2X(I)=FD2X(I)-FE2FL(I)
576.          IF(TT.LT.0) PRINT,I,FE2X(I),'=FE2X',FE2FL(I)
577.          END WHILE
578.          FE21=FE2(I)=FE2X(I)
579.          DFE2OX=-DT*YA1*(KOX1*H1**(-2)+KOX2)
580.         1*FE21
581.          DFE2B=-KB(I)*YA1*FE21*DT
582.          UT=UT+(DFE2OX+DFE2B)*DX(I)*8.64D+08/DT
583.    C
584.    C              FE3 IS CALCULATED
585.    C
586.    112   ZFE3=-(DFE2OX+DFE2B)*1000.+OE3(I)+FE3FL(I)+TOE3C-TFE3CX(I)
587.          FE3(I)=ZFE3/(1.-Z4/FE31*RHOB(I)*FFR(I)*FPY(I)/(120.*BF
588.         1*WC(I))*1000.)
589.          IST=1
590.          WHILE(FE3(I).LT.0..AND.IST.LT.20)
591.          FE3FL(I)=FE3FL(I)/2. ; TFE3CX(I)=TFE3CX(I)/2.
592.          FE3(I)=FE3(I)-FE3FL(I)+TFE3CX(I)
593.          IF(IST.EQ.19) PRINT,I,FE3(I),'=FE3',FE3FL(I),'=FE3FL',TFE3C(I)
594.          IST=IST+1; END WHILE
595.          IF(M.GT.1) Z4=FE3(I)*Z4/FE31  ; AFE22=AFE22*FE3(I)/FE31
596.          FE3(I)=FE3(I)-TOE3C+TFE3CX(I)
597.    C
598.    C              H IS CALCULATED
599.    C
600.          H(I)=((RHOB(I)*FFR(I)*FPY(I)/(120.*WC(I))*(-16.*
601.         1Z4-2.*Z3)+DFE2OX+DFE2B)*1000.+HFL(I)-6.*DT*1000*FLS(I)*RLS(I)/
602.         2WC(I)*LS(I)**(2./3.)*OH(I))/(1.+6.*DT*1000.*FLS(I)*RLS(I)/WC(I)
603.         3*LS(I)**(2./3.))
604.          IST=1
605.          IF(H(I)+OH(I).LT.0.0) THEN
606.          STH=(RHOB(I)*FFR(I)*FPY(I)/(120.*WC(I))*(-16.*
607.         1Z4-2.*Z3))*1000.
608.          STL=1.0D-07-OH(I)
609.          AST=(STH+STL)/2.
610.          WHILE(DABS(STH-STL).GT..001*DABS(STH))
611.          H(I)=AST+OH(I)
612.          HFL(I)=FLUX(1)/WC(I)
613.          H(I)=((RHOB(I)*FFR(I)*FPY(I)/(120.*WC(I))*(-16.*
614.         1Z4-2.*Z3)+DFE2OX+DFE2B)*1000.+HFL(I)-6.*DT*1000.*FLS(I)*RLS(I)/
615.         2WC(I)*LS(I)**(2./3.)*OH(I))/(1.+6.*DT*1000.*FLS(I)*RLS(I)/WC(I)
616.         3*LS(I)**(2./3.))
617.          IF(H(I).GT.AST) THEN
618.          STL=AST
619.          ELSE; STH=AST; END IF
620.          AST=(STH+STL)/2.
621.          IF(TT.LT.0) PRINT,I,M,IST,STH,'=HH',H(I),'=H',AST,
622.         1'=AST',STL,'=HL',HFL(I),'=HFL'
623.          IST=IST+1
624.          IF(IST.GT.20) THEN
625.          DFE2B=DFE2B/2.
626.          KB(I)=KB(I)/2.
627.          END IF
628.          END WHILE
629.          END IF
630.    C
631.    C              SO4 IS CALCULATED
632.    C
633.          ASO4=-2.*(Z3+Z4)*1000.*RHOB(I)*FFR(I)*FPY(I)/
634.         1(120.*WC(I))
635.          ST(I)=OST(I)+ASO4+STFL(I)
636.          IF(ST(I).LT.0.) THEN
```

```
637.          IST=1
638.          STH=2.*OST(I)+ASO4
639.          STL=0.0
640.          AST=(STH+STL)/2.
641.          WHILE(DABS(ST(I)-AST).GT..001*DABS(AST))
642.          ST(I)=AST
643.          STFL(I)=FLUX(4)/WC(I)
644.          ST(I)=OST(I)+ASO4+STFL(I)
645.          IF(ST(I).GT.AST) THEN
646.          STL=AST
647.          ELSE; STH=AST; END IF
648.          AST=(STH+STL)/2.
649.          IF(TT.LT.0) PRINT,I,IST,ST(I),'=ST',AST,'=AST',STFL(I)
650.          IST=IST+1
651.          END WHILE
652.          END IF
653.    C
654.    C               CA IS CALCULATED
655.    C
656.          ACALS=(LSO(I)-LS(I))*FLS(I)*1000./WC(I)
657.          CA(I)=OCA(I)+ACALS+CAFL(I)
658.          IF(CA(I).LT.0.) THEN
659.          IST=1
660.          STH=2.*OCA(I)+2.*ACALS
661.          STL=CA(I)
662.          AST=(STH+STL)/2.
663.          WHILE(DABS(CA(I)-AST).GT..001*DABS(AST))
664.          CA(I)=AST
665.          CAFL(I)=FLUX(6)/WC(I)
666.          CA(I)=OCA(I)+ACALS+CAFL(I)
667.          IF(CA(I).GT.AST) THEN
668.          STL=AST
669.          ELSE; STH=AST; END IF
670.          AST=(STH+STL)/2.
671.          IF(TT.LT.0)PRINT,I,IST,CA(I),'CA',AST,'=AST',CAFL(I),'=CAFL',ACALS
672.         1,LS(I),'=LS',LSO(I),'=LSO',RLS(I),'=RLS',FLS(I),'=FLS'
673.          IST=IST+1
674.          END WHILE
675.          END IF
676.          IF(I.EQ.33)  PRINT,I,'= I',H(I),'= H',FE3(I),'= AFE3',Z,'= AFE3T'
677.         1,Z1,'=Z1',Z2,'= Z2',Z3,'= Z3',Z4,'= Z4',G1(I),'= G1'
678.          IF(M.GT.70) H(I)=H1
679.          IF(M.GT.70) FE3(I)=FE31
680.    C
681.    C               COMPLEXES ARE ADJUSTED
682.          CALL CHEMI(4,H(I),FE3(I),FEOOH(I),AFE3T(I),G1(I))
683.    C
684.          IF(M.GT.70) H(I)=H1
685.          IF(M.GT.70) FE3(I)=FE31
686.          FE32=FE3(I)
687.          IF(FE3(I).LT.0.0) PRINT,'     Z4 IS TOO LARGE IN LAYER',I
688.          IF(FE3(I).EQ.0.0) FE3(I)=1.0D-25
689.          IF(FE31.NE.0.0) FEMAX=DMAX1(FEMAX,DABS(FE31-FE32)/FE31)
690.          HMAX=DMAX1(HMAX,DABS(H1-H(I))/H(I))
691.          IF(M.GT.78) PRINT126,I,H(I),H1,FE3(I),FE31,YA1,YAX(I),KB(I),KBA(I)
692.    317   IF(FE3(I).LT.1.0D-34) THEN; PRINT,'FE3=0',I; FE3(I)=0.0; END IF
693.          END IF
694.    114   PYMAX=DMAX1(PYMAX,DABS(PY(I)-PYX(I)))
695.          IF(M.EQ.1) THEN
696.          ZLS=LS(I)
697.          IF(RLS(I)*FLS(I).NE.0.0) THEN
698.          LS(I)=(LSO(I)**(1./3.)-DT*RLS(I)*H(I)
699.         1)**3
700.          IF(LS(I).LT.0.) LS(I)=0.0
701.          END IF
702.          IF(ZLS.GT.0.) LSMAX=DMAX1(LSMAX,1.-LS(I)/ZLS)
703.          END IF
704.          PYX(I)=PY(I)
705.          PYO2(I)=Z3*DX(I)
706.          PYF(I)=Z4*DX(I)
707.          FCMAX=DMAX1(FCMAX,DABS((TFE3C(I)-TFE3CX(I))/TFE3C(I)))
708.    115   CONTINUE
709.          IF(M.EQ.80)THEN; PRINT,'   *ERROR* MUST RESTART';GO TO 200;END IF
710.    C*************************************************************C
711.    C                                                             C
712.    C               CONVERGENCE IS CHECKED                        C
713.    C                                                             C
714.    C*************************************************************C
```

```
715.          IF(M.GT.50) PRINT2,M,AMAX,BMAX,PYMAX,HMAX,FEMAX,FERMAX
716.     2    FORMAT(/,1X,' M= ',I3,' AMAX=',D11.3,' BMAX=',D11.3,
717.         1' PYMAX=',D11.3,' HMAX=',D11.3,' FE3MAX=',D11.3,
718.         2' FERMAX=',D11.3)
719.          IF(OPRINT.GE.3) THEN
720.          DO 900 I=1,N
721.     900  PRINT12,I,X(I),YA(I),YB(I),NA(I),NB(I),UA(I),UB(I),R2,PY(I)
722.          END IF
723.          IF(M.LT.35) THEN
724.          IF(AMAX.GT.10.*E1) GO TO 500
725.          IF(BMAX.GT.10.*E1) GO TO 500
726.          IF(PYMAX.GT.E1) GO TO 500
727.          IF(HMAX.GT.E1*1000.) GO TO 500
728.          IF(FEMAX.GT.E1*1000.) GO TO 500
729.          END IF
730.     999  FORMAT(1X,I2,2X,6D11.4)
731.          MSWEEP=MSWEEP+1
732.     901  IF(OPRINT.GE.1.OR.MSWEEP.GT.20) PRINT902,MSWEEP,M,RMAX,KBMAX,
733.         1FLMAX,LSMAX,FCMAX
734.     902  FORMAT(37X,'AFTER SWEEP',I4,5X,'AND',I4,' ITERATIONS',/
735.         1,10X,'RMAX=',D11.3,8X,'KBMAX=',D11.3,8X,'FLMAX=',D11.3,8X,
736.         2'LSMAX=',D11.3,'FCMAX=',D11.3)
737.          IF(OPRINT.GT.1) PRINT2,M,AMAX,BMAX,PYMAX,HMAX,FEMAX,FERMAX
738.          IF(MSWEEP.LT.25)  THEN; M=0
739.          IF(OPRINT.EQ.4) PRINT785,(I,YA(I),I=1,N)
740.          IF(OPRINT.EQ.4) PRINT785,(I,YAX(I),I=1,N)
741.          IF(OPRINT.EQ.4) PRINT788,(I,KB(I),I=1,N)
742.          IF(OPRINT.EQ.3) PRINT788,(I,KBA(I),I=1,N)
743.          DO 786 I=2,N
744.          FE2(I)=(FE2X(I)+FE2(I))/2.
745.          YA(I)=(YA(I)+YAX(I))/2.; YB(I)=(YBX(I)+YB(I))/2.
746.          IF(MSWEEP.EQ.1.OR.MSWEEP.EQ.11.OR.MSWEEP.EQ.16) THEN
747.          KBH(I)=DMAX1(KB(I),KBA(I)); KBL(I)=DMIN1(KB(I),KBA(I))
748.          ELSE
749.          IF(KBA(I).GT.KB(I)) THEN; KBL(I)=KB(I)
750.          IF(KBA(I).LT.KBH(I)) KBH(I)=KBA(I)
751.          ELSE; KBH(I)=KB(I); IF(KBA(I).GT.KBL(I)) KBL(I)=KBA(I);END IF
752.          END IF
753.          IF(KBL(I)*KBH(I).GT.0.) THEN; KB(I)=DSQRT(KBL(I))*DSQRT(KBH(I))
754.          ELSE; KB(I)=(KBH(I)+KBL(I))/2.; END IF
755.          IF(KB(I)*YA(I)*FE2(I).LT.1.0D-30) KB(I)=0.0
756.     786  CONTINUE
757.          IF(FLMAX.GT..0005) GO TO 450
758.          IF(RMAX.GT.E1*10.) GO TO 450
759.          IF(KBMAX.GT.E1*1000.) GO TO 450
760.          IF(FCMAX.GT..001) GO TO 450
761.          END IF
762.          IF(OPRINT.GE.0) PRINT2,M,AMAX,BMAX,PYMAX,HMAX,FEMAX,FERMAX
763.          PRINT787
764.     787  FORMAT(/)
765.     110  PRINT788,(I,KB(I),I=1,N)
766.     788  FORMAT((12X,3(5X,'I = ',I3,2X,'KB = ',D10.4)))
767.     785  FORMAT((2X,3(5X,'I = ',I3,2X,'YB = ',D15.9)))
768.     C*****************************************************************C
769.     C                                                                 C
770.     C                              OUTPUT                             C
771.     C                                                                 C
772.     C*****************************************************************C
773.     130  PRINT10,TT,MM
774.          IF(MBAT.EQ.1) WRITE(NBAT,850) TT
775.     850  FORMAT(F10.1)
776.     10   FORMAT('1',45X,'AFTER',F10.1,' DAYS',/,37X,
777.         1'SOLUTION WAS FOUND IN ',I4,' ITERATIONS',/)
778.          PRINT11
779.          PRINT211
780.     11   FORMAT(/,1X,'LAYER',4X,'DEPTH',5X,
781.         1'O2',07X,'CO2',08X,'NO2',09X,'NCO2',9X,'UO2PY',7X,
782.         2'UO2FEOX',4X,'UO2HB/OR',3X,'CHOX/BACTOX',3X,'XPY/XLS')
783.     211  FORMAT(11X,'CM',7X,'MOLE FRACTION',7X,'MOLES/CM**2-SEC',16X,
784.         1'MOLES/CM**3-SEC',8X,'-',4X,'MOLES/CM**3',6X,'-',/)
785.          NCI=KBMAX=Z=0.
786.     C
787.     C              CALCULATE CONSTITUENTS ENTERING THE WATER TABLE
788.     C
789.          I=N+1
790.          Z1=FLUX(1)
791.          Z2=FLUX(2)
792.          Z3=FLUX(3)
793.          Z4=FLUX(4)
794.          Z5=FLUX(5)
795.          Z6=FLUX(6)
```

```
796.          Z8=FLUX(7)
797.          DO 124 J=2,N
798.          I=N+1-J
799.          NCI=YBX(I)=PHI(I)*PR/TE(I)*DX(I)/DT*(YAO(I)-YA(I)+YBO(I)-YB(I)
800.         1+YAO(I+1)-YA(I+1)+YBO(I+1)-YB(I+1))/2.+NCI
801.     124  CONTINUE
802.           DO 125 I=1,N
803.          H2CO3(I)=DCO2(TE(I))*YB(I)
804.          IF(I.NE.N) THEN
805.          D1=DX(I)
806.          D3=DX(I+1)
807.          D2=D1+D3
808.          T2=(T(I)*D3+T(I+1)*D1)/D2
809.          TE2=(TE(I)*D3+TE(I+1)*D1)/D2
810.          DAB2=DAB(TE2)
811.          DAC2=DAC(TE2)
812.          DBC2=DBC(TE2)
813.          YA3=YA(I+1)
814.          YA1=YA(I)
815.          X3=X(I+1)
816.          X1=X(I)
817.          YB3=YB(I+1)
818.          YB1=YB(I)
819.          YA2=(D1*YA3+D3*YA1)/D2
820.          YB2=(D1*YB3+D3*YB1)/D2
821.          Z10=1
822.          WHILE(Z10.GT.1.0D-14)
823.          Z11=NAI(I); Z12=NBI(I)
824.          NAI(I)=T2*DAB2*DAC2/(YB2*(DAC2-DAB2)-YA2*DAB2+DAB2)*(Z12*
825.         1YA2/(T2*DAB2)+YBX(I)*YA2/(T2*DAC2)-PR/TE2*(YA3-YA1)/(X3-X1))
826.          NBI(I)=T2*DAB2*DBC2/(YA2*(DBC2-DAB2)-YB2*DAB2+DAB2)*(NAI(I)*
827.         1YB2/(T2*DAB2)+YBX(I)*YB2/(T2*DBC2)-PR/TE2*(YB3-YB1)/(X3-X1))
828.          Z10=DABS(NAI(I)-Z11)+DABS(NBI(I)-Z12)
829.          END WHILE
830.          END IF
831.          R(I)=NB(I)/NA(I)
832.          U3=U(I)*YA(I)
833.          U1=U3
834.          UAO(I)=U3
835.          U3=-U1*BO*2.
836.          U3=U3/DX(I)
837.          U4=DMIN1(0.0D+00,2.*YA(I)*HBACT(I)*(TE(I)
838.         1-273.))
839.          D1=X(I)+DX(I)/2.
840.          OE2OX(I)=-FE2(I)*YA(I)*(KOX1*H(I)**(-2)+KOX2)
841.          YAX(I)=U2=1./4.*WC(I)*OE2OX(I)
842.          U2=U2+1./4.*WC(I)*(-KB(I)*YA(I)*FE2(I))
843.          Z=DMAX1(Z,DABS(PY(I)-PYO(I)))
844.          FE2OX=YAX(I)*4.*DT
845.          FE2B=-KB(I)*YA(I)*FE2(I)
846.          TFE2B=FE2B*DT*WC(I)
847.          OE2B(I)=FE2B
848.          DXFO(I)=DXF(I)*AFE3T(I)*FE3(I)*DELTAF(I)/(L*DELTAF(I)*ALPHA(I)*KSF
849.         1*(1.-PY(I))+DCF)
850.          IF(DABS(NB(I)).LT.1.0D-20) NB(I)=0.0
851.     123  PRINT12,I,X(I),YA(I),YB(I),NA(I),NB(I),U1,U2,U4,FE2OX,PY(I)
852.          IF(MBAT.EQ.1) WRITE(NBAT,851) I,X(I),YA(I),YB(I),NA(I),NB(I),U1,
853.         1Z11,PY(I)
854.          PRINT13,D1,NAI(I),NBI(I),PYF(I)/PYO2(I),TFE2B
855.         1,LS(I)
856.          IF(MBAT.EQ.1) WRITE(NBAT,13) D1,NAI(I),DELTAO(I)
857.     126  FORMAT(1X,I3,8(1X,D10.4))
858.     125  CONTINUE
859.     12   FORMAT(1X,I4,1X,F8.1,2F10.4,3X,2(D10.4,3X),4(D10.3,2X),2X,F6.3)
860.     13   FORMAT(6X,F8.1,20X,2(3X,D10.4),25X,2(2X,D10.3),4X,F6.3)
861.     851  FORMAT(1X,I4,1X,F8.1,2F10.4,3X,2(D10.4,3X),/,2(D10.4,3X),
862.         1F7.4)
863.          PRINT15
864.          PRINT215
865.          DZ7=Z7=TFE=0.0
866.          DO 128 I=1,N
867.          Z7=Z7+(PYO2(I)+PYF(I))*FPY(I)
868.          IF(I.GT.1) DZ7=DZ7+FPY(I)*DX(I)
869.          IF(I.NE.1) CALL CHEMI(1,H(I),FE3(I),FEOOH(I),AFE3T(I),PYX(I))
870.          IF(I.NE.1) TFE=(PYX(I)+PY(I)*1000.*FFR(I)*FPY(I)*RHOB(I)/(120.*
871.         1WC(I)))*DX(I)*WC(I)+TFE
872.          OHBOX(I)=DMIN1(0.0D+00,2.*YA(I)*HBACT(I)*(TE(I)-273.))
873.          Z11=AFE3T(I)*1000.-G1(I)**9
874.          PH=-DLOG10(H(I))
875.          IF(MBAT.EQ.1) WRITE(NBAT,16) I,PH,FE2(I),FE3(I),FEOOH(I),HC(I),
```

```
     10SO4(I),OIO(I),FE2OX,TFE2B
      PRINT16,I,PH,FE2(I),FE3(I),FEOOH(I),HC(I),OSO4(I),OIO(I),
     1H2CO3(I),CA(I),Z11
      IF(TT.GE.32.) KBO(I)=DMAX1(KB(I),KBA(I),1.0D-15)
      IF(KB(I)+KBO(I).LT.1.0D-12) GO TO 128
      IF(KB(I).NE.0.0) THEN; X1=DABS(KB(I)-KBO(I))/KB(I)
      ELSEIF(KBO(I).EQ.1.0D-15) THEN; X1=0.; ELSE; X1=100.; END IF
      KBMAX=DMAX1(DABS(KB(I)-KBO(I))/KBO(I),KBMAX,X1)
      KBMAX=KBMAX
128   CONTINUE
      Z7=86400.*Z7/(DT*DZ7)
15    FORMAT('1',1X,'LAYER',4X,'PH',7X,'FE2',9X,'FE3',7X,'FEOOH',
     17X,'ACIDITY',7X,'SO4',6X,'IONIC STR',5X,'H2CO3',
     28X,'CA',7X,'TFE3CMPLX')
215   FORMAT(17X,'------------------------------------------ MOLES/L',
     1'----------------------------------------',7X,'-',/)
16    FORMAT(1X,I4,1X,F8.2,3X,9(D9.3,3X))
      IF(OPRINT.EQ.3) PRINT7
7     FORMAT(5X,'H',6X,'SO4',5X,'HSO4',4X,'FE3',5X,'FEOH',
     13X,'FEOH2',3X,'FEOH3',3X,'FEOH4',
     22X,'FE2OH2',3X,'FESO4',2X,'FEHSO4')
      TFED=TFE-TFEO
      TFEO=TFE
      TFE=(TFED+(Z2+Z3)*DT/864000.-DT*INFILR*(FE3(1)+FE2(1)))/TFE
      IF(TT.EQ.0.0) TFE=0.0
      DO 127 I=1,N
      PH=-DLOG10(H(I))
      IF(OPRINT.EQ.2)PRINT8,H(I),OSO4(I),OHSO4(I),OE3(I),OEOH(I),
     1OEOH2(I),OEOH3(I),OEOH4(I),OE2OH2(I),OESO4(I),OEHSO4(I)
 127  CONTINUE
8     FORMAT(1X,11D10.3)
      IF(TT.GT..0) THEN; TUT=TUT+UT*DT/86400.
      TZ1=TZ1+Z1*DT/86400.
      TZ2=TZ2+Z2*DT/86400.
      TZ3=TZ3+Z3*DT/86400.
      TZ4=TZ4+Z4*DT/86400.
      TZ5=TZ5+Z5*DT/86400.
      TZ6=TZ6+Z6*DT/86400.
      TZ7=TZ7+Z7*DT/86400.
      TZ8=TZ8+Z8*DT/86400.
      END IF
      PRINT14,TFE,Z7,TZ7
14    FORMAT(//,1X,'T',34X,'INCREMENTAL FRACTIONAL IRON MASS BALANCE',/,
     11X,'T',50X,D10.4,//,1X,'T',31X,'FRACTIONAL PYRITE CONSUMPTION',
     2' PER M**2 PER DAY',/,1X,'T',50X,D10.4,//,1X,'T',32X,'TOTAL ',
     3'FRACTIONAL PYRITE CONSUMPTION PER M**2',/,1X,'T',50X,D10.4)
      PRINT18
18    FORMAT(/,1X,'T',32X,'MOLES ENTERING THE WATER TABLE PER M**2 PER',
     1' DAY')
      PRINT19,Z1,Z5,Z2,Z3,Z4,Z6,Z8
19    FORMAT(1X,'T',17X,'H',9X,'ACIDITY',10X,'FE3',10X,'FE2',7X,'TOTAL',
     1' SULFATE',6X,'CALCIUM',8X,'H2CO3',/,
     21X,'T',12X,D10.4,4X,E10.4,4X,3(D10.4,4X),2X,2(D10.4,4X),//)
      PRINT20
20    FORMAT(1X,'T',32X,'TOTAL MOLES TO ENTER THE WATER TABLE PER M**2')
      PRINT19,TZ1,TZ5,TZ2,TZ3,TZ4,TZ6,TZ8
      PRINT720,(I,R(I),I=2,N)
720   FORMAT(//,6(10X,4('I= ',I3,2X,'R= ',F7.4,5X),/))
C
C                TIME INCREMENT IS ADJUSTED
C
      NBAT=NBAT+1
      D=1
      IF(TT.EQ.0.) THEN
      MSWEEP=MM=M=0
      TT=TT+DT/86400.
      GO TO 400
      ELSE
      IF(MM.GT.80) GO TO 140
      IF(MT.EQ.1) THEN
      IF(KBMAX.LE.4.0) THEN
      DDT=DMIN1(DDT*2.,1.0D+12)
      DT=DDT=DMIN1(DT*2.,1.5768D+07)
      GO TO 140
      DT=DDT-TT*86400.
      WHILE(DT.LE.0.)
      DT=DDT+DT
      END WHILE
      ELSE
      DT=DDT
```

```
956.          END IF
957.          DT=DMIN1(DT,1.5768D+07)
958.          END IF
959.    140   IF(TT.LE.32.) THEN
960.          IF(TT+DT/86400..GT.32.) DDT=DT=86400.*2.
961.          END IF
962.          TT=TT+DT/86400.
963.          END IF
964.          MSWEEP=MM=M=0
965.          IF(TT.GE.ET) GO TO 200
966.          GO TO 400
967.    C*************************************************************C
968.    C                                                             C
969.    C                        DATA IS DUMPED IF TIME               C
970.    C                           LIMIT IS EXCEEDED                 C
971.    C                                                             C
972.    C*************************************************************C
973.    200   PRINT,'      *****EXECUTION EXCEEDS TIME ALLOWED, JOB DUMPED*****'
974.          WRITE(42,202) OPRINT,O,N,NBAT,MBAT,MT,E1,PR,DT,DDT,TT,ET,TUT,
975.         1TZ1,TZ2,TZ3,TZ4,TZ5,TZ6,TZ7,TZ8,KSO,DCO,KSF,DCF,L,INFILR,TFEO
976.          WRITE(42,201) (YA(I),I=1,N)
977.          WRITE(42,201) (YB(I),I=1,N)
978.          WRITE(42,201) (PY(I),I=1,N)
979.          WRITE(42,201) (PYO(I),I=1,N)
980.          WRITE(42,201) (TE(I),I=1,N)
981.          WRITE(42,201) (TO(I),I=1,N)
982.          WRITE(42,201) (X(I),I=1,N)
983.          WRITE(42,201) (DX(I),I=1,N)
984.          WRITE(42,201) (T(I),I=1,N)
985.          WRITE(42,201) (UAN(I),I=1,N)
986.          WRITE(42,201) (UA(I),I=1,N)
987.          WRITE(42,201) (UAO(I),I=1,N)
988.          WRITE(42,201) (ALPHA(I),I=1,N)
989.          WRITE(42,201) (PHI(I),I=1,N)
990.          WRITE(42,201) (WC(I),I=1,N)
991.          WRITE(42,201) (RHOB(I),I=1,N)
992.          WRITE(42,201) (RHOFR(I),I=1,N)
993.          WRITE(42,201) (FFR(I),I=1,N)
994.          WRITE(42,201) (FPY(I),I=1,N)
995.          WRITE(42,201) (FEOOH(I),I=1,N)
996.          WRITE(42,201) (ST(I),I=1,N)
997.          WRITE(42,201) (FE3(I),I=1,N)
998.          WRITE(42,201) (FE2(I),I=1,N)
999.          WRITE(42,201) (H(I),I=1,N)
1000.         WRITE(42,201) (DXF(I),I=1,N)
1001.         WRITE(42,201) (DXFO(I),I=1,N)
1002.         WRITE(42,201) (OE2B(I),I=1,N)
1003.         WRITE(42,201) (OE2OX(I),I=1,N)
1004.         WRITE(42,201) (KB(I),I=1,N)
1005.         WRITE(42,201) (KBO(I),I=1,N)
1006.         WRITE(42,201) (OIO(I),I=1,N)
1007.         WRITE(42,201) (HC(I),I=1,N)
1008.         WRITE(42,201) (HBACT(I),I=1,N)
1009.         WRITE(42,201) (OHBOX(I),I=1,N)
1010.         WRITE(42,201) (R(I),I=1,N)
1011.         WRITE(42,201) (OE3(I),I=1,N)
1012.         WRITE(42,201) (OE2(I),I=1,N)
1013.         WRITE(42,201) (OH(I),I=1,N)
1014.         WRITE(42,201) (YAO(I),I=1,N)
1015.         WRITE(42,201) (YBO(I),I=1,N)
1016.         WRITE(42,201) (GA(I),I=1,N)
1017.         WRITE(42,201) (GB(I),I=1,N)
1018.         WRITE(42,201) (CA(I),I=1,N)
1019.         WRITE(42,201) (LS(I),I=1,N)
1020.         WRITE(42,201) (LSO(I),I=1,N)
1021.         WRITE(42,201) (RLS(I),I=1,N)
1022.         WRITE(42,201) (FLS(I),I=1,N)
1023.         WRITE(42,201) (H2CO3(I),I=1,N)
1024.         WRITE(42,201) (OH2CO3(I),I=1,N)
1025.   201   FORMAT(1X,2D28.18)
1026.   202   FORMAT(1X,5I5,I10,2(1X,F10.8),/,1X,4D17.10,/,5(1X,D17.10),/,
1027.        11X,4D18.10,2E13.6,/,1X,4E13.6,D17.10)
1028.         STOP
1029.         END
1030.   C*************************************************************C
1031.   C                                                             C
1032.   C                        D.O. FUNCTION                        C
1033.   C              DO*YA = GRAMS O2 PER ML                        C
1034.   C                                                             C
1035.   C*************************************************************C
```

```
      DOUBLE PRECISION FUNCTION DO(T)
      REAL*8 T
      DO=.032*10.**(2237.8/T-15.803+.018117*T)
      RETURN
      END
C*****************************************************************C
C                                                                 C
C                        D.CO2. FUNCTION                          C
C          DCO2=HENRY'S LAW TEMP. DEPEND. COEFFICIENT             C
C                                                                 C
C*****************************************************************C
      FUNCTION DCO2(T)
      REAL*8 T
      DCO2=.03388
      RETURN
      END
C*****************************************************************C
C                                                                 C
C                          FUNCTION DAB                           C
C                                                                 C
C            THIS FUNCTION CALCULATES THE TEMPERATURE DEPENDANT   C
C     O2-CO2 DIFFUSION COEFFICIENT.                               C
C                                                                 C
C*****************************************************************C
      DOUBLE PRECISION FUNCTION DAB(T)
      IMPLICIT REAL*8 (A-H,P-Z)
      DAB=1.56D-05*T**1.661/DEXP(61.3/T)
      RETURN
      END
C*****************************************************************C
C                                                                 C
C                          FUNCTION DAC                           C
C                                                                 C
C            THIS FUNCTION CALCULATES THE TEMPERATURE DEPENDANT   C
C     O2-N2 DIFFUSION COEFFICIENT.                                C
C                                                                 C
C*****************************************************************C
      DOUBLE PRECISION FUNCTION DAC(T)
      IMPLICIT REAL*8 (A-H,P-Z)
      DAC=1.13D-05*T**1.724
      RETURN
      END
C*****************************************************************C
C                                                                 C
C                          FUNCTION DBC                           C
C                                                                 C
C            THIS FUNCTION CALCULATES THE TEMPERATURE DEPENDANT   C
C     N2-CO2 DIFFUSION COEFFICIENT.                               C
C                                                                 C
C*****************************************************************C
      DOUBLE PRECISION FUNCTION DBC(T)
      IMPLICIT REAL*8 (A-H,P-Z)
      DBC=3.15D-05*T**1.57/DEXP(113.6/T)
      RETURN
      END
C*****************************************************************C
C                                                                 C
C                          FUNCTION FLUX                          C
C              CALCULATES LEACHING RATE FOR H,HC,FE3,FE2,ST       C
C     AND IS BASED ON CONCENTRATIONS AT OLD TIME STEP ONLY.       C
C                                                                 C
C*****************************************************************C
      DOUBLE PRECISION FUNCTION FLUX(MO)
      IMPLICIT REAL*8 (A-H,O-Z)
      REAL*4 INFILR
      DIMENSION HCFL(50),OH(50),OE3(50),OE2(50),OST(50),OHC(50),S(50),
     1X(50),DX(50),A(50,50),OEOH(50),OEOH2(50),OEOH3(50),OEOH4(50),
     2OE2OH2(50),OESO4(50),OEHSO4(50),OSO4(50),OHSO4(50),OIO(50),
     3OEOOH(50),ST(50),FE2(50),H(50),FE3(50),HC(50),GA(50),GB(50),
     4CA(50),OCA(50),H2CO3(50),OH2CO3(50)
      COMMON/ACHCAL/OIO,OEOH,OEOH2,OEOH3,OEOH4,OE2OH2,OESO4,
     2OEHSO4,OEOOH,OSO4,OHSO4,ST,FE2,OH,OE3,OE2,
     3OST,CA,OCA,H2CO3,OH2CO3,I/AHADJ/HC,OHC,HCFL,GA,GB
     4/AFLUX1/H,FE3,X,DX,DT,INFILR,N
      IF(MO.GT.0) GO TO 25
      NN=N+1
      H(NN)=FE3(NN)=FE2(NN)=OH(NN)=OE3(NN)=OE2(NN)=OST(NN)=OHC(NN)=0.
      HC(NN)=OEOH(NN)=OEOH2(NN)=OEOH3(NN)=OEOH4(NN)=OE2OH2(NN)=0.
      CA(NN)=OCA(NN)=ST(NN)=OEHSO4(NN)=OESO4(NN)=OSO4(NN)=OHSO4(NN)=0.
      H2CO3(NN)=OH2CO3(NN)=0.
      X(NN)=X(N)+DX(N)/2.
      DO 10 II=2,N
```

```
1118.          BASE=X(II-1)+DX(II-1)/2.
1119.          S(II)=0.0
1120.          DO 10 K=II,NN
1121.          S(II)=S(II)+1./(X(K)-BASE)
1122.    10    CONTINUE
1123.          DO 20 II=2,NN
1124.          DO 20 J=2,II
1125.          IF(J.EQ.NN) GO TO 20
1126.          BASE=X(J-1)+DX(J-1)/2.
1127.          A(II,J-1)=(1./(X(II)-BASE))/S(J)
1128.    20    CONTINUE
1129.          A(NN,N)=1.0
1130.          DO 22 J=1,N
1131.          SS=0.0
1132.          IF(J.NE.1) THEN
1133.          DO 23 K=2,J
1134.          SS=A(J,K-1)+SS
1135.    23    CONTINUE
1136.          ELSE
1137.          SS=1.0
1138.          END IF
1139.          DO 22 L=J,N
1140.          A(L+1,J)=A(L+1,J)*SS
1141.    22    CONTINUE
1142.          FLUX=1.0
1143.          IF(MO.EQ.-1) PRINT1,((A(KK,LL),KK=1,NN),LL=1,N)
1144.    1     FORMAT(1X,4F10.5)
1145.          RETURN
1146.    25    CI=TI=0.0
1147.          IF(MO.EQ.2) GO TO 39
1148.          IF(MO.EQ.3) GO TO 49
1149.          IF(MO.EQ.4) GO TO 59
1150.          IF(MO.EQ.5) GO TO 69
1151.          IF(MO.EQ.6) GO TO 79
1152.          IF(MO.EQ.7) GO TO 89
1153.          DO 30 J=2,I
1154.          CI=A(I,J-1)*2.*OH(J-1)/(OH(J-1)+H(J-1))*H(J-1)+CI
1155.          TI=A(I,J-1)+TI
1156.    30    CONTINUE
1157.          Y=2.*OH(I)/(OH(I)+H(I))*H(I)
1158.          GO TO 100
1159.    39    DO 40 J=2,I
1160.          Y=2.*FE3(J-1)/(FE3(J-1)+OE3(J-1))*OE3(J-1)+OEOH(J-1)+OEOH2(J-1)
1161.         1+OEOH3(J-1)+OEOH4(J-1)+OE2OH2(J-1)+OEHSO4(J-1)+OESO4(J-1)
1162.          CI=A(I,J-1)*Y+CI
1163.          TI=A(I,J-1)+TI
1164.    40    CONTINUE
1165.          Y=2.*FE3(I)/(FE3(I)+OE3(I))*OE3(I)+OEOH(I)+OEOH2(I)+OEOH3(I)--
1166.         1OEOH4(I)+OE2OH2(I)+OEHSO4(I)+OESO4(I)
1167.          GO TO 100
1168.    49    DO 50 J=2,I
1169.          CI=A(I,J-1)*2.*FE2(J-1)/(FE2(J-1)+OE2(J-1))*OE2(J-1)+CI
1170.          TI=A(I,J-1)+TI
1171.    50    CONTINUE
1172.          Y=2.*FE2(I)/(FE2(I)+OE2(I))*OE2(I)
1173.          GO TO 100
1174.    59    DO 60 J=2,I
1175.          Y=OSO4(J-1)+OHSO4(J-1)+OEHSO4(J-1)+OESO4(J-1)
1176.          CI=A(I,J-1)*2.*Y/(Y+ST(J-1))*ST(J-1)+CI
1177.          TI=A(I,J-1)+TI
1178.    60    CONTINUE
1179.          Y=OSO4(I)+OHSO4(I)+OEHSO4(I)+OESO4(I)
1180.          Y=2.*Y/(Y+ST(I))*ST(I)
1181.          GO TO 100
1182.    69    DO 70 J=2,I
1183.          DENOM=HC(J-1)+OHC(J-1)
1184.          CI=A(I,J-1)*2.*HC(J-1)/DENOM*OHC(J-1)+CI
1185.          TI=A(I,J-1)+TI
1186.    70    CONTINUE
1187.          Y=2.*HC(I)/(HC(I)+OHC(I))*OHC(I)
1188.          GO TO 100
1189.    79    DO 80 J=2,I
1190.          DENOM=CA(J-1)+OCA(J-1)
1191.          CI=A(I,J-1)*2.*CA(J-1)/DENOM*OCA(J-1)+CI
1192.          TI=A(I,J-1)+TI
1193.    80    CONTINUE
1194.          Y=2.*CA(I)/(CA(I)+OCA(I))*OCA(I)
1195.          GO TO 100
1196.    89    DO 90 J=2,I
1197.          DENOM=H2CO3(J-1)+OH2CO3(J-1)
1198.          CI=A(I,J-1)*2.*H2CO3(J-1)/DENOM*OH2CO3(J-1)+CI
1199.          TI=A(I,J-1)+TI
```

```
90      CONTINUE
        Y=2.*H2CO3(I)/(H2CO3(I)+OH2CO3(I))*OH2CO3(I)
100     IF(I.EQ.NN) GO TO 110
        FLUX=(CI-Y*TI)*INFILR*DT/DX(I)
        RETURN
110     FLUX=CI*INFILR*864000.
        RETURN
        END
C*****************************************************************C
C                                                                 C
C              SUBROUTINE FOR CALCULATING DELTA                   C
C                                                                 C
C*****************************************************************C
        SUBROUTINE DELCAL(A,PY,DELTA,DELTB)
        IMPLICIT REAL*8 (A-Z)
        REAL*4 KSO,KSF,DCO,DCF,L
        COMMON/ADEL/KSO,DCO,KSF,DCF,L
        PY1=1.0
        Y=DSQRT(KSO*A/DCO)
        R=(1.-PY/PY1)*L
        C=(DEXP(-Y*R)-DEXP(Y*(R-2.*L)))/(DEXP(Y*(R-2.*L))+DEXP(-Y*R))
        DELTA=C/(Y*(1.+R*KSO*C/(DCO*Y)))
        Y=DSQRT(KSF*A/DCF)
        R=(1.-PY/PY1)*L
        C=(DEXP(-Y*R)-DEXP(Y*(R-2.*L)))/(DEXP(Y*(R-2.*L))+DEXP(-Y*R))
        DELTB=C/(Y*(1.+R*KSF*C/(DCF*Y)))
        RETURN
        END
C*****************************************************************C
C                                                                 C
C                        THOMAS'S ALGORITHM                       C
C                                                                 C
C*****************************************************************C
        SUBROUTINE THOMAS(A,B,C,D,N,X)
        DOUBLE PRECISION A(N),B(N),C(N),D(N),X(N),W(50),G(50),DEN(50)
        W(1)=C(1)/B(1)
        G(1)=D(1)/B(1)
        DO 1 I=2,N
        DEN(I)=B(I)-A(I)*W(I-1)
        IF(I.NE.N) W(I)=C(I)/DEN(I)
        G(I)=(D(I)-A(I)*G(I-1))/DEN(I)
1       CONTINUE
        X(N)=G(N)
10      X(N-1)=G(N-1)-W(N-1)*X(N)
        N=N-1
        IF(N.GT.1) GO TO 10
        RETURN
        END
C*****************************************************************C
C                                                                 C
C                        SUBROUTINE HADJ                          C
C                                                                 C
C              THIS ROUTINE ADJUSTS THE H PRODUCED TO             C
C       ACCOUNT FOR NEUTRALIZATION BY THE GANGUE MATERIAL.        C
C                                                                 C
C*****************************************************************C
        SUBROUTINE HADJ(AH,OH,I,H)
        IMPLICIT REAL*8 (A-H,O-Z)
        DIMENSION HC(50),OHC(50),HCFL(50),GA(50),GB(50)
        COMMON/AHADJ/HC,OHC,HCFL,GA,GB
        MMM=0
        IF(AH.LE.0..OR.GA(I).LT.-9.) THEN
        H=OH+AH
        HC(I)=OHC(I)+HCFL(I)
        WHILE(HC(I).LT.0.)
        HCFL(I)=HCFL(I)/2.
        HC(I)=HC(I)-HCFL(I)
        MMM=MMM+1; IF(MMM.GT.10) THEN; PRINT,'     ***ERROR***1120'
        GO TO 732
        END IF
        END WHILE
732     RETURN
        END IF
        M=1; Z1=1.0
        AL=OH
        AG=DMIN1(1.0D+01**(-GA(I)),OH+AH)
        AM=(AL+AG)/2.-OH
        WHILE(DABS(Z1-AM).GT..0001*AM)
        Z1=AM
        APH=-(DLOG10(OH)+DLOG10(OH+AM))/2.
        AAH=AH*(1.-DEXP(GB(I)*(GA(I)-APH)))
        IF(AM.LT.AAH) THEN
        AL=AM+OH
```

```
      ELSE
      AG=AM+OH
      END IF
      AM=(AL+AG)/2.-OH
      M=M+1
      IF(M.GT.50) PRINT,I,OH,'=H',AAH,'=AAH',' HC IS NOT CONVERGING'
      IF(M.GT.50) STOP
      END WHILE
      H=OH+AM
      HC(I)=OHC(I)+AH-AM+HCFL(I)
      WHILE(HC(I).LT.0.)
      HCFL(I)=HCFL(I)/2.
      HC(I)=HC(I)-HCFL(I)
      MMM=MMM+1; IF(MMM.GT.80) THEN; PRINT,'      ***ERROR***1132'
      GO TO 733; END IF
      END WHILE
733   RETURN
      END
C*****************************************************************C
C                                                                 C
C                        SUBROUTINE CHEMI                         C
C                                                                 C
C         THIS ROUTINE CALCULATES THE IONIC STRENGTH, ACTIVITY    C
C   COEFFICIENTS, AND CONCENTRATIONS OF THE FERRIC SPECIES FOR    C
C   ANY GIVEN PH, ST, TFE3, AND TFE2.  IT RETURNS THE ACTIVITY    C
C   COEFFICIENTS AND THE TOTAL IRON(III) ACTIVITY.                C
C                                                                 C
C*****************************************************************C
      SUBROUTINE CHEMI(MO,H,FE3,FEOOH,AFE3T,DELIO)
      IMPLICIT REAL*8 (A-H,O-Z)
      REAL*8 IO,DELFE(50)
      REAL*4 KSP,K11,K12,K13,K14,K22,KML,KMHL,KA2
      DIMENSION OH(50),OIO(50),OE3(50),OEOH(50),OEOH2(50),HC(50),
     1OEOH4(50),OE2OH2(50),OESO4(50),OEHSO4(50),OSO4(50),OE2(50),
     2OEOH3(50),OHSO4(50),OEOOH(50),OST(50),ST(50),FE2(50),TFE3C(50),
     3HCFL(50),OHC(50),GA(50),GB(50),CA(50),OCA(50),H2CO3(50),OH2CO3(50)
      COMMON/ACHEMI/FE31,HH1,TFE3C,KSP,KA2,K11,K12,K13,K14,K22,KML,KMHL,
     1MCHEMI/ACHCAL/OIO,OEOH,OEOH2,OEOH3,OEOH4,OE2OH2,OESO4,
     2OEHSO4,OEOOH,OSO4,OHSO4,ST,FE2,OH,OE3,OE2,OST,CA,OCA
     3,H2CO3,OH2CO3,I/AHADJ/HC,OHC,HCFL,GA,GB
      M=1; X=0.0
      IF(MO.LE.0) THEN
      DELFE(I)=0.
      OEOOH(I)=FEOOH
      IO=0.5*H+1.5*ST(I)
      FEOH=FEOH2=FEOH3=FEOH4=FE2OH2=FESO4=FEHSO4=0.
      ELSEIF(MO.GT.1) THEN
      X2=Z1=FE3RI=FE3
      HR=H
      CALL HADJ(HR,OH(I),I,H)
      H=HH1; FE3=X2=FE31
      IO=OIO(I); FEOH=OEOH(I); FEOH2=OEOH2(I)
      FEOH3=OEOH3(I); FEOH4=OEOH4(I); FE2OH2=OE2OH2(I)
      FESO4=OESO4(I); FEHSO4=OEHSO4(I); OFEOOH=OEOOH(I)+FEOOH
      ELSE
      X2=FE3; X=IO=OIO(I)
      END IF
      G1=10.**(-.5*(DSQRT(IO)/(1.+DSQRT(IO))-.3*IO))
      G2=G1**4
      G3=G1**9
      G4=G1**16
      GO TO 25
20    IO=0.25*(H+HSO4+FEOH2+FEOH4+FESO4+4.0*(FE2(I)+SO4+FEOH+FEHSO4)
     1+8.0*HC(I)+9.0*FE3+16.0*FE2OH2)+IO/2.
      IF(IO.GT.120.) PRINT,I,'= I',M,'=M',ST(I),'= ST',FE2(I),'=FE2'
      IF(IO.GT.120.)PRINT2,H,PH,SO4,HSO4,FE3,FEOH,FEOH2,FEOH3,FEOH4,
     1FE2OH2,FESO4,FEHSO4,FEOOH
      IF(IO.GT.120.) PRINT,FE3RI,' =FE3RI',FE3R,' =FE3R',HR,' =HR',
     1DELFE(I),'=DELFE',FE3E,'=FE3E',H6,'=H6',HC(I),'=HC',IO,'=IO'
      IF(M.GT.15) THEN; IO=X; END IF
      G1=10.**(-.5*(DSQRT(IO)/(1.+DSQRT(IO))-.3*IO))
      G2=G1**4
      G3=G1**9
      G4=G1**16
25    IF(MO.EQ.4) THEN
      Z1=FE3
      H6=H=DMAX1(H,OH(I)/100.)
      FE3E=KSP/G3*(G1*H)**3
      FE3R=FE3RI-G3*FE3E*(K11/(H*G1*G2)+K12/(H**2*G1**3)+K13/
     1(H**3*G1**3)+K14/(H**4*G1**5)+G3*FE3E*K22/(G4*H**2*G1**2)
     2+KML*SO4*G2/G1+KMHL*HSO4*G1/G2)+OEOH(I)+OEOH2(I)+OEOH3(I)
     3+OEOH4(I)+OE2OH2(I)+OESO4(I)+OEHSO4(I)
      FEOOH=OEOOH(I)-FE3E+FE3R
```

```
      IF(FEOOH.GT.0.) THEN
      FE3=FE3E
      ELSE
      FEOOH=0.0
      FE3=(FE3RI+OEOOH(I)+OEOH(I)+OEOH2(I)+OEOH3(I)+OEOH4(I)+
     1OE2OH2(I)+OESO4(I)+OEHSO4(I))/(1.+G3*(K11/(H*G1*G2)+K12
     2/(H**2*G1**3)+K13/(H**3*G1**3)+K14/(H**4*G1**5)+G3*FE3*K22
     3/(G4*H**2*G1**2)+KML*SO4*G2/G1+KMHL*HSO4*G1/G2))
      END IF
      IF(FE3.LE.0.0) FE3=DMAX1(0.0D+00,FE3R+DELFE(I))
      H1=DMAX1(OH(I)/10.,H); HA=10.; MMMM=1 ; IF(M.EQ.1) MMMM=1
      WHILE(DABS(HA-H).GT..001*H.AND.MMMM.LT.2)
      MMMM=MMMM+1; IF(I.EQ.32) PRINT,MMMM,HA,'=HA',H,'=H'
      HA=H
      AH=HR+3.*(FEOOH-OEOOH(I))-(OEOH(I)+2.*(OEOH2(I)+OE2OH2(I))
     1+3.*OEOH3(I)+4.*OEOH4(I)+OHSO4(I)+OEHSO4(I))+FE3*G3*
     2(K11/(H1*G1*G2)+2.*K12/(H1*H1*G1**3)+3.*K13/(H1**3*G1**3)+4.*K14/
     3(H1**4*G1**5)+2.*K22*G3*FE3/(G4*H1**2*G1**2)+KMHL*HSO4*G1/G2)
     4+HSO4
      CALL HADJ(AH,OH(I),I,H)
      H2=DMAX1(OH(I)/100.,H)
      IF(H.EQ.OH(I)/100.) HC(I)=OHC(I)/10.
      END WHILE
      IF(M.EQ.9)THEN
      IF(H2.GT.H1) THEN
      HH=H2; HL=H1
      ELSE
      HH=H1; HL=H2
      H=(HL+HH)/2.
      END IF
      ELSEIF(M.GT.9) THEN; IF(H.LT.H1) THEN;HH=H1
      ELSE; HL=H1; END IF
      H=(HL+HH)/2.
      IF(I.GT.35) PRINT88,HR,FE3RI,FE3R,FE3,FE3E,FEOOH,H,HL,HH,H2,IO
      ELSEIF(M.LT.9) THEN
      H=(H1+H2)/2.
      IF(I.GT.33) PRINT,I,H1,'=H1',H2,'=H2'
      END IF
88    FORMAT(1X,F10.5,' =HR ',F10.5,' =FE3RI ',F10.5,' =FE3R ',F10.5,
     1' =FE3 ',F10.5,' =FE3E ',F10.5,' =FEOOH ',/,1X,F10.5,' =H ',
     2F10.5,' =HL ',F10.5,' =HH ',F10.5,' =H2 ',F10.5,'= IO ',/)
      GO TO 27
      END IF
      IF(MO.LE.0) THEN
      X2=Z1=FE3=.2*(H*G1)**3/G3
      FEOOH=OEOOH(I)-FE3-FEOH-FEOH2-FEOH3-FEOH4-2.*FE2OH2-FESO4-FEHSO4
      IF(FEOOH.LT.0.0) THEN
      FEOOH=0.0
      END IF
      END IF
27    IF(FE3.LT.0.0) THEN
      PRINT28,I,M
28    FORMAT(//,35X,'WARNING',/,10X,'FE3 .LT. 0.0;     TOTAL COMPLEXES
     1EXCEED FEOOH',/,5X,'PROGRAM WAS EXECUTING LAYER',I4,', ITERATION'
     2I4,' IN SUBPROG CHEMI')
      PRINT,FE3RI,' =FE3RI',FE3R,' =FE3R',HR,' =HR',
     1DELFE(I),'=DELFE',FE3E,'=FE3E',H6,'=H6'
      PRINT2,H,PH,SO4,HSO4,FE3,FEOH,FEOH2,FEOH3,FEOH4,FE2OH2,
     1FESO4,FEHSO4,FEOOH
      STOP
      END IF
      SO4=ST(I)/(1.+H*KA2*G2+KML*FE3*G3*G2/G1+KMHL*H*FE3*KA2*G1*G3)
      HSO4=H*SO4*KA2*G2
      FEOH=FE3*K11*G3/(G1*G2*H)
      FEOH2=FE3*K12*G3/(G1**3*H**2)
      IF(FEOH.GT.1000.)PRINT,FE3,'=FE3',FEOH,'=FEOH',H,G1,G2,G3,'1354'
      FEOH3=FE3*K13*G3/(H**3*G1**3)
      FEOH4=FE3*K14*G3/(H**4*G1**5)
      FE2OH2=(FE3/H)**2*K22*(G3/G1)**2/G4
      FESO4=FE3*KML*SO4*G2*G3/G1
      FEHSO4=FE3*KMHL*HSO4*G1*G3/G2
      IF(MO.GT.1) THEN
      DELFE(I)=FEOH+FEOH2+FEOH3+FEOH4+2.*FE2OH2+FEHSO4+FESO4-
     1OEOH(I)-OEOH2(I)-OEOH3(I)-OEOH4(I)-2.*OE2OH2(I)-OEHSO4(I)-
     2OESO4(I)
      END IF
      IF(DABS(FE3-X2).LE..001*FE3) THEN
      IF(DABS(IO-X)/IO.LE..01) GO TO 30; END IF
      X=IO
      X2=FE3
```

```
1446.          M=M+1
1447.          GO TO 20
1448.     30   AFE3T=((G1*(FEOH2+FEOH4+FESO4)+G2*(FEOH+FEHSO4)+2.*G4*FE2OH2
1449.         1+FEOH3)/(FE3*G3)+G3)/1000.
1450.          TFE3C(I)=FEOH+FEOH2+FEOH3+FEOH4+2.*FE2OH2+FEHSO4+FESO4+FEOOH
1451.          IF(MO.LE.1) THEN
1452.          DELIO=FE3+FE2(I)+FEOOH+FEOH+FEOH2+FEOH3+FEOH4+2.*FE2OH2+
1453.         1FESO4+FEHSO4
1454.          OEOH(I)=FEOH; OEOH2(I)=FEOH2; OEOH3(I)=FEOH3
1455.          OEOH4(I)=FEOH4; OE2OH2(I)=FE2OH2; OEOOH(I)=FEOOH; OESO4(I)=FESO4
1456.          OEHSO4(I)=FEHSO4;OSO4(I)=SO4; OHSO4(I)=HSO4; OST(I)=ST(I)
1457.          OHC(I)=HC(I); OCA(I)=CA(I); OH2CO3(I)=H2CO3(I)
1458.          IF(MO.EQ.-1) THEN; OH(I)=H; OE2(I)=FE2(I); OE3(I)=FE3; END IF
1459.          ELSE; DELIO=G1
1460.          END IF
1461.          OIO(I)=IO
1462.          IF(I.EQ.32) GO TO 60
1463.          IF(MCHEMI) 40,50,60
1464.     40   RETURN
1465.     50   PRINT1,I,M,IO
1466.     1    FORMAT(/,10X,'LAYER ',I4,', # ITERATIONS = ',I2,5X,
1467.         1'IONIC STRENGTH = ',F6.4)
1468.          RETURN
1469.     60   PRINT1,M,IO
1470.          PH=-(DLOG10(G1*H))
1471.          PRINT2,H,PH,SO4,HSO4,FE3,FEOH,FEOH2,FEOH3,FEOH4,FE2OH2,
1472.         1FESO4,FEHSO4,FEOOH
1473.     2    FORMAT(7X,'H',8X,'PH',7X,'SO4',7X,'HSO4',6X,'FE3',7X,'FEOH',/,
1474.         13X,D8.2,3X,F6.3,3X,4(D8.2,2X),//,5X,'FEOH2',5X,'FEOH3',5X,'FEOH4',
1475.         24X,'FE2OH2',5X,'FESO4',4X,'FEHSO4',4X,'FEOOH',/,3X,7(D8.2,2X))
1476.          PRINT3,FE3,AFE3T*FE3
1477.     3    FORMAT(/,5X,'FERRIC IRON',8X,'TOTAL FERRIC',
1478.         1' IRON ACTIVITY',/,6X,D10.4,6X,D10.4)
1479.          RETURN
1480.          END
1481.     //DATA.FT51F001 DD UNIT=BAT,FILES=$DXDT1
1482.     //DATA.FT52F001 DD UNIT=BAT,FILES=$DXDT2
1483.     //DATA.FT53F001 DD UNIT=BAT,FILES=$DXDT3
1484.     //DATA.FT54F001 DD UNIT=BAT,FILES=$DXDT4
1485.     //DATA.FT55F001 DD UNIT=BAT,FILES=$DXDT5
1486.     //DATA.FT42F001 DD VOL=REF=MEN.P65440.D1J.LIB,
1487.     //  DSN=MEN.P65440.D1J.DMNLS8,
1488.     //  DCB=(RECFM=FB,LRECL=100,BLKSIZE=3100),
1489.     //  SPACE=(TRK,(3,5),RLSE),DISP=(NEW,KEEP)
1490.     //DATA.INPUT DD *
1491.      1                                IDUMP
1492.      0                                OPRINT
1493.      0                                MBAT
1494.     2.                                L
1495.     4.                                RADIUS
1496.     100.                              Y DIMENSION
1497.     100.                              Z DIMENSION
1498.     .0000001                          DCO
1499.     .000000083                        KSO
1500.     .0000001                          DCF
1501.     .0000044                          KSF
1502.     .00000291                         KLS
1503.     1.                                P
1504.     82.3                              RG
1505.     .00001                           E1
1506.      10300.                           ET
1507.              1                        MT
1508.     50.                               INFILR (CM/YR)
1509.      50.                              MWLS
1510.      3.                               RHOLFR
1511.     1000.                             DEPTH
1512.     20                                NL
1513.     1.                                VINC
1514.      1                                NPL
1515.     0.                                X2
1516.     .21                               YA
1517.     .0003                             YB
1518.     10.                               T
1519.     .313                              PHI(.180, .216)
1520.     .7                                WC
1521.     .75                               FFR
1522.     1.80                              RHOB(1.67,1.80)
1523.     0.0025                            FPY
1524.     .0                                FFEO
1525.     2.1                               RHOFF
```

```
1526.     15.                                   TE
1527.     2.50000000                            GA(0.523,-10.)
1528.        1.11000                            GB(1.11)
1529.     0.0                                   HBACT
1530.      1.0                                  RLS
1531.      .00083                                FLS
1532.     0.0  0.0  0.0  .00025  .00025
1533.     .00025  .00025  .00025  .00025  .00025
1534.     .02325  .0025 .0025  .0025  .0025
1535.     .0025  .0025  .0025  .0025  .0025  .0025
1536.     0.0 -0.3D-12 0.0 0.0 0.0
1537.     0.0  0.0  0.0  0.0  0.0
1538.     0.0  0.0  0.0 0.0 0.0
1539.     //DATA.FT43F001 DD DSN=MEN.P65440.D1J.DMNLS7,
1540.     //  DISP=(OLD,KEEP),VOL=REF=MEN.P65440.D1J.LIB,
1541.     //  DCB=(RECFM=FB,LRECL=100,BLKSIZE=3100),
1542.     //  SPACE=(TRK,(17,3),RLSE)
1543.     /*
1544.     // EXEC PGM=UMSG,PARM=(INTERACT,'TO D1J JOB DONE')
?
```

Example Output from Run 4

```
                                  AFTER SWEEP  21      AND   5 ITERATIONS
RMAX=  0.871D-03        KBMAX=  0.517D+00        FLMAX=  0.115D-01        LSMAX=  0.0        FCMAX=  0.281D-01
                                  AFTER SWEEP  22      AND   4 ITERATIONS
RMAX=  0.787D-03        KBMAX=  0.277D+00        FLMAX=  0.645D-02        LSMAX=  0.0        FCMAX=  0.145D-01
                                  AFTER SWEEP  23      AND   1 ITERATIONS
RMAX=  0.115D-02        KBMAX=  0.226D+00        FLMAX=  0.798D-02        LSMAX=  0.0        FCMAX=  0.697D-02
                                  AFTER SWEEP  24      AND   3 ITERATIONS
RMAX=  0.618D-03        KBMAX=  0.139D+00        FLMAX=  0.269D-02        LSMAX=  0.0        FCMAX=  0.397D-02
                                  AFTER SWEEP  25      AND   1 ITERATIONS
RMAX=  0.883D-03        KBMAX=  0.183D+00        FLMAX=  0.669D-02        LSMAX=  0.0        FCMAX=  0.825D-03

M=   1 AMAX=  0.162D-04 BMAX=  0.114D-17 PYMAX=  0.174D-05 HMAX=  0.441D-04 FE3MAX=  0.300D-03 FERMAX=  0.137D+00

I =   1  KB = 0.0            I =   2  KB = 0.9984D-08     I =   3  KB = 0.7760D-08
I =   4  KB = 0.1091D-07     I =   5  KB = 0.1639D-07     I =   6  KB = 0.2811D-07
I =   7  KB = 0.6228D-07     I =   8  KB = 0.7992D-07     I =   9  KB = 0.4408D-08
I =  10  KB = 0.0            I =  11  KB = 0.0            I =  12  KB = 0.0
I =  13  KB = 0.0            I =  14  KB = 0.0            I =  15  KB = 0.0
I =  16  KB = 0.0            I =  17  KB = 0.0            I =  18  KB = 0.0
I =  19  KB = 0.0            I =  20  KB = 0.0            I =  21  KB = 0.0
```

AFTER 6166.0 DAYS
SOLUTION WAS FOUND IN 155 ITERATIONS

LAYER	DEPTH	O2	CO2	NO2	NCO2	UO2PY	UO2FEOX	UO2HB/OR	CHOX/BACTOX	XPY/XLS
1	-0.5	0.2100	0.0003	0.6720D-10	0.2024D-13	0.0	-0.861D-26	0.0	-0.381D-18	0.0
	0.0			0.6715D-10	0.2023D-13			0.100D+01	0.0	0.0
2	25.0	0.1754	0.0003	0.5362D-10	0.1615D-13	-0.235D-13	-0.210D-13	0.0	-0.166D-09	0.345
	50.0			0.3185D-10	0.9593D-14			0.810D+00	-0.928D-06	0.0
3	75.0	0.1411	0.0003	0.3050D-10	0.9187D-14	-0.164D-13	-0.360D-13	0.0	-0.359D-09	0.231
	100.0			0.2924D-10	0.8806D-14			0.208D+01	-0.159D-05	0.0
4	125.0	0.1083	0.0003	0.2777D-10	0.8365D-14	-0.119D-13	-0.450D-13	0.0	-0.320D-09	0.184
	150.0			0.2639D-10	0.7949D-14			0.358D+01	-0.199D-05	0.0
5	175.0	0.0777	0.0003	0.2472D-10	0.7450D-14	-0.857D-14	-0.560D-13	0.0	-0.265D-09	0.186
	200.0			0.2315D-10	0.6977D-14			0.621D+01	-0.248D-05	0.0
6	225.0	0.0500	0.0003	0.2114D-10	0.6371D-14	-0.584D-14	-0.727D-13	0.0	-0.200D-09	0.235
	250.0			0.1922D-10	0.5794D-14			0.119D+02	-0.322D-05	0.0
7	275.0	0.0264	0.0003	0.1644D-10	0.4955D-14	-0.353D-14	-0.106D-12	0.0	-0.132D-09	0.343
	300.0			0.1376D-10	0.4148D-14			0.288D+02	-0.468D-05	0.0
8	325.0	0.0091	0.0003	0.7729D-11	0.2329D-14	-0.205D-14	-0.238D-12	0.0	-0.230D-09	0.641
	350.0			0.1812D-11	0.5438D-15			0.115D+03	-0.105D-04	0.0
9	375.0	0.0068	0.0003	0.1499D-11	0.4499D-15	-0.567D-14	-0.693D-14	0.0	-0.122D-09	0.957
	400.0			0.1181D-11	0.3540D-15			0.176D+01	-0.307D-06	0.0
10	425.0	0.0053	0.0003	0.1059D-11	0.3177D-15	-0.492D-14	-0.177D-17	0.0	-0.784D-10	0.969
	450.0			0.9330D-12	0.2799D-15			0.311D+00	0.0	0.0
11	475.0	0.0041	0.0003	0.8333D-12	0.2501D-15	-0.402D-14	-0.126D-17	0.0	-0.556D-10	0.975
	500.0			0.7307D-12	0.2193D-15			0.271D+00	0.0	0.0
12	525.0	0.0032	0.0003	0.6503D-12	0.1953D-15	-0.324D-14	-0.918D-18	0.0	-0.406D-10	0.979
	550.0			0.5676D-12	0.1704D-15			0.267D+00	0.0	0.0
13	575.0	0.0024	0.0003	0.5033D-12	0.1512D-15	-0.259D-14	-0.681D-18	0.0	-0.301D-10	0.982
	600.0			0.4373D-12	0.1313D-15			0.278D+00	0.0	0.0
14	625.0	0.0019	0.0003	0.3863D-12	0.1161D-15	-0.205D-14	-0.510D-18	0.0	-0.226D-10	0.985
	650.0			0.3340D-12	0.1003D-15			0.302D+00	0.0	0.0
15	675.0	0.0014	0.0003	0.2937D-12	0.8825D-16	-0.162D-14	-0.386D-18	0.0	-0.171D-10	0.987
	700.0			0.2524D-12	0.7582D-16			0.336D+00	0.0	0.0
16	725.0	0.0011	0.0003	0.2205D-12	0.6625D-16	-0.129D-14	-0.295D-18	0.0	-0.130D-10	0.988
	750.0			0.1878D-12	0.5643D-16			0.379D+00	0.0	0.0
17	775.0	0.0009	0.0003	0.1623D-12	0.4878D-16	-0.103D-14	-0.229D-18	0.0	-0.101D-10	0.989
	800.0			0.1363D-12	0.4095D-16			0.429D+00	0.0	0.0
18	825.0	0.0007	0.0003	0.1155D-12	0.3472D-16	-0.834D-15	-0.182D-18	0.0	-0.807D-11	0.990
	850.0			0.9440D-13	0.2837D-16			0.482D+00	0.0	0.0
19	875.0	0.0006	0.0003	0.7699D-13	0.2314D-16	-0.698D-15	-0.150D-18	0.0	-0.665D-11	0.991
	900.0			0.5935D-13	0.1784D-16			0.530D+00	0.0	0.0
20	925.0	0.0005	0.0003	0.4406D-13	0.1324D-16	-0.612D-15	-0.130D-18	0.0	-0.577D-11	0.991
	950.0			0.2863D-13	0.8607D-17			0.560D+00	0.0	0.0
21	975.0	0.0005	0.0003	0.1434D-13	0.4310D-17	-0.570D-15	-0.121D-18	0.0	-0.533D-11	0.992
	1000.0			0.0	0.0			0.559D+00	0.0	0.0

LAYER	PH	FE2	FE3	FEOOH	ACIDITY	SO4	IONIC STR	H2CO3	CA	TFE3CMPLX
1	5.00	0.100D-14	0.100D-14	0.0	0.100D-14	0.100D-14	0.105D-03	0.102D-04	0.100D-14	0.216D+05
2	2.91	0.381D-03	0.253D-03	0.283D-01	0.490D-09	0.192D-02	0.681D-02	0.102D-04	0.100D-14	0.268D+01
3	2.80	0.104D-02	0.700D-03	0.651D-01	0.952D-03	0.415D-02	0.189D-01	0.102D-04	0.100D-14	0.208D+01
4	2.80	0.121D-02	0.886D-03	0.610D-01	0.397D-02	0.631D-02	0.363D-01	0.102D-04	0.100D-14	0.226D+01
5	2.80	0.140D-02	0.105D-02	0.548D-01	0.737D-02	0.870D-02	0.558D-01	0.102D-04	0.100D-14	0.241D+01
6	2.80	0.164D-02	0.123D-02	0.384D-01	0.117D-01	0.117D-01	0.802D-01	0.102D-04	0.101D-14	0.257D+01
7	2.80	0.204D-02	0.145D-02	0.270D-01	0.184D-01	0.167D-01	0.118D+00	0.102D-04	0.109D-14	0.278D+01
8	2.80	0.104D-01	0.167D-02	0.0	0.295D-01	0.301D-01	0.208D+00	0.102D-04	0.146D-14	0.319D+01
9	2.80	0.736D-02	0.112D-04	0.0	0.200D-01	0.189D-01	0.133D+00	0.102D-04	0.257D-14	0.285D+01
10	2.80	0.609D-02	0.138D-05	0.0	0.170D-01	0.161D-01	0.113D+00	0.102D-04	0.515D-14	0.275D+01
11	2.80	0.557D-02	0.862D-06	0.0	0.157D-01	0.149D-01	0.105D+00	0.102D-04	0.101D-13	0.271D+01
12	2.80	0.526D-02	0.605D-06	0.0	0.150D-01	0.143D-01	0.998D-01	0.102D-04	0.183D-13	0.269D+01
13	2.80	0.507D-02	0.451D-06	0.0	0.145D-01	0.138D-01	0.967D-01	0.102D-04	0.304D-13	0.268D+01
14	2.80	0.492D-02	0.352D-06	0.0	0.142D-01	0.135D-01	0.946D-01	0.102D-04	0.466D-13	0.269D+01
15	2.81	0.482D-02	0.281D-06	0.0	0.140D-01	0.133D-01	0.931D-01	0.102D-04	0.665D-13	0.270D+01
16	2.81	0.473D-02	0.235D-06	0.0	0.139D-01	0.132D-01	0.921D-01	0.102D-04	0.893D-13	0.272D+01
17	2.81	0.467D-02	0.200D-06	0.0	0.138D-01	0.131D-01	0.913D-01	0.102D-04	0.114D-12	0.273D+01
18	2.82	0.462D-02	0.173D-06	0.0	0.137D-01	0.130D-01	0.907D-01	0.102D-04	0.138D-12	0.275D+01
19	2.82	0.458D-02	0.153D-06	0.0	0.136D-01	0.129D-01	0.903D-01	0.102D-04	0.161D-12	0.277D+01
20	2.82	0.456D-02	0.138D-06	0.0	0.136D-01	0.129D-01	0.900D-01	0.102D-04	0.181D-12	0.279D+01
21	2.82	0.453D-02	0.126D-06	0.0	0.136D-01	0.129D-01	0.898D-01	0.102D-04	0.202D-12	0.280D+01

T INCREMENTAL FRACTIONAL IRON MASS BALANCE
T -.2644D-03

T FRACTIONAL PYRITE CONSUMPTION PER M**2 PER DAY
T -.2960D-04

T TOTAL FRACTIONAL PYRITE CONSUMPTION PER M**2
T -.2563D+00

T MOLES ENTERING THE WATER TABLE PER M**2 PER DAY

	H	ACIDITY	FE3	FE2	TOTAL SULFATE	CALCIUM	H2CO3
T	0.2054D-02	0.1853D-01	0.5355D-04	0.6126D-02	0.1760D-01	0.2900D-12	0.1392D-04

T TOTAL MOLES TO ENTER THE WATER TABLE PER M**2

	H	ACIDITY	FE3	FE2	TOTAL SULFATE	CALCIUM	H2CO3
T	0.1106D+02	0.1485D+03	0.2763D+00	0.3445D+02	0.1277D+03	0.6294D-03	0.8585D-01

TECHNICAL REPORT DATA
(Please read Instructions on the reverse before completing)

1. REPORT NO	2	3. RECIPIENT'S ACCESSION NO.
4. TITLE AND SUBTITLE Atmosphere and temperature within a reclaimed coal-stripmine and a numerical simulation of acid mine drainage from stripmined lands		5. REPORT DATE 6. PERFORMING ORGANIZATION CODE
7. AUTHOR(S) D. B. Jaynes, A. S. Rogowski, and H. B. Pionke		8. PERFORMING ORGANIZATION REPORT NO. 3
9. PERFORMING ORGANIZATION NAME AND ADDRESS Northeast Watershed Research Center USDA-ARS, 110 Research Building A University Park, Pennsylvania 16802		10. PROGRAM ELEMENT NO. 11. CONTRACT/GRANT NO. EPA-IAG-D5-E763
12. SPONSORING AGENCY NAME AND ADDRESS U.S. Environmental Protection Agency Office of Research & Development Office of Energy, Minerals & Industry Washington, D.C. 20460		13. TYPE OF REPORT AND PERIOD COVERED Interim 9/1/75-8/31/80 14. SPONSORING AGENCY CODE EPA-ORD

15. SUPPLEMENTARY NOTES
This project is part of the EPA-planned and coordinated Federal Interagency Energy/Environment R&D Program.

16. ABSTRACT

Oxygen, O_2, carbon dioxide, CO_2 and temperature were measured with depth along a transect of an acid, reclaimed, coal stripmine over a two year period. Spoil-atmosphere O_2 concentrations decrease with depth but approach zero only in a small portion of the transect. Most of the mine remains well oxygenated (O_2 > 10% by volume) down to 12-meters depth. CO_2 concentrations ranged from near atmospheric levels to greater than 15%. At some locations, especially within 2 meters of the surface, variations in O_2 and CO_2 are correlated with changes in the spoil temperature. Spoil temperatures in layers below 3 meters remain in a range conducive to iron-oxidizing, bacterial activity year around. Flux ratios of CO_2 and O_2 and the source/sink rates of the two gases indicate that carbonate neutralization of the acid produced by pyrite oxidation is the dominant source of CO_2.

In a second phase of the study, a numerical model describing the production and removal of acid and acid by-products from reclaimed coal-stripmines is presented. Both direct oxygen and bacterially catalyzed pyrite oxidation is considered. The pyrite oxidation rate is assumed to be controlled by first-order, solid-liquid kinetics and simple diffusion of oxidant into reactive, coarse, stone fragments. Oxygen supply into the reclaimed profile is considered to be governed by one-dimensional, gas diffusion.

17. (Circle One or More) KEY WORDS AND DOCUMENT ANALYSIS

a. DESCRIPTORS			b. IDENTIFIERS/OPEN ENDED TERMS	c. COSATI Field/Group
Ecology Environments Earth Atmosphere Environmental Engineering Geography Other	Hydrology, Limnology Biochemistry Earth Hydrosphere Combustion Refining	Energy Conversion Physical Chemistry Materials Handling Inorganic Chemistry Organic Chemistry Chemical Engineering		6F 8A 8F 8H 10A 10B 7B 7C 13B

18. DISTRIBUTION STATEMENT	19. SECURITY CLASS *(This Report)*	21. NO. OF PAGES
	20. SECURITY CLASS *(This page)*	22. PRICE

EPA Form 2220-1 (9-73)